Università dell'Insubria

Dipartimento di Scienza ed Alta Tecnologia

Ph.D. Program in Chemical and Environmental Sciences

XXX cycle

Pedostratigraphical and geochronological characterization of late Pleistocene to Holocene depositional sequences from the Po Plain: loess and paleosols as paleoseismological markers

Ph.D. Candidate
Chiara Frigerio

Supervisor
Prof. Alessandro M. Michetti

Co-supervisors
Prof. Franz Livio
Prof. Andrea Zerboni

Ph.D. Coordinator
Prof. Norberto Masciocchi

Academic Year 2016-2017

Ai miei Genitori

Contents

Abstract

Loess represents one of the main paleoenvironmental archives recording Quaternary environmental changes. In Italy, and in particular at the Po Plain Loess Basin (PPLB), loess accumulation and conservation was promoted by local environmental conditions during the Upper Pleistocene. The cold and dry climate of glacial periods led to loess generation and deposition; whereas, the wetter and warmer conditions typical of the interglacial/interstadial periods promoted pedological processes on loess deposits, resulting in loess-paleosol pedosedimentary sequences. In the PPLB, loess sequences are generally thin and seldom outcropping. Looking at the distribution of these sequences, most of the developed loessial sequences are preserved in association with morphotectonic structures, such as isolated hills, uplifted terraces, and topographic highlands formed due to tectonically-induced drainage diversion. These landforms represent the surface expression of the complex interplay between the Pleistocene climatic changes and the compressional active tectonics which characterize the Po Plain foredeep. The morphotectonic features emerge a few meters above the surrounding fluvial plain because their moderate tectonic uplift rates are higher than regional denudation and sedimentation rates. For this reason, isolated hills and uplifted terraces acted as sedimentary traps for aeolian sediments, and preserved them. This means that loess can be a valuable stratigraphic marker, suitable to document the tectonic activity of the Po Plain. therefore, the main goal of this PhD project is to demonstrate that the loess/paleosols sequences might represent a key sedimentary record suitable not only to investigate the Quaternary climate change, but also to calibrate the fault slip rates and the deformational history of the Quaternary seismic sources in the active tectonic setting of the Po Plain.

For this purpose, I identified in the PPLB four key loess-paleosols sequences preserved in setting controlled by active compressional tectonics: Solero (AL), Rivarone (AL), Pecetto di Valenza (AL) in the Monferrato area (Western Po Plain) and Monte Netto, in the central sector of the Po Plain.

The Solero and Rivarone loess-paleosols sequences are located at the top of two fluvial terraces, the Alessandria and Valenza plateaux respectively, displaying fluvial deposits covered by one loessic cover. The Pecetto di Valenza sequence is located in a secondary valley free from the drainage network due to a phenomenon of river piracy. It displays, from the bottom, a marly bedrock, followed by a colluvial deposit cover with two loess covers at its top. This pedosedimentary sequence is affected by a recent paleoseismic reverse surface faulting, representing the first evidence of repeated Late Quaternary coseismic surface ruptures in this sector of the Po Plain. Monte Netto is an isolated hill, showing a complex loess-paleosols sequence, resting upon fluvial/fluvioglacial deposits, displaced by an

outcropping secondary anticline with some related faults. The paleoenvironmental and paleoseismological reconstructions of this sequence has already been proposed in Livio et al., 2014 and Zerboni et al., 2015. Nevertheless, a new outcrop exposed in 2016 opened a new paleoseismological laboratory suitable to confirm and to add further details at the hypothesis expressed in the previous works.

Each site has been investigated through an innovative approach, integrating pedostratigraphy and micropedology, radiometric dating and, where clear tectonic evidence have been identified (at Pecetto di Valenza and Monte Netto sites) structural analysis.

The choice to adopt the Optically Stimulated Luminescence (OSL) and the Thermally Transferred – OSL (TT-OSL) dating methods as a radiometric dating technique, resulted successful.

In the Monferrato area, the comparison of the luminescence dating obtained for the loess deposits at the study sites, allowed to constrain to the Upper Pleistocene the formation and evolution of the Alessandria and Valenza plateaux, which have never been dated through direct radiometric dating. Moreover, I demonstrate that the formation of the Alessandria plateau is linked to the rearrangement, for tectonic reasons, of the Tanaro river drainage network, rather than to the tectonic deactivation of the Monferrato Frontal thrust (Giraudi, 2015).

At Monte Netto the geochronological characterization of the loess deposits, obtained through the OSL/TT-OSL dating method allowed to detail the paleoseicmological evolution proposed in the previous studies. the deposition of the loess cover resulted connected to the moment in which the topographic surface stabilized, linked, in turn, to the growing of the anticline. Here I demonstrated how loess can preserve the tectonic information and allow to constrain a tectonic evolution.

Loess played the same role at the Pecetto di Valenza site, preserving the deformation induced by earthquake surface reverse faulting and giving constraints to the sequence of events that characterized this site. In fact, the structural analyses and a 2D balanced retrodeformation of the section, integrating radiometric dating and constraints from the pedostratigraphical analysis, especially for the micropedological one, allowed identifying at least two different phases of deformation, and more than five fault scarp forming events, which caused a total net displacement of ca. 4.8 m during the past ca. 40 ka. In this paleoseismological reconstruction, the micropedology of soil thin sections played a key role: the observations at microscopic scale of features linked to the tectonic deformation and the study of their crosscutting relationship, allowed to identify at least two deformative events that were not visible at macroscopic scale.

The importance of the constraints obtained from the application of the micropedological approach into the paleoseismological one, gave rise to the idea that micropedology can be a useful tool to fill, or at least reduce, the incompleteness of the paleoseismic record, providing important clues into the paleoseismological reconstructions. To demonstrate this hypothesis, I individuated into the new outcrop excavated in 2016 at Monte Netto, a good laboratory, that, together with the Pecetto di Valenza one, allowed me to obtain promising preliminary results. The main one is that the identification of features formed during specific climatic phases and subsequently disturbed by surface deformation, can provide relative geochronological constraints useful to detail paleoseismological reconstructions.

The constraints obtained from the study of the loess-paleosols sequences analysed in this project, highlight how loess-paleosol sequences can be a valuable stratigraphic marker suitable to document the Late Quaternary tectonic activity of the Po Plain. Moreover, I showed that from the study of the interaction between aeolian sedimentation and active tectonics, it is possible to provide relevant hints for a correct assessment of the seismic potential of an area and the related hazard assessment.

1. Introduction

1.1 The Po Plain and the overlooked earthquake hazard

The Po Plain (Northern Italy) is an area of moderate seismicity and tectonic activity, located in an active tectonic setting.

Italy, indeed, is a tectonically active region, as testified by the distribution of earthquakes (Fig. 1). Earthquakes show prevalent compressional focal mechanisms at the fronts of Alps and Apennines and extensional mechanisms along the Apennines backbone, confirmed by in-situ stress measurements (e.g., borehole breakouts; Montone *et al.*, 2004). Alps and Apennines are therefore responsible of the tectonic evolution of the Italian landscape. They show markedly different characters (Carminati et al., 2004a; 2010).

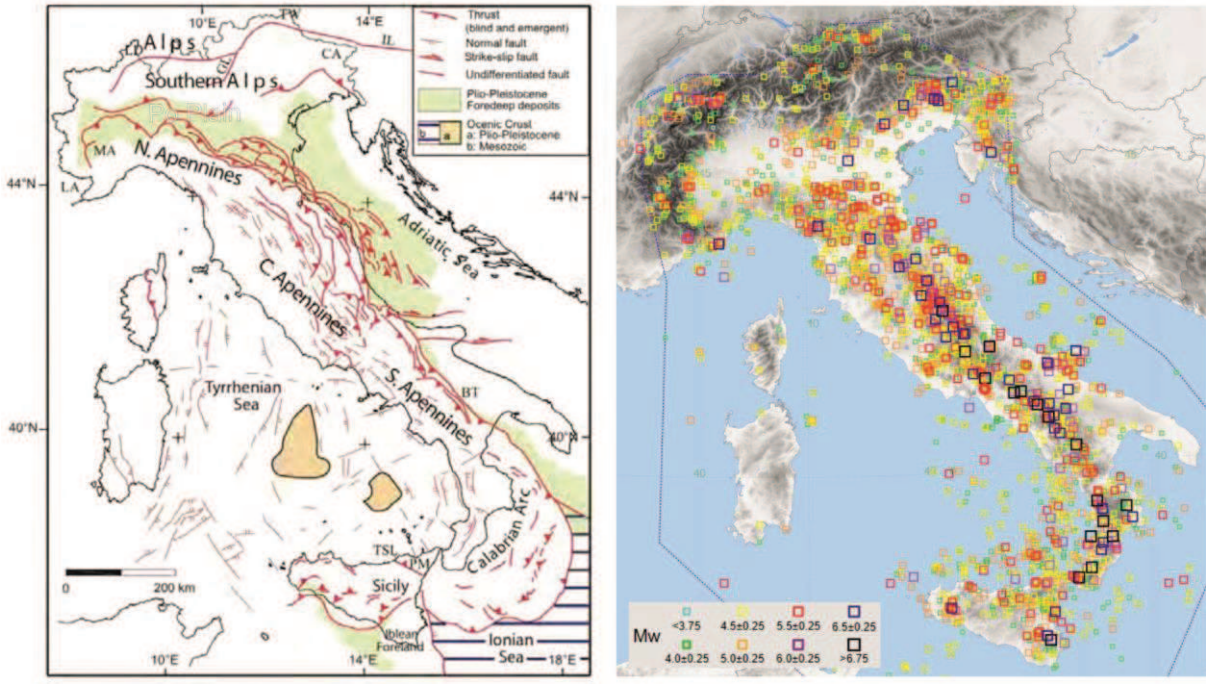

Fig. 1: On the left: simplified structural map of Italy (modified from Scrocca, 2006). LA: Ligurian Alps; MA: Monferrato Apennines; IL: Insubric Line; CA: Carnian Alps; GL: Giudicarie Line; LD: Lepontine dome; TW: Tauern Window; PM: Peloritani Mountains; BT: Bradanic trough; TSL: Taormina-Sangineto Line. On the right: seismicity map of Italy from the CPTI (Catalogo Paramentrico dei Terremoti Italiani, from the year 1000 AD to 2014) catalogue (Rovida et al., 2016).

The Alps display double-verging growth, with the involvement of large volumes of basement and the exhumation of metamorphic rocks (thick-skinned tectonics). The Apennines, instead, are a single-verging belt, mostly characterized by thin-skinned tectonics and associated to a radial "eastward" translation (coupled to extensional tectonics in the Ligurian-Provençal, Tyrrhenian, and western

Apennines areas). The Apennines generated an arc from the northern Apennines down to Sicily, possibly merging with the Maghrebides along the northern Africa coast. The different evolution of the Alpine and Apenninic belts is mirrored by the different geometry of the respective foredeep or foreland basins (shallow in the Alps and deep in the Apennines), as recorded also by the dip of the foreland monocline (shallow in the Alps and steeper in the Apennines; Mariotti and Doglioni, 2000). The geometry of the compressional structures is mainly controlled by active geodynamic processes and paleogeography (distribution of structural highs and lows, inherited from the Mesozoic rifting) (Carminati et al., 2010).

In this framework, the Po Plain is the foredeep basin in northern Italy, where the junction between the southern Alps and the northern Apennines is located [e.g., Castellarin et al., 1985; Castellarin and Vai, 1986; Castellarin et al., 1992; Doglioni, 1993; Giglia et al., 1996; Castellarin and Cantelli, 2000; Fantoni et al., 2004; Carminati et al., 2004; Mosca et al., 2009]. As stated above, this is a region characterized by moderate historical seismicity, where earthquake hazard is perceived as marginal (e.g., Crescimbeni et al., 2014; Carnelli and Frigerio, 2016). Since the Po Plain is the most economically developed region of Italy, hosting ca. 15 million of people, and characterized by a dense industrial network, understanding the local seismic hazard is of critical societal value. After the recent seismic sequence in Modena (May 20 and 29, 2012; Mw 6.1 and 6.0. respectively), this topic has been largely debated in the literature (e.g., Malagnini et al., 2012; Meletti et al., 2012; Michetti et al., 2012). The issue, which is the background motivation of this PhD project in Environmental Sciences, is well illustrated in Fig. 1. The instrumental seismicity of N Italy in the period 1981 to 2002 (from CSI 1.1; Castello et al., 2006) shows the typical situation of the Po Plain, with very low seismicity clustered along the Southern Alps and Apennines piedmont belts. When we use a larger historical time window, provided by the excellent record available in Italy for the last millennium, the picture is quite different (Fig. 1; relevant seismic events from the year 1000 AD to 2014, CPTI catalogue – Catalogo Parametrico dei Terremoti Italiani, Rovida et al., 2016). Note the very low level of instrumental seismicity along the whole Po Plain, in comparison with the strong (Mw 6 – 6.9) historical seismic events, which are frequent in the eastern sector, rare in the central sector of the Po Plain and absent in the western one. These observations highlight the presence of a seismicity gradient from East to West, which is in good agreement with the available geological and geodetic data showing a similar westward decreasing of the Quaternary to ongoing shortening rates (e.g., Falletti et al., 1995; Mosca et al., 2009; Michetti et al., 2012 and reference therein). Moreover, the available historical and instrumental data clearly suggest that the Po Plain might host seismic events much stronger than the ones occurred in 2012. For instance, both the Verona 1117 and Brescia 1222 earthquakes had larger earthquake magnitude, in the order of Mw 6.5 to 7.0. Also, the ITHACA catalogue of capable faults (Vittori et al., 1988; ITHACA, 2017, web page:

http://www.isprambiente.gov.it/it/progetti/suolo-e-territorio-1/ithaca-catalogo-delle-faglie-capaci) for the Po Plain shows that seismogenic structures similar to the ones responsible for the Verona, Brescia and Modena events are present in other sectors of the Po Plain, indicating that the seismic hazard of the region is underestimated (Comerci et al., 2016; Berlusconi et al., 2016; Fig. 3).

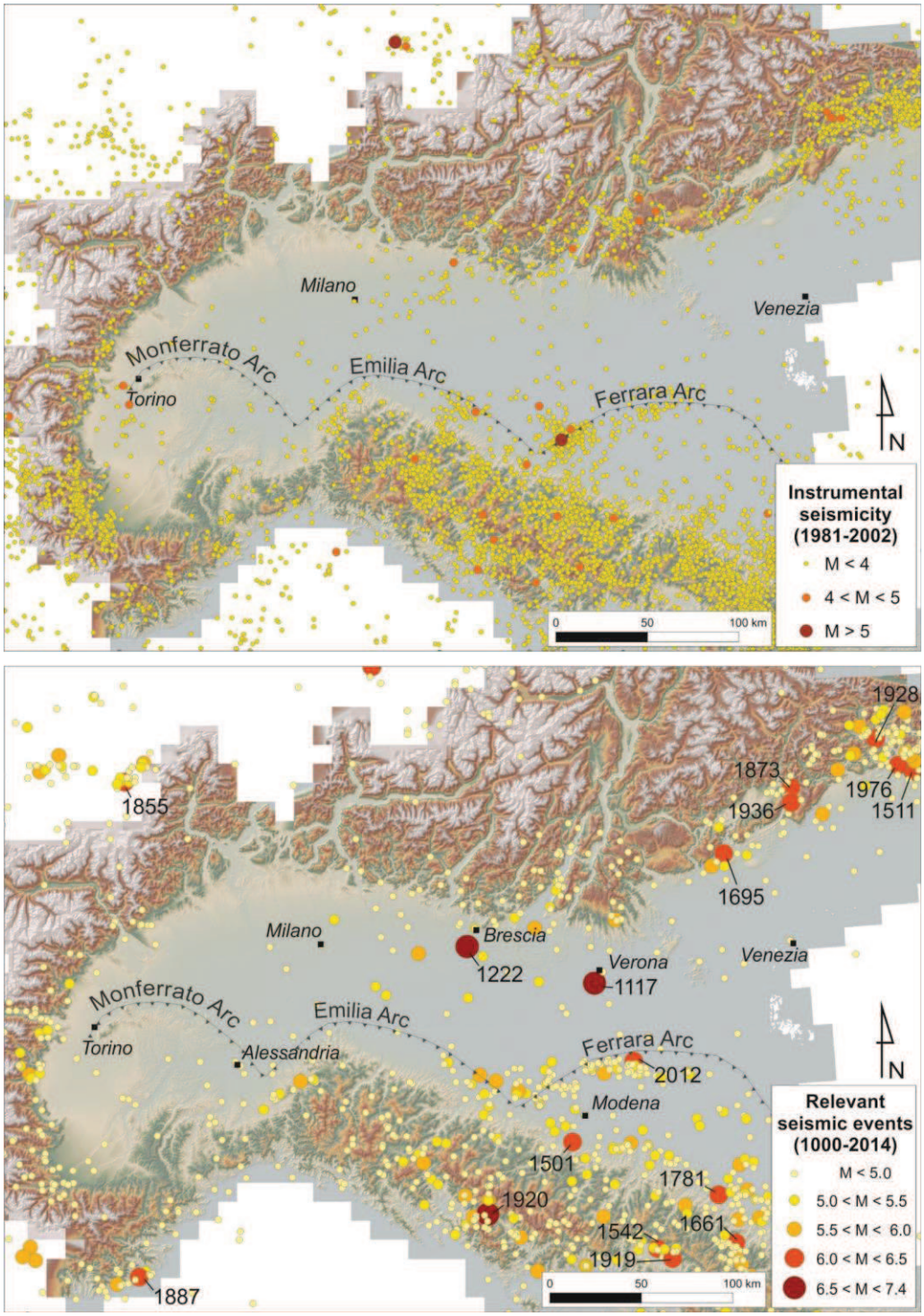

Fig. 2: Seismicity of N Italy: a) instrumental events in the period 1981 to 2002 (from CSI 1.1; Castello et al., 2006); b) relevant seismicity from the CPTI (Catalogo Parametrico dei Terremoti Italiani, from the year 1000 AD to 2014) catalogue (Rovida et al., 2016), except for the 1222 Brescia event, which is relocated based on Guidoboni and Comastri (2005). For historical events, Mw is estimated from macroseismic data.

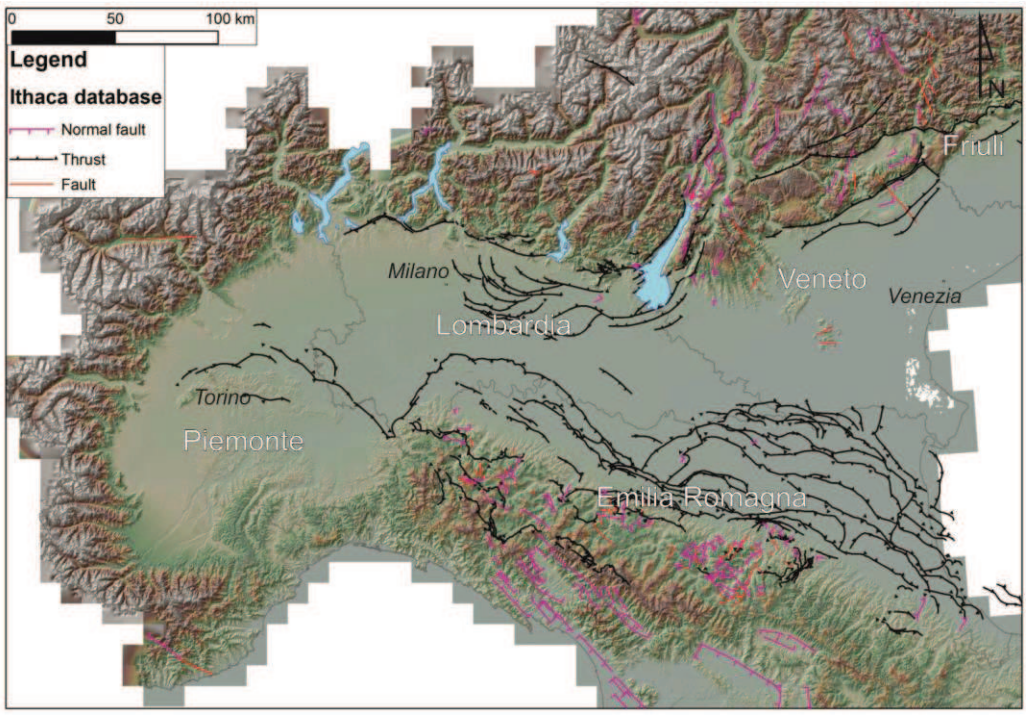

Fig. 3: Map of capable faults buried beneath the Po Plain, extracted from the Ithaca database.

One major point of debate is the assessment of the maximum credible earthquake magnitude in the W Po Plain, which remains an open issue (e.g., Michetti et al., 2012; Giraudi, 2015). The seismic catalogue shows no event with Mw greater than ca. 5.6 west of the longitude of Brescia (45,53659° N, 10,23206° E). But the seismic catalogue in Italy is certainly not complete, at least for strong events happened before the year ca. 1000 A.D., as was demonstrated, for instance, in the Pollino Region (e.g., Cinti et al., 1997; Michetti et al., 2000). In fact, the Po Plain is a homogeneous structural and tectonic foredeep domain, and there is no apparent physical discontinuity which might justify the absence of strong earthquakes in the Piedmont and western Lombardy area. Moreover, evidence of recent and active tectonics is described in the whole Po Plain, including the western sector (e.g., Carraro et al., 1995; Burrato et al., 2003; Benedetti et al., 2003; Boccalettiet al., 2011; Giraudi, 2014; 2015; Turrini et al., 2015; 2016).

The present-day physiographic setting of the Po Plain is the result of the complex interplay between the effects of major Pleistocene climatic changes (i.e., sea level fluctuations, glaciations, fluvial incision, alluvial mega-fan accretion in the piedmont belts, pedogenesis) and the compressional active tectonics (uplift, subsidence, folding and faulting). The surface expression of this active tectonic shortening can be represented by:

a) isolated hills, some tens of meters higher than the surrounding alluvial plain, induced by the late Quaternary growth of fault-propagation anticlines (e.g., San Colombano, Monte Netto, Castenedolo, Romanengo, Trino Vercellese; Fig. 4; Cremaschi & Papani, 1975; Boccaletti et al., 2004; Livio et al.,

2009; Ponza et al. 2010; Galadini et al., 2012; Michetti et al., 2012; Bresciani & Perotti, 2014; Livio et al., 2014);

b) faults scarps in the Northern Apennines foothills and Po River terraces (e.g., Ghiardo, Broni-Stradella Fault, Valenza, Poirino plateaux; Fig. 4; Carraro et al., 1995; Benedetti et al., 2003; Boccaletti et al., 2011; Giraudi,2014; 2015);

c) tectonically-induced drainage diversion (Oglio River, Tanaro River; Burrato et al., 2003; Forno, 1982; Carraro et al., 1995; Michetti et al., 2012; Bonadeo, 2014 and references therein).

The widespread presence of such morphotectonic structures, hint of active tectonics, suggests that the seismotectonic potential, in terms of maximum magnitude, of the Central and Western part of the Po Plain is similar to the one known for the Eastern part (e.g., Michetti et al., 2012; Bonadeo, 2014; Turrini et al., 2015). Conversely, a change in recurrence interval, along a E-W gradient, can be supposed: several thousands of years in the western area and much more frequent to the East. The only way to prove this hypothesis is to look over longer time windows than the historical one in the western sector, integrating the study of the Quaternary landscape and paleoseismology. Such an approach (e.g., Serva, 1990; Cinti et al., 1997; Michetti et al., 2012; Caputo et al., 2015) can provide valuable information regarding the seismotectonic evolution of this area, useful to assess its seismogenic potential. In this line, the morphotectonic structures cited above, emerging a few meters above the plain and being free from the drainage system and from the main erosive surface processes, are well preserved and become an ideal setting able to record paleoseismic information. Further characteristics that promote the preservation of these structures and therefore their suitability for paleoseismological structure, are moderate tectonic uplift rates (max 1 mm/a over the Pliocene to present; Castellarin et al., 2006; Scrocca et al., 2006; Boccaletti et al., 2011; Michetti et al., 2012; Forno and Lucchesi, 2016), which are still typically higher than regional denudation and sedimentation rates (0.4-0.5 mm/a; Bartolini et al., 1996; Scardia et al., 2012).

1.2 The loess/paleosols sequences as a key to understand the seismic landscape

As stated above, a reliable assessment of the local seismo-tectonic potential of the Po Plain, can arise only from the paleoseismological analysis of the Quaternary landscape, in particular isolated hills, uplifted terraces and tectonically-induced drainage changes. These morphotectonic structures, located where the uplift rate exceeds the erosion/sedimentation rate, in addition to the peculiarity presented in the previous paragraph, also present the characteristic to act as sedimentary traps for aeolian sediments, i.e. loess (Cremaschi 1987; 1990a; 2004; Cremaschi et al., 2011).

Loess consists of silty sediments which have been transported and accumulated by aeolian activity.

Aeolian sedimentation is a widespread phenomenon, favoured by local environmental conditions, that characterized the Po Plain during the Late Pleistocene. During glacial periods, cold and arid climate as well as the availability of source material and enhanced wind activity led to loess accumulation. Then, during warmer and less arid interglacial and interstadial phases, sediments underwent pedogenesis and weathering, resulting in loess/paleosols pedosedimentary sequences.

Loess present typical textural and mineralogical characteristics.

From a textural point of view, the loess deposits are characterized by a sigmoid, asymmetric grain size distribution curve (Fig. 4; Cremaschi, 1990a). Sorting is high to moderate, with a median varying between 5 phi and 7.5 phi and considerable asymmetry in the fine tail. The sand content is generally very low (1-10%) and the clay fraction varies between 5 and 40%. The differences in grain size depend both on the sorting which affected loess particles during transport and on post-depositional weathering (Cremaschi, 1987b). Post-depositional weathering processes have strongly modified the original texture of most of the loess lying on the top of stable surface.

The mineralogy of the Po Plain loess is rather homogeneous. The sandy fraction is composed mainly by quartz and by small amount of feldspars and muscovite. The heavy minerals, varying in percentage from 0.4 to 1%, consist mostly of minerals in metamorphic paragenesis (amphiboles, epidotes, disthene, garnets, etc.). This association is characteristic of the fluvial and fluvioglacial Late Pleistocene deposits of the Po Plain which thus represent the source of the aeolian dusts (Cremaschi, 1979; 1978a; 1978b, 1990a). The clay minerals in loess deposits are mainly constituted by vermiculite and illite, while halloysite is scarce. The calcium carbonate content in loess should have been generally low (below 5%), but its real amount is very difficult to evaluate, due to the weathering phenomena which affected loess deposits.

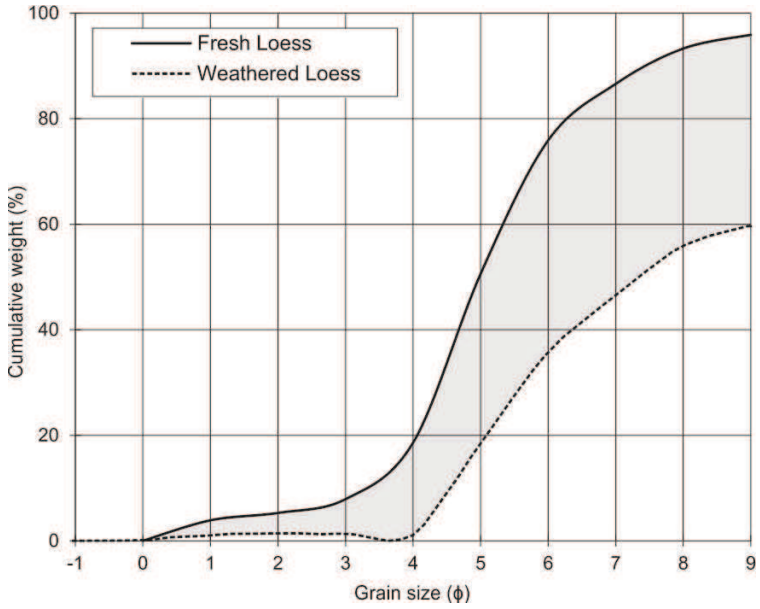

Fig. 4: The grain size distribution of the loess in Northern Italy. The curves for the unweathered and weathered loess are shown.

About the stratigraphy, loess deposits are systematically associated with Palaeolithic artifacts which constitute a valuable independent chronostratigraphic marker for dating and correlation. The artifacts included in loess deposits, typically present sharp edges, which, therefore, did not undergo post-depositional transportation. Their surfaces, instead, are affected by impact traces, due to abrasion of aeolian quartz grains: this fact points to an aeolian transportation for the loess sediments into which the artifacts are buried (Cremaschi, 1990a). As stated above, the loess sedimentation in the Po Plain is typical of the Late Pleistocene. Several stratigraphic sequences (Cremaschi, 1987a; 1979; 1990a) indicate that two main phases of sedimentation occurred during the Upper Pleistocece: the first during the Early Pleniglacial, systematically associated with Mousterian artifacts, the second, which occurred during the Second Pleniglacial, is systematically associated with Upper Palaeolithic artifacts.

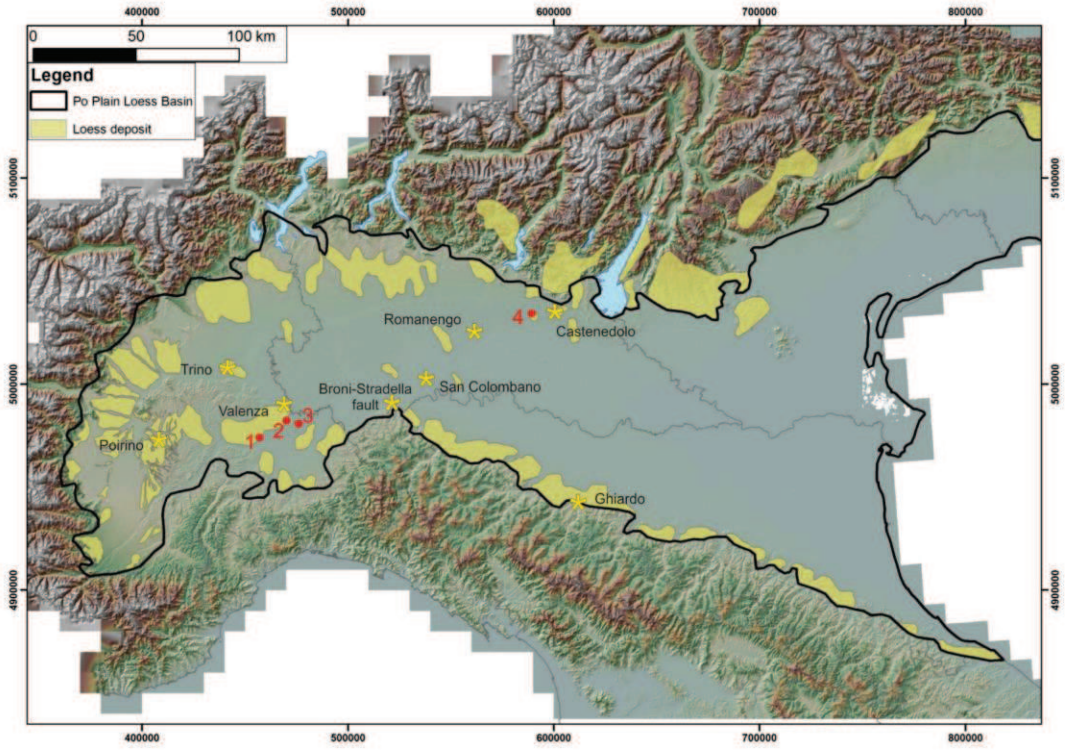

Fig. 5: Map of the Po Plain Loess Basin showing the distribution of the main loess deposits in the Po Plain. Modified after Cremaschi, 1990a and Forno, 1990. The yellow stars locate the main morphotectonic structures cited in the text; the red dots locate the site object of this study: 1- Solero; 2- Rivarone; 3- Pecetto di Valenza; 4- Monte Netto.

Looking at the map of the distribution of loess deposits in the Po Plain Loess Basin (PPLB, Amit and Zerboni, 2013; Fig. 5), can be observed that they are widespread on the Pleistocene terraces contouring the Po Valley fringes. On fluvial terraces, loess is found all along the Apennine edge, from Piedmont to the Marche region. At the southern margin of the Prealps, from the Piedmont province to the Tagliamento River, loess deposits are recognized on fluvioglacial terraces and moraine ridges belonging to the glacial stages older than isotope stage 2. At the foothill of the Alps, loess deposits contour upper Pleistocene moraine systems. In the piedmont belt of both the Apennines and the S Alps, hilltop loess is well preserved on the small isolated hills. Therefore, observing the location of the morphotectonic landforms illustrated above, there is a clear correspondence with the loess covers. This means that loess can be a valuable stratigraphic marker suitable to document the tectonic activity of the Po Plain. Moreover, when a loess/paleosols sequence is faulted, it is possible to constrain the timing of the deformation. Therefore, the study of the interaction between aeolian sedimentation and active tectonics can allow to define the uplift/deformation rates, the number, the magnitude and the recurrence interval of paleoearthquakes along a specific section of a capable fault (i.e., active faults that have the potential for generating displacement at or near the ground surface; e.g., Azzaro et al., 1998; IAEA, 2010).

The study of loess covers from this point of view, is a novelty: a revision of the existing literature underlines how loess is only used as a sedimentary record for paleoenvironmental reconstructions, both in Italy and in the rest of the world. For example, in a substantial amount of papers focused on the Asian Plateau (e.g., Kumar et al., 1996; Sing et al, 2006; Srivastava et al. 2009; YunYi and ZhengTang, 2010), although performed in settings controlled by active faults, loess strata are considered only as one of the sedimentary events that characterized the analysed area. The Authors do not take into account that the aeolian deposition could be favoured by a moment of tectonic stability, missing, therefore, an important constraint for the paleoseismological reconstruction. Also the Italian paleoseismological studies performed in correspondence of loessic cover, in particular in the PPLB, do not recognized these deposits as marker useful the constrain the Quaternary tectonic activity, but simply as the last deposition event completing a sedimentary succession (Sacco, 1889; Corsi et al; 1969; Forno, 1979; Biancotti and Cortemiglia, 1981; ENEL, 1984;. Giraudi et al.; 2003; Festa et al., 2009; Balestro et al., 2009; Giraudi, 2014; 2015; 2016).

In this light, while the background motivation of this research project is the assessment of the seismic hazard, the main goal is to demonstrate that loess/paleosols sequences might represent a key sedimentary record able to calibrate the fault slip rates and the deformational history of the Quaternary seismic sources in the active tectonic setting of the Po Plain.

From the study of loess/paleosols sequences is possible to take multiple advantages, useful to better characterize the paleoseismological reconstruction. The main one is that loess sediments are suitable for radiometric dating, in particular for luminescence dating (e.g., Duller, 2008; Roberts, 2008; Rhodes, 2011; Duller and Wintle, 2012): accurate chronological constraints derived from Pleistocene loess can be a useful tool for defining the capability of Quaternary faults. Today, there is a lack of radiometric dating for the Quaternary deposits infilling the Po Plain area and covering the surface of terraces and isolated reliefs: this gap represents one of the main obstacle to a more precise definition of the Quaternary dynamics and to the characterization of the tectonic activity of this area. This lack, probably, is due to the difficulty to date sediments deposited during the glacial periods, poor in organic matter, thus unsuitable for radiocarbon dating. The few studies that tried to reconstruct the evolution of the Po Plain, mostly used relative chronology (e.g., intensity of weathering and degree of soil development; Arduino et al., 1984).

Therefore, this project identifies in the Optically Stimulated Luminescence (OSL) and in the Thermally Transferred – OSL (TT-OSL) an innovative radiometric dating technique suited to date loess/paleosols sequences and to constrain the paleoseismological evolution of this area from a geochronological point

of view. One of the main value of this method is that allows to extend the dating range up to 150 ka year, compared with the only 40 ka years of radiocarbon.

Like all dating methods, also the OSL/TT-OSL one does not date directly a specific event, but provides limits *post* or *ante quem*, i.e., a time interval in which the studied event developed. This means that in the case of condensed or discontinuous sequences, where it is usually possible to date only few samples, the time interval constrained can be very long and important information can be lost in the hiatus. Only a continuous process, that is the soil development, can record the paleoenvironmental and also the paleoseismological information. Soils and paleosols (i.e., soils formed long periods ago that have no relationship in their chemical and physical characteristics to the present-day climate or vegetation), in fact, are usually considered as a paleoenvironmental archives: they can continuously record into their natural organization, in form of permanent features, the processes and events occurred throughout history, even though the depositional setting is characterized by low and discontinuous rates. In this line, the loess deposits affected by pedogenesis become suitable to document multiple kinds of information. This possibility to detail the gap between an event and the limit *post*/*ante quem* through the study of the pedogenized loess deposits represents the second main advantage that can be taken from the studiy of loess/paleosols sequences.

The analytical method used to decipher the information recorded in the soil organization and into its permanent features, called *pedofeatures* (defined by Stoops, 2003, as “discrete fabric units present in soil materials that are recognizable from an adjacent material by difference in concentration in one or more components or by a difference in internal fabric), is the micropedology of soil thin sections. This technique allows reconstructing the evolution processes and the event that have interested the studied soil. Since the pedofeatures are the result of the interaction between soil forming factors, such as time, topography, vegetation/organism, parent material and, mostly, climate (Jenny, 1941), soils, paleosols and all the pedogenized deposits (loess included) are considered relevant indicators of the climatic and environmental changes that characterized an area. In particular, they preserve information on changes occurred due to the alternation between glacial and interglacial periods, which, in soil science, can be translated as the alternation between cycles of biostasy and rhexistasy (Erhart, 1951).

Nevertheless, the observation conducted during this research project, bring me to state that the pedofeatures can record, not only the climatic information, but also the paleoseismological ones. Soils and paleosols are generally considered in the paleoseismological studies as marker for event horizon (sensu Pantosti et al., 1993; McCalpin, 2009). However, the potentiality of soils/paleosols to record past event also into their natural organization, has been largely overlooked until now. Indeed, a detail

review of the available literature on this topic, presented in the following section, highlights that micropedology is barely integrated to the paleoseismological research.

The same works cited above, focusing on the Asian Plateau (e.g., Kumar et al., 1996; Sing et al, 2006; Srivastava et al. 2009; YunYi and ZhengTang, 2010), used the micromorphology of soil thin section to characterize the nature of the loess strata and interlayered soil horizons close to active faults. Nevertheless, these works did not consider the identification and interpretation of micro-pedofeatures directly related to tectonic movements.

Micropedology is largely used to the recognition of glaciotectonic deformations in glacigenic sediments and derived soils, thus reconstructing glacial dynamics (e.g., Khatwa and Tulaczyk, 2001; Larson et al., 2011; Menzies and Reitner, 2016). In these papers, deformation pedofeatures recognized in thin-sections, such as rotation structures, microshears, grain stacks, deformation bands, edge-to-edge crushing events, and shear zones, are interpreted as evidence of variation of the shear stress levels in the till/soil. Even if the abovementioned pedofeatures were described in glacigenic sediments suffering glaciotectonic, these studies represent a good analogue for coseismic-induced deformations and offer a number of hints for paleoseismological analysis.

Early works that applied the micromorphological approach to faulted sequences (Douglas, 1981; Douglas et al., 1983) described the effect of faulting on pedological features comparing un-faulted soils with soil breccias. The main outcomes of these seminal studies underlined that i) soil breccia zones have a specific microstructure (massive with vughs-type voids without clay coatings on their rim), and ii) induced orientations of the discrete elements of fabric are common. In the latter case, the principal directions of constituents are triggered by the direction of movement of the fault. Nevertheless, these works only describe the differences between faulted and un-faulted material, without identifying elements useful to reconstruct the correct sequence of events that characterized the studied site, thus without any reference to earthquake surface faulting. Therefore, these papers did not use soil microstructures in the framework of a paleoseismic analysis.

Later, Jim (1990) confirmed that the distribution patterns of the groundmass is a sensitive and reliable indicator of the stress-strain history of a soil, and made use of soil mechanics, structural geology, and agricultural engineering to interpret the possible stress-strain components that rearrange fabric units with a preferred orientation. The morphological product of a shear deformation on soils is the presence of relatively long and straight voids with oriented-clay coatings and well developed oriented clays around embedded grains (striated b-fabric). This work also provided a conceptual model summarizing the conditions promoting the rearrangement of the elements of fabric, including tectonic deformation.

More recently, Cetin (1995, 1998, 2000) converged in observing that during faulting: i) the soil material moved along a fault is anisotropically consolidated or compacted, recording in its microstructure the local faulting stress; ii) pores, clays, and coarse mineral constituents are reoriented with their longer axes oriented along the maximum principal stress direction. In these papers, a comprehensive paleoseismic discussion of pedofeatures is not offered and are focussed on the effect of active faulting on soil-pore and particle orientations in the fault zone, in order to determine minimum and maximum principal stress directions. Nevertheless, this approach, as applied in Cetin (1998), can be useful in determining strain orientation, when fault displacement is not observed, but traces of ductile folding are present at the site. The latter case explains how the study of the orientation patterns of the discrete elements of fabric at microscale is helpful in reconstructing stress direction. The author also suggests, in a methodological perspective, cutting the undisturbed soil blocks for thin sections into smaller chips at right angles to each other, to obtain oriented thin sections and derive the real attitude of planar features and anisotropy. This method was originally proposed by Brewer (1976). Moreover, these cases highlight that the number and degree of orientation of the individual features increase proportionally to the increase of the shear strain, thus resulting in the striated b-fabric.

Jeong and Cheong (2005) published one of the first specific contributions of micromorphology of soil thin sections in paleoseismic investigations. They carried out an approach combining mineralogy, micromorphology, and chemistry strengthened by using microanalytical tools (electron microscopy and microchemical analysis) in addition to the optical observation of soil thin sections. Jeong and Cheong (2005) investigated a deformed weathering profile and associated fault gouge in Korea (Yangsan Fault System): they observed that, due to the disturb by tectonic movements, clay and silt-sized particles i) formed in the intensively weathered soil horizons, ii) have been transported through the profile, and iii) accumulated in the C horizon and occasionally also into the bedrock. The translocation of fine mineral constituents occurs via microfissures and voids of fault, thus recording a sequence of disturbance. In this way, they recognised a greater number of faulting events larger than expected from field observations, thus suggesting a more complex paleoseismic history for the considered outcrops. From the methodological point of view, the major point of this work is that the investigation at the microscopic scale offers much more information than the macroscopic one, providing, for instance, essential details to the reconstruction of the seismic history of a region, including important clues to reconstruct the recurrence intervals of earthquakes. However, the Authors defined the chronology of the seismic events considering the neoformation of minerals and their transformation observed in soil thin sections, without identifying specific morphologic features recording evidence of earthquake surface rupture events.

Vanneste et al. (2008) highlight the micromorphological analysis as a tool to identify paleoearthquakes along active faults. They analysed thin sections from two paleoseismic trenches across the Geleen Fault (Belgium) identifying the most recent large paleoearthquake on that fault segment. These thin sections were already studied and presented in a previous paper (Van den Berg et al., 2002), but the results were not fully integrated within the paleoseismic analysis, becoming, therefore one of the main purpose of Vanneste et al. (2008). Here, they recognized a colluvial wedge that was not visible at the macroscale, thanks to the observation in soil thin sections of fragments of clay coatings/infillings with rounded boundaries, suggesting a mechanical transport, consistent with a reworking of the underlying soil material. Moreover, they identified coarse mineral grains vertically oriented, interpreted as sand-dykes resulting from liquefaction. The position of these features respect to the colluvial wedge into the soil profile indicates that liquefaction and the faulting event occurred contemporaneously, both contributed to the formation of the colluvial wedge itself, and this produced features which allow to unequivocally identify the most recent large paleoearthquake. These observations enable better defining the paleoseismic history of the Geleen Fault, providing useful information regarding the surface displacement and the magnitude of each event. Therefore, the main remark of this work is that where macroscopic evidence is vague, micromorphology may provide critical information that helps to identify paleoseismic features as fault splays, fissures, event horizon, colluvial wedges, buried soils, and deformed stratification.

A valuable contribution of micromorphology to paleoseismic analysis is also underlined in Verbeeck et al. (2017). They evaluate the co-seismic character and movement history of the Rauw Fault (Belgium), which lack geomorphological expression and historical/present seismicity. The micropedology of the fault gouge material revealed fragmented oriented clays, which suggest fast co-seismic rupturing instead of fault creep.

The main observation that can be drawn from this review of the existing literature is that soil horizons may preserve reliable microscopic evidence formed under stress/deformation conditions after past earthquakes. Nevertheless, the interpretation of micropedological data in paleoseismology is largely lacking so far. In this work, another goal is to show how the micropedological approach could provide critical information, helping to identify paleoseismic features, where macroscopic evidence is vague, including new or additional constraints into the paleoseismological reconstruction built up on the basis of crosscutting relations.

Summarizing, the loess/paleosols sequences preserved in setting controlled by active compressional tectonics may record paleoseismological evidence that can be time-constrained through a geochronological characterization and deciphered in detail through a

pedostratigraphical/micropedological approach. The integration of these approaches into the paleoseismological practice, represents a novelty. The study of key sedimentary records, as the loess/paleosols sequence, through this integrated paleoseismological approach, can provide important hints for defining the fault slip rates, the magnitude, the earthquake recurrence intervals and related implications for seismic hazard assessment. In this sense, the suitability of loess/paleosols as a marker for paleoseismic studies has been proved at Monte Netto site (Livio et al., 2014; Zerboni et al., 2015). This example, described in the next paragraph, constitutes the starting point from which derives the research strategy adopted for the present PhD project.

1.3 Research strategy and site selection

The case of Monte Netto represents the first example where a loess/paleosols sequence becomes a suitable stratigraphic marker for paleoseismic analysis.

The research hypothesis which led to the identification of this site was based on the detailed analysis of the area to the south of Brescia, that is described as the epicentral area of one of the strongest known historical earthquake in Northern Italy, the 25 December 1222 event (Io = IX-X MCS; e.g., Guidoboni, 1986; Serva, 1990). During this event, historical sources describe the occurrence of significant environmental effects. The working hypothesis was that if such a strong earthquake is repeated in a recent geological time-interval, we should be able to detect the cumulative effects of coseismic ground deformation in the landscape. For this purpose, systematic field mapping has been performed in this area, along the main tectonic structures, previously defined by regional analysis, using an extensive database of seismic profiles provided by ENI E&P for hydrocarbon explorations, and calibrated by several deep boreholes (Livio et al., 2009). Along the Capriano del Colle Fault System (CPCFS), the small isolated hill of Monte Netto has been identified as its structural culmination, representing the topographic expression of the structural relief of the underlying growing Quaternary structures (e.g., Desio, 1965; Livio et al., 2009). Here, in the *Danesi* clay quarry at the top of the hill, a highly deformed fluvial and fluvioglacial deposits, underneath a 2 to 4 m thick loess/paleosols sequence, has been identified (Livio et al., 2014; Zerboni et al., 2015). The structural analysis of this outcropping sequence, together with OSL/radiocarbon age and pedostratigraphic constraints on the exposed loess layers, allow to unravel the growth history of a secondary fault-related fold, linked to the blind CPCFS backthrust. One of the main outcome of this investigation was that the formation of the exceptional thick loess deposit compared to other occurrences at the margin of the Po Plain, generally limited to a few tens of centimetres up to 1 m (for more details see Cremaschi, 1987; 1990) was favoured by the presence of a tectonically-controlled topographic obstacle. The continuous growth of the anticline that displaced geological strata at the top of the hill strengthened the role played by the hill as a local sediment trap for aeolian silt, allowing the existence of a depositional sink for most of the Upper Pleistocene (Zerboni et al., 2015). This positive interaction between the tectonically induced surface deformation and the aeolian deposition, suggests that loess/paleosols sequence can be particularly promising as stratigraphic marker, suitable to record tectonically induced near-surface deformation and earthquake surface faulting.

From this study, moreover, arose the idea that micropedology could help deciphering more tectonic events than the ones identified at macroscopic scale. Indeed, a thin section sampled in a system of

subvertical fractures, showed planar voids filled by a clay-rich plasma, displaying different generations of clay infillings characterized by different colours and textures. These differences indicated several infillings, whose formation required a multistep process of fissures opening and infilling by pedogenetic clay: these events have been interpreted as related to subsequent coseismic movements (Livio et al., 2014).

Due to the success of this kind of investigation, I decided to demonstrate the hypothesis of loess as stratigraphic marker able to record paleoseismological information at each scale, in an area where the loess covers and landforms of tectonic origin are well expressed, but historical evidence of strong earthquakes producing surface faulting, such as the 1222 Brescia event, are missing. The Monferrato area, located in the W Po Plain foreland basin, represent the ideal setting. The map in Fig. 5 shows for this area a dense distribution of loess deposits. Their preservation is mainly due to the westward decreasing of the Quaternary to ongoing sedimentation/erosion rate, but it is also promoted by morphotectonic structures, such as the ones cited above, that acted as sedimentary trap for wind-blown sediments. Most of the landforms characterizing this area take origin from tectonic activity, closely related to the recent evolution of the westernmost of 3 major structural fronts characterizing the Po Foreland Basin. Therefore, this setting become particularly suitable for applying the same investigation approach used at Monte Netto. Indeed, several field surveys allowed to identify three significative sites: Solero, Rivarone and Pecetto di Valenza.

The first two ones, present well-preserved loess/paleosols sequences, whose OSL/TT-OSL dating and pedostratigraphical analysis allowed to decipher the uplift rates of the fluvial terraces in which they are located (paragraphs 3.1; 3.2).

The Pecetto di Valenza site present a complex pedosedimentary sequence with two loess covers at its top, and it is also affected by a recent paleoseismic reverse surface faulting. Here I had the opportunity to document the first evidence of repeated Late Quaternary coseismic surface rupture in this sector of the Po Plain. I integrated pedosedimentary data, structural analysis, OSL/TT-OSL/radiocarbon dating, allowing to reconstruct the recent paleoenvironmental evolution and the deformation history of this site (paragraph 3.3; Frigerio et al., 2017). The data obtained confirm the preservation of the structural features thanks to the local geomorphic and geological setting, where, also here, the aeolian sedimentation recorded a positive feedback with the tectonically induced surface deformation. In particular, the micropedological approach, as highlighted in the case of the Monte Netto site (Livio et al., 2014), played a key role into the paleoseismological reconstruction: the identification of peculiar pedofeatures, help to decipher two of the major stages in the sequence of tectonic events.

As illustrated above, due to the importance of the information that is possible to take from the application of this approach, I decided to investigate the potentiality of micropedology of soil thin sections if integrated into the paleoseismological practice. For this purpose, I started to outline in a separate paper (in preparation) the guidelines for the use of this original approach. I intend to a) define the ideal setting of applicability of such approach; b) define diagnostic criteria useful to identify crosscutting relationship recorded into pedofeatures, microstructure and micromass, in order to help recognizing the number of events and their chronology; c) present a collection of microphotographs, showing typical microfeatures interpreted as the results of the interplay between soil forming processes and tectonic activity, intended as a first step toward the creation of an atlas of "seismopedofeatures" in thin section.

About this issue, preliminary outcomes will be presented in paragraph 5.3.2. The most meaningful microphotographs shown, come from a new outcrop exposed at Monte Netto during the 2016 excavations. Along this wall, a thrust fault zone, cutting through a fluvial and overlying syn-growth loess-paleosols sequence, has been finally revealed confirming the previous work of Livio et al., 2014, where the surface folding observed, was interpreted as the fault-propagation fold of a near-surface thrust. Therefore, this new outcrop offered the opportunity to investigate its fault geometry and characteristics through the paleoseismological approach integrated with the micropedological one, successfully applied at the Pecetto di Valenza site. The preliminary pedostratigraphic and micropedologic results useful to reconstruct the deformation history of this new outcrop will be presented in paragraph 4.2. Moreover, these data will be used in a paper (Livio et al., in preparation), where the kinematic retrodeformation of the main fault plane and associated fold, points out that underlying stratigraphy can significantly change the potential of surface faulting form an upward propagation fault.

The strategy above illustrated constitutes the guideline of this research project, that, therefore, is outlined as follows. Chapter 2 presents all the methods applied into this study, that constitute an innovative integrated paleoseismological approach. Chapter 3 and 4 described the results obtained from the application of the integrated paleoseismological approach, respectively at Monte Netto and Pecetto di Valenza, that will be discuss in chapter 5. Finally, in chapter 6 the main conclusions are presented.

1.4 Goals

The framework presented in the previous paragraphs highlights that the main goals of this research project are:

1. Demonstrate the potentiality of loess/paleosols sequence, preserved in setting controlled by active compressional tectonics, as valuable stratigraphic marker suitable to record tectonic evidence useful to reconstruct the paleoseismological evolution of an area.
2. Provide robust radiometric constraints, through the Optical Stimulated Luminescence (OSL) and the Thermally Transferred-OSL (TT-OSL) methods, to the loess/paleosols sequences identified in this research study. The geochronological characterization of the Monferrato area, constitutes a novelty, since all the studies performed till today are based on relative dating.
3. Demonstrate how the micromorphology of soil thin sections can be a useful tool to fill, or at least reduce, the incompleteness of the paleoseismic record, through the identification at microscopic scale of paleoseismic evidence that can provide new or additional constraints to the paleoseismological reconstruction.
4. Define an innovative paleoseismological approach integrating pedostratigraphy/micropedology, radiometric dating (OSL/TT-OSL and AMS-14C) and structural analysis able to provide a correct reconstruction of the recent landscape evolution, and, in particular, important clues to define the number, the magnitude, the recurrence interval of paleoearthquakes, and, therefore, relevant implications for the seismic hazard assessment.

2. Approach and methodology

In this chapter I present all the methodology applied in the framework of this work. Their integration into the traditional paleoseismological practice, gives rise to an innovative approach able to provide useful information that can detail the paleoseismological evolution of o site.

2.1 Literature data mining

The field reconnaissance strategy, aimed to identify evidence of active tectonics suitable for paleoseismological analysis, has been set up following the available literature.

The study of the Po Plain from a paleoseismological point of view has been correctly sketched out almost 40 years ago, in the framework of the Italian Nuclear Program and the related "Progetto Finalizzato Geodinamica", leaded by CNR (National Research Council of Italy) (e.g., Bigi et al., 1990; CNR, 1992; Serva, 1990). The main purpose of these investigation was to assess the seismic potential of this area, in the light of a possible nuclear power-plant siting. Since then, however, while the active tectonics of the eastern southern Alps (e.g., Benedetti et al., 2000; Galadini et al., 2005; Burrato et al., 2008; Poli et al., 2008), the Apennine margin of the Po Plain (e.g., Benedetti et al., 2003; Boccaletti and Martelli, 2004; Scrocca et al., 2007; Toscani et al., 2009; Boccaletti et al., 2011), and the central Soutehr Alps piedmont belt (Livio et al., 2009; Galadini et al., 2012; Berlusconi et al., 2013; Livio et al., 2014) have been carefully reconsidered, no systematic detailed studies have been performed in the region W of the longitude of Brescia. Bonadeo (2014) faced this issue collecting all the literature produced during 80's, that, since then, has not been updated. The analysis of geological, geomorphological, geophysical and seismological data available from the scientific literature and from private and public database integrated with field analysis conducted in the central sector of the western Po Plain, allowed to provide a new regional seismotectonic models for this area. Such model constituted the background for the investigation presented in Frigerio et al., 2017: the field reconnaissance along the thrust crossing the Alessandria plain to the North, identified by Bonadeo (2014) as a structure able to produce surface faulting, allowed to identify the Pecetto di Valenza site.

In the framework of this project, the revision of the existing literature included the following points.

- Analysis of the ITHACA catalogue (Italy Hazard from Capable faults; ISPRA, http://sgi.isprambiente.it/geoportal/catalog/content/project/ithaca.page) and DISS 3 database (Database of Individual Seismogenic Sources, Versione 3.2.0; DISS Working Group, 2015): Quaternary fault and seismogenetic structures database in which the potential sources of Mw > 5.5 earthquakes are mapped.

- Analysis of the lithostratigraphic, structural and neotectonic setting: CNR, 1980; 1982; 1983; 1987; 1990; Mosca, 2006; Mosca et al., 2009; Irace et al., 2009; Piana et al., 2017.
- Analysis of the Quaternary deposits: Carta Geologica d'Italia 1:50.000 (CARG project), 1:100.000; Foglio Geologico n. 156 "Torino Est" (Festa et al., 2009a; 2009b) and n. 157 "Trino" (Dela Pierre et al., 2003a; 2003b).
- Analysis of subsurface data from:
    - Banca Dati Geotecnica di Arpa Piemonte (https://www.arpa.piemonte.gov.it/approfondimenti/temi-ambientali/geologia-e-dissesto/bancadatiged/banca-dati-geotecnica): boreholes stratigraphy and geotechnical investigations for the characterization of Quaternary deposits.
    - VIDEPI project (UNIMIG; http://unmig.sviluppoeconomico.gov.it/videpi): seismic profiles for hydrocarbon exploration.
    - ENEL, 1984a; 1984b: investigations performed by ENEL in the framework of the project aimed to the nuclear power-plant siting of PO1 and PO2 sites. The documentation has been made available courtesy by SOGIN (https://sogin.it), a Company in charge for the management of nuclear wastes and decommissioning of abandoned nuclear sites.
- Analysis of the morpho-topographic elements through 10m DEM, extracted from the Regione Piemonte topo maps (CTR, 1:10.000 scale) and from aerial photos.
- Analysis of the historical and instrumental seismicity catalogues:
    - CPTI15 Catalogue (Catalogo Parametrico dei Terremoti Italiani; Rovida et al., 2016) from the year 1000 to 2014;
    - CSI catalogue (Catalogo della Sismicità Italiana; Castello et al., 2006): instrumental events in the period 1981-2002.

2.2 Logging and soil profiles field description

Excavation of trenches in deformation zones or identification of natural displaced outcrops represents the starting point for paleoseismic studies. Before a trench or an outcrop can be logged, must be cleaned well enough to expose the structures, stratigraphy and soil horizons. After that, a 1m or 2m-spaced reference net is constructed. Pedostratigraphic levels (*sensu* Costantini and Priori, 2007), which indicate sets of horizons formed from parent materials having the same origin and age deposition are identified, logged and fully digitalized. Log horizon and the crosscut relationships with structural features are carefully considered and digitalized in order to chronologically constrain the relative age

and progressive deformation affecting the studied outcrop (McCalpin, 2009; Livio et al., 2009, 2014; Zerboni et al., 2015).

Field descriptions and horizon designations are made following the internationally accepted guidelines (FAO, 2006). The B horizons of the buried paleosols of the sequence were defined in the international classification systems (James et al., 1998; WRB, 2006; Soil Survey Staff, 2010; Zerboni et al., 2011, 2015).

For each horizon, the following field properties are reported:

- textural class of the fine earth fraction
- colour (according to Munsell Soil Color Charts: Munsell® Color, 1994)
- size, shape and resistance of aggregates
- size and frequency of pores and roots
- thickness and boundary depth (with distinctness and topography)
- possible presence of pedofeatures (clay coatings, nodules, mottles, etc.)

2.3 Grain size analysis

For sedimentiological analyses we collected a homogeneous and representative sample, variable in weight between 0.5 and 1 kg; sample were collected every 15-20 cm in order to highlight any differences invisible to the naked eye (Ministero per le Politiche Agricole, 1999). Sampling was always performed from the bottom to the top of the pedostratigraphic sequence in order to avoid pollution of the lower horizons (Cremaschi and Rodolfi, 1991; Giordano, 1999)

The particle size distribution of a soil is the distribution of its mineral particles into size classes. It is a fundamental property on which depend many other chemical and physical properties of soils, and its determination is the basis of a correct classification of a soil (Ministero per le Politiche Agricole, 1999). Knowing the particle size, it is then possible to derive the texture of the sample, i.e. the proportion of the constituents of the earth end of the soil, grouped into size classes (McRae, 1991). Grain size analysis is performed with both sieving and the aerometer method.

2.3.1 Sieving and aerometer method

For particle size analysis, it was used the fine earth fraction in quantities of about 100 g. The portion to be subjected to analysis was obtained by one or more subsequent quartering, so arranged that the sub-sample was representative of the original sample. The obtained fraction was weighed and then pre-treated with hydrogen peroxide (H_2O_2, 130 volumes) in order to destroy organic matter, which, by favouring aggregate formation, interferes with the analysis. Each sample was then analysed using two

distinct methodologies applied to different granulometric fractions: the distribution of sand (particles of diameter varying between 2 mm and 63 µm) was determined by sieving, the distribution of silt (particles of diameter varying 63 and 2 µm) was determined by the aerometer method (Gale and Hoare, 1991; ASTM D 422). Sand sieving was conducted on wet samples, using a column of 6 mesh sieves with decreasing values (2000, 850, 500, 250, 150 and 63 µm) under a constant stream of water to favour particle passage through the sieve. The sieves were then dried and weighed in order to obtain the amount of sand fraction for every class. The fraction of the sample passing through the 63 µm sieve was collected in water tanks and left to settle for at least 24 hours; the volume of water has been progressively reduced by siphoning to obtain a total volume smaller than 1000 ml. The material thus obtained was analysed by aerometry with the aerometer method, into columns of 1 l volume after treatment with calgon (i.e. 3 g of sodium hexametaphosphate for each column). The aerometric analysis exploits Stokes law according to which settling velocity of a particle is proportional to its size. Density of the suspension thus tends to decrease with the passage of time and its variation depends on the size of the particles contained in the column. The measurement of density and temperature at standard intervals over 24 hours allows therefore to establish the amount of silt present in the sample. The data obtained by sieving and aerometry are then unified into frequency cumulative curves that allow an effective visualisation of the distribution of the constituents of the soil into dimensional classes.

2.3.2 Laser diffraction

Measurement procedure, using Malvern MS-2000 laser diffraction analyser, included: hand sieving and separation of the < 2 mm size fraction, dissolving of organic matter in 8% H_2O_2 for 3 days, stirring for 5 min in 40 ml of distilled water with 3 drops of sodium hexametaphosphate, and ultrasonication for 30 s. Three replicates of each sample were then subjected to 3 consecutive runs at a pump speed of 1850 RPM. The laser diffraction raw data was transformed into Particle Size Distributions (PSD) using Mie scattering model, with optical parameters of RI = 0.52 and A = 0.1 (Eshel et al., 2004). The data were also converted to the broad categories of gravels (> 2 mm), sand (0.063–2 mm), and fines (< 0.063 mm).

2.4 Micropedological analysis of soil thin sections

The sampling for the micropedological soil thin section has been performed through the use of Kubiena boxes, which allowed to take samples of undisturbed soil. Kubiena boxes are appropriate metal containers with removable lid and bottom which allow to extract and transport undisturbed soil samples; they are inserted in the profile and once extracted retain inside them a prism of undisturbed

soil. On each Kubiena box was reported the original orientation of the sample, information needed in order to properly interpret the information derived from the observation of the corresponding thin section (Kubiena, 1953; Stoops, 2003).

The undisturbed samples were then sent to an external laboratory for thin section preparation according to the standard method described in Murphy (1986). An initial drying for the total water removal is followed by the impregnation in epoxy resins (polystyrene); after a variable period of duration of some weeks, necessary for allowing the resin to harden, the sample was cut and polished, to obtain a thin section about 20-30 μm thick. The sections were then observed under a petrographic microscope (Olympus BX41), al parallel (PPL), cross-polarised (XPL) and oblique incident light (OIL), using different objectives with magnification of 2, 10, 20 and 40x. Sections were described according to the terminology of Bullock et al. (1985) and Stoops (2003), whereas some concepts of Brewer (1964) were also taken into account. The interpretation of thin sections was performed according Stoops et al. (2010). For each section has been described:

• Microstructure and porosity: type of microstructure, aggregate size and shape, void type, abundance, spatial arrangement, shape and size.

• Groundmass: c/f limit, ratio and relative distribution; nature, degree of weathering, size and frequency of coarse mineral and organic constituents; nature, colour, limpidity, interference colours and b-fabric of the micromass.

• Soil pedofeaures: nature, size, shape, variability, abundance and spatial arrangement of the different figures soil.

2.5 Radiometric dating

2.5.1 AMS-^{14}C dating

Analyses performed by BETA Analytic only on the samples from Pecetto di Valenza site. Calib 7.0 software (Stuiver et al., 2013) and the INTCAL13 curve (Reimer et al., 2013) were used for AMS-^{14}C ages calibration (2σ range).

2.5.2 OSL/TT-OSL dating

The Optically Stimulated Luminescence (OSL) and Thermally Transferred – OSL (TT-OSL) dating methods are the main radiometric dating techniques adopted in this project. I had the opportunity to attend the luminescence dating laboratory at Geological Survey of Israel, and, under the supervision of Dt. Naomi Porat, to date all the samples collected in the framework of this research project.

2.5.2.1 Principles of OSL dating

The use of optically stimulated luminescence (OSL) for dating sediments was firstly proposed by Huntley et al. (1985). The OSL signal acquired during the previous burial period is reset (bleached) by sunlight during sediment transport prior to deposition. Quartz or feldspar minerals are commonly used for OSL dating of sediments, but where available, quartz is the preferred dosimeter because the physical basis of OSL production is better understood and the quartz signal is more rapidly bleached in nature (Preusser et al., 2009). Hence, in this research, all measurements are made using the OSL signal from quartz.

The natural OSL signal of mineral grains builds up once sediment is buried and no longer exposed to sunlight. Since that moment, the sediment starts to interact with the radiation from uranium (U), thorium (Th), potassium (K) and cosmic rays. At sub-atomic level, the total amount of radiation interacting with the crystal (ionization), provides energy to electron to rise from the valence band, to the conduction band, leaving "holes" in the valence band. From here, electrons become trapped at defects sites and remain for a period of time: the deeper the trap below the conduction band, the more stable the electron and the longer it stays trapped (i.e., trap depth). When the crystal is stimulated by heat or by exposure to light, the electrons from this trap recombine with holes at luminescence centres and emit a photon of light: the luminescence signal (Aitken, 1990). The amount of light emitted is proportional to the number of trapped electrons, and hence is related to the total amount of energy received from irradiation. The process of stimulation and eviction of the electrons, i.e., signal bleaching, is achieved with stimulation by heat or light resulting in a thermoluminescence (TL) or OSL signal respectively. If the grain is stimulated sufficiently to evict all the trapped electrons, it is described as being fully bleached. OSL is generally very much more rapidly reset than TL (Godfrey-Smith et al., 1998) thus making it more suitable for dating sediments where the bleaching occurs

The radiation to which a grain is exposed during burial derives from a number of different sources, and consists of alpha and beta particles, and gamma rays. Quartz grains contain very little internal radioactivity, so the majority of the radiation they receive is derived from U, Th, K contained within the surrounding sediment, as well as a small level of cosmic radiation.

The radiation flux at a sampling location is termed the dose rate, and can be obtained either by field or by geochemical laboratory measurements; in the case of this project, the latter have been carried out.

The amount of radiation that a grain has received during burial can be determined by measuring the OSL signal from the natural dose (i.e. that received during burial), and the OSL signals from a series of laboratory irradiations of known dose. These laboratory measurements are used to calibrate the OSL

signal derived from the natural dose, and thus determine the laboratory dose that is equivalent to the dose received by the grains in nature; this is termed the equivalent dose (D_e). The SI (Système International) unit of absorbed radiation is the Gray (Gy): one Gray is equivalent to one joule of energy being deposited in each kilogramme of a sample. Since the OSL signal is bleached on exposure to light during sediment transport, the D_e normally represents the amount of radiation received following deposition and burial after the last transport event. The development of a measurement protocol, the single-aliquot regenerated-dose protocol (SAR; Murray and Wintle, 2000; see paragraph 2.5.2.4) has made possible to rapidly measure a number of the D_e values for a sample, with each D_e value being calculated from a single aliquot (i.e., sub sample) allowing to obtain a dataset of De values.

By deriving the equivalent dose of a sample from the D_e dataset, and the environmental dose rate at the sampling location, the age of a sample can be found using this equation:

$$\text{Age (years)} = \frac{\text{Equivalent Dose } (D_e) \text{ (Gy)}}{\text{Dose Rate (Gy/year)}}$$

2.5.2.2 Sampling

More than one samples were collected from each loess/paleosols sequence presented in this project. To prevent any exposure to sunlight, samples were collected by hammering iron tube into the exposed sections; where sediments were highly indurated, the samples were taken as blocks, wrapped in opaque black plastic for transport to the laboratory. The innermost material was extracted from the tubes under weak orange-red light at the luminescence dating laboratory of GSI. The outer surfaces of the blocks, which had been exposed to daylight during sampling, were removed in the laboratory and the resulting sub samples prepared for OSL measurements. A complementary sediment sample for dose rate measurements was collected from each sampling point.

2.5.2.3 OSL sample preparation

I prepared the samples provided for OSL analysis under an appropriate low-level orange lighting, which did not affect the OSL signal.

Very fine quartz sand (90-125 or 75-125 μm) was extracted for OSL dating using routine laboratory procedures (Porat, 2007; Davidovich et al., 2012). After wet sieving for the selected grain size, carbonates were dissolved with 10% HCl solution. The rinsed and dried sample was passed through a LB-1 Frantz magnetic separator, using a current of 1.4 A on the magnet, to remove heavy minerals and most feldspars (Porat, 2006). Etching in concentrated (40%) HF for 40 minutes removed any remaining feldspars and the outer 20 μm of the individual quartz grains, followed by soaking in 16% HCl overnight,

to dissolve any fluorides which may have precipitated (Porat et al., 2015). The purified quartz was placed on 9.8 mm aluminium discs (aliquots) using 2 mm masks and silicon spray as an adhesive (~200 grains for each aliquots).

2.5.2.4 OSL analysis

2.5.2.4.1 Equipment used

All luminescence measurements were undertaken using TL/OSL DA-12 or DA-20 Risø readers (Bøtter-Jensen and Murray, 1999), equipped with blue LEDs (Thomsen et al., 2006). Irradiation was by a calibrated 90Srβ source and the luminescence signal was detected through 7 mm U-340 filters.

2.5.2.4.2 Measurement of D_e: the SAR protocol

The single-aliquot regenerative-dose (SAR) protocol (Murray and Wintle, 2000) allows the determination of multiple D_e estimates by analysis of the OSL signals from individual aliquots, with each aliquot potentially giving rise to an estimate of D_e.

The standard SAR procedure proposed by Murray and Wintle (2000) that I applicated is reported in table 1:

Steps	Treatment	Signal
1	Preheat (160 – 300°C) for 10s	
2	OSL stimulation at 125°C for 40s	L_n
3	Test dose beta irradiation	
4	Cut-heat to 160°C for 0s	
5	OSL stimulation at 125°C for 40s	T_n
6	Beta irradiation of regeneration dose ($D_{1\text{-}n}$)	
7	Preheat (160 – 300°C) for 10s	
8	OSL stimulation at 125°C for 40s	L_x
9	Test dose beta irradiation	
10	Cut-heat to 160°C for 0s	
11	OSL stimulation at 125°C for 40s	T_x
12	Repeat steps 6 – 11 with further regeneration doses	

Table 1: Single aliquot regeneration sequence (Murray and Wintle, 2000). The growth of the signal with dose is characterised by administering a number of laboratory doses (regeneration doses) of different sizes and measuring the resulting OSL signals L_1, L_2, etc. After each measurement the luminescence sensitivity is measured by giving a fixed dose and measuring the resulting OSL signal (T_1, T_2, etc).The effect of changes in sensitivity can be corrected for by taking the ratio of the luminescence signal (L_x) to the response to the fixed dose (T_x).The plot of the sensitivity-corrected OSL (L_x/T_x) as a function of the laboratory dose (bottom) can be used to calculate D_e for that aliquot when the ratio of the initial measurements on the natural sample (L_n/T_n) is projected onto the dose response curve.

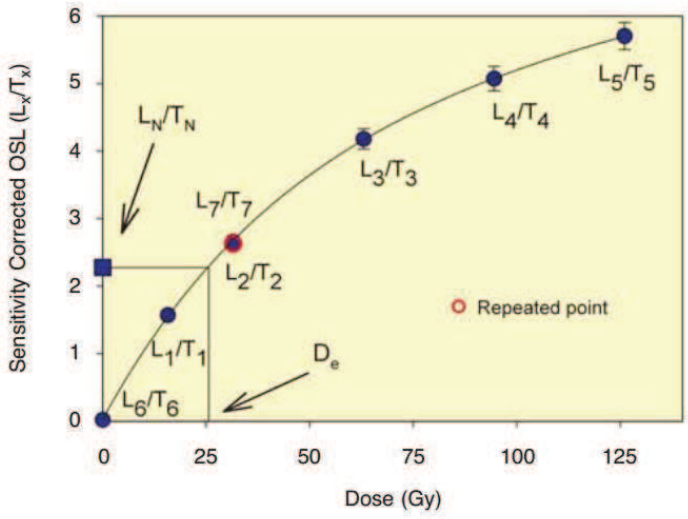

Fig. 6: Typical SAR dose response curve for a quartz aliquot (from Kalambo Falls, Zambia). Modified after Duller (2008).

Before each luminescence measurements, the aliquot is heated between 160-300° C for 10 seconds. The purpose of the preheat stage is to remove thermally unstable charge from optically-sensitive traps, so that the OSL signal comes only from electrons that would have been stored safely through the burial period. Prior to measurement of the test dose OSL, a cut-heat is administered. This is normally held for 0 s, and performed at a lower temperature than the preheat, to minimise any temperature-induced sensitivity change associated with this thermal treatment.

The more suitable preheat temperatures are selected according to dose recovery tests (Wintle and Murray, 2006) over a range of temperatures carried out on selected samples from each site. This test involves removing the trapped electron population from the sample, thus mimicking the resetting of the sample at the time of the event being dated.

This involves exposing 12 aliquots of the younger sample for each site, to daylight. Then, the aliquots are irradiated with a known dose, which should be of similar magnitude to the expected natural D_e: in this way, complications introduced as samples become close to saturation at high dose values, are assessed implicitly.

The 'known' dose is then treated as unknown and the conventional SAR protocol is applied to each aliquot in order to determine the given dose. The ratio of the measured dose (i.e. that found by construction of a growth curve) to the given dose should be one if the SAR procedure is working successfully. If a sample fails a dose recovery test, then it is unlikely that the D_e calculated for the sample will be correct.

Moreover, the dose recovery test is usually performed using a range of different preheat temperature. This experiment forces differing amounts of sensitivity change and is performed to assess whether the

D_e values remain consistent as the temperature changes; if not, one can select the most suitable preheat temperature for a given sample. The temperature range that gives consistent results for the D_e values is termed the preheat plateau (Murray and Wintle, 2000).

During the measurements of the 12 aliquots through the standard SAR procedure, two aliquots for each sample measured at various preheat temperature and cut-heat.

The SAR protocol has advantage to allow to make replicate measurements of D_e for each sample. Thus it is routinely possible to assess the reproducibility of D_e within each sample. Replicate determinations of D_e would be expected to form a normal or log-normal distribution. Averaging the replicate D_e measurements, should give an increase in the precision of the age calculated.

2.5.2.4.3 Measurement of dose rate

The radiation dose received by the sample each year comes from four types of environmental radiation: alpha particles (α), beta particles (β), gamma rays (γ) and cosmic rays. In the framework of this project, they are measured by ICP-MS (for U and Th) and ICP-AES (for K) at the Geochemistry Lab of the Geological Survey of Israel.

Note that the measurements are made on dried sub-samples. Water between mineral grains in the environment absorbs some of the radiation, meaning that only a proportion of the radiation emitted by U, Th and K is absorbed by mineral grains. The larger the amount of water, the less radiation is absorbed by minerals. Therefore, it's important to try to estimate the water content throughout the burial period. In this project, reasonable values have been obtained by measuring the modern-day water content, as the mass of water divided by the mass of dry sediment, multiplied by 100.

The cosmic dose rates are evaluated using the burial depth.

2.5.2.5 Limits of luminescence dating

2.5.2.5.1 Suitability of material

The quality of luminescence dating depends on these assumptions:

a) the sample contains grains that were completely bleached at deposition;
b) variations in the annual dose due to small-scale differences in the concentrations of uranium, thorium and potassium are small;
c) no post-depositional mixing has occurred.

As stated above, a way to assess the suitability of the material to the luminescence dating, is the possibility to make replicate measurements on sub-samples of the same material. If the mineral grains

were exposed to sufficient daylight to reset the OSL signal at deposition, the variation between aliquots must be very small.

If replicate measurements of De are not similar, the most common cause is that the trapped electron population in the different mineral grains of the sample was not completely reset during the event being dated. This is called incomplete bleaching. For example: when rivers transport sediments, mineral grains are moved through the surface environment and might be exposed to daylight more than once before their final deposition. This insufficient exposition to daylight leaves a residual population of trapped electron, for which the sample is incompletely bleached and the age will be overestimated.

This means that it is always important to consider the depositional context from which a sample has been collected when assessing the most likely cause of scatter in the distribution of De values.

2.5.2.5.2 Range of dating

Dating Quaternary sediments using the fast component of OSL signal become a well-established method (e.g., Murray and Olley, 2002; Duller, 2004; Rittenour, 2008; Madsen and Murray, 2009). The range of ages over which this signal can be used varies depending upon the dose rate experienced by the sediment during burial and the maximum dose that can be measured using the fast OSL component signal. The typical dose response curve for a single aliquot quartz dominated by the fast component OSL signal is reported in Fig. 7.

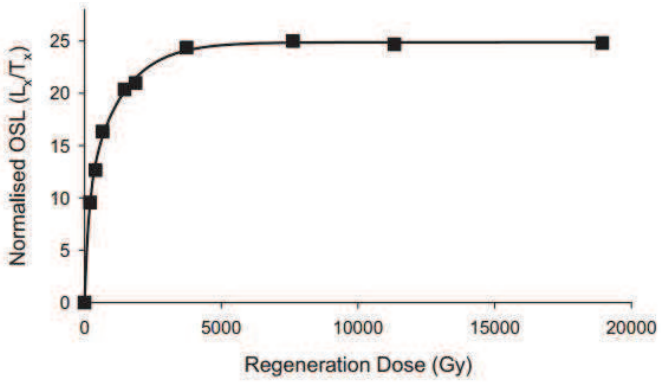

Fig. 7: Dose response curve obtained from a multiple aliquot regenerative dose procedure using OSL measurement on a sample of quartz. Modified after Duller and Wintle (2012).

While D_e values reported in literature typically fall in the range 55-110 Gy (Roberts and Duller, 2004; Jain et al., 2005), care must be taken when D_e is measured on a dose response curve comes to saturation. In such situation, the OSL signal increases as the size of the prior radiation dose increases. At first, this increase with dose is almost linear, but at some stage the traps within the crystal where electrons can be stored become full. As this happens, the luminescence signal grows more slowly, until

all the traps become full. After that the luminescence signal stops to increase despite the continuing exposure to radiation. This is known as saturation.

This saturation imposes an upper limit to luminescence dating and increases error in the De value, because as the dose response curve flattens, small uncertainties in the value of the natural signal being projected have a larger impact on De values. In addition, D_e is more difficult to assess, because of the impact of systematic uncertainties in the measurement of the dose response curve, thus ages obtained with De values close to the limit of saturation should be regarded with additional caution. Wintle and Murray (2006) suggest that it is only prudent to work in the range where the natural signal (L_N /T_N) is 85% or less of the maximum luminescence signal obtainable.

Nevertheless, a number of attempts have been made to obtain other luminescence signals from quartz with larger D_e values, trying to extend the OSL age range.

Wang et al., (2006a,b) described measurements of a Thermally Transferred Optically Stimulated Luminescence (TT-OSL) signal from quartz which continued to grow at doses of many thousands of Gray, long after the fast component OSL signal had become saturated. This TT-OSL signal exhibits growth to the highest dose and has the potential to extend the age range of luminescence dating by at least an order of magnitude (Fig. 8)

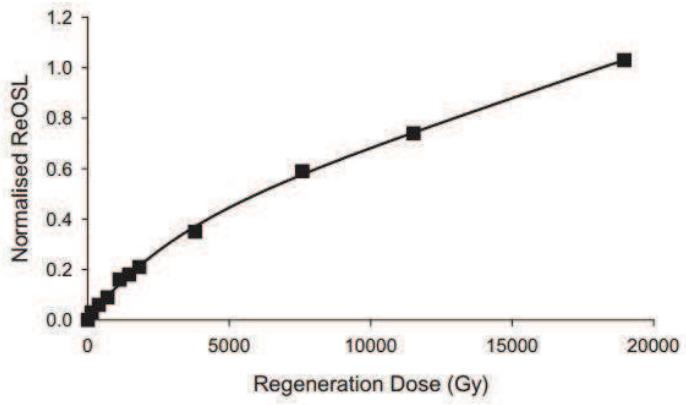

Fig. 8: Dose response curve obtained from a multiple aliquot regenerative dose precedure using TT-OSL measurements on a sample of quartz, substracting the BT-OSL component to give the recuperated OSL (ReOSL). Redrawn after Wang et al. (2006b) and Duller and Wintle (2012).

2.5.2.5.2.1 TT-OSL dating method

This method uses the thermal transfer to increase the OSL signal: heating the aliquot to higher and higher temperatures will progressively release charge from deeper traps to shallower sites, available for standard OSL extraction. Despite this insensitivity of the TT-OSL signal to light, some authors (Tsukamoto et al., 2008; Kim et al., 2009; Porat et al., 2009; Table 2) tried to assess the bleaching for its signal.

They measured the resetting of the TT-OSL signal exposing some sample to a solar simulator in the laboratory. They noticed that the TT-OSL signal decreased slowly to 10% of the signal remaining after exposure to the solar simulator for two weeks (Fig. 9. The fast component of the OSL signal would have been removed in a few seconds.

Sample	Environment	OSL D_e (Gy)	TT-OSL D_e (Gy)	Source
IEE208	Loess, China	3.6 ± 0.2	18.7 ± 1.2	Wang et al. (2006a)
IEE209	Loess, China	3.0 ± 0.4	10.0 ± 2.1	Wang et al. (2006a)
IEE210	Loess, China	4.3 ± 0.6	10.4 ± 2.4	Wang et al. (2006a)
DEK-1	Coastal dune, South Africa	0.74 ± 0.02	17.2 ± 0.8	Tsukamoto et al. (2008)
KR-17	Desert sand sheet, Israel	~0.2	~5	Porat et al. (2009)
CH04/2/3	Loess, China	1.1 ± 0.0	13.3 ± 2.5	Stevens et al. (2009)
DB_{Mod}	Beach sand, South Africa	Not given	15–30 Gy (TT-OSL) 40–50 Gy (BT-OSL)	Jacobs et al. (2011)
YSG-OSL02	Suspended sediment, Yellow River, China	1.6 ± 0.5	282 ± 38	Hu et al. (2010)
HYK-OSL03	Overbank deposits, Yellow River, China	2.7 ± 0.4	259 ± 108	Hu et al. (2010)

Table 2: Residual doses measured in young or modern sample using OSL and TT-OSL. Modified after Duller and Wintle (2012).

They also measured "modern" samples that have been exposed to daylight during natural depositional processes. Residual doses measured from this modern samples using the TT-OSL signal are reported in Table 2.2. Note that a) the residual D_e derived from TT-OSL measurements is larger than those from OSL; b) for aeolian sediment, the magnitude is not so large if compared with samples of fluvial origin (the two last samples in Table 2); c) the residual D_e values measured using TT-OSL are almost two orders of magnitude greater than the D_e values obtained using OSL on the same samples.

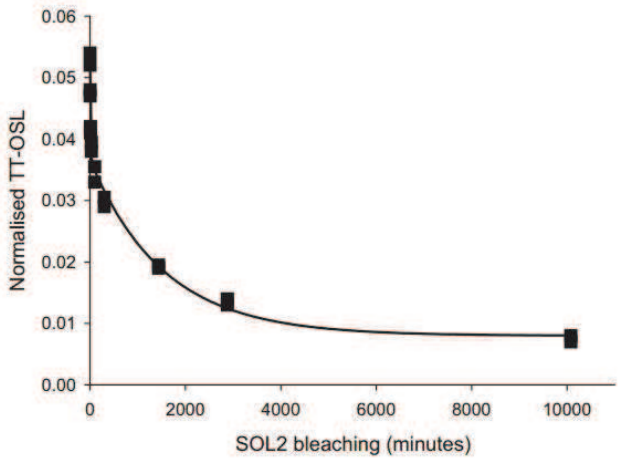

Fig. 9: Reduction of the TT-OSL signal after differnt duration to exposure to a solar stimulator. Redrawn from Kim et al (2009) and Duller and Wintle (2012).

Therefore, comparing the OSL residual D_e value with the TT-OSL one, it is clear that signal bleaching strongly depends on the depositional environment. Suspended sediments or overbank deposits coming from a fluvial environment show a high TT-OSL residual D_e value: for this reason the applicability of the TT-OSL dating method to such a setting is limited or results have to be carefully considered. Moreover, from Fig. 9 it is clear that much a longer light exposure is required to bleach the TT-OSL signal, compared to fast-component OSL (i.e., some weeks vs some seconds). Therefore, the

application of the TT-OSL method should be restricted to samples coming from stabilized environment, thus containing grains expected to have been well-bleached at deposition.

2.5.2.5.2.1.1 Measurements of TT-OSL signal

Wang et al (2006b) thought that the TT-OSL signal that they observed was composed of charge from two different sources: basic transfer (resulting in BT-OSL) and recuperation (resulting in ReOSL). BT-OSL is the thermally transferred signal that is due to charge originating in deep traps which is hard to remove optically. A large trapped charge population was supposed to exist in these traps and the amount of charge transferred will be the same in each cycle. In contrast, the ReOSL signal decreases exponentially

with the number of transfer cycles. Wang et al. (2006b) fitted their TT-OSL data with the sum of a constant (basic transfer) and an exponentially decreasing component (recuperation), and these are shown on Fig. 10.

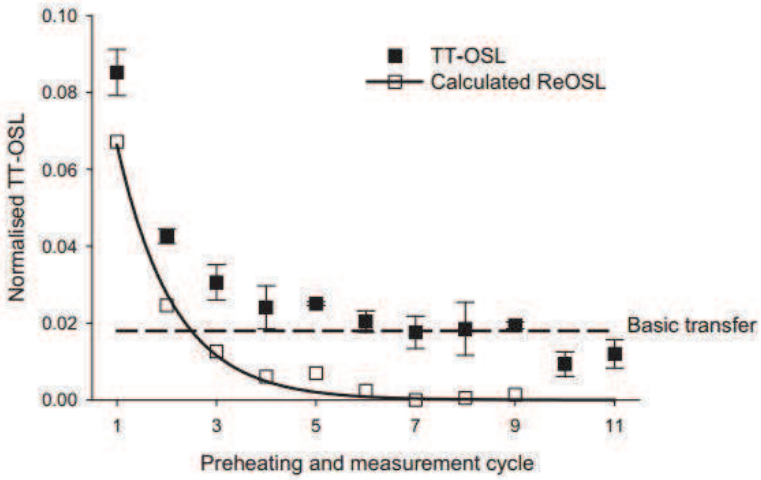

Fig. 10: The TT-OSL signal from an aliquot of quartz. The aliquot is heated at 260 °C for 10 s and the resulting TT-OSL signal is measured. This cycle of heating and TT-OSL measurement was repeated 11 times and the TT-OSL signal signal decreases each time. After 7 cycles the TT-OSL signal stabilises: this was interpreted by Wang et al., 2006b as BT-OSL. By substracting the BT-OSL signal, Wang et al., 2006b calculated the recuperated OSL (ReOSL) signal, which has been fitted with a single exponential decay function. Adapted from Wang et al., 2006b and after Duller and Wintle (2012).

Since the BT-OSL signal is light-insensitive, thermally stable, and independent of dose (Rhodes, 1988), it needs to be measured and subtracted from the TT-OSL signal to isolate the main component of the TT-OSL, ReOSL. It is the ReOSL that is used to construct the dose response curve to obtain De.

However, recently has been shown that the contribution of the BT-OSL signal as measured using the protocol presented was a very small portion of the TT-OSL and their study implied that it may not be necessary to make a separate measurement of the BT-OSL. Therefore Porat et al., 2009 developed a simplified TT-OSL protocol (Table 3) that I applied for the samples object of this study. Such a protocol

fulfils the main requirements of a SAR protocol, i.e. appropriate correction for sensitivity changes for each TT-OSL measurement and complete zeroing of ReOSL between cycles.

Steps	Treatment	Signal
1	Dose (natural or lab)	
2	Preheat at 200–260 °C for 10 s	
3	Blue stimulation at 125 °C for 300 s	
4	Preheat at 260 °C for 10 s	
5	Blue stimulation at 125 °C for 100 s;	$L_{TT\text{-}OSL}$
6	Give test dose, D_t	
7	Preheat at 220 °C for 10 s	
8	Blue stimulation at 125 °C for 100 s;	$T_{TT\text{-}OSL}$
9	Heat at 300 °C for 100 s	
10	Return to 1	

Table 3: Simplified TT-OSL SAR protocol from Porat et al. (2009).

Moreover, Porat et al. (2009) demonstrates for a preheat of 180 °C that the ReOSL is almost three times higher than that for a preheat of 260 °C. This suggests that it would be advantageous to use a lower temperature for the preheat in step 2, both to increase the magnitude of the TT-OSL signal and to reduce the relative contribution of the measured BT-OSL.

2.6 *Structural analysis*

Structural data were collected using an Android mobile equipped with the Fieldmove CLINO app by Midland Valley. FaultKin v.6 (Allmendinger et al., 2001) was used for kinematic analysis of fault dataset and TruDisp v.1.0.2 (Nieto-Fuentes et al., 2014) for true slip calculations from separation field measurements.

3. The Monferrato area

The Monferrato Arc is the westernmost of the 3 major structural fronts of the Po Foreland Basin, enclosing the most external thrust fronts of the northern Appenines (Fig. 11a,b; Pieri and Groppi, 1981). The tectonic activity of the Po Plain is closely related to the recent evolution of these structural belts, mainly buried in the Central and Eastern sector below the Plio-Pleistocene sedimentary infilling (Emilia and Ferrara Arcs; Fig. 11a), but emerging, or very shallow, in the West along the Monferrato Arc.

For the purpose of this project we conducted our field mapping along the eastern Monferrato Arc, that previous investigations indicated as a suitable area for paleoseismic analysis, due to the presence of uplifted terraces, isolated reliefs and tectonically induced drainage diversion (e.g., Michetti et al., 2012; Bonadeo, 2014; Giraudi, 2014; 2015; 2016). Indeed, we identified three key sites, Solero, Rivarone and Pecetto di Valenza (Fig. 11b,c), that will be illustrated in the following paragraphs.

The geological framework of the Monferrato Arc is illustrated in Fig. 11b,c. From the point of view of Cenozoic stratigraphy and evolution, the most important phase in the building of the N Apennines mountain belt, the Monferrato is the north-easternmost geo-structural domain of the Tertiary Piemonte Basin. It consists of a Oligocene to Messinian sedimentary succession of mainly terrigenous deposits, that unconformably overlies Cretaceous-Eocene Ligurian units (Fig. 11c; Dela Pierre et al., 2003a). The structural setting of the eastern Monferrato is mainly characterized by buried NE-verging thrust systems (Fig. 11c) and NW-SE trending open to tight folds. Since Early Miocene the Monferrato acted as a structural high between the Alessandria thrust-top Basin and the Po Foreland Basin (Falletti et al., 1995; Rossi et al., 2009; Irace et al., 2009). The evolution of this area was significantly controlled, to the North, by the activity of the most external buried structural front. During Pliocene and Pleistocene, this induced the further uplift of the Monferrato Oligocene-Miocene successions and their northward overthrusting onto the Plio-Quaternary stack of the Po Foreland Basin (Giraudi, 2014, 2015; Irace et al. 2015).

The Cretaceous-Eocene substratum is poorly exposed and crops out only within tectonic slices. The overlying succession, including also the Pliocene and Early Pleistocene, is made up of 8 major synthems (Fig. 11c), split by seven regional unconformities (Dela Pierre et al., 2003a, 2003b; Festa et al., 2009a, 2009b; Carta Geo Piemonte 250K).

The synthem 1 is introduced by Lower Oligocene fan-delta deposits that are followed by Oligocene-Lower Burdigalian slope fine-grained and silica-rich deposits. The synthems 2 and 3 consist of shelf deposits (the lower carbonate and the upper mixed) of Burdigalian to Langhian age. The synthem 4 is

made up of Tortonian hemipelagic sediments abruptly followed by the Messinian primary gypsum. The synthem 5 consists of resedimented gypsum units, followed by sandy-muddy deltaic to shelfal sediments included in the synthem 6 (Upper Messinian). The synthem 7 corresponds to the Pliocene transgressive-regressive succession represented by basin to outer shelf up to coastal plain alluvial sediments, which mark the onset of continental deposition. The Pliocene succession is succeeded by the coarse-grained fluvial deposits of the synthem 8 (Lower Pleistocene) representing the stratigraphic base of the Quaternary continental sedimentation in the Po Foreland and Alessandria basins.

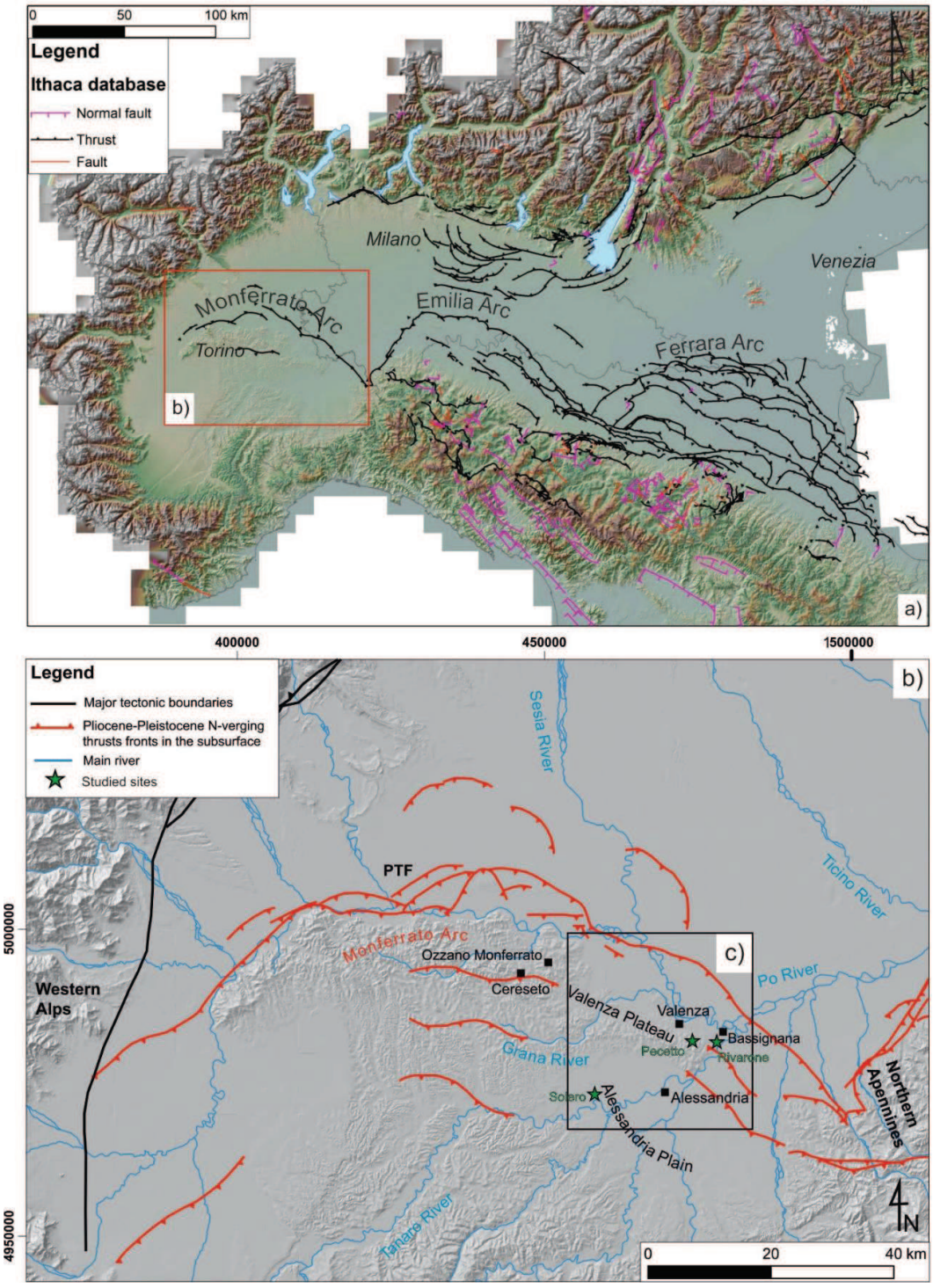

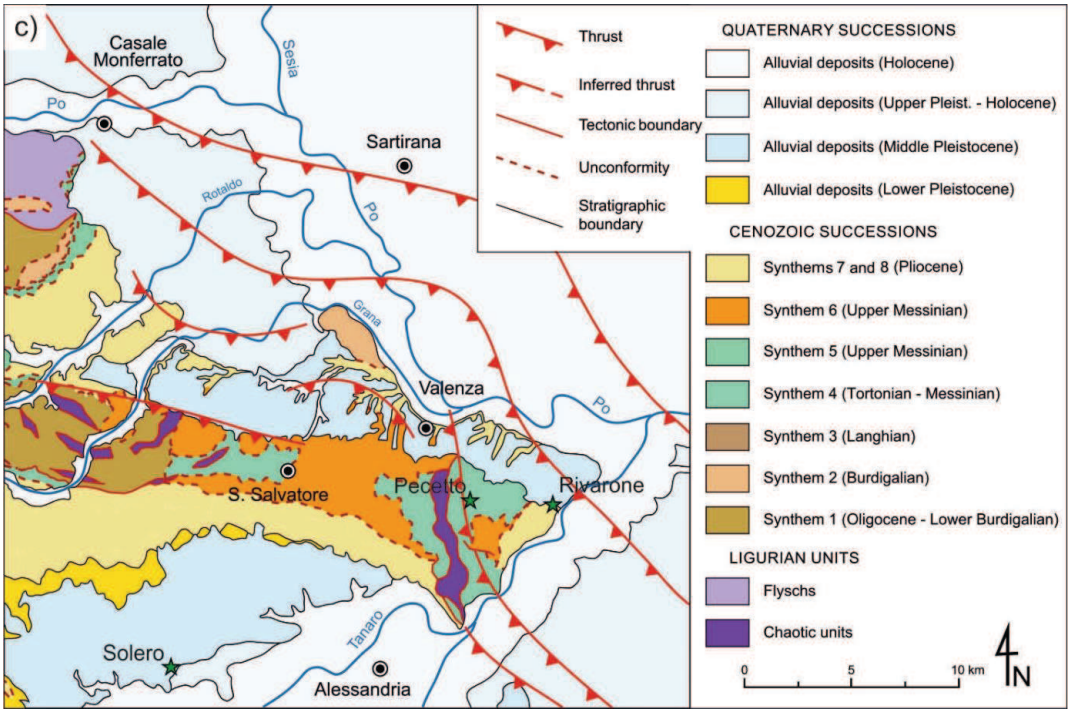

Fig. 11: Location map of the study area: a) structural setting of the Po Plain (from Ithaca database) highlighting the major frontal arc of the N Appenine. The red box locates the Monferrato arc, represented in b): simplified structural setting of the Monferrato Arc and W Po Plain (PTF: Padane Thrust Front). The black box represents c): geologic sketch of the E Monferrato Arc and adjoining Po alluvial plain (modified after Piana et al., 2017). Note that the loess covers are not mapped. The location of the studied sites is also shown. Modified after Frigerio et al., 2017

3.1 *Solero*

The Solero site is located on the Alessandria plateau, which is a terrace extending between the Monferrato Hills to the Tanaro River (Fig. 11c,b). This site is ca. 25 km far from the Rivarone site and ca. 20 km far from the Pecetto di Valenza one.

In correspondence of a quarry wall, a complex pedostratigraphic sequence up to 6 m thick has been identified. The description of the sequence has been divided in an uppermost and a lowermost part, as shown in Fig. 12. The entire sequence has also been sampled for luminescence dating and sedimentological analysis. The field descriptions, the results of the grain size analysis and the luminescence dating results are reported in the following paragraph.

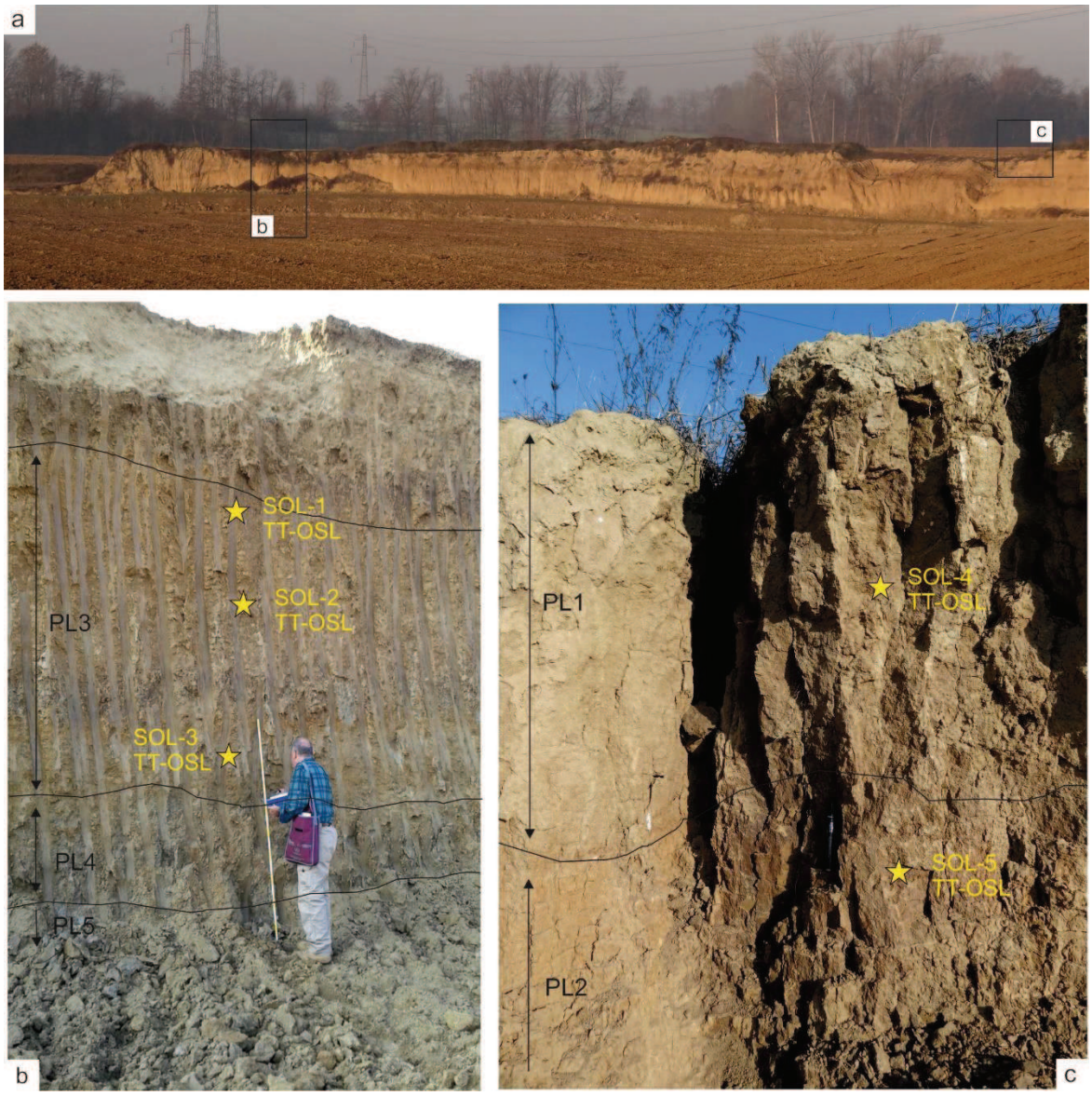

Fig. 12: General view of the Solero quarry; the black box locates the lower part (b) and upper part (c) of the outcrop. The position of the samples for TT-OSL dating and the results are indicated.

3.1.1 Soil profiles field description

The sequence exposed at the Solero site presents five pedostratigraphic levels (sensu Costantini and Priori, 2007) that, according to the field properties, show sets of horizons developed from parent materials having the same origin (Table 4). The parent material that identify the pedostratigraphic levels are loess (PL1) and fluvial materials (PL2, PL3, PL4 and PL5).

Horizon	Depth (cm)	Description	Pedostratigraphic level
Bt(x)	0-80	Silty clay; pale brown (10 YR 6/4); massive structure to weakly developed coarse platy structure; very firm; common medium and fine pores; common clay coatings; gradual lower boundary.	PL1
2Btc	80-130	Clayey silt; reddish brown (5 YR 4/3); massive to prismatic angular blocky structures; very firm; common medium and fine pores; common Fe-Mn and clay coatings on peds and voids; common Fe-Mn nodules; abrupt wavy lower boundary.	PL2
3Btc	130-150	Silty clay; dark yellowish brown (10 YR 4/6); massive; firm; common medium and fine pores; common clay coatings on voids; common Fe-Mn nodules decreasing toward the bottom; gradual lower boundary.	PL3
3Btg	150-210	Clay, slightly silty; yellowish brown (10 YR 5/8); frequent, medium brownish yellow (10 YR 6/8) mottles; massive structure to weakly developed prismatic structure; firm; common medium and fine pores; few fine Fe-Mn nodules decreasing toward the bottom; common clay coating on voids and peds; common hydromorphic mottles; gradual lower boundary.	PL3
3Bt1	210-255	Silty clay; yellowish brown (10YR 5/6); common, medium brownish yellow (10 YR 6/8) mottles; massive structure to weakly developed prismatic structure; firm; common medium and fine pores; common Fe-Mn and clay coatings on peds; few fine Fe-Mn nodules; clear lower boundary.	PL3
3Bg	255-340	Silty, slightly clayey; light red (2.5 YR 6/8); common, fine brownish yellow (10 YR 6/8) mottles; massive; firm; few medium and fine pores; medium to fine Fe-Mn nodules decreasing toward the bottom; very few clay coatings on voids; gradual lower boundary.	PL3
3Bcg	340-370	Silty, slightly clayey; light red (2.5 YR 6/8); massive; few medium and fine pores; medium to fine abundant Fe-Mn nodules; very few clay coatings on voids; common hydromorphic mottles; abrupt lower boundary.	PL3
3Bt2	370-390	Clay, slightly silty; light red (2.5 YR 6/8); massive; firm; common medium and fine pores; common clay coatings on voids and peds; few fine Fe-Mn nodules; gradual lower boundary.	PL3
3Bt3	390-415	Clayey silt; light red (2.5 YR 6/8); massive; firm; few medium and fine pores; common clay coatings on voids and peds; few fine Fe-Mn nodules; gradual lower boundary.	PL3
4Bcg	415-420	Silty, slightly clayey; light red (2.5 YR 6/8); massive; firm; few medium and fine pores; medium to fine abundant Fe-Mn nodules; very few clay coatings on voids; common hydromorphic mottles; abrupt lower boundary.	PL4
4Bt	420-440	Silty clay; brownish yellow (10 YR 6/6); common, fine light reddish brown (2.5 YR 6/3) mottles; massive; firm; common fine pores; very few and fine Fe-Mn nodules; abrupt lower boundary.	PL4
4BC	440-470	Fine sand; brownish yellow (10 YR 6/6); common, fine light reddish brown (2.5 YR 6/3) mottles; massive; firm; common fine pores; common Fe-Mn coatings on voids and peds; gradual lower boundary.	PL4
5BC	> 470	Clay; bluish gray (gley 2 6/1); frequent, medium brownish yellow (10 YR 6/8) mottles; massive; firm; few fine pores; common fine and medium Fe-Mn nodules; lower boundary not exposed	PL5

Table 4: Field properties of the Solero section.

PL1 consists of ca. 80 cm-thick silty-clay Bt(x) horizon, developed on an aeolian parent material, showing a moderate degree of weathering (common clay coatings). It presents a massive to platy structure, compact and pale brown colour, gradually passing downward to PL2. PL2 is represented by 2Btc horizon, constituted of clayey silt material, with a massive to prismatic angular blocky structure, including common Fe-Mn nodules and clay coatings. The boundary to the underlying PL3 is abrupt. The latter is represented by several yellowish brown to light red B horizons, rich in clay and developed on coarse silty materials. The high degree of clay illuviation is expressed in 3Btc, 3Btg, 3Bt1, 3Bt2 and 3Bt3 horizons, displaying common clay coating on voids and peds surfaces. Moreover, brownish yellow mottles and Fe-Mn nodules decreasing with depth, related to hydromorphic conditions, have been identified (3Btc, 3Btg, 3Bg and 3Bcg horizons). The boundary to the underlying PL4 is gradual. PL4 consists of 4Bcg, 4Bt, and 4BC horizons. These horizons are developed in a silty clay material passing downward to a fine sand material, showing an increasing degree of clay mobilization and accumulation of Fe-Mn nodules. Finally, the lowermost part of the sequence (pedostratigraphic level PL5) is developed in a massive bluish gray clayey material, probably deposited in a water body (decantation): in fact, hydromorphic pedofeatures (Fe-Mn coatings and nodules) are well expressed.

3.1.2 Grain size analysis

Grain size analysis (Fig. 13) were carried out on the Solero pedosedimentary sequence to characterize the fine earth (<2 mm) fraction, by sieving and aerometer method. One soil/sediment sample has been analysed for each horizon.

From the top to the base of the sequence, the cumulative grain size distribution curve of the pedostratigraphic level PL1 show a characteristic sigmoidal pattern, typical of loessic sediments. The curve is unimodal and well-sorted, with a strong positive skewness, where the sand and silt values are about 75%. In the pedostratigraphic level PL2, the sampled horizon shows completely different grain size distribution and poor sorting, with a moderate clay and sand content, respectively 40% and 15%. The third pedostratigraphic level PL3 shows well-sorted asymmetric (positive skewness) sigmoidal curves, but shifted toward the coarse fraction. Moreover, the clay content decrease toward the bottom of the PL, ranging from 30 % (3Bct horizon) to about 20 % (3Bt3 horizon). The PL4 pedostratigraphic level still shows unimodal and well-sorted asymmetric sigmoidal curves, but different sand values, ranging from 10% (4Bcg horizon) up to about 50% (4BC horizon). The lowermost pedostratigraphic level shows another different grain size distribution, poorly sorted and shifted toward the fine fractions.

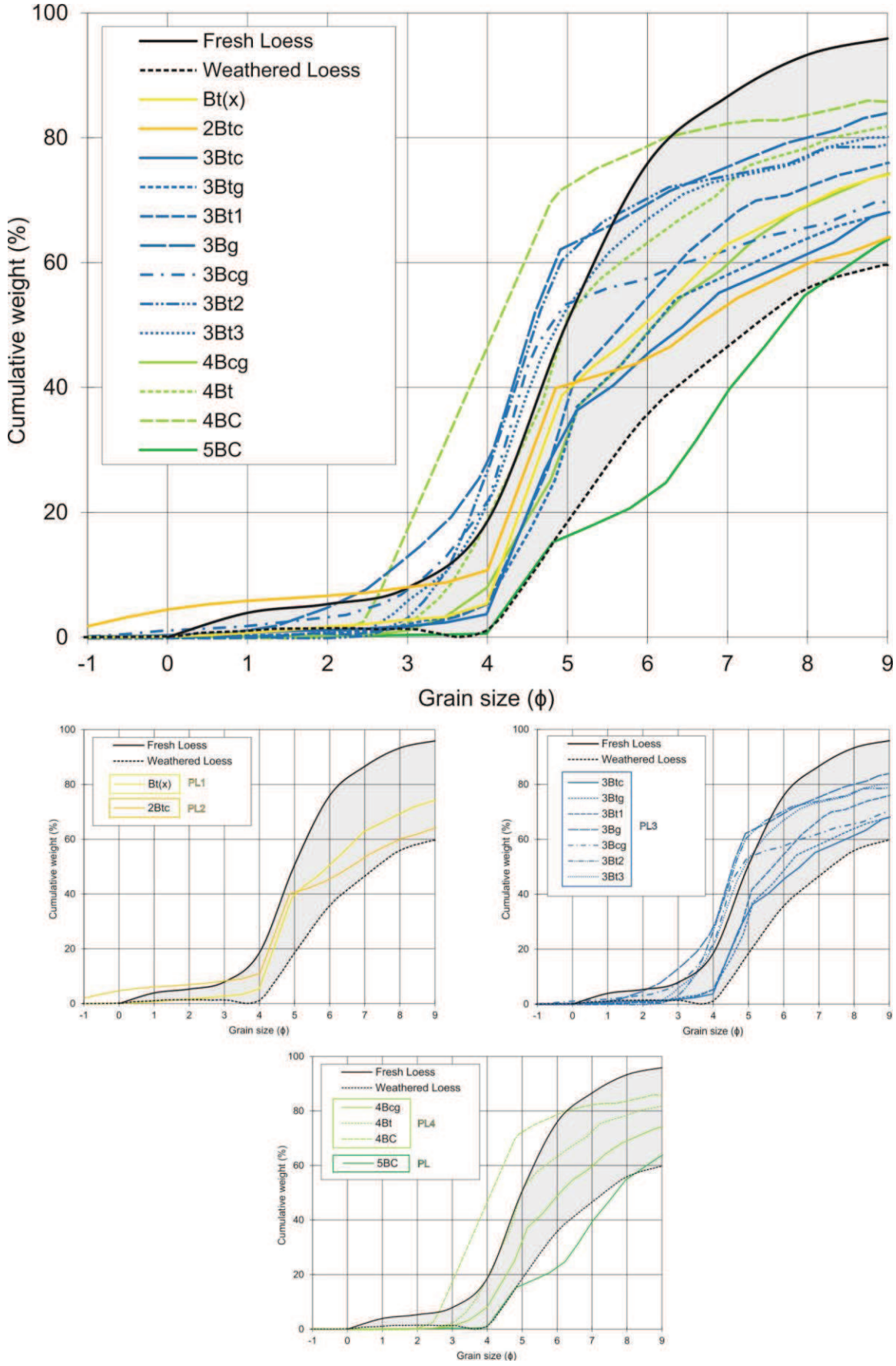

Fig. 13: Cumulative grain size curves for the pedostratigraphical levels compared to variability of grain size distribution in loess deposits in the PPLB according to Cremaschi (1987; 2004). The shadow area indicates the field of existence of loess.

3.1.3 TT-OSL dating

Sample	Burial Depth (m)	Soil horizon	Water contents (%)	K (%)	U (ppm)	Th (ppm)	Dose Rate (Gy/ka)	Aliquots	O-D	DE (Gy)	Age (ka)
SOL-4	0.30	Bt(x)	10	1.67	3.5	14.5	3.32 ± 0.13	10	15	253 ± 12	76 ± 5
SOL-5	1.05	2Btc	10	1.44	3.5	13.8	3.05 ± 0.12	10	19	485 ± 30	159 ± 12
SOL-1	1.15	3Btg	10	1.83	3.3	13.8	3.36 ± 0.11	8	15	546 ± 34	162 ± 11
SOL-2	2.35	3Bg	10	1.58	2.3	8	2.53 ± 0.08	8	15	545 ± 29	216 ± 13
SOL-3	3.2	3Bt3	10	1.83	2.3	9.7	2.83 ± 0.09	5	17	*1361 ± 252	*481 ± 90

*Table 5: TT-OSL data and ages for the Solero samples. The Central age model (CAM) was used to obtain representative De values, with standard errors propagated to the age errors; except for the sample indicated with * which De values has been calculated through the Unweighted model. No. of aliquots = the number of aliquots accepted for De determination out of those measured; OD = over dispersion.*

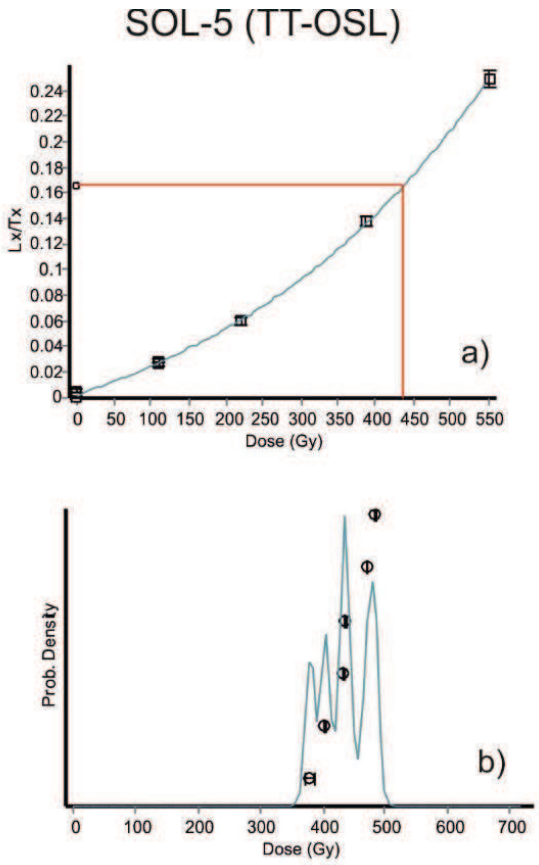

Fig. 14: a) dose response curve for sample SOL-5; b) a probability density function plot for the same sample, with individual De value and errors. A normal distribution with over-dispersion (OD) <20% indicates adequate bleaching.

The luminescence ages obtained at Solero site range from 481 ± 90 ka to 76 ± 5 ka (Table 5). The uppermost sample (SOL-4), collected in a pedostratigraphic unit developed on loess material, date

back to 76 ± 5 ka. The others samples, collected in the underlying units developed on a fluvial material, show ages in stratigraphic order. The sampling positions are indicated in Fig. 12.

SOL-4 and SOL-5 samples were taken as undisturbed blocks, cleaned in the luminesce dating laboratory of the Geological Survey of Israel with appropriate low level orange lighting. The other three samples (SOL-1, SOL-2 and SOL-3) have been collected by hammering iron tubes into the excavated section. The purified quartz was extracted following the procedures described in paragraph 2.5.2.3.

A sample test performed on 2 aliquots of 2 mm for each sample, using the single aliquot regenerative dose (SAR) protocol (Murray and Wintle, 2000) showed high De values, suggesting that the OSL signal was saturated. Therefore, it was agreed to measure the De value using the thermally transferred OSL (TT-OSL) signal, applying the protocol of Porat et al., 2009.

The purified quartz was placed on 9.8 mm aluminium discs (aliquots) using 5 mm masks and silicon spray as adhesive. Five to ten aliquots were measured for each sample. The dose response curves have been constructed from four dose points (Fig. 14a), two of which have been repeated and two zero-dose points. After the removal of the aliquots with a recycling ratio exceeding 10%, the central age model (CAM; Galbraith and Roberts, 2012) was used to obtain a representative De value, with standard errors, which were propagated to the age errors (except for SOL-4 sample, whose De value has been obtained through the unweighted average between all its aliquots). The TT-OSL De distribution for each sample presents a very little scatter, lower than 20% (Fig. 14b): this suggest that the sample was exposed to sunlight only briefly, enough to bleach some of the OSL signal but not enough to bleach any of the TT-OSL signal (Zaidner et al., 2016). Therefore, all the TT-OSL age obtained can be considered representative of the original time of deposition.

3.2 *Rivarone*

The Rivarone section is located on the left bank of the Tanaro river, near Rivarone village (Fig. 11b,c), which is ca. 25 km far from Solero site and ca. 8 km far from the Pecetto di Valenza one. The site is divided in two outcrops, namely RVA (upstream) and RVB (downstream), separated by a distance of ca. 200m (see location in Fig. 15). The sequence outcropping at RVB, in turn, is divided into an upper (RVB_top) and a lower part (RVB_bottom). The RVB_bottom sequence one is in stratigraphic continuity respect to RVB_top, but is exposed ca. 25 m downstream (Fig. 15).

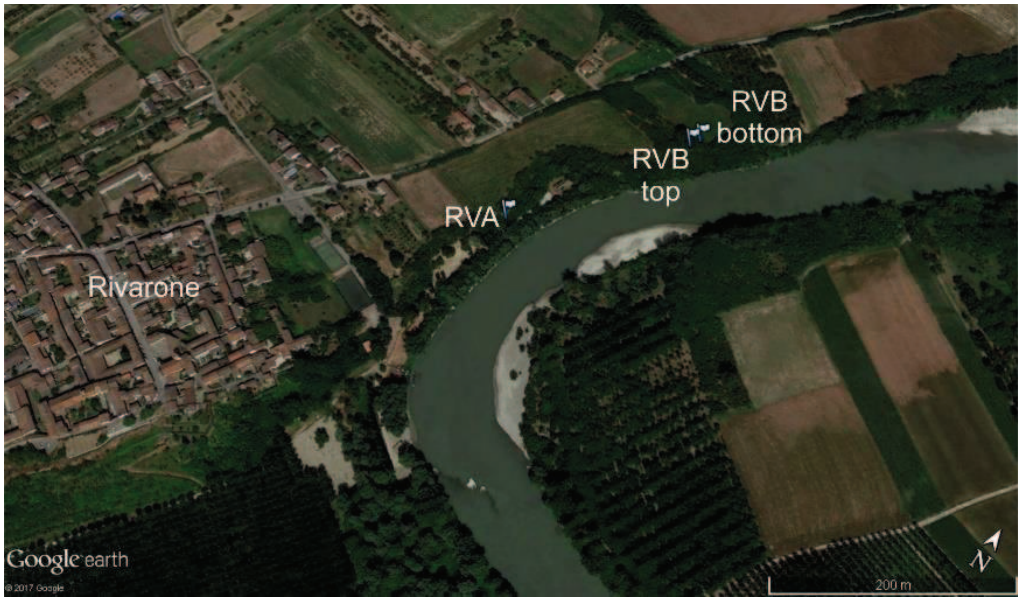

Fig. 15: Oblique view (Google Earth base image) of the Rivarone site. RVA locates the upstream sequence, while RVB the downstream one, in turn divided into an upper part, RVB_top, and a lower part, RVB_bottom.

Both RVA and RVB sequences have been described and sampled for luminescence dating and sedimentological analysis. The field descriptions, the results of the grain size analysis and the luminescence dating results are reported in the following paragraphs.

3.2.1 Soil profiles field description

3.2.1.1 RVA-sequence field properties

The pedostratigraphic sequence at RVA is characterized by several B horizons developed on aeolian/fluvial material (Fig. 16), which properties are reported in detail in Table 6.

Fig. 16: General view on the RVA sequence. The coloured lines indicate the lower boundary of each horizons showed in detail in the following figures (black boxes).

The upper ca. 3 m of this outcrop have not been evaluated, since the material is clearly reworked by ploughing. The first two undisturbed horizons present a clayey silt to sandy silt yellowish material with a massive to weakly developed poliedric structure. The following Bk1, Bk2 and Bk3 horizons, are developed on coarse silty pale yellow material and show abundant $CaCO_3$ nodules, possibly due to the occurrence of carbonate mobilization and recrystallization (a detail is illustrated in the inset of Fig. 17). Below, several Bc horizons (Btc1, Btc(x), Btc2 and Btc3) pale yellow coloured, mostly developed on silty/sandy material have been recognized. They present weakly to strong prismatic structure with Fe-Mn nodules increasing with depth. The underlying set of yellowish Bt horizons are developed on silty sandy material, in particular: a Btk horizon with common pedofeatures ($CaCO_3$ nodules and mottles) associated with carbonate translocation processes; a Bc(w) horizon characterized by Fe-Mn nodules increasing toward bottom. The sequence closes with a layer of fine gravel, lowly pedogenized.

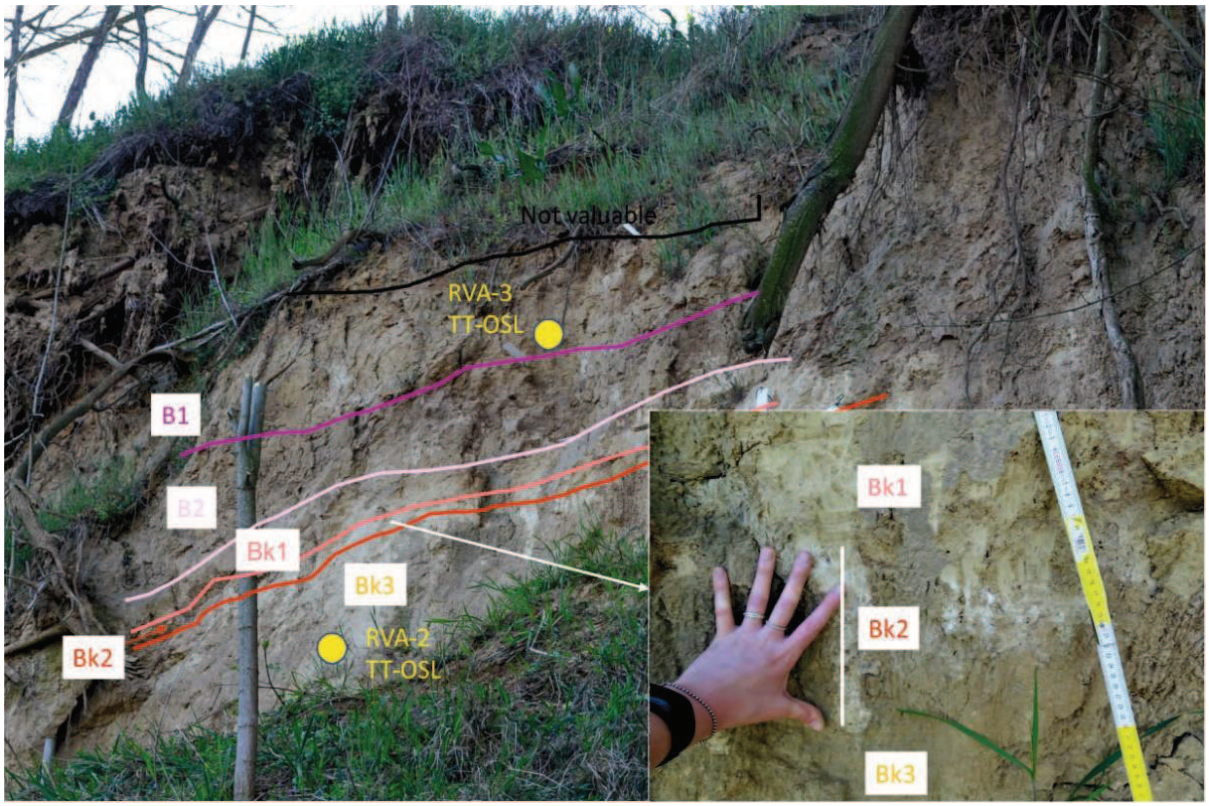

Fig. 17: Close view on the upper part of the RVA sequence; see Fig. 16 for location. The horizons and their lower boundary are indicated. The inset represent a further zoom on the Bk1 horizon characterized by abundant CaCO3 nodules. The position of the samples for the TT-OSL dating are also indicated.

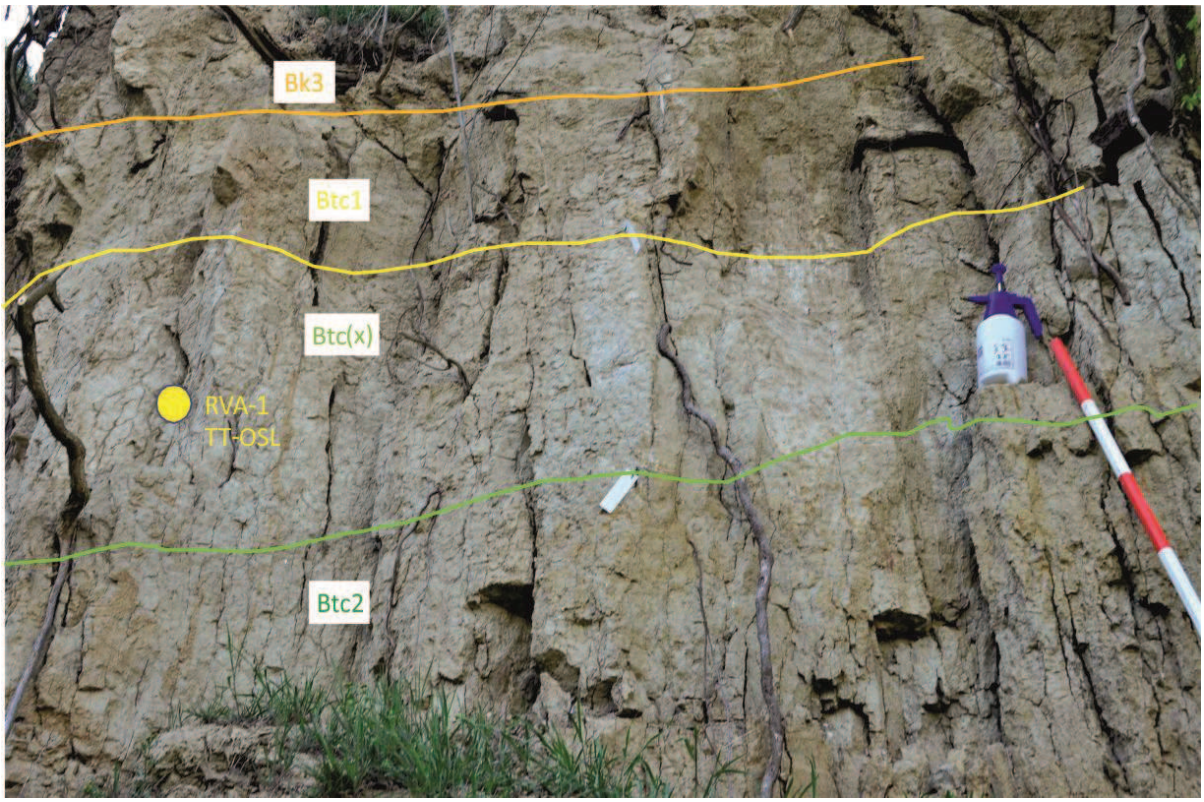

Fig. 18: Focus on the intermediate part of the RVA sequence; see Fig. 16 for location. The horizons, their lower boundary and the position of the sample RVA-1 dated with the TT-OSL method are indicated.

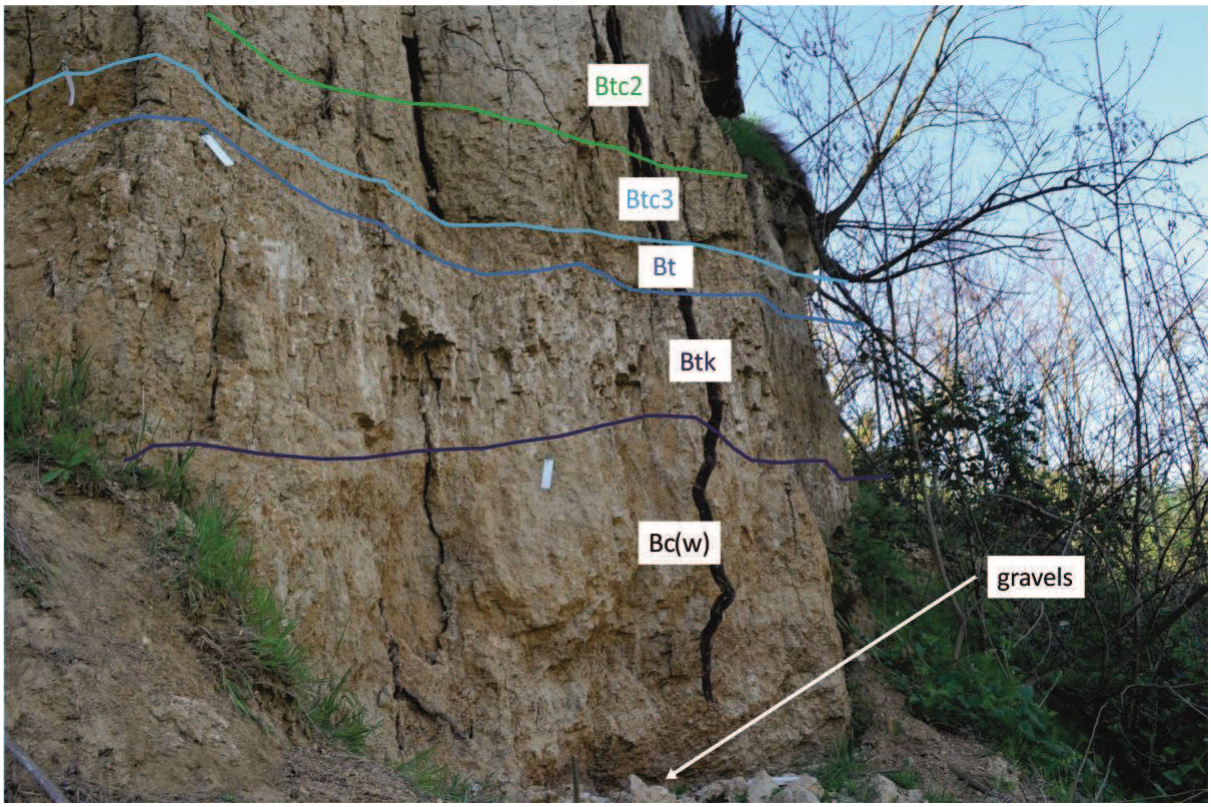

Fig. 19: Close view on the lower part of the RVA sequence; see Fig. 16 for location. The horizons and thei lower boundary are indicated.

Horizon	Depth (cm)	Description
---	0-300	Reworked by anthropic activity
B1	300-330	Clayey silt; light yellowish brown (10 YR 6/4); massive structure to weakly developed coarse poliedric structure; firm; abundant medium pores; rare Fe-Mn and clay coatings on voids and peds; gradual and linear lower boundary.
B2	330-370	Silty sandy; light yellowish brown (10 YR 6/4); massive to weakly developed coarse poliedric structure; firm; common medium pores; rare Fe-Mn coatings on peds and void; rare fine Fe-Mn nodules; gradual and linear lower boundary.
Bk1	370-405	Silty sandy, slightly clayey; pale yellow (2.5 Y 7/4); massive; very firm; few coarse pores; rare fine Fe-Mn nodules; common coarse $CaCO_3$ nodules; clear and wavy lower boundary.
Bk2	405-425	Silty sandy, slightly cleyey; pale yellow (2.5 Y 8/3); massive; very firm; few coarse pores; abundant coarse $CaCO_3$ nodules; gradual and linear lower boundary.
Bk3	425-500	Silty clay, slightly sandy; yellow (2.5 Y 7/6); massive; very firm; common fine pores; abundant $CaCO_3$ mottles; gradual and linear lower boundary.
Btc1	500-555	Sandy silty; pale yellow (2.5 Y 7/4); massive structure to weakely developed columnar structure; firm; common medium pores; frequent clay coatings on void and peds; gradual and linear lower boundary.
Btc(x)	555-635	Silty, slightly clayey; pale yellow (2.5 Y 8/3); slightly coarse platy structure to weakely developed columnar structure; firm; very few and fine pores; frequent madium Fe-Mn nodules increasing toward bottom; frequent clay coatings on void and peds; gradual and linear lower boundary.
Btc2	635-705	Silty, slightly sandy; pale yellow (2.5 Y 7/3); common brownish yellow mottles (10 YR 6/8); strongly developed coarse poliedric/prismatic structure; very firm; abundant fine pores and few coarse pores; frequent fine Fe-Mn nodules; frequent clay coatings on void and peds; gradual and linear lower boundary.
Btc3	705-741	Silty, slightly sandy; pale yellow (2.5 Y 7/4); strongly developed coarse prismatic structure; very firm; few very fine pores; common Fe-Mn coatings on peds and voids; freqeunt fine to coarse Fe-Mn nodules; frequent clay coatings on void and peds; clear and linear lower boundary.
Bt	741-756	Silty, slightly sandy; very pale yellow (10 YR 7/3); massive structure to weakly developed prismatic structure; very firm; common fine pores; few Fe-Mn coatings; frequent clay coatings on void and peds; clear and linear lower boundary.
Btk	756-831	Silty, slightly sandy; yellow (10 YR 7/6); few reddish yellow mottles (7.5 YR 7/6); strongly developed prismatic structure; very firm; few fine pores; common coarse $CaCO_3$ nodules; frequent $CaCO_3$ mottles; frequent clay coatings on void and peds; gradual and wavy lower boundary.
Bc(w)	831-941	Silty sandy; yellow (2.5 Y 7/6); massive structure to weakly developed prismatic structure; very firm; few fine pores; coarse Fe-Mn nodules increasing from common to frequent toward bottom; clear and wavy lower boundary.
---	941-951	Fine gravel; lower boundary not exposed.

Table 6: Field properties of RVA sequence at Rivarone site

3.2.1.2 RVB-sequence

As mentioned above, the RVB sequence is divided into an upper and a lower part (Fig. 20; 21; 22). Two pedostratigraphic level have been recognized, divided by a clear erosive surface (Fig. 20) and described in detail as illustrated in Table 7. The upper part, RVB_top, presents at its top a deposit 185 cm-thick, which has not been evaluated due to its reworked characteristics, probably induced by ploughing activity: a fragment of a modern-day clay pigeon has been found inside this deposit. The first pedostratigraphic level is developed on an aeolian material. It is composed by two yellowish brown Bt horizons (Bt(x) and Btc), displaying a moderate degree of clay illuviation. In particular, Btc horizon, characterized by frequent Fe-Mn nodules, becomes a marker horizon of the erosive surface that divides this PL from the lowermost. The abrupt limit marked by this horizon of Fe-Mn nodules can be followed for ca. 25 m, until getting to the outcropping RVB_bottom sequence.

The second pedostratigraphic level is composed of several pale yellow to brownish yellow B horizon developed on silty clay material. Pedofeatures related to illuvial processes are well represented in 2Bt(g), 2Bt, 2Btk and 2Bt(c) horizons. Pedofeatures related to the carbonate traslocation process, in the form of $CaCO_3$ nodules and mottles, are locally well expressed in 2Btk and 2Bk horizons. 2Bc horizon presents evidence of hydromorphic process as frequent Fe-Mn nodules.

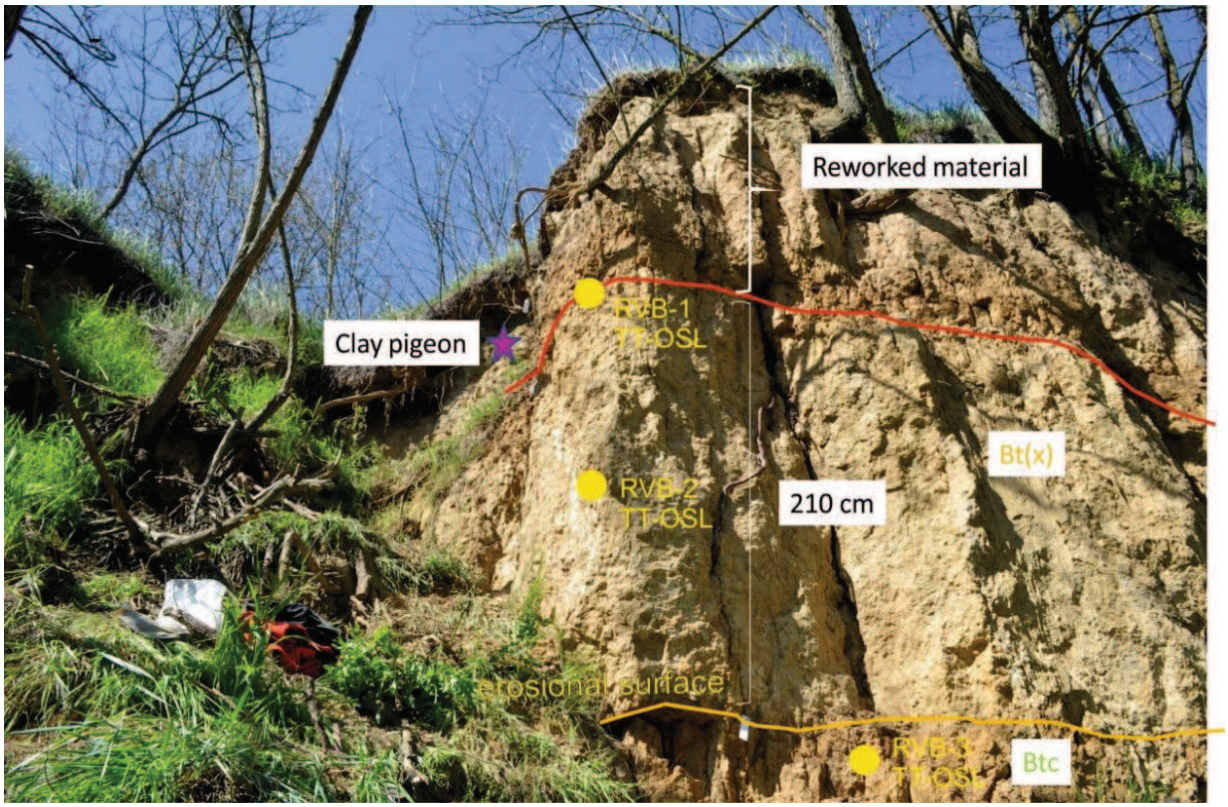

Fig. 20: General view on the top of the RVB sequence. The horizons, their lower boundary and the position of the samples dated with the TT-OSL method are indicated.

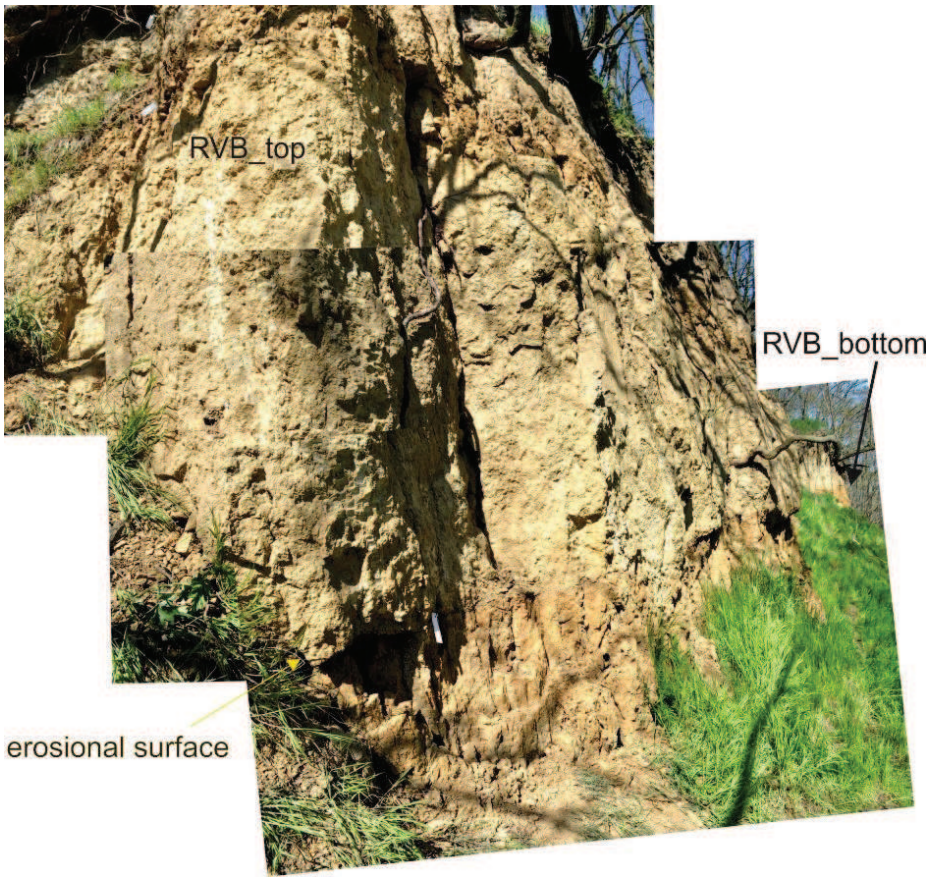

Fig. 21: Focus on the continuous erosional surface passing from the top to the bottom part of the RVB sequence.

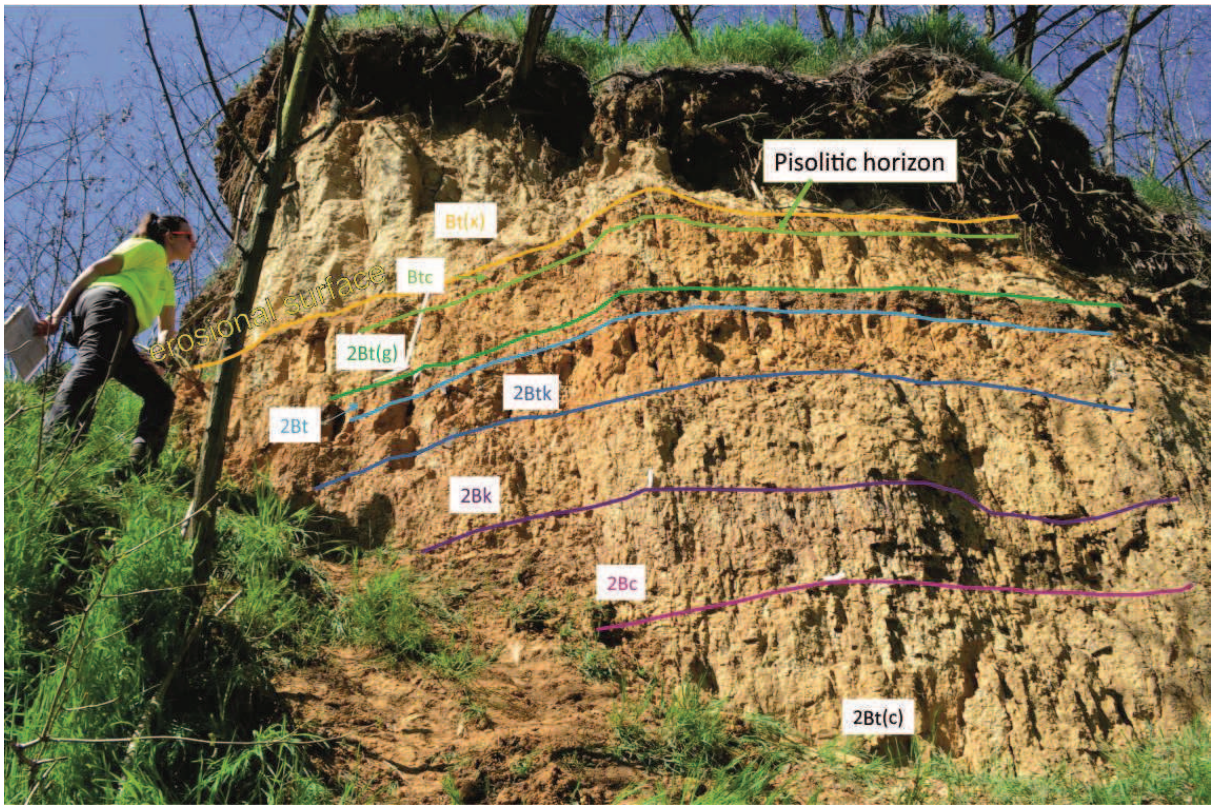

Fig. 22: General view on the RVB_bottom sequence. The horizons, their lower boundary are indicated.

Horizon	Depth (cm)	Description	Pedostratigraphic level
---	0-185	Not evaluable	---
Bt(x)	185-395	Silty clay; light yellowish brown (10 YR 6/4); massive structure to weakly columnar/prismatic structure; firm; common medium pores; very few and very fine roots; rare Fe-Mn nodules; common Fe-Mn coating on voids and peds; very few clay coating on peds; clear and wavy lower boundary.	PL1
Btc	395-410	Clayey silt; brownish yellow (10 YR 6/6); common very pale brown mottles (10 YR 8/3); moderately developed coarse granular structure; slightly firm; few very fine pores; frequent coarse Fe-Mn nodules; locally coarse CaCO3 nodules; clear and wavy lower boundary.	PL1
2Bt(g)	410-460	Silty, slightly clayey; yellowish brown (10 YR 5/6); frequent light gray mottles (2.5 Y 7/2); strongly developed coarse polyedric structure; very firm; common Fe-Mn coatings on voids and peds; few clay coatings on void and peds; abrupt and linear lower boundary.	PL2
2Bt	460-472	Clayey, slightly silty; brownish yellow (10 YR 6/6); common pale yellow mottles (2.5 Y 8/2); strongly developed coarse polyedric structure; firm; frequent Fe-Mn coatings; abrupt and linear lower boundary.	PL2
2Btk	472-512	Silty clay; yellowish brown (10 YR 5/6); very few pale yellow mottles (2.5 Y 8/2); moderately developed coarse prismatic/columnar structure; very firm; rare coarse roots; frequent coarse nodules of CaCO3; frequent coatings of Fe-Mn on voids and peds; gradual and linear lower boundary.	PL2
2Bk	512-577	Silty; yellow (10 YR 7/6); frequent very pale yellow mottles (10 YR 7/4); moderately developed coarse prismatic/columnar structure; firm; abundant medium pores; frequent Fe-Mn coatings on voids and peds; frequent fine CaCO3 mottles; gradual and linear lower boundary.	PL2
2Bc	577-637	Silty; yellow (2.5 Y 7/6); common yellowish brown mottles (10 YR 5/6); moderately developed coarse prismatic structure; firm; frequent Fe-Mn coatings on peds and voids; coarse Fe-Mn nodules increasing toward bottom; locally fine CaCO3 mottles; clear and linear lower boundary.	PL2
2Bt(c)	637-737	Clayey, slightly silty; yellow (2.5 Y 7/6); strongly developed coarse polyedric structure; firm; abundant medium pores; locally Fe-Mn coatings on peds; lower boundary not exposed.	PL2

Table 7: Field properties of RVB sequence at Rivarone site

3.2.2 Grain size analysis

3.2.2.1 RVA-sequence particle size distribution

Grain size analysis of the RVA-sequence were carried out by sieving and aerometer method on one soil/sediment sample for each horizon (Fig. 23).

As highlighted by the field properties, the grain size analysis confirm the development of the whole sequence on an aeolian/fluvial material. In particular, the uppermost two soil horizons (B1 and B2) present well-sorted cumulative grain size distribution curves, with a positive skewness. The underlying three horizons (Bk1, Bk2 and Bk3) still shows well-sorted asymmetric (positive skewness) sigmoidal curve, but shifted toward the coarse fraction, where the sand and silt values range up to 90%. This shifting can be explained by the frequent presence of $CaCO_3$ concrections characterizing these horizons that increase the amount of the coarse fraction. From Bc1 to Bw horizon, the grain size distribution

curves are unimodal, passing from well-sorted to moderately-sorted toward the bottom of the sequence: there is in fact an increasing of the clay content from 20% (Bc1 horizon) to 40% (Bw horizon). The lowermost two horizons (Bk4 and Bc(w)) present a slightly poor sorting, with a moderate content of clay and the coarse fraction well represented (between 15 and 20% of sand).

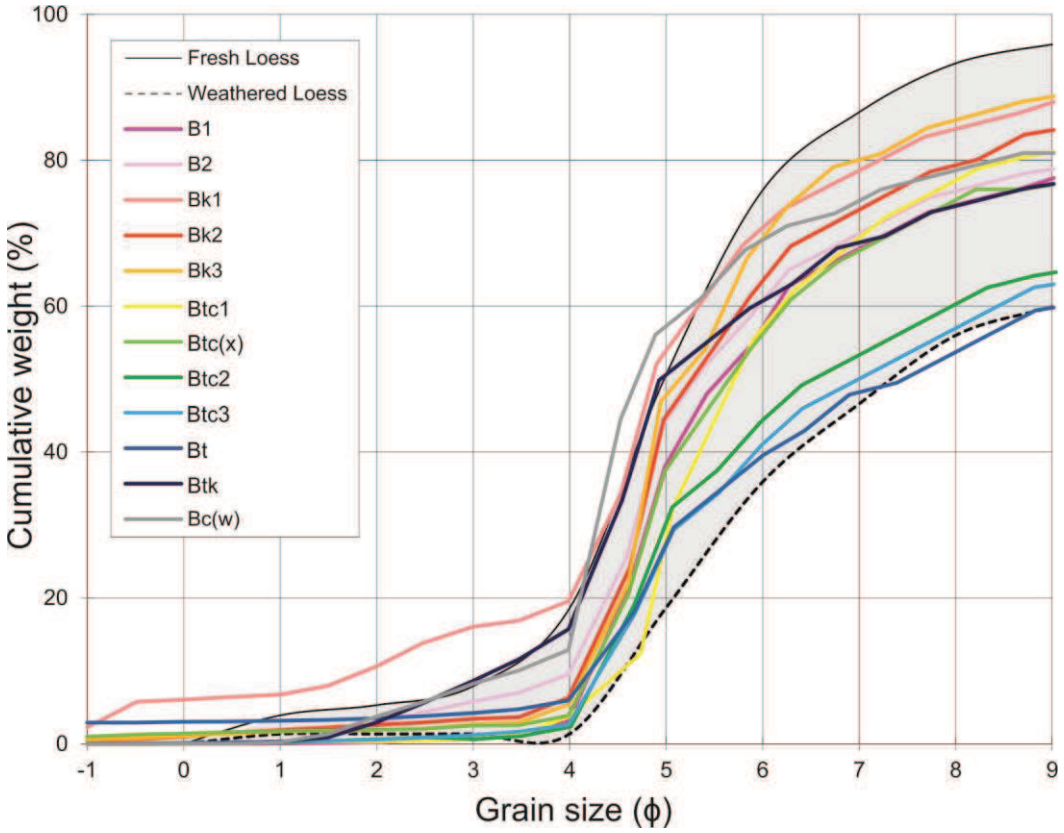

Fig. 23: Cumulative grain size curves compared to variability of grain size distribution in loess deposits in the PPLB according to Cremaschi (1987; 2004). The shadow area indicates the field of existence of loess.

3.2.2.2 RVB-sequence particle size distribution

Also the grain size analysis of the RVB-sequence were carried out on one soil/sediment sample for each horizon (Fig. 24) through the sieving and aerometer method.

The cumulative grain size distribution curves of the uppermost pedostratigraphic level PL1 show characteristic sigmoidal patterns. Curves are unimodal and well-sorted, with a positive skewness and the sand and silt values ranging up to 30%. In the pedostratigraphic level PL2, the sampled horizons pass from poorly sorted, at the top of the PL, to slightly sorted at the bottom: the clay content, in fact, decreases toward depth from 60% (2Bt(g) horizon) to about 20% (2Bt(c) horizon). Note, in the 2Bc horizon, the well represented coarse fraction which is due to the abundant presence of Fe-Mn nodules that increase the sand amount changing the trend of the curve.

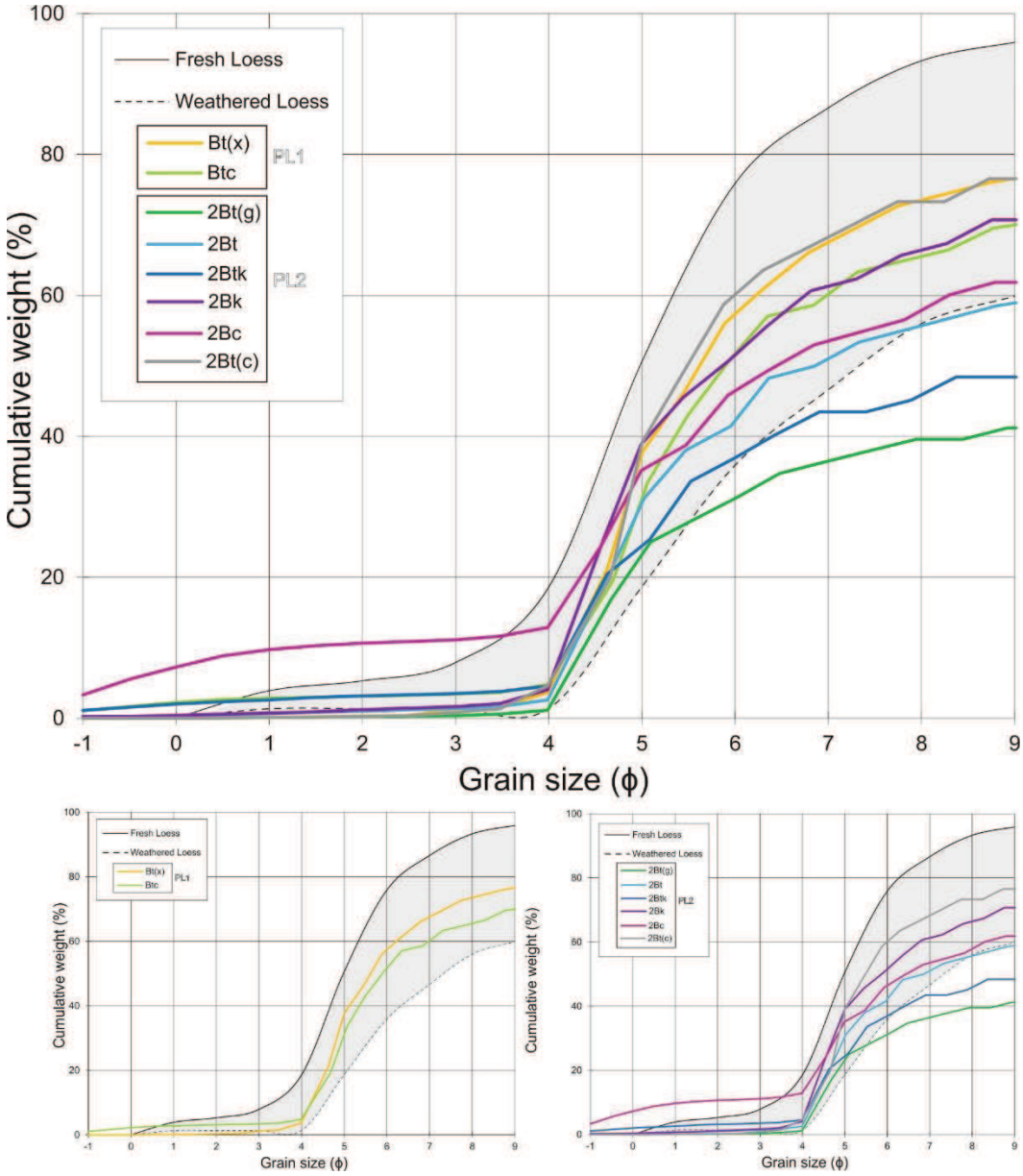

Fig. 24: Cumulative grain size curves for the pedostratigraphical levels compared to variability of grain size distribution in loess deposits in the PPLB according to Cremaschi (1987; 2004). The shadow area indicates the field of existence of loess.

3.2.3 TT-OSL dating

Sample	Burial Depth (m)	Soil horizon	Moisture content %	Dose rate (Gy/ka)	No. of aliquots	OD (%)	De (Gy)	Age (ka)
RVA-3	3.2	B1	10	3.50±0.13	10/10	6	441±41	126±12
RVA-2	4.55	Bk3	10	3.85±0.14	8/10	65	1803±710	469±185
RVA-1	5.95	Bc(x)	10	2.70±0.11	10/10	19	541±106	200±40
RVB-1	1.9	Bt(x)	10	3.18±0.12	10/10	22	297±65	87±21
RVB-2	3.0	Bt(x)	10	3.77±0.13	10/10	25	510±155	135±41
RVB-3	4.0	Btc	10	2.71±0.11	10/10	19	573±123	211±46

Table 8: TT-OSL data and ages for the Rivarone samples. The Unweighted model was used to obtain representative De values, with standard errors propagated to the age errors. No. of aliquots = the number of aliquots accepted for De determination out of those measured; OD = over dispersion.

The luminescence ages obtained at Rivarone site are presented in Table 8. RVA-2 and RVA-3 samples have been collected by hammering iron tubes into the exposed section; while all the other samples were taken as undisturbed blocks, cleaned in the luminesce dating laboratory of the Geological Survey of Israel with appropriate low level orange lighting. The sampling positions are indicated in Fig. 20. The purified quartz was extracted following the procedure described in paragraph 2.5.2.3.

A *sample test* performed on 2 aliquots of 2 mm for each sample, using the single aliquot regenerative dose (SAR) protocol (Murray and Wintle, 2000) showed high De values, suggesting that the OSL signal was saturated. Therefore, it was agreed to measure the De value using the thermally transferred OSL (TT-OSL) signal, applying the protocol of Porat et al., 2009.

The purified quartz was placed on 9.8 mm aluminium discs (aliquots) using 5 mm masks and silicon spray as adhesive. Ten aliquots were measured for each sample. The dose response curves have been constructed from four dose points (Fig. 25a,c), two of which have been repeated and two zero-dose points. After the removal of the aliquots with a recycling ratio exceeding 10%, the De values have been obtained calculating the unweighted average between all the aliquots of the same sample. The distribution of the TT-OSL De values of most samples presents a very little scatter, lower than 20% (Fig. 25d), except for RVA-2, showing a OD value of 65 % (Fig. 25b). The large scatter of this latter sample may be due to fluvial reworking of the parent material leading to partial bleaching of the quartz grain; thus, the age of 469 ± 185 ka is not reliable.

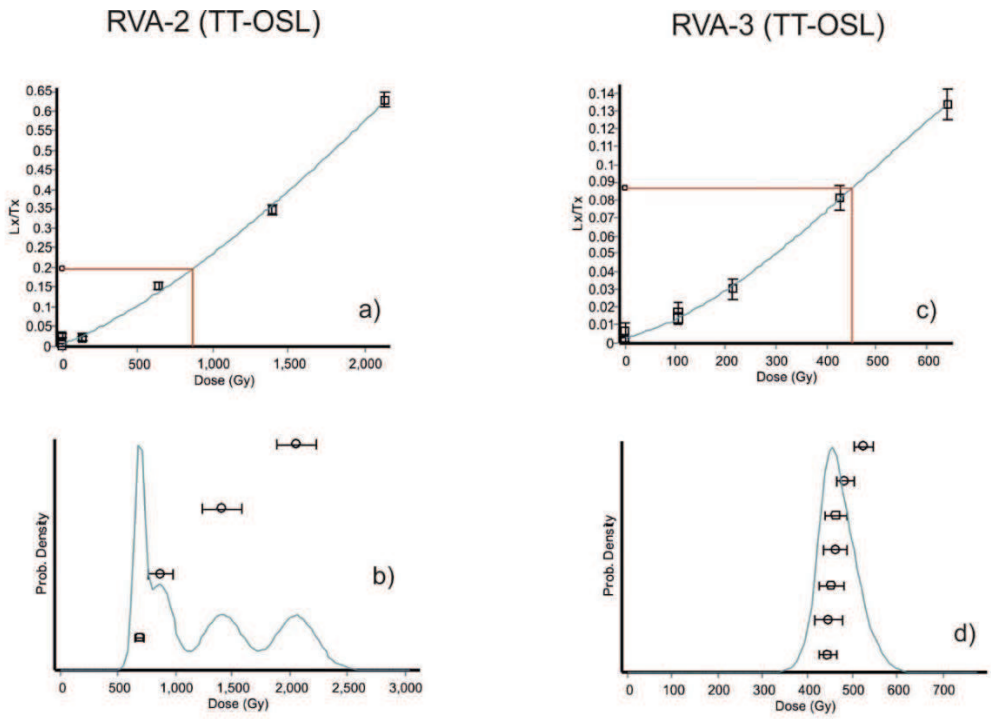

Fig. 25: TT-OSL analysis for the Rivarone site samples; a) dose response curve for RVA-2 sample; b) the probability density function plot of 2 mm aliquots measured for the same sample. The positively-skewed distribution with OD = 65% is typical of the poorly bleached material; c) dose response curve for sample RVA-3; d) a probability density function plot for the same sample with individual De values and error. Note the normal distribution with over dispersion OD < 20 %, typical of well bleached material.

3.3 *Pecetto di Valenza*

The field mapping conducted along the eastern sector of the Monferrato Arc, allows us to identify the Pecetto di Valenza site (Fig. 11b,c), which is ca. 20 km far from the Solero site and ca. 8 km from the Rivarone one. This site presents a recent paleoseismic reverse surface faulting affecting a complex pedosedimentary sequence with two loess covers at its top. Here, we had the opportunity to document the first evidence of repeated Late Quaternary coseismic surface rupture along the Monferrato Arc. In the following, we integrate pedosedimentary data, structural analyses, radiocarbon dating (Accelerator Mass Spectrometry, AMS-^{14}C) and OSL/TT-OSL dating of sediments, with the aim to reconstruct the recent paleoenvironmental evolution and deformation history of this site. We discuss the results of new geological field mapping at near regional scale (1:25.000). Then, we describe the stratigraphy, paleopedology, AMS-14C dating, OSL/TT-OSL dating and structural analysis at site scale of the sequence exposed at Pecetto di Valenza. Finally, we show how these data are useful to redefine the seismic hazard of a region, which seems totally unprepared to cope with the effects of a local strong earthquake.

3.3.1 Bedrock geology and quaternary deposits of the near-regional area

In the Pecetto di Valenza area the oldest sediments correspond to the Argille Varicolori (AVC; Fig. 26), correlative with the Ligurian units of the Apennines, of Upper Cretaceous-Middle Eocene age (Dela Pierre et al., 2003a). Here, the AVC sediments are tectonically deformed to form hundreds of meter thick tectonic mélange, characterized by a block-in-matrix fabric (cf. Festa & Codegone, 2013; Festa et al., 2015). The tectonic mélange is part of a major NS-striking sub-vertical deformation zone, bordered by two main high-angle tectonic detachments, oriented obliquely to the Eastern Monferrato trend (NW-SE). In fact, this tectonic feature interrupts the open fold observed in the western sector of the investigated area. The AVC matrix consists of purple, green and grayish claystones and shalestones affected by a pervasive, scaly cleavage and it includes dm-sized exotic blocks of Upper Jurassic - Lower Cretaceous Maiolica wackestones. Where the matrix is better exposed, the scaly cleavage is steeply E-dipping and shows an average N-S direction (i.e. nearly parallel to the main marginal faults). Along the eastern border of the deformation zone, hundreds of meter wide and lozenge-shaped tectonic slab of the Cenozoic succession have been mapped within the varicoloured matrix. The upper stratigraphic boundary of AVC with the overlying succession is not preserved.

The Cenozoic stratigraphic succession is basically represented by the deposits of Tertiary Piemonte Basin synthems 4 and 6 (Figs. 3.1c and 3.13). Both East and West of the deformation zone, the succession consists of Tortonian-Lower Messinian hemipelagic sediments (Sturani & Sampò, 1973)

referred to as the Marne di Sant'Agata Fossili (SAF), containing lenticular bodies with erosional base of sandy-gravelly resedimented deposits (SAFa). The SAF show a cyclic organization, evidenced by the rhythmical alternation of homogeneous bioturbated grey marls and brownish silty clays. The upper (Messinian) part of the unit is locally followed by an euxinic succession of thinly laminated shales (eu), yielding scattered carbonate concretions. To the East of the deformation zone, in the surroundings of Pecetto di Valenza, the SAF become carbonate and silica-enriched, yielding abundant diatomitic facies (Pavia, 1989; Gaudant et al., 2010). The SAF are unconformably topped by the shallower sandy-muddy deltaic deposits known as the Cassano-Spinola Formation (CCS; Boni & Casnedi, 1970), Late Messinian in age. On the whole, the investigated succession is affected by N-S and NNE-SSW trending high-angle to E-dipping fault systems, both reverse and normal.

The Pecetto site, that is the focus of this paper, formed on the reverse fault zone that displaces the lower Messinian marly bedrock, recognized in the easternmost part of the study area (Fig. 26a).

The main Quaternary morphological feature of the Pecetto di Valenza area is represented by the Valenza Plateau, an alluvial terrace 1.5 - 2.5 km wide that stretches for about 20 km between the Grana and the Tanaro rivers, right tributaries of the Po River (Figs. 11b and 27a). Interposed between the Eastern Monferrato hills and the Po Plain, the plateau is separated from the active meandering belt of the Po river by a scarp with decreasing height: 40 m at Valenza and 15 m at the eastern termination of the alluvial terrace, near Bassignana. A detailed analysis of 5-m-resolution DTM shows that the plateau is largely covered by coalescing flat alluvial fans (mean slope gradient 0.5°) fed by minor tributaries draining the northern flank of the Eastern Monferrato reliefs. Since the late Pleistocene, the gradual dismantling of the Valenza Plateau operated by the Po River (in turn forced by the clastic deposition of the Sesia and Ticino rivers) caused a local steepening of the stream network gradient and a generalized entrenchment of the alluvial fans (Fig. 26a).

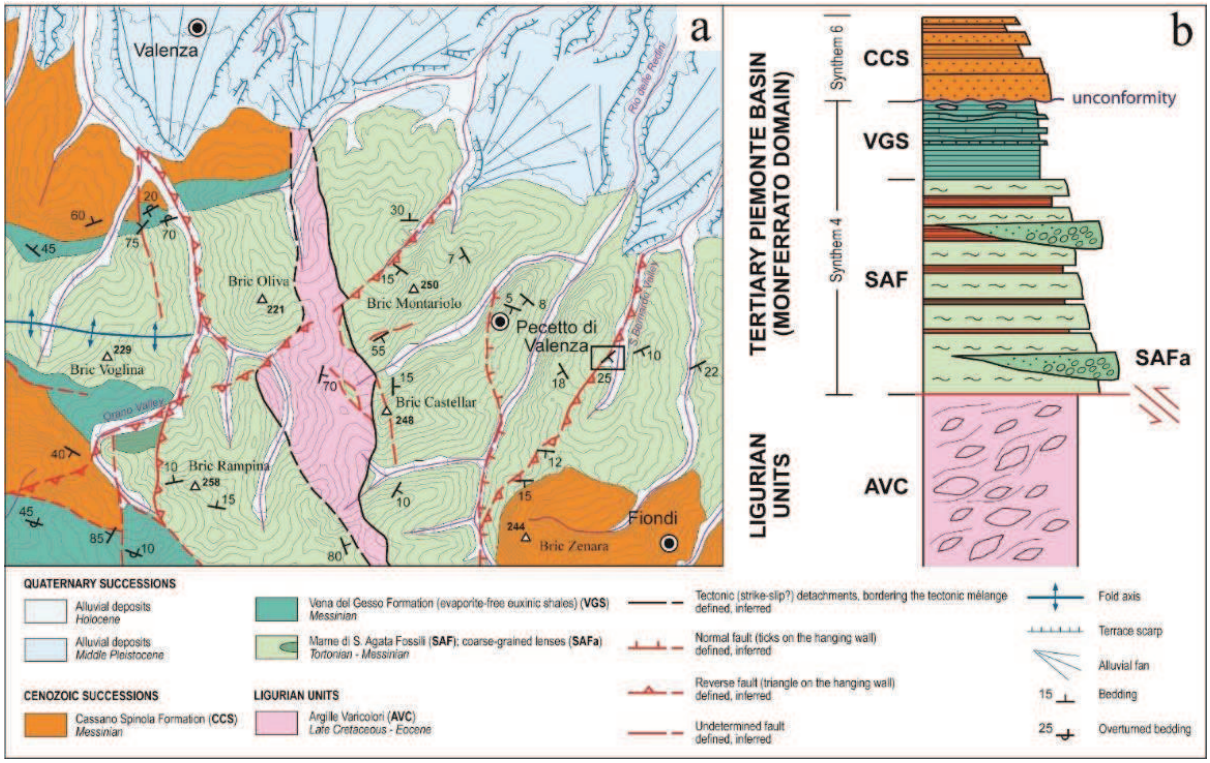

Fig. 26: Near regional setting of the study area; a) geological map of the Pecetto di Valenza area; the location of the Pecetto site is indicated by the black box, which also locates Fig. 3.14b; b) stratigraphic log of the Paleogene-Neogene succession. Note that loess is not mapped. From Frigerio et al., 2017.

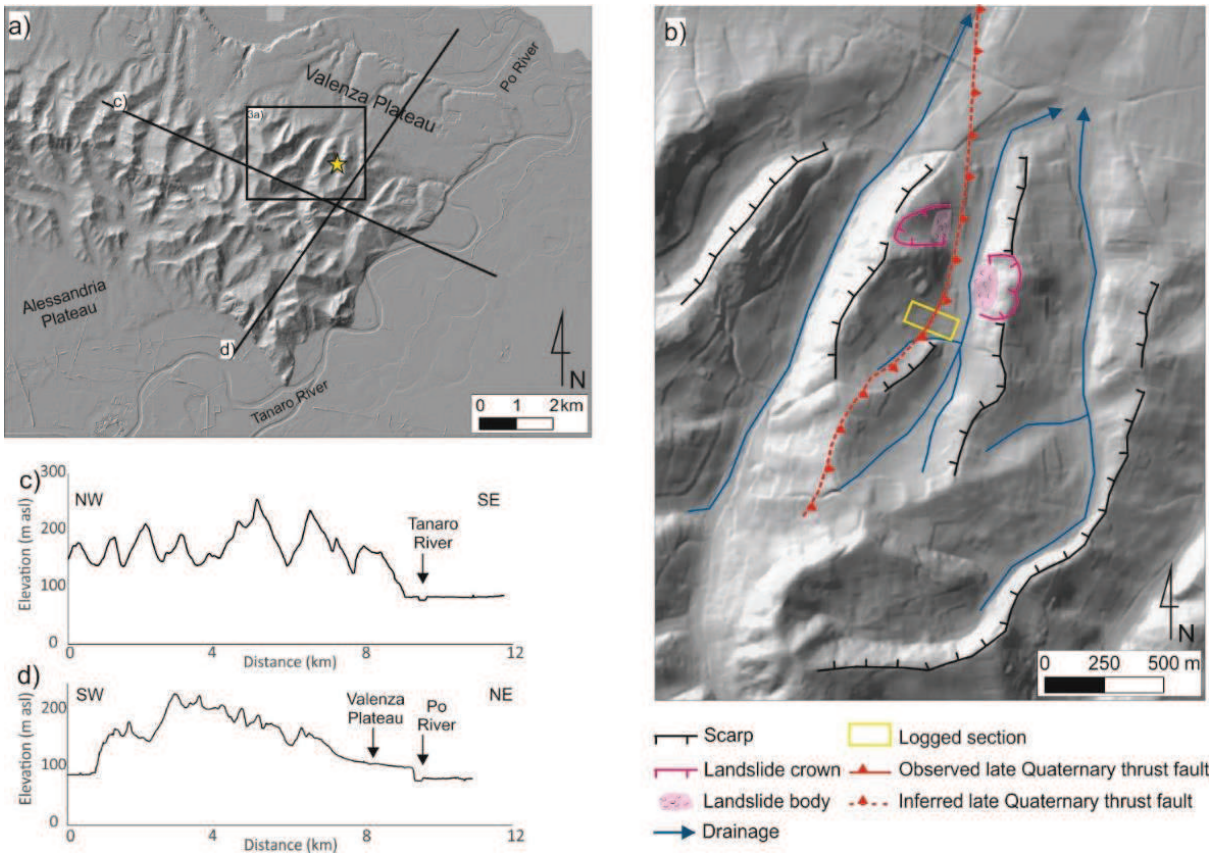

Fig. 27: Geomorphic setting of the Pecetto site; a) hillshade model derived from a 5m resolution DEM illustrating the E part of the Monferrato Hills, bounded by the Valenza and Alessandria Plateau; the star locates the Pecetto site, the box locates Fig. 26a; b) morphotectonic map of the Pecetto di Valenza site; basemap of a hillshade model derived from a 5m resolution DEM; c) and d) topographic profiles crossing the Pecetto di Valenza hilly area, whose traces are shown in Fig. 27a.

According to stratigraphic logs carried out on some outcrops along the fluvial terrace scarp and on two quarry located close to Valenza and Bassignana, the stratigraphic sequence of the Valenza plateau (fl2; Fig. 26b) can be summarized as follow.

- A basal unit up to 5-6 m thick made up of reddish yellow (5YR) fluvial silts and clayey silts, with a massive structure and with a strongly developed coarse prismatic structure. Abundant Fe-Mn oxide-rich fracture coatings and millimetric nodules are visible along the whole profile. At the contact with the pre-Quaternary succession (represented by the sandy deposits of the Cassano-Spinola Formation and by the sandy-gravel deposits of the Villafranchian succession Auct.) a well-developed calcrete horizon is visible, presumably deriving by leaching of the overlying parent material; in some cases the carbonatic horizon is made up of abundant centimetric CaCO3 nodules or veins scattered in the host sediments; in other cases calcium carbonate forms massive calcrete horizon up to 20-30 cm thick; instead, in a few places calcrete forms stockwork of randomly oriented millimetric carbonatic veins.

- The upper unit consists of yellow/yellowish brown (10YR) fluvial and aeolian silts, with a massive and poorly developed coarse prismatic structure. Fe-Mn oxide-rich fracture coatings are visible mainly

toward the bottom of the unit. The base of the unit is marked by a sharp contact with the underlying units, evidenced by a high concentration of Fe-Mn nodules. Within the alluvial fan sequence at least 3-4 subunits, each 3-5 m thick, can be recognized and evidenced by weakly developed multiple paleosols. According to some borehole logs, the maximum thickness of the upper unit can be estimated in 20-25 m.

In the hilly area (Fig. 27a,b), valley bottoms are covered by thin (1-3 m) unconsolidated silty and sandy-silty alluvial deposits (fl1); these are the result of the reworking of colluvial deposits formed at expense of weathered pre-Quaternary bedrock.

3.3.2 The integrated paleoseismological analysis

As already mentioned, during the geological field mapping we observed evidence for recent paleoseismic events at the Pecetto di Valenza site (Fig. 28).

Fig. 28: General view of the Pecetto di Valenza section; arrow shows the position of the pedosedimentary column in Fig. 30; detail on reverse faults F3 (b) and F1(c), displacing the overlying PL3 colluvial deposit.

At this site, we performed detailed investigations including: (i) logging of the exposed section and soil profiles field description; (ii) sampling for pedosedimentary analyses; (iii) extraction of oriented and undisturbed samples for micromorphological analyses of thin sections; (iv) radiocarbon and luminescence dating; (v) description of the structural features at the mesoscale and slip inversion analyses. The method applied are descripted in chapter 2.

3.3.2.1 Logging and soil profiles field description

The Pecetto di Valenza site (Figs. 28) presents a stratigraphic section, 10 m long and up to 4 m deep, excavated for building construction works in the vicinity of the southern margin of the Valenza Plateau. The geomorphologic setting of the site is shown in Fig. 27b. The section (Fig. 28) trends ESE-WNW and shows a lower Messinian marly bedrock (Catanzariti R. and Da Prato S., 2016 pers. com.) overlaid by a complex pedosedimentary sequence, which includes a paleosol developed on colluvial sediments capped by a succession of weathered loess deposits. The latter thickens upslope, from SE toward NW, suggesting that these deposits infilled a former small paleovalley flowing parallel to the direction of the main slope with a thalweg located in a sector to the NW (Fig. 27b). Successive phases of deposition, pedogenesis and erosion are documented in the section. Almost the entire sedimentary sequence is affected by reverse faulting, which offsets the bedrock, paleosols and loess. As illustrated in Figs. 26a and 27b, the dip of the fault zone is opposite of the dip of the main slope.

Log units are based on the definition of pedostratigraphic levels and soil horizons; two more Log units have been mapped, resulting from the interplay between tectonic deformation of the bedrock and pedogenic illuviation of clay along fractures and joints. These are an example of well-developed fault gouges, and pockets of colluvium distributed along the main fault strands.

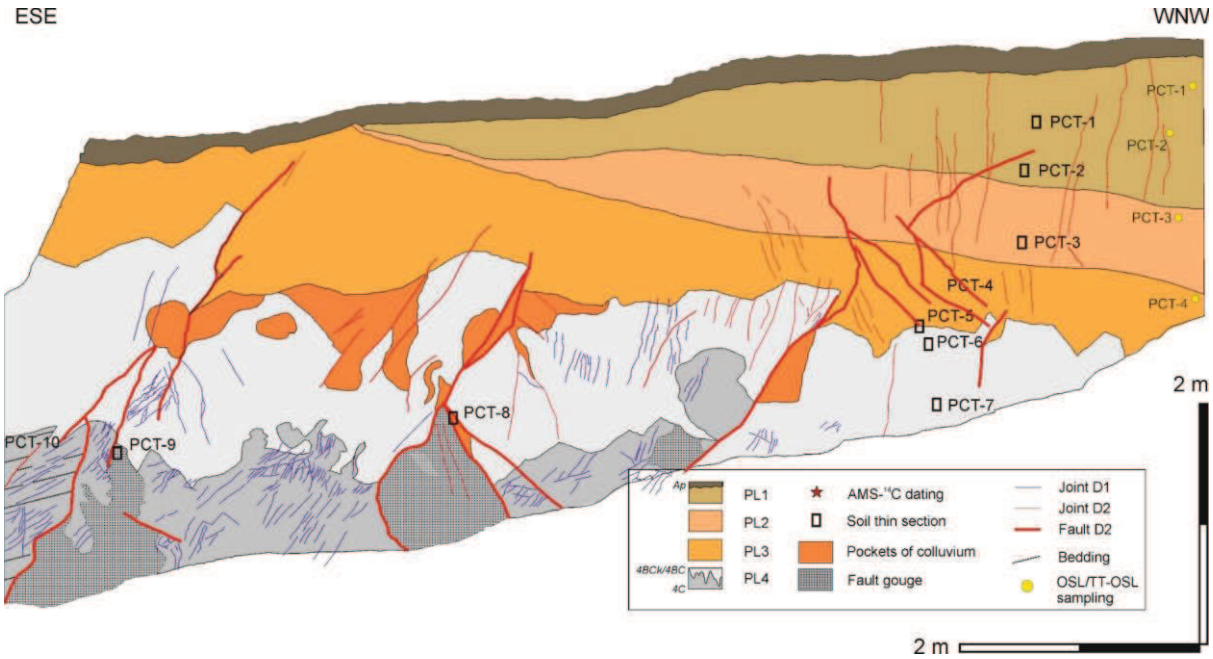

Fig. 29: Detailed Log of the outcrop, from the 1:10 scale field survey; the position of samples collected for AMS dating (Table 11), OSL-TT-OSL dating (Table 12) and thin sections analysis (Table 10) are indicated; F1, F2 and F3 are the fault strands shown in Fig. 52.

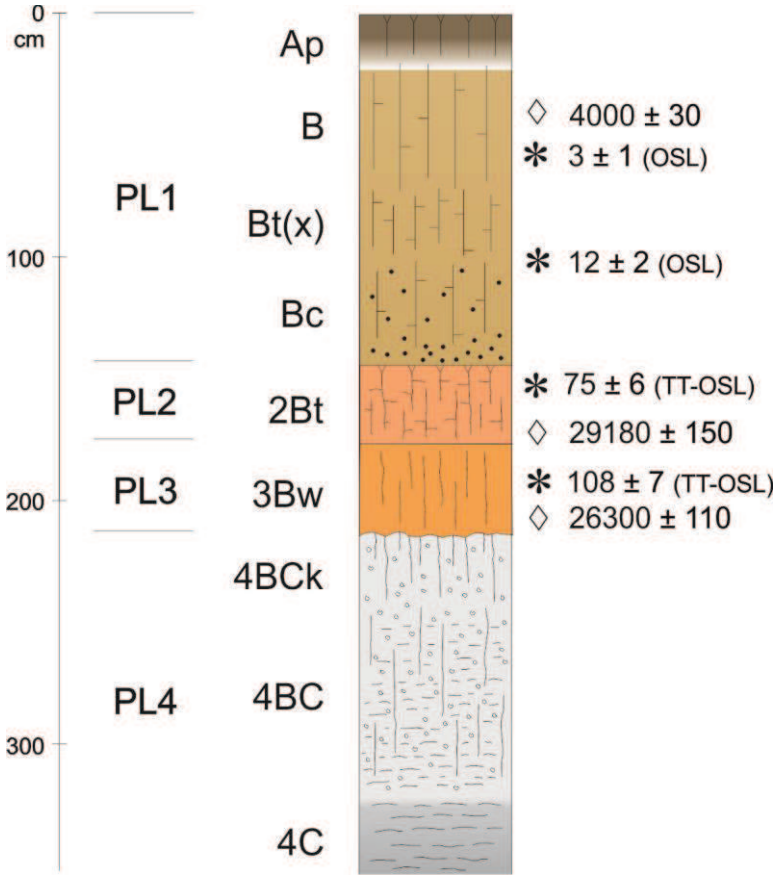

Fig. 30: Pedostratigraphic column illustrating the distribution of soil horizons and the pedostratigraphic levels. The results of AMS-14C (stars), OSL/TT-OSL (diamonds) dating and the position of samples for thin sections are indicated.

As shown in Figs. 28 and 29, the complex pedosedimentary sequence is better represented in the WNW part of the outcrop, where deposits are typically thicker. The distribution of soil horizons and pedostratigraphic levels is presented in the stratigraphic column of Fig. 30. From a paleopedological point of view, the section includes a series of B horizons developed on different parent materials, distinguished on the basis of field description and laboratory analyses (mostly grain-size). The parent materials that identify the four pedostratigraphic levels are: loess (PL1 and PL2), colluvial deposits (PL3) and the marly bedrock (PL4). The horizons of each PL underwent specific pedogenetic processes. A detailed field description is in Table 9. In the following, PLs are detailed from top to bottom. PL1 consists of a ca. 20 cm-thick Ap horizon, rich in organic matter and showing a weakly developed blocky structure. In the eastern portion of the outcrop, the lower boundary of this PL is an erosive surface that truncates the top PL2; whereas, in the western part, the Ap horizon is followed by three silty-clay B, Bt(x), and Bc horizons, all pertaining to PL1. They present a massive to platy structure, compact and light yellow colour. Moreover, the Bc horizon includes common Fe-Mn nodules, whose concentration increases downward. The boundary to the underlying PL2 is sharp. This level is represented by a 2Bt horizon consisting of a strong brown silty clay material, with a coarse and wellexpressed prismatic structure, gradually passing downward to PL3. The latter is a clay-rich, dark reddish brown, and it is the residual 3Bw horizon of a strongly developed paleosol. Evidence for intense clay illuviation, strong weathering, and abundant Fe-Mn coatings points to the occurrence of a strong and prolonged pedogenetic process acting on colluvial sediments. The lower boundary of PL3 is a sharp erosional contact that truncates the underlying bedrock. Reverse faulting systematically displaces the base of the unit. The 4BCk, 4BC, and 4C horizons constitute PL4. They were developed on the local weathered bedrock (Marne di S. Agata Fossili, early Messinian). They display a concentration of $CaCO_3$ nodules, possibly due to the occurrence of carbonate mobilization and recrystallization, and a decrease towards the bottom of clay coatings on voids and structural joints. Calcium carbonate-bearing pedofeatures are particularly common in the upper part of the PL, where a possible calcrete (Wright and Tucker, 1991) has been identified. The 4C horizon also presents common Fe-Mn coatings on structural joints and little evidence for clay illuviation, but still preserves the properties of the bedrock.

Horizon	Depth (cm)	Description	Parent material	Pedostratigraphic level
Ap	0-20	Silt loam; dark yellowish brown (10YR 4/4); weakly developed fine subangular blocky structure; friable; common medium and fine pores; abundant organic matter; common fine and medium roots; gradual lower boundary.	loess	PL1
B	20-70	Silty clay; pale yellow (2.5Y 7/4); massive structure to weakly developed coarse platy structure; firm; common fine pores; gradual lower boundary.	loess	PL1
Bt(x)	70-100	Silty clay; pale yellow (2.5Y 7/4); massive structure to strongly developed coarse platy structure; very firm; common medium pores; gradual lower boundary.	loess	PL1
Bc	100-140	Silt clay; light yellowish brown (10YR 6/4); massive; firm; few medium pores; common to abundant fine Fe-Mn nodules increasing towards the bottom; few clay coatings; clear lower boundary.	loess	PL1
2Bt	140-175	Silty clay; strong brown (7.5YR 5/6); strongly developed coarse prismatic structure; slightly firm; few fine and medium pores; gradual lower boundary.	loess	PL2
3Bw	175-215	Clay; dark reddish brown (2.5YR 3/4); strongly developed prismatic structure, with coarse aggregates; moderately firm; few fine to medium pores; common coatings of yellowish brown (10YR 5/6) clay on peds; common Fe-Mn coatings on peds and voids; abrupt wavy lower boundary.	Colluvium	PL3
4BCk	215-240	Weathered marl; light gray (5Y 7/2); massive; firm; very few small pores; very common fine CaCO3 nodules; common clay coatings along joints; irregular lower boundary.	Marl	PL4
4BC	240-320	Weathered marl; light gray (5Y 7/2); frequent, medium pale brown (10YR 6/3) and few fine reddish brown (5YR 4/4) mottles; massive; firm; very few small pores; very common fine CaCO3 nodules; few clay coatings on voids and structural joints; clear wavy lower boundary.	Marl	PL4
4C	> 320	Weathered marl; light gray (5Y 7/2); massive; firm; very few small pores; common Fe-Mn coatings on voids and structural joints; few clay coatings on voids and structural joints; lower boundary not exposed.	Marl	PL4

Table 9: Field properties of the Pecetto di Valenza section; colours are according to Munsell, 1994.

3.3.2.2 Grain size analysis

The particle size distribution of the pedostratigraphic sequence at Pecetto di Valenza site has been obtained both by sieving and aerometer method and by masterizer analyzer. In the first case, one soil/sediment sample was analysed for each horizon; in the other case, a sample every 15 cm has been analysed.

From both analysis, it's possible to observe that the whole Pecetto pedosedimentary sequence is characterized by sandy and silty parent materials, where the coarsest particles do not exceed 2 mm (Figs. 31 and 32).

The cumulative grain size distribution curves obtained from the sieving and aerometer method (Fig. 31) shows for the samples from PL1, the characteristic sigmoidal patterns of loessic sediments; curves are well-sorted, with a positive skewness (Cremaschi, 1987). The sand + silt content ranges between 80% (Bc horizon) and 90% (B horizon), depending on the relative contribution of clay due to illuviation processes. In PL2, horizon 2Bt show again a well-sorted asymmetric (positive skewness) sigmoidal curve; in this case sand + silt content is around 70%. PL3, represented by 3Bw horizon, shows a different grain size distribution, marked by a poor sorting and a sand and silt values around 65-70%. Finally, PL4 is very similar to PL3.

The grain size of horizons B, Bt(x), Bc, and 2Bt can be compared with the reference theoretical curves elaborated for fresh and weathered loess from the Po Plain (Cremaschi, 1987). This comparison allows also estimating the degree of loess weathering along a section (Zerboni et al., 2015).

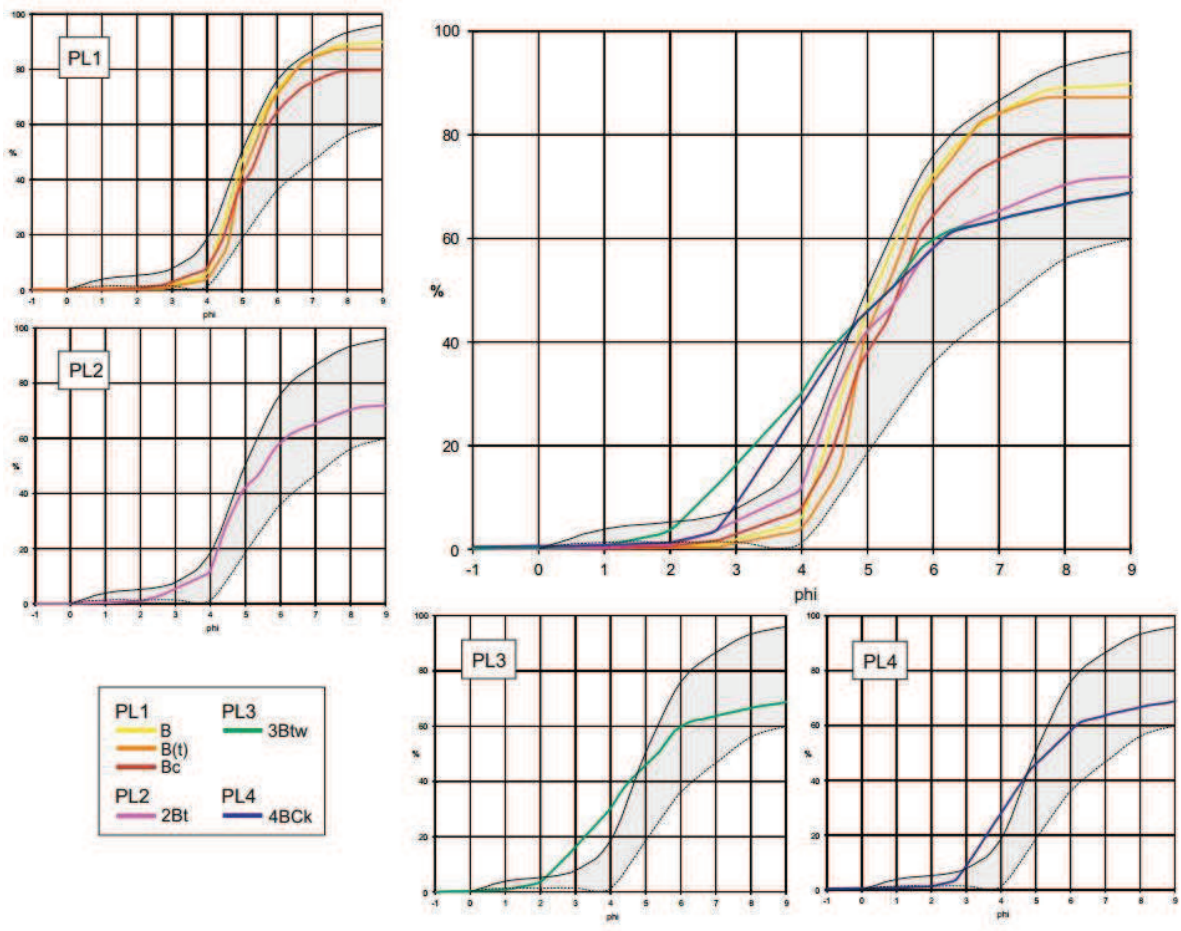

Fig. 31: Cumulative grain size curves for the pedostratigraphic levels compared to variability of grain size distribution in loess deposits in the PPLB according to Cremaschi (1987, 2004). The shadow area indicates the field of variability of loess; the black solid curve indicates the fresh loess, the dashed black curve indicates weathered loess.

The PSD curve obtained with the mastersizer analyser after dissolving the organic matter in 8% H2O2 for 3 days, (Fig. 32) highlights the bimodal behaviour of the weathered loess (horizon Bc from PL1 and PL2), with a peak in the silt fraction between 40 and 55 micron. This peak corresponds to the sedimentaryfraction of the parent material; a further peak in the clay fraction is related to an enrichment of the fine fraction after pedogenesis.

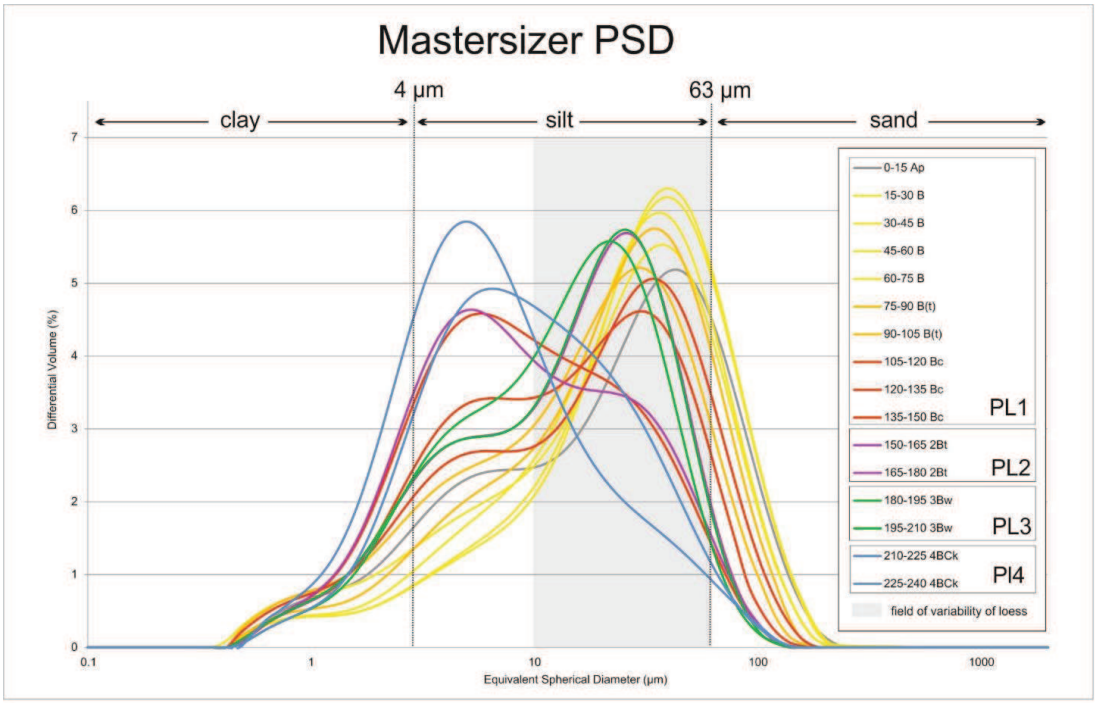

Fig. 32: Particle size distribution of sediments sampled along the whole pedostratigraphic sequence every 15 cm. The shadowed area indicates the field of variability of loess.

3.3.2.3 Thin section micromorphology

Seven undisturbed blocks (PCT-1 to PCT-7) for micromorphology of soil thin sections (Figs. 33 and 34) were extracted from the western part of the pedostratigraphic section. Three further blocks have been sampled in the eastern part of the outcrop: a sample from the fault damage zone (PCT-8), and two samples from the fault gouge (PCT-9, PCT-10). The location of samples is indicated in Fig. 29 and a detailed description of the micromorphological properties of each slide is provided in Table 1.

Sample name	Horizon	Pedostratigraphic level	Porosity					Micro structure	Mineral coarse fraction				Organic coarse fraction	c/f related distribution (c/f limit 10 µm)	Micromass
			Chambers	Channels	Planes	Vesicles	Vughs		Quartz	Micas	Others	Microfossils ineriithed from bedrock			
PCT-1	B	PL1	-	5-15%	< 2%	15-30%	-	Massive	40%	50%	10%	-	Roots residues (< 5%)	Close porphyric (ratio 60/40)	Dominant: yellowish gray, cloudy, crystallitic, locally striated; locally: brown, opaque, crystallitic
PCT-2	Bc	PL1	-	< 5%	< 2%	15-30%	-	Massive	50%	40%	10%	-	-	Close porphyric (ratio 60/40)	Yellowish brown, cloudy, crystallitic; locally: brown, cloudy, crystallitic
PCT-3	2Bt	PL2	< 5%	15-30%	15-30%	-	15-30%	Massive	60%	20%	20%	-	Roots residues (< 2%)	Close porphyric (ratio 50/50)	Dominant: brownish yellow, cloudy, crystallitic; few depleted areas: yellowish gray, cloudy, crystallitic
PCT-4	3Bw	PL3	5-15%	< 5%	15-30%	-	-	Massive	40%	30%	30%	-	-	Single spaced porphyric (ratio 25/75)	Dominant: reddish brown, opaque, crystallitic, locally striated; very few depleted areas: yellowish brown, cloudy, crystallitic
PCT-5	3Bw/4BCk	PL3	5-15%	-	15-30%	-	-	Subangular blocky	40%	30%	20%	10%	-	Double spaced porphyric, locally open pophyric (ratio 20/80)	Dominant: reddish brown, opaque, striated; few depleted areas: yellowish brown, limpid, crystallitic
PCT-6	4BC	PL4	30-50%	-	30-50%	-	-	Massive	30%	20%	20%	30%	-	Open porphyric (ratio 15/85)	Yellowish orange, cloudy, striated
PCT-7	4BC	PL4	< 2%	-	15-30%	-	-	Massive (locally bridged grain microstructure	20%	20%	10%	50%	-	Single spaced porphyric, locally concave gefuric (ratio 50/50)	Dominant: yellowish gray, cloudy, cross-striated; few depleted areas: gray, limpid, crystallitic
PCT-8	-	-	-	-	15-30%	-	-	Massive	40%	20%	10%	30%	-	Close porphyric to open (ratio 40/60)	Reddish brown, cloudy, cross-striated, locally granostriated
PCT-9	-	-	-	-	5-15%	-	5-15%	Massive	30%	30%	10%	30%	-	Open porphyric (ratio 20/80)	Yellowish gray, opaque, undifferentiated
PCT-10	-	-	-	-	5-15%	-	-	Massive	25%	15%	10%	50%	-	Open porphyric (ratio 20/80)	Yellowish gray, opaque, undifferentiated

Sample name	Horizon	Pedostratigraphic level	Pedofeatures								
			Textural pedofeatures		Amorphous pedofeatures			Crystalline pedofeatures			Passage features
			In situ clay coatings and infillings	Fragmented clay coatings/infillings	Fe-Mn nodules		Fe-Mn hypocoatings	In situ calcite coatings and infillings	Calcite hypocoatings	Calcite nodules	
					Orthic	Disorthic					
PCT-1	B	PL1	Yellowish brown dusty < 2%	-	5-15%	5-15%	-	-	5-15%	-	< %5
PCT-2	Bc	PL1	Yellowish brown limpid 5-15%; brownish dusty < 5%	-	15-30%	15-30%	-	-	-	-	< 2%
PCT-3	2Bt	PL2	Brownish dusty 15-30%; brownish dusty layered 5-15%	-	-	15-30%	< 5%	-	-	-	< 5%
PCT-4	3Bw	PL3	Brownish dusty < 5%	Brownish dusty < 5%	-	15-30%	5-15%	-	-	-	-
PCT-5	3Bw/4BCk	PL3	Orange dusty laminated and not laminated 5-15%	-	-	15-30%	-	-	< 5%	15-30%	-
PCT-6	4BC	PL4	Pale yellow dusty 15-30%; orange limpid 15-30%	Pale yellow dusty < 5%	30-50%	-	-	5-15%	5-15%	5-15%	-
PCT-7	4BC	PL4	Brownish dusty < 2%	-	15-30%	-	< 5%	-	-	15-30%	-
PCT-8	-	-	Yellowish brown dusty < 2%	-	15-30%	15-30%	-	-	-	< 5%	-
PCT-9	-	-	Yellow dusty < 2%	-	< 5%	< 5%	< 5%	-	-	5-15%	-
PCT-10	-	-	Yellow dusty 5-15%	-	15-30%	15-30%	5-15%	-	-	5-15%	-

Table 10: Micromorphological properties of the samples horizons.

The thin sections from the pedostratigraphic levels PL1 (sample PCT-1, PCT-2) and PL2 (slide PCT-3), whose soils developed on the same parent material (loess), show a close porphyric c/f (coarse/fine) related distribution and a massive microstructure. The dominant color of the micromass in PL1 ranges from yellowish gray to yellowish brown, locally brown for the presence of amorphous organic matter. In PL2, the micromass is brownish yellow and presents few sub-vertical yellowish gray depleted areas. The mineral fraction of slides from PL1 consists of frequent (40-50%) quartz and mica grains; in PL2, instead, the quartz grains are dominant (60%), mica grains become common (20%), and igneous minerals are also present. Vesicles mostly constitute the porosity of PL1; in PL2 pores include common channel, planes, and vughs.

Thin sections PCT-4 and PCT-5 derive from the colluvial unit PL3. The slide PCT-4 looks uniform both at the mesoscale and microscale; the slide PCT-5, coming from the transition between the 3Bw and 4BCk horizons, instead, shows some different characteristic. At the mesoscale, in fact, the transition from the 3Bw horizon to the 4BCk horizon can be observed: soil fragments from the upper level appear reworked and included in the underlying weathered marls. From the micromorphological point of view, the thin section PCT-4 presents a single spaced porphyric c/f related distribution and a massive microstructure. On the contrary, thin section PCT-5 shows a double-spaced porphyric c/f related distribution, which locally becomes open porphyric, and a sub-angular blocky structure. In both PCT-4 and PCT-5 thin sections the micromass is reddish brown, opaque, with crystallittic to striated b-fabric and locally few yellowish brown depleted areas are evident. The quartz and mica grains are frequent (30-40%) and also the igneous minerals are common. Moreover, in slide PCT-5 few microfossils inherited from the underlying weathered bedrock are preserved.

PCT-6, from PL4, presents a c/f related distribution ranging from single to open porphyric. The latter is evident also in PCT-7, but therein it locally becomes concave gefuric; a bridged grain microstructure corresponds to this c/f related distribution, while generally the microstructure is massive. The color of the micromass ranges from yellowish orange to yellowish gray and it is cloudy and striated/cross-striated; the thin section PCT-7 also presents few gray depleted areas. The frequency of quartz and mica grains decreases to 20-30%; on the contrary, the amount of microfossils inherited from the bedrock is higher with respect to slides PCT-1 to PCT-5, increasing up to 30% in PCT-6 and 50% in PCT-7 (Fig. 34c). The porosity of PCT-6 consists of frequent planes and chambers, while in PCT-7 planes are common.

Textural, amorphous and crystalline pedofeatures, albeit increasing the level of complexity of the described pedosedimentary sequence, are useful in the interpretation of postsedimentary processes. From the top to the bottom of the pedostratigraphic profile the following observation can be made:

- PL1, in its upper B horizon, is characterized by the presence of rare yellowish brown dusty clay coatings (PCT-1); while in its deeper part, the Bc horizon (slide PCT-2), few yellowish brown limpid clay coatings (Fig. 33b) and very few brownish dusty clay coatings are present. Coarse orthic and disorthic Fe-Mn nodules (Fig. 33a) are common in PCT-1 (horizon B) and frequent in PCT-2 (horizon Bc). Few calcite hypocoatings, related to channel voids left by roots passage, have been also identified in PCT-1.
- PL2 (PCT-3 thin section, from the 2Bt horizon) presents common brownish clay coatings (Fig. 33c), layered when thicker; the amorphous pedofeatures consist of common disorthic Fe-Mn nodules (Fig. 3.20d) and few Fe-Mn hypocoatings.
- Very few brownish dusty clay coatings (Fig. 33f) and fragments characterize the 3Bw horizon of the PL3 (PCT-4 thin section); the lower part of PL3, where the transition from 3Bw to 4BC horizon (PCT-5) is located, presents few orange dusty laminated and not laminated clay coatings and infillings. Common disorthic Fe Mn nodules (Fig. 33e) are present and in the section PCT-5 few Fe-Mn hypocoatings also exist. Calcite coatings and nodules appear only in thin section PCT-5.
- In PL4 common pale yellow dusty clay coatings and fragments and orange limpid clay coatings (Fig. 34a) and infillings have been identified in the 4BC horizon (sample PCT-6); while in the lower part of the 4BC horizon, rare brownish dusty clay coatings are present (PCT-7). The orthic Fe-Mn nodules are frequent at the top of the level and decrease toward the bottom, where, in PCT-7, very few Fe-Mn hypocoatings have been found. The upper part of PL4 is characterized by few calcite coatings, nodules (Fig. 34a) and hypocoatings; the nodules become more common in the deeper PCT-7 thin section (Fig. 34b), while calcite coatings and hypocoatings have not been identified.

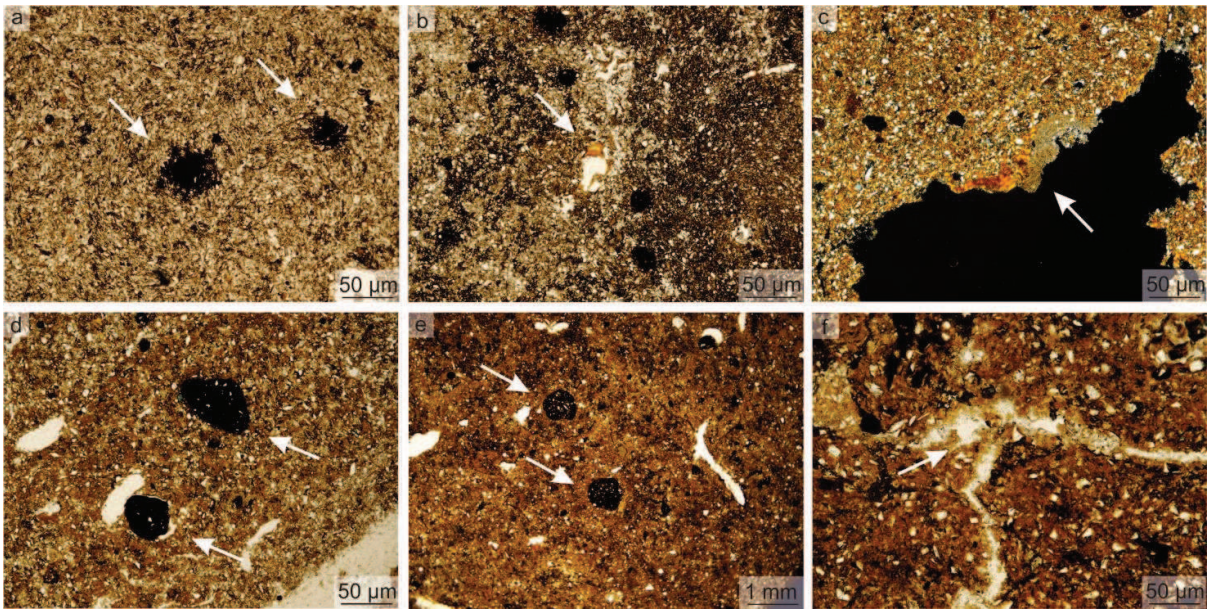

Fig. 33: Photomicrographs of thin sections illustrating pedofeatures related to the loessial (PL1 and PL2) and colluvial (PL3) units. a) Ortich Fe-Mn nodules (indicated by arrows) in the massive microstructure in the B horizon of PL1, PPL (PCT-1). b) Yellowish brown clay coating (indicated by arrows) in the Bc horizon of PL1, PPL (PCT-2). c) Brownish dusty clay coating (indicated by arrows) in 2Bt horizon, PPX (PCT-3). d) Disorthic Fe-Mn nodules (indicated by arrows) in 2Bt horizon of PL2, PPL (PCT-3). e) Reddish brown micromass with interspersed disorthic Fe-Mn nodules (indicated by arrows) in the 3Bw horizon of PL3, PPL (PCT-4). f) Brownish dusty clay coatings (indicated by arrows) along planar voids in the 3Bw horizon of PL3, PPL (PCT-4).

The PCT-8 thin section, presents some peculiarities due to its position inside the damage zone. At the mesoscale, a set of subvertical fractures (corresponding to planar voids at the microscale) and some fragments of marl are observed. At the microscale, the c/f related distribution is close to open porphyric and the microstructure is massive. The micromass is reddish brown, cloudy, cross-striated, locally granostriated and in particular the micromass particles present a parallel sub-vertical orientation (Fig. 34d) aligned along tectonic strain axis. The mineral coarse fraction is composed of frequent (40%) quartz grains, common (20-30%) mica grains and microfossil and few (10%) igneous minerals. The pedofeatures are represented by rare yellowish brown dusty clay coatings, few orthic and disorthic Fe-Mn nodules and rare calcite nodules.

The thin sections PCT-9 and PCT-10 were sampled in correspondence of the fault gouge. The first one appears chaotic, with soil fragments highly weathered by illuvial clay, pinched in the weathered marl. The second slide presents Fe-Mn oxides along planar voids macroscopically consisting of systematic joints, which are crosscut by an illuviated fault gouge (Fig. 34e) and locally deformed in a small-scale kink band anticline, due to a rotational component along the fault gouge.

At the microscale, PCT-9 and PCT-10 present almost the same characteristics, namely an open porphyric c/f related distribution and a massive microstructure. The micromass is yellowish gray, opaque, and undifferentiated. The total amount of quartz, mica, and igneous minerals is between 10

and 30%, while the microfossils are up to 30% in PCT-9 and 50% in PCT-10. The pedofeatures consist in very few yellow dusty clay coatings and infillings; very few to few orthic and disorthic Fe-Mn nodules and coatings; few calcite nodules

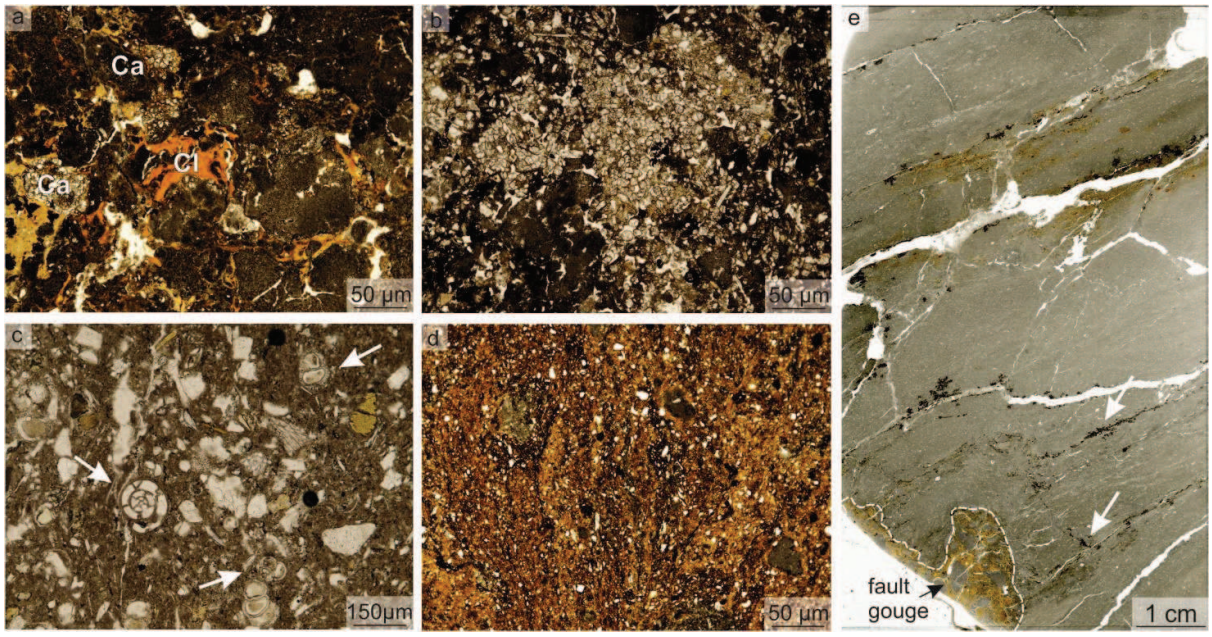

Fig. 34: Photomicrographs of thin sections illustrating (a-c) pedofeatures related to the weathered marls of PL4: a) Orange limpid clay infilling (Cl) and calcite nodules (Ca) in the weathered marls of 4BC horizon, PPL (PCT-6). b) Irregular calcite nodule in the 4BC horizon, PPL (PCT-7). c) Microfossils (indicated by arrows) inherited from the bedrock in the 4BC horizon, PPL (PCT-7). d) Photomicrograph of thin section PCT-8, illustrating the parallel orientation of the constituents of the micromass in a pocket of colluvium (Unit CLa), 4X, PPL. e) Scan of thin section PCT-10 sampled from the fault gouge (Unit FB): the red arrows indicate D1 structural joints, which are crosscut by the gouge associated to D2 fault.

3.3.2.4 Radiometric dating

3.3.2.4.1 AMS-14C dating

AMS-^{14}C dating (Table 11) was performed by Beta Analytic on the organic fraction of three samples, collected at the top of PL1 (PEC-1), at the bottom of PL2 (PEC-2) and at the uppermost part of PL4 (PEC-3), at depths ranging from 60 to 210 cm. The uppermost sample was dated at 4000 ± 30 years BP (4525 - 4415 cal age BP), while PEC-2 and PEC-3 were dated at 29180 ± 150 and 26300 ± 110 years BP (33705 - 33060 and 30810 - 30445 cal age BP), respectively.

Sample name	Pedostratigraphic level	Depth (cm)	δ13C ‰	Uncal 14C age (years BP)	Cal 14C age (±2σ) (years BP)
PEC-1	PL-1	60	- 22.9	4000 ± 30	4525-4415
PEC-2	PL-3	170	-24	29180 ± 150	33705-33060
PEC-3	PL-4	210	- 23.4	26300 ± 110	30810-30445

Table 11: AMS-^{14}C for the Pecetto di Valenza section; 2σ range is calculated using Calib 7.0 software (Stuiver et al., 2013) and INTCAL13 calibration curve (Reimer et al., 2013). Analysis performed by Beta Analytic Lab.

3.3.2.4.2 OSL/TT-OSL dating

Sample	Burial Depth (m)	Water contents (%)	K (%)	U (ppm)	Th (ppm)	Dose Rate (Gy/ka)	No. of aliquots	OSL / TT-OSL	O-D	DE (Gy)	Age (CAM) (ka)
PCT-1	0.4	10	2.06	3.7	16.6	3.85 ± 0.14	15/21	OSL	87	10 ± 2	3 ± 1
PCT-2	0.8	10	2.06	3.9	17	3.86 ± 0.14	18/20	OSL	60	47 ± 5	12 ± 2
PCT-3	1.25	10	1.99	3.5	15.3	3.63 ± 0.15	10	TT-OSL	21	270 ± 18	75 ± 6
PCT-4	1.6	10	1.7	3.2	15.2	3.31 ± 0.13	10	TT-OSL	14	358 ± 16	108 ± 7

Table 12: OSL and TT-OSL data and ages for the Pecetto di Valenza samples, performed at the luminescence laboratory of the Geological Survey of Israel. The central age model (CAM) was used to obtain representative De values, with standard errors propagated to the age errors. No. of aliquots — the number of aliquots accepted for De determination out of those measured. OD — over-dispersion.

The luminescence ages obtained at Pecetto di Valenza site range from 108 ± 7 ka to 3 ± 1 ka (Table 12). One sample has been collected from the lower part of the weathered loessial PL2 level, dating back to 108 ka. Three other samples have been collected within the PL1 level, which yielded an age between 75 and 3 ka. The ages are in stratigraphic order.

The four sediment samples were collected by hammering iron tubes into the excavated section. The sampling positions are indicated in Fig. 29. The purified quartz was extracted in the luminesce dating laboratory of the Geological Survey of Israel following the procedures described in paragraph 2.5.2.3. The two uppermost samples (PCT-1 and PCT-2) have been dated using the OSL method, while the two lowermost ones (PCT-3 and PCT-4) have been dated by TT-OSL dating method (Table 12). This choice is based on the preliminary *sample test*, in which two aliquots for each sample were measured using the conventional single aliquot regenerative dose (SAR) protocol. The purpose of this test was to determine the maximum dose that can be given to a sample in the subsequent measurements and to check if the luminescence signal reaches the saturation. In the case of PCT-3 and PCT-4 the signal reached the saturation, therefore has been decided to perform the TT-OSL method.

The purified quartz from PCT-1 and PCT-2 was placed on 9.8 mm aluminium discs (aliquots) using 2 mm masks and silicon spray as an adhesive. Equivalent dose (De) was measured using the SAR protocol (Murray and Wintle, 2000). The OSL signal of the quartz is dominated by the fast component (Fig. 35). Preheat temperatures were selected according to dose recovery tests over a range of temperatures carried out on PCT-1 sample. These showed that a recovery of 95-100 % is achieved using a pre-heat of 10 s at 220 °C, a test dose of ~ 9 Gy and a test dose pre-heat of 5 s at 200 °C (Fig. 36).

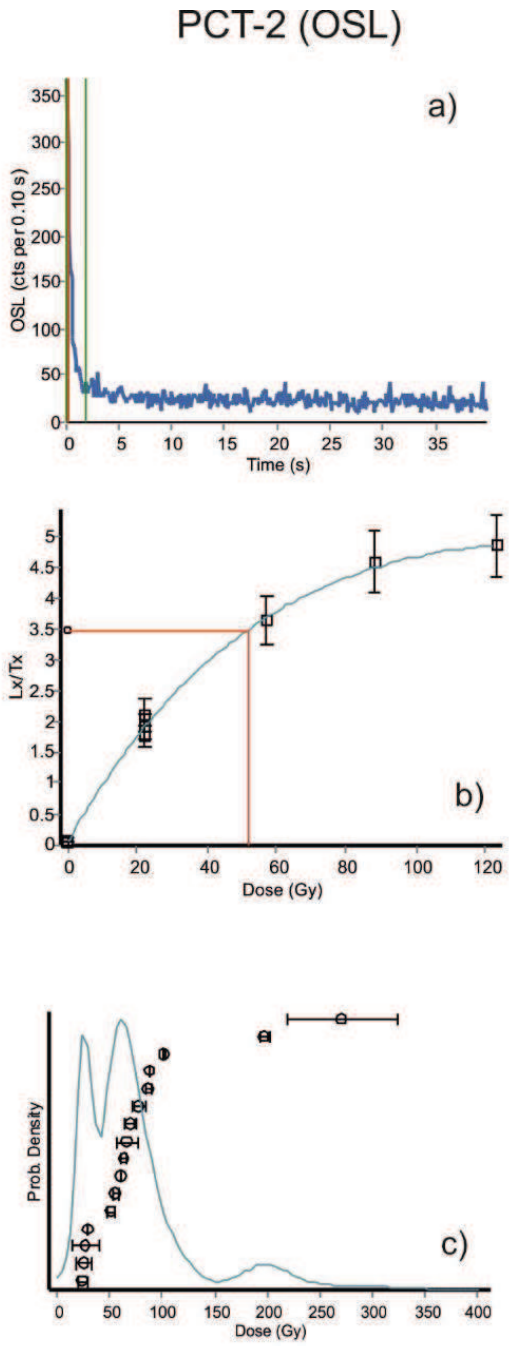

Fig. 35: OSL results for sample PCT-2: a) the first seconds of the natural OSL signal; b) dose response curve for the same aliquot; c) A probability density function plot with individual De values and errors. Note the positively-skewed distribution with OD = 60% indicating an inadequate bleaching of the material.

Twenty aliquots were measured for each sample. Each aliquot was irradiated stepwise and normalized until the natural signal was regenerated. Dose response curves were constructed from five dose points (Fig. 35b), two of which were repeats (a regular recycling point and an IR depletion ratio point) and two zero-dose points. After distinct outliers were removed (the ones with a recycling ratio up to 10%), the central age model (CAM; Galbraith and Roberts, 2012) was used to obtain a representative De value, with standard errors, which were propagated to the age errors.

The homogeneity of the samples is expressed by the over-dispersion (OD) parameter which represents the scatter in the De values (Fig. 35c). For PCT-1 and PCT-2 the OD values is more than 60%, indicating that the samples have heterogeneous depositional histories. The most likely source of this scatter is related to partial bleaching during any steps of the transport (Arnold and Roberts, 2009), or post-depositional reworking. Therefore, the PCT-1 and PCT-2 OSL ages are only a rough estimate of their deposition time.

The purified quartz from PCT-3 and PCT-4 was placed on 9.8 mm aluminium discs using 5 mm masks and silicon spray as an adhesive. The equivalent dose (De) measurement used the simplified SAR protocol for TT-OSL from Porat et al., 2009. For each sample ten aliquots have been measured. The dose response curves have been constructed from four dose points (Fig. 37a), two of which have been repeated and two zero-dose points. Both samples showed recycling ratios lower than 10%, implying that the protocol is appropriate. Also here, the most representative De value for each sample was calculated using the central age model. The distribution of the De values is close to normal (Fig. 37b), with OD values of 21 % for PCT-3 and 14 % for PCT-4, indicating that the samples were exposed to sunlight for a short period, enough to bleach some of the OSL signal but not any of the TT-OSL signal (Zaidner et al., 2017). Therefore, the TT-OSL ages for PCT-3 and PCT-4 can be considered representative of a pristine deposition.

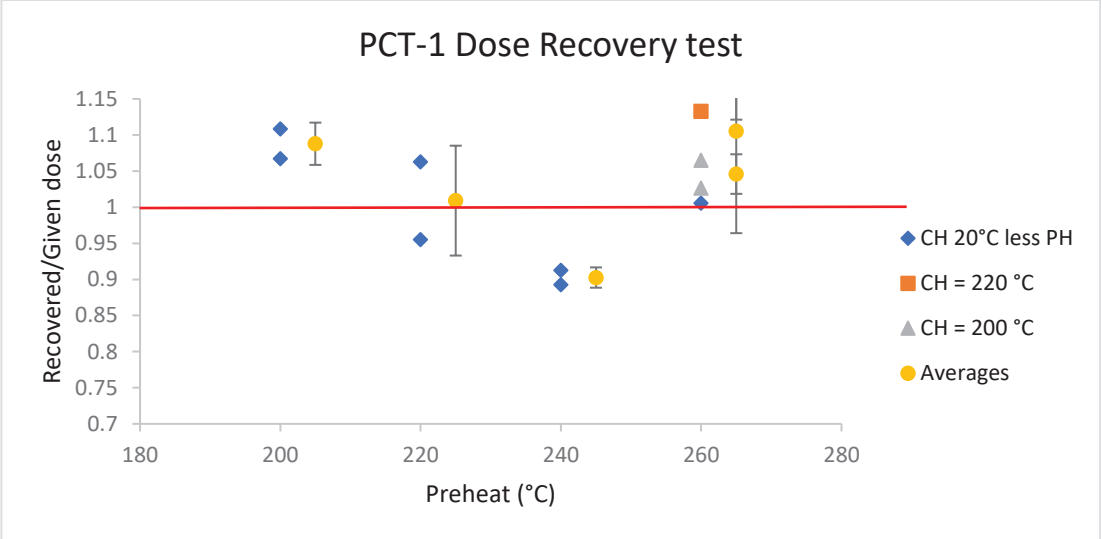

Fig. 36: Dose recovery over a range of pre-heat temperatures for sample PCT-1. Test dose (TD) preheat was at 20 °C below pre-heat temperature in all cases. Dose recovery of over 95% is achieved using pre-heat temperature of 220 °C and TD pre-heat of 200 °C. Individual aliquots are shown as diamonds, triangles and squares, while averages with errors as full circles.

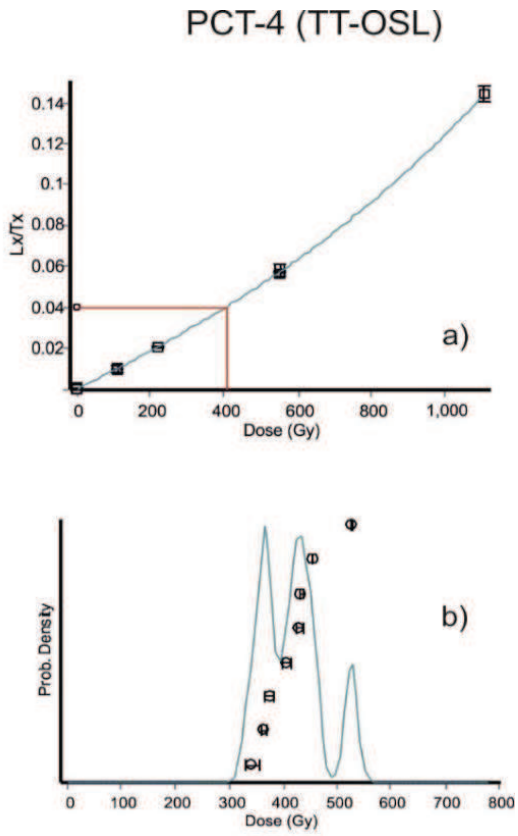

Fig. 37: TT-OSL results for sample PCT-4: a) dose response curve for an aliquot; b) a probability density function plot with individual De values and errors. Note the almost normal distribution, with OD < 20% indicating well bleached material.

3.3.2.5 Structural data

Bedrock is uniformly dipping N140°/25° and no folding is present. A first set of systematic jointing, ca. NNE-SSW striking, affects the bedrock marls, with abundant Fe-Mn coatings present at the joint surface (Fig. 38b). We define these features as pertaining to a first deformation phase (D1) recorded by this surface. These joints, showing no evidence of shear components, are mode I extensional fractures. The unfolding of the data, according to the local bedding orientation, gives an average orientation for this set of N109°/59°, thus possibly consistent with a local extensional regime. Weathering of the bedrock (4BCk/4BC of PL4) partially bleaches the D1 joints.

A major reverse fault zone cuts through the marls (PL4), displacing the base of PL3, the base of PL2, and, in one point, the base of PL1. The fault zone consists of several fault strands, steeply dipping to the ESE, characterized by anastomosed slip planes showing clear kinematic indicators (i.e. slickensides). Secondary conjugate WNW-dipping faults are also present. A well-developed fault gouge is present in the fault damage zone with cm-scale angular to sub-angular bedrock fragments included in an abundant matrix. We define all these structural features as belonging to D2 deformation set, systematically crosscutting or deforming D1 set (Fig. 38). Two sets of conjugate joints, with orientations close to those ones of the faults (i.e., N96°/39° and N279°/62°; Fig. 38b), can be ascribed to D2: these

joints do not have a clear crosscut relationship with D1 joints but they are not bleached by weathering of the bedrock and crosscut younger units (PL3 and PL1). All D2 reverse faults cut through PL3 and one fault strand displaces the base of PL2 and some fragments from the base of PL3 are included in the fault gouge (Fig. 34e).

We calculated total net slip from separation on the logged section, basing on the relative orientation of the faults, slickensides, mark horizon and line of observation (Xu et al. 2009; TruDisp software; Nieto-Fuentes et al. 2014). The four main fault strands, considering the base of Unit PL3 as the marker horizon, record a total net displacement of 4.8 m.

We performed a slip inversion analysis from fault data with kinematic indicators. The software FaultKin v.6 (Allmendinger et al., 2001) was used to make the calculations. Firstly, we followed a kinematic approach (i.e., Unweighted Moment Tensor Solution) to derive strain axes from fault geometry and slip direction. This method assumes that slip direction on fault is parallel to the maximum resolved shear rate of a large-scale homogeneous strain rate tensor (e.g., Marret and Allmendinger, 1990). The collected data (n. 20 faults) point to a N304° sub-horizontal axis of compression and sub-vertical extension one, thus consistent with a compressive regime with a NW-SE oriented shortening axis. If we consider only the principal fault strands (n. 4) with a measurable offset at the base of PL3 and we perform a slip inversion kinematic analysis weighted on the relative true displacement, we obtain a similar strain axis distribution, with maximum shortening axis close to horizontal, after performing a backrotation of the data according to local bedding.

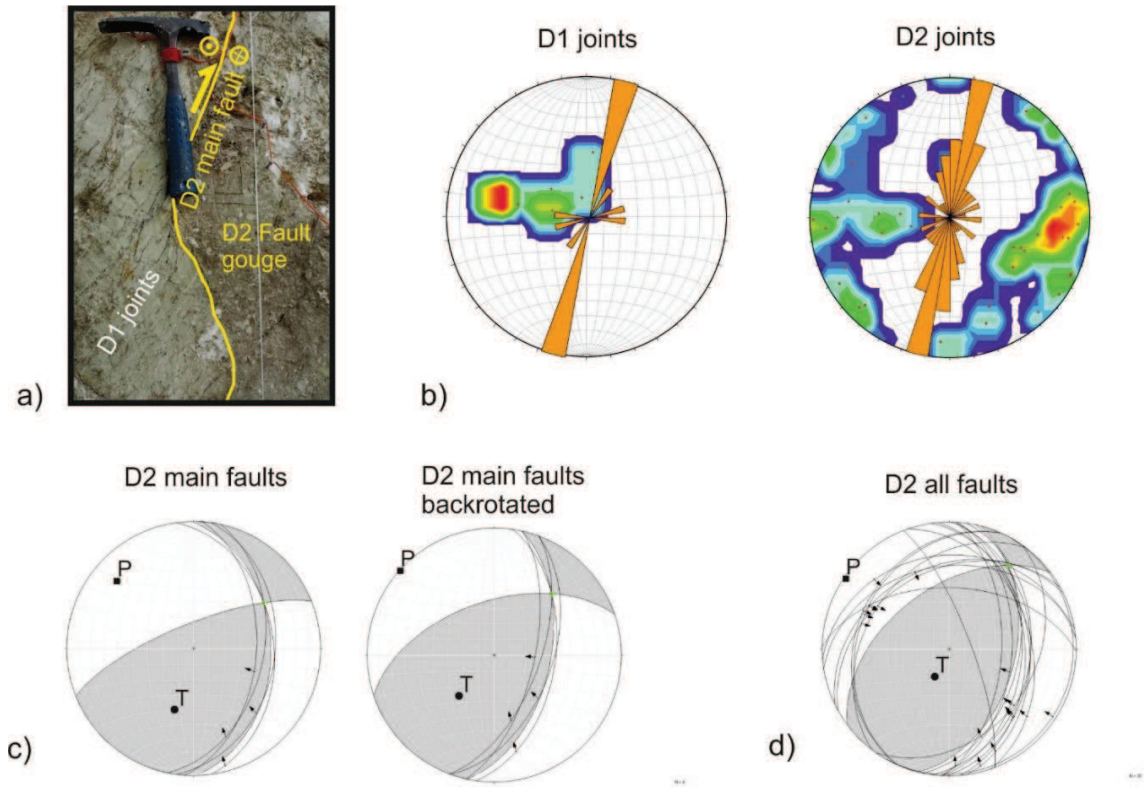

Fig. 38: a) detail on the fault zone where D1 structural joints are systematically crosscut by D2 faults and associated gouge; b) orientation of D1 and D2 joint sets; c) kinematic strain analysis of D2 main faults, weighted on their calculated slip, performed according to their present orientation or after backrotation of the local bedding: stretching (T) and shortening (P) axes are indicated; d) kinematic analysis performed on the whole faults dataset. All the stereonets are equiareal lower hemisphere.

4. The Monte Netto site

Monte Netto (Capriano del Colle, northern Italy) is an isolated hill (e.g., Desio, 1965), located along a buried structural front of the central Southern Alps, facing the most external buried fronts of the northern Appeninnes beneath the Po Plain foredeep (e.g., Castellarin and Vai, 1986; Castellarin et al., 2006; Fantoni et al., 2004; Fig. 39). The emergence of the hill is due to the recent growing of an anticline related to a fault system composed of a main south-vergent forethrust and an associated high-angle backthrust (Livio et al., 2009; 2014).

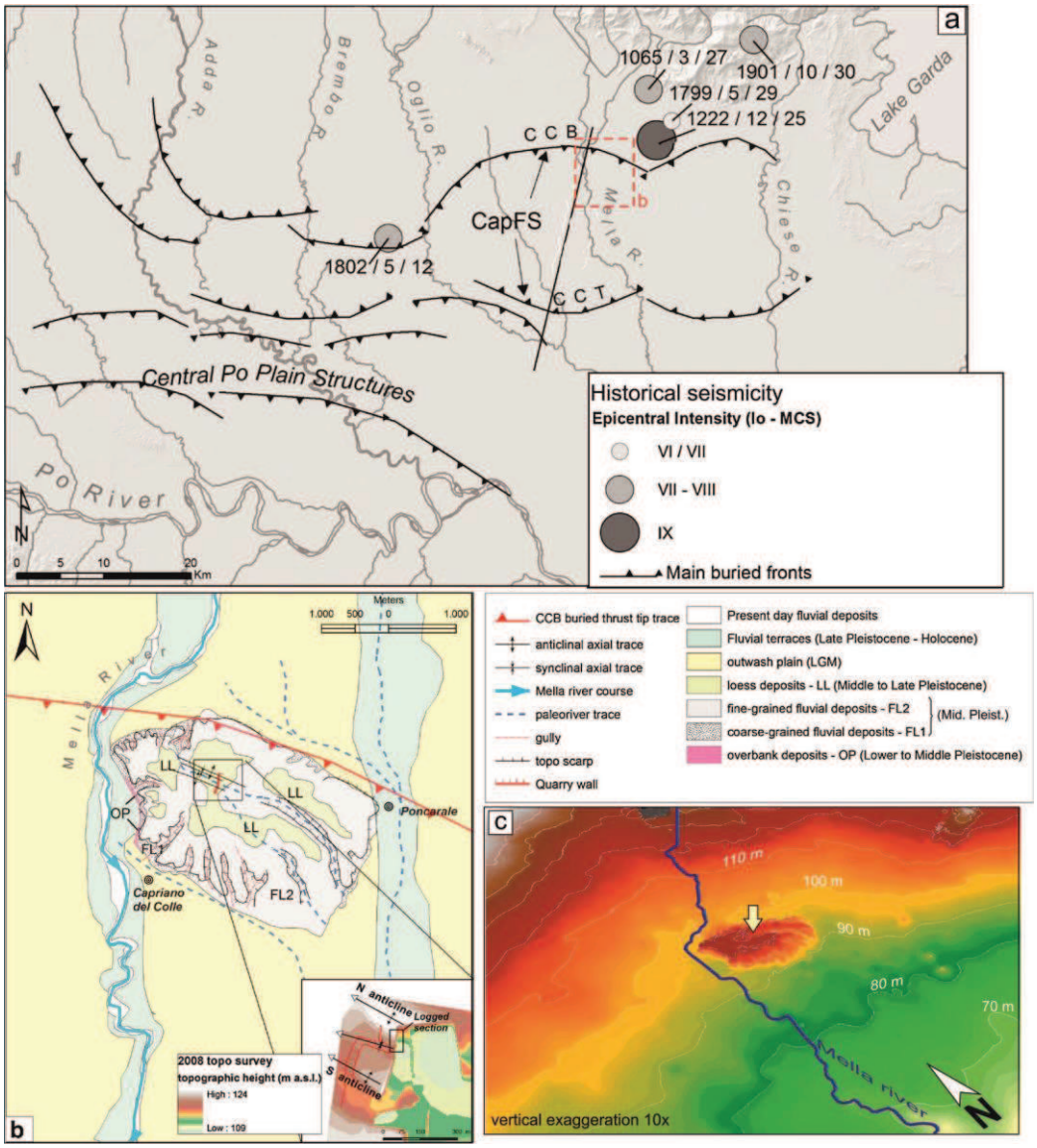

Fig. 39: Monte Netto site; a) map of buried thrust (modified after Livio et al., 2014) as revealed by the analysis of an extensive database of seismic reflection lines (courtesy of ENI E&P) and historical and instrumental seismicity data (CPTI catalogue; Rovida et al., 2016); b) geological sketch map of the Monte Netto area and (inset) detail on a topo survey of the quarry area (Livio et al., 2014), acquired in 2008: the hinge traces of the outcropping fold underline that structural relief is closely mimicked by topography; c) 3-D persepctive of the Monte Netto hill elaborated from a 20 m digital elevation model. The white arrow indicates the location of the studied quarry.

At the top of the hill, during excavation works at the Danesi clay quarry, an outcrop ca. 4 m deep displaying a sequence of loess deposit interlayered with paleosols with different degrees of maturity has been exposed (Fig. 40; Livio et al., 2014; Zerboni et al., 2015). The peculiarity of this site is the occurrence of tectonic deformation that affected the loess and paleosol horizons in the form of faults and folds (Fig. 40b; Livio et al., 2009; 2014). Here, cross-disciplinary investigations of the interplay between sedimentation, erosional processes, pedogenesis, earthquake surface faulting and active tectonics allowed reconstructing the Late Quaternary evolution and the local seismic hazard (Livio et al., 2014; Zerboni et al., 2015). The paleopedological analysis, including field description of the sequence, micropedological analysis and radiocarbon and luminescence dating, allowed to reconstruct the evolution of this pedostratigraphic sequence (Zerboni et al., 2015). The methods of investigation here applied are the same descripted in chapter 2, except for radiocarbon and luminescence dating.

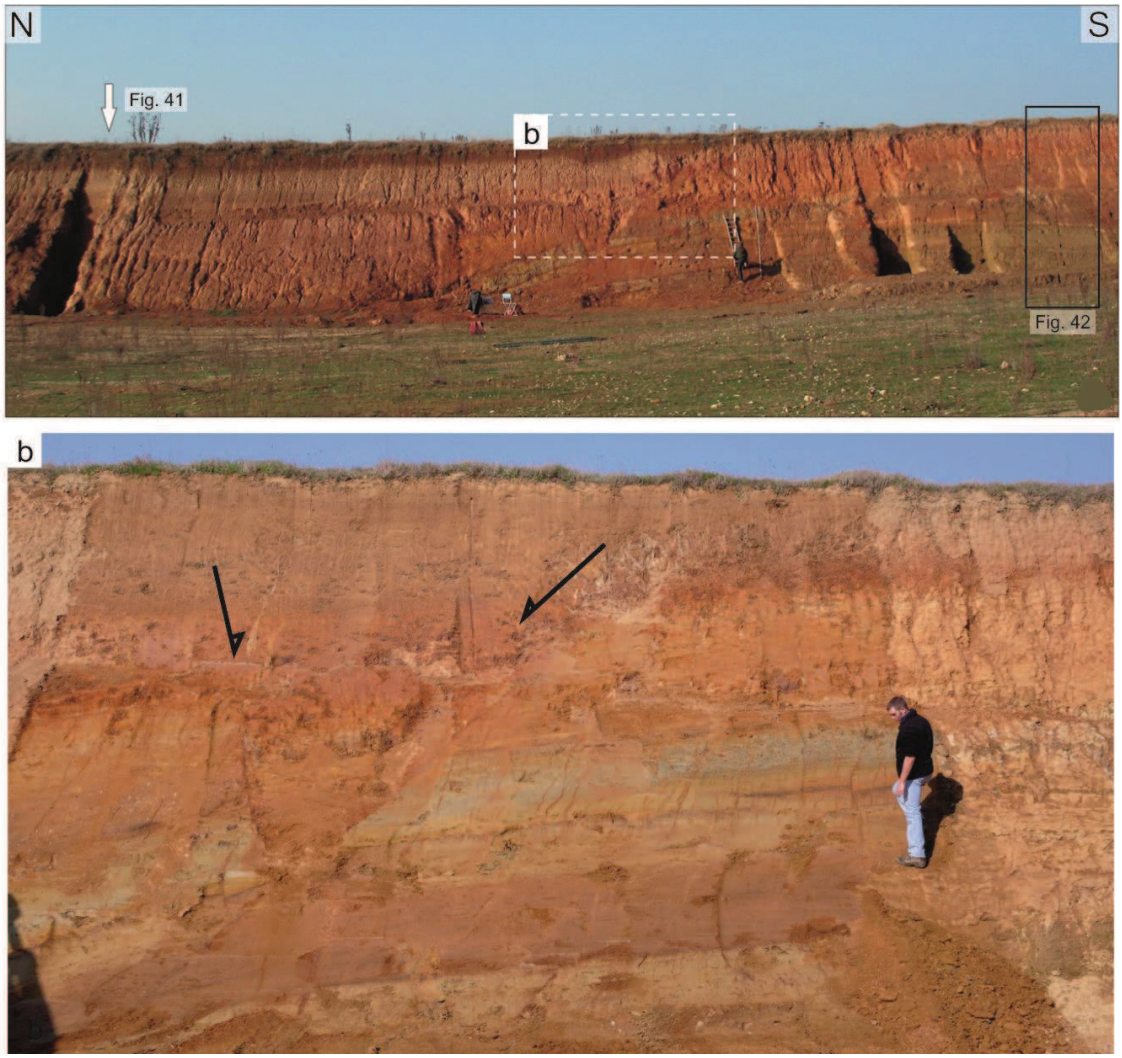

Fig. 40: Exposure at Monte Netto; a) the central part of the section, which includes loess, paleosols and fluvial sediments forms an anticline (the anticline crest is on the right). The white arrow indicates the thickest sequence, represented in Fig. 4.3; while the black box locates the condensed sequence at the top of the anticline, represented in Figure 4.4. The white box locate figure b): the brittle, secondary, fold-related faulting, dislocating loess strata and paleosols in the central part of the anticline (modified after Zerboni et al., 2015).

The AMS-^{14}C analysis was performed on three samples (see Fig. 41 for the position) at the CEDAD Laboratory (Lecce, Italy) on the total organic fraction after removing contaminants by acid-base-acid treatment. The dates were calibrated (2σ range) using Calib 7.0 software (Stuiver et al., 2013) and INTCAL13 (Reimer et al., 2013). The ages obtained are reported in Table 13. The OSL analysis were performed on three samples (see Fig. 40b for the position) at the luminescence dating laboratory of Innsbruck. The samples were prepared following the standard techniques proposed by Wintle (1997). The D_e was measured for 24 aliquots of each sample, using the double single-aliquot regenerative-dose protocol; then, the central age model (CAM; Galbraith et al., 1999) was used to obtain a representative De value. The ages obtained are reported in Table 14.

The pedostratigraphic characterization presented in Zerboni et al., 2015, has been conducted where the loess/paleosols sequence was better expressed, in correspondence with the synclinal part of the fold. This is illustrated in Fig. 41. The lowermost soils, developed on fluvial/fluvioglacial and colluvial sediments (PL5 and PL4) likely formed during MIS 7 and MIS 5 interglacials. Dust accumulation started when climate reached glacial conditions and the Po Plain was an arid steppe during the MIS 4. Finally, a long polycyclic cold phase, interrupted by brief interstadials, permitted the formation of the overhead loess units (PL3, PL2, PL1).

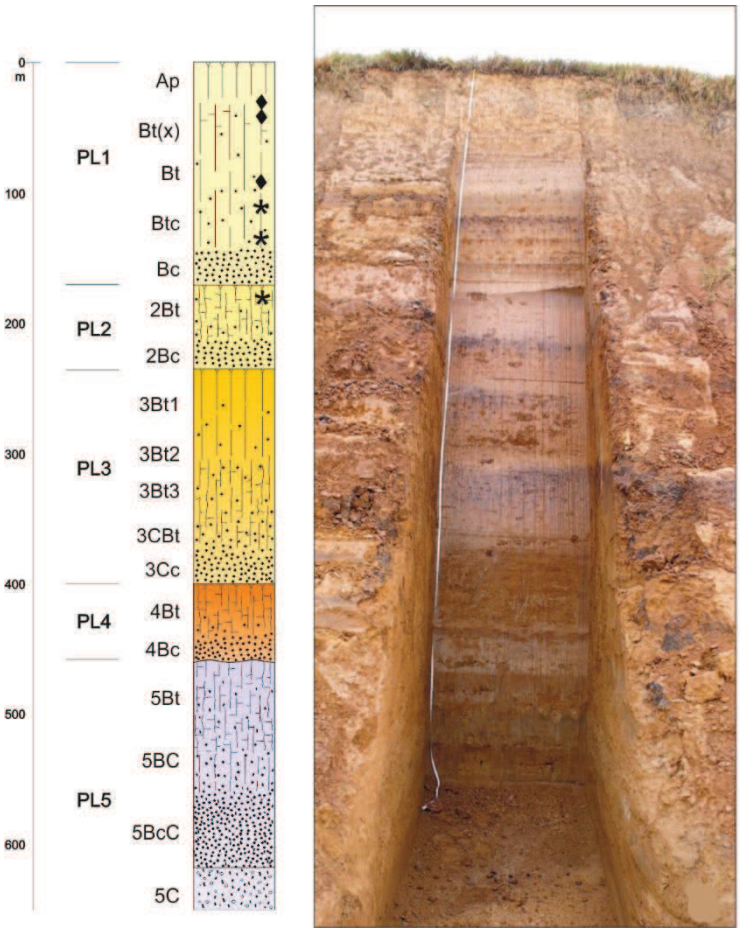

Fig. 41: On the right, the main investigated profile investigated in Zerboni et al., 2015, located at the southern fringe of the quarry and drawn on the left. The position of the OSL (stars) and AMS-^{14}C (diamonds) dating are indicated.

Sample	Pedostratigraphic level	No. of aliquots	Dose Rate (Gy/ka)	DE (Gy)	Age (ka)
CC01	PL1	24	7.37 ±0.88	146 ± 3	19.9 ± 2.3
CC02	PL1	24	7.01 ±0.83	173 ± 4	24.6 ± 2.9
CC03	PL2	24	7.22 ±0.89	321 ± 9	44.4 ± 5.4

Table 13: OSL ages for the Monte Netto section dated in Zerboni et al., 2015

Sample name	Pedostratigraphic level	Depth (cm)	δ13C ‰	Uncal 14C age (years BP)	Cal 14C age (±2σ) (ka BP)
CAP01	PL1	40	- 22.5 ± 0.3	4635 ± 45	5574-5094
CAP02	PL3	50	-28 ± 0.3	6485 ± 50	7483-7287
CAP03	PL4	100	-33.7 ± 0.5	13313 ± 75	16241-15772

Table 14: Details of dosimetry calculations for samples dated from the Monte Netto section (Zerboni et al., 2015)

The integration of these investigations with the structural tectonic ones provided also the paleoseismological evolution of Monte Netto area. As mentioned above, the origin of the anticline at the core of the section was triggered by a buried backthrust. The superficial expression of this blind fault is a complex system of fault-related folds, which deform the fluvial/fluvioglacial sediments. This process, probably occurring during the Middle Pleistocene, led to the uplift of the parent material of PL5, its weathering under warm interglacial conditions (MIS 7?) and its subsequent truncation (MIS 6?). The continuous growth of the structural crest of the anticline led to the asymmetric development of the sequence. The emergence of a morphological relief allowed the onset of erosional processes and the deposition of a thick colluvial unit (PL4) at the base of the anticline (MIS 6?). PL4 also underwent strong pedogenesis under interglacial conditions (MIS 5?) and was then buried by loess deposited under glacial conditions (possibly MIS 4 and definitely during MIS 3 and MIS 2). These loess deposits, whose deposition and preservation has been favoured by the topographic obstacle represented by the Monte Netto hill, act as valuable stratigraphic marker of tectonically induced near-surface deformation.

4.1 The 2013 condensed loess/paleosols sequence

During the INQUA-AEOMED field-trip workshop 'Reconsidering Loess in Northern Italy' (Po Plain, July 2013; Amit and Zerboni, 2013), aimed at better understanding the process of Po Plain loess formation, transportation, accumulation, distribution and its association with soil formation and climate, five main loess sequences in the Southern Alps and Apennines piedmont belts have been sampled for OSL/TT-OSL dating. The Monte Netto site was among these sequences. Unfortunately, the pedostratigraphic sequence located on the synclinal part of the fold described in Livio et al. (2014) and Zerboni et al. (2015) no longer existes, due to the progression of the excavation work in the quarry. Nevertheless, the southernmost part of the wall, in correspondence with the top of the anticline, has been preserved and therefore sampled for the luminescence analysis (Fig. 42). Due to the growing of the anticline described in Livio et al. (2009; 2014), this sequence (NMNT hereafter) show a condensed stratigraphy compared to the one described in the synclinal part of the fold (see above; OMNT hereafter). Indeed, it is represented only by three pedostratigraphic levels. The detailed field descriptions are reported in Table 15. The first pedostratigraphic level is represented by a thin sequence of B horizons (Bt and Bc), displaying a higher degree of clay illuviation and a darker colour. The intermediate pedostratigraphic level is constituted by the 2Bt and 2Bc horizons, developed in a slightly coarser parent material. They also exhibit a high degree of clay mobilization and accumulation of Fe-Mn nodules. The lowermost PL of the sequence is represented by fluvial sediments, which are slightly weathered at their top.

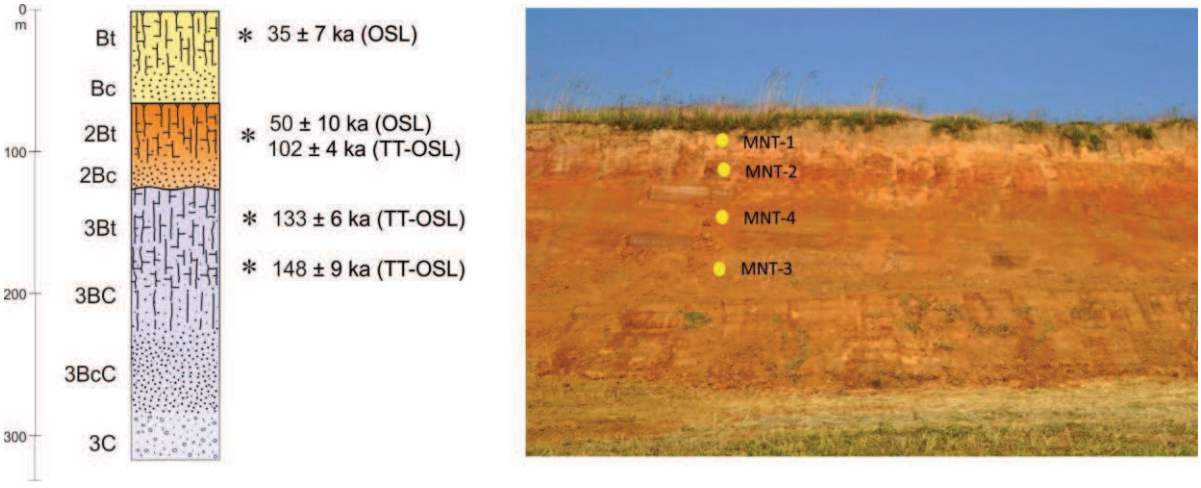

Fig. 42: The condensed pedostratigraphic sequence identified in 2013 (NMNT) at the top of the anticline at Monte Netto site: on the left is represented the pedostratigraphic column with the distribution of soil horizons. The position of OSL/TT-OSL dating results are also indicated.

Horizon	Depth (cm)	Description
Bt	0-40	Silt loam; yellowish brown (10YR 5/4); common mottles very dark grayish brown (10YR 3/2); subangular blocky structure; firm; very few fine Fe –Mn nodules; common clay coatings; very few small pores; gradual lower boundary
Bc	40-60	Silt loam; very dark brown (10YR 2/2); massive; abundant (60 –80 %) coarse to fine Fe – Mn nodules (up to 1 cm) in the silty clay matrix; yellow (2.5Y 7/8) matrix; firm; few small pores; abrupt lower boundary
2Bt	60-100	Clay loam; yellowish red (5YR 4/6); common mottles black (5YR 2.5/1) to dark reddish brown (5YR 2.5/2); subangular blocky structure; moderately firm; common clay coatings; few to common Fe–Mn coatings; very few Fe –Mn fine nodules; few small pores; gradual lower boundary
2Bc	100-120	Clay loam; very dark brown (10YR 2/2) to dark reddish brown (5YR 3/3); massive; abundant (60 –80 %) coarse to fine Fe –Mn nodules (up to 1 cm) in the silty clay matrix; reddish brown (5YR 4/4) silty matrix; firm; few small pores; abrupt lower boundary
3Bt	120-190	Silty clay loam; strong brown (7.5YR 5/8); common mottles dark reddish brown (5YR 3/4); subangular blocky structure; firm; few small pores; common Fe–Mn nodules; common Fe –Mn coatings; common clay coatings; gradual lower boundary
3BC	190-130	Clay loam; strong brown (7.5YR 5/8); common mottles dark reddish brown (5YR 3/4); subangular blocky structure; firm; few small pores; very common Fe –Mn nodules (locally abundant); very common Fe–Mn coatings; common clay coatings; gradual lower boundary
3BcC	130-220	Loam; very dark brown (10YR 2/2); massive; abundant (60 –80 %) coarse to fine Fe–Mn nodules in the silty clay matrix; strong brown (7.5YR 4/6) silty sandy matrix; firm; very few calcium carbonate nodules; few small pores; abrupt lower boundary
3C	>220	Sequence of unweathered sediments including strata of clay, silt, sand, coarse sand and fine gravel; laminated to massive; very few calcium carbonate nodules; very few Fe–Mn nodules; lower boundary not reached

Table 15: Field properties of NMNT sequence

Four samples for the new luminescence dating were collected by hammering iron tubes into the NMNT section. The sampling positions are indicated in Fig. 42. The uppermost sample (MNT-1) was collected in a unit developed on aeolian parent material (loess); MNT-2 was sampled on a soil developed on the fluvial material composing the underlying PL with an aeolian contribution; MNT-4 and MNT-3 were collected in units composed of fluvial/fluvioglacial materials only in part affected by weathering. The purified quartz was extracted in the luminesce dating laboratory of the Geological Survey of Israel following the procedures described in paragraph 2.5.2.3.

The luminescence dating results are shown in Tables 16 and 17. Note that each sample has been dated using both OSL and TT-OSL methods: since during the *sample test* all the samples showed De values greater than 100 Gy, it was decided to measure De values also using the TT-OSL signal.

Sample	Burial Depth (m)	Dose Rate (Gy/ka)	OSL / TT-OSL	No. of aliquots	O-D	DE (Gy)	Age (ka)
MNT-1	0.80	2.96 ± 0.09	OSL	6	17	103 ± 21	**35 ± 7**
			TT-OSL	10	13	*290±12	*98±5
MNT-2	1.80	3.43 ± 0.12	OSL	5	16	171 ± 34	**50 ± 10**
			TT-OSL	10	8	*351 ± 9	***102 ± 4**
MNT-4	2.90	3.26 ± 0.11	OSL	6	69	289 ± 222	89 ± 68
			TT-OSL	8	8	*434 ± 14	***133 ± 6**
MNT-3	4.50	3.41 ± 0.12	OSL	6	23	168 ± 46	49 ± 14
			TT-OSL	8	14	*505 ± 26	***148 ± 9**

Table 16: OSL and TT-OSL data and ages for the NMNT sequence. The Central Age Model (CAM) was used for the samples dated with TT-OSL (indicated with a star), to obtain representative De values, with standard errors propagated to the age errors. The Unweighted model has been used to calculate the De values for all the other samples dated with OSL. No. of aliquots = the number of aliquots accepted for De determintation out of those measured. OD = over dispersion. Final ages considered in this project are in bold.

Sample	Burial Depth (m)	Water contents (%)	K (%)	U (ppm)	Th (ppm)	Dose Rate (Gy/ka)
MNT-1	0.8	10	1.16	3.8	14.5	2.96 ± 0.09
MNT-2	1.8	10	1.33	5	15.8	3.43 ± 0.12
MNT-4	2.9	10	1.41	4.5	14.5	3.26 ± 0.11
MNT-3	4.5	10	1.49	4.4	15.7	3.41 ± 0.12

Table 17: Dose rate for the NMNT samples.

The OSL ages were obtained measuring the equivalent dose on 5/6 aliquots of 2 mm from each sample, following the conventional SAR protocol (Murray and Wintle, 2000). The OSL signal of the quartz is dominated by the fast component (Fig. 44a). Preheat temperatures were selected according to dose recovery tests over a range of temperatures carried out on MNT-1 sample. These showed that a recovery of 95-100 % is achieved using a pre-heat of 10 s at 220 °C, a test dose of ~ 9 Gy and a test dose pre-heat of 5 s at 200 °C (Fig. 43).

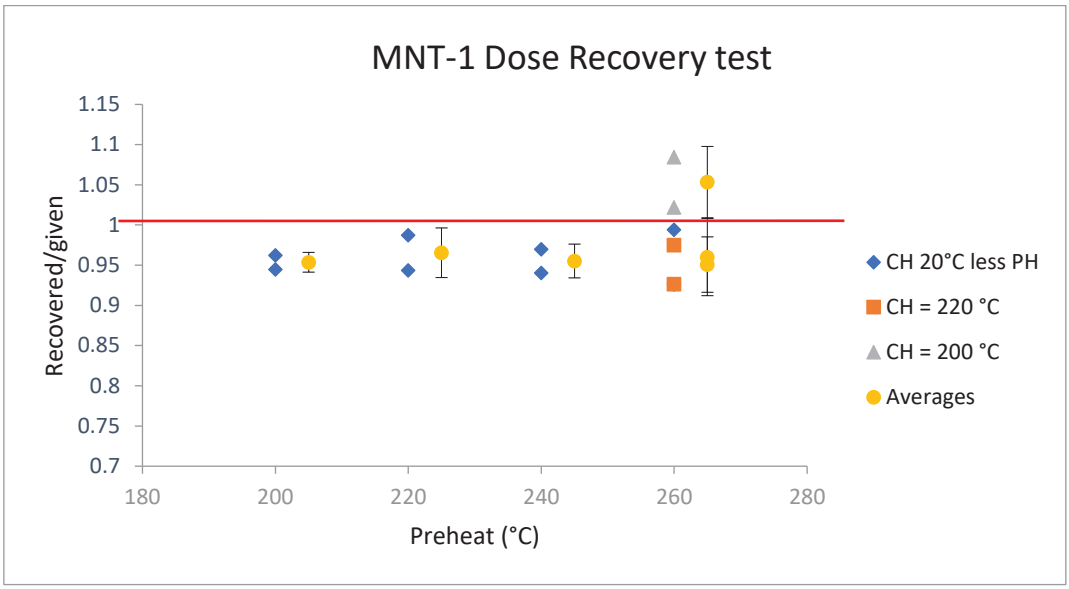

Fig. 43: Dose recovery over a range of pre-heat temperature for sample MNT-1. Test dose preheat was at 20 °C below pre-heat temperature in all cases. Dose recovery of over 95% is achieved using a pre-heat 220 °C, and a test dose pre-heat of 5 s at 200 °C. Individual aliquots are shown as diamonds, triangles and squares, while averages with errors as full circles.

Dose response curves were constructed from five dose points (Fig. 44b), two of which were repeats (a regular recycling point and an IR depletion ratio point) and two zero-dose points. All samples showed recycling ratios smaller than 10%. The De values have been obtained through the unweighted average between all the aliquots of the same sample. The little scatter for the OSL ages of MNT-1 and MNT-2 (OD < 20%) indicates that the grains have been homogeneously bleached (Arnold and Roberts, 2009): thus, 35 ± 7 ka and 50 ± 10 ka, are reliable ages. Instead, the OSL ages for MNT-4 and MNT-3, present a large scatter (OD > 20%; Fig. 44c), meaning that the sediments were partially exposed to light, otherwise, the samples might have been contaminated by mineral grains not bleached, transported in the lower part of the sequence due to pedoturbation. Moreover, these ages are not in stratrigraphical order and are not consistent with similar units dated in other studies (Muttoni et al., 2003; Scardia et al., 2006) and with reliable models describing the seismo-tectonic evolution of the hill (Livio et al., 2014). Therefore, they were not taken into account.

The TT-OSL ages were obtained measuring the De values on eight to ten 5 mm aliquots for each sample, using the protocol of Porat et al., 2009. The dose response curves have been constructed from four dose points (Fig. 44d), two of them have been repeated and two zero-dose points. After distinct outliers were removed (aliquots showing a recycling ratio upper than 10%), the central age model (CAM; Galbraith and Roberts, 2012) was used to obtain a representative De value, with standard error, which were propagated to the age errors. All the samples present a very little scatter in the TT-OSL distribution (Fig. 44f), suggesting that the samples were exposed to sunlight briefly, enough to bleach some of the OSL signal but not enough to bleach any of the TT-OSL signal (Zaidner et al., 2017).

Therefore, all the TT-OSL ages should be considered representative of the original time deposition. Nevertheless, the uppermost sample (MNT-1), dates 99 ± 14 ka, which is not coherent with the ages obtain for the corresponding unit in Livio et al., 2014 and Zerboni et al., 2015: therefore, this age, has not been considered.

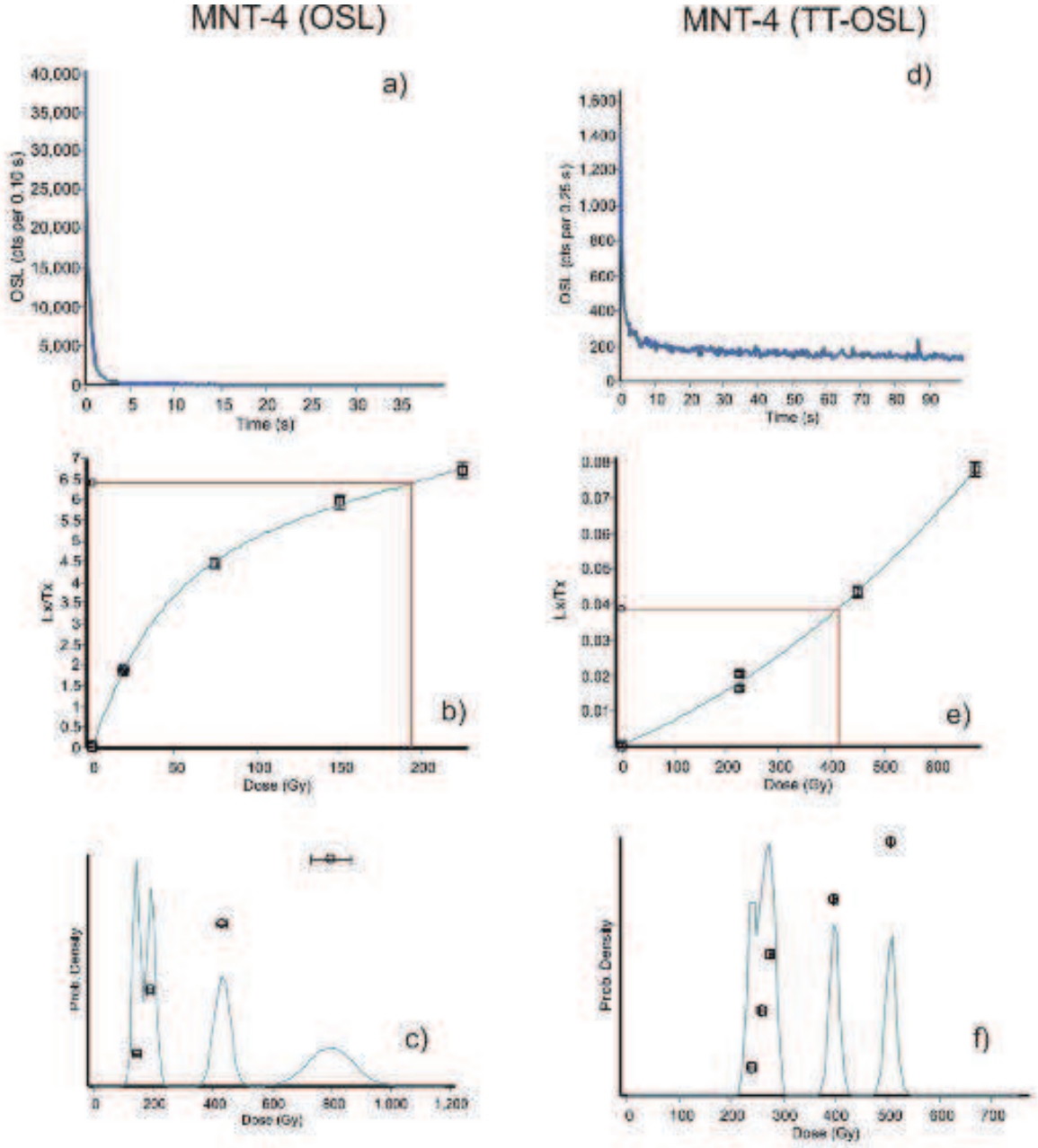

Fig. 44: OSL, on the left and TT-OSL, on the right, results for MNT-4 sample; a) the first seconds of the natural OSL signal. Note that the signal decays to less than 1% within 2 s; b) dose response curve for the OSL signal; c) a probability density function plot of 2 mm aliquots measured on the same sample: note the positively-skewed distribution with OD = 69%, typical of poorly bleached material; d) the first seconds of the TT-OSL signal; e) dose response curve for the TT-OSL signal; f) the probability density function plot measured between the aliquot of the same sample: note the almost normal distribution with over dispersion OD < 20%, indicating adequate bleaching.

Summarizing, the OSL/TT-OSL ages considered in this project are in bold in Table 16. These data, together with the field ones, will be used to compare the pedostratigraphic levels of NMNT with the OMNT ones, providing further details about their origin and evolution (see paragraph 5.2).

4.2 *The new 2016 outcrop*

In 2016, new excavations work at the *Danesi* quarry, finally exposed the fault modelled by Livio et al., (2014) through the kinematic restoration of the structural evidence linked to the growing of the anticline and recorded in the OMNT sequence. The ca. 6 m-wide fault zone (see location in Fig. 45) shows a deformed sequence composed by fluvial pre-growth strata (PGS in Fig. 46) and 5 stacked layers of syn-growth overbank and aeolian pedogenized deposits (GS1 to 5 in Fig. 46). Correlations with dated units exposed in previously analyzed OMNT section (Livio et al., 2014, Table 18) offers the opportunity to constraints the age of the new deformed sequence to Early – Middle Pleistocene to present.

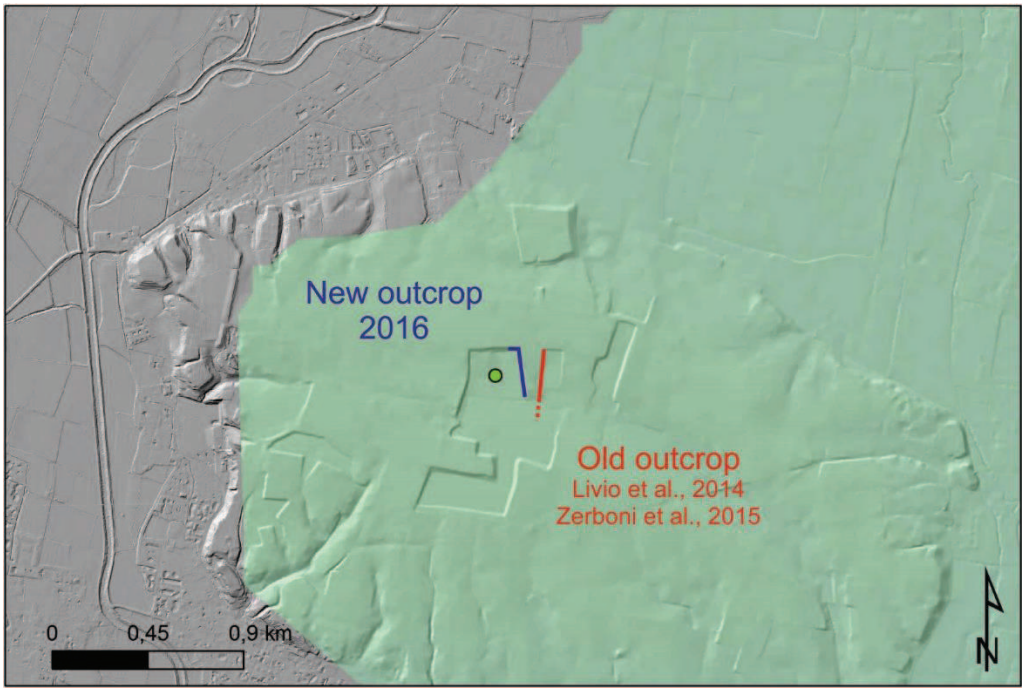

Fig. 45: Hillshade model of the Danesi quarry at Monte Netto site; in green the one derived from a 5 x 5 m DEM, in gray the one derive from the 1 m LIDAR. The position of the 2016 outcrop and the old one published in Livio et al., 2014 and Zerboni et al., 2015 are indicated.

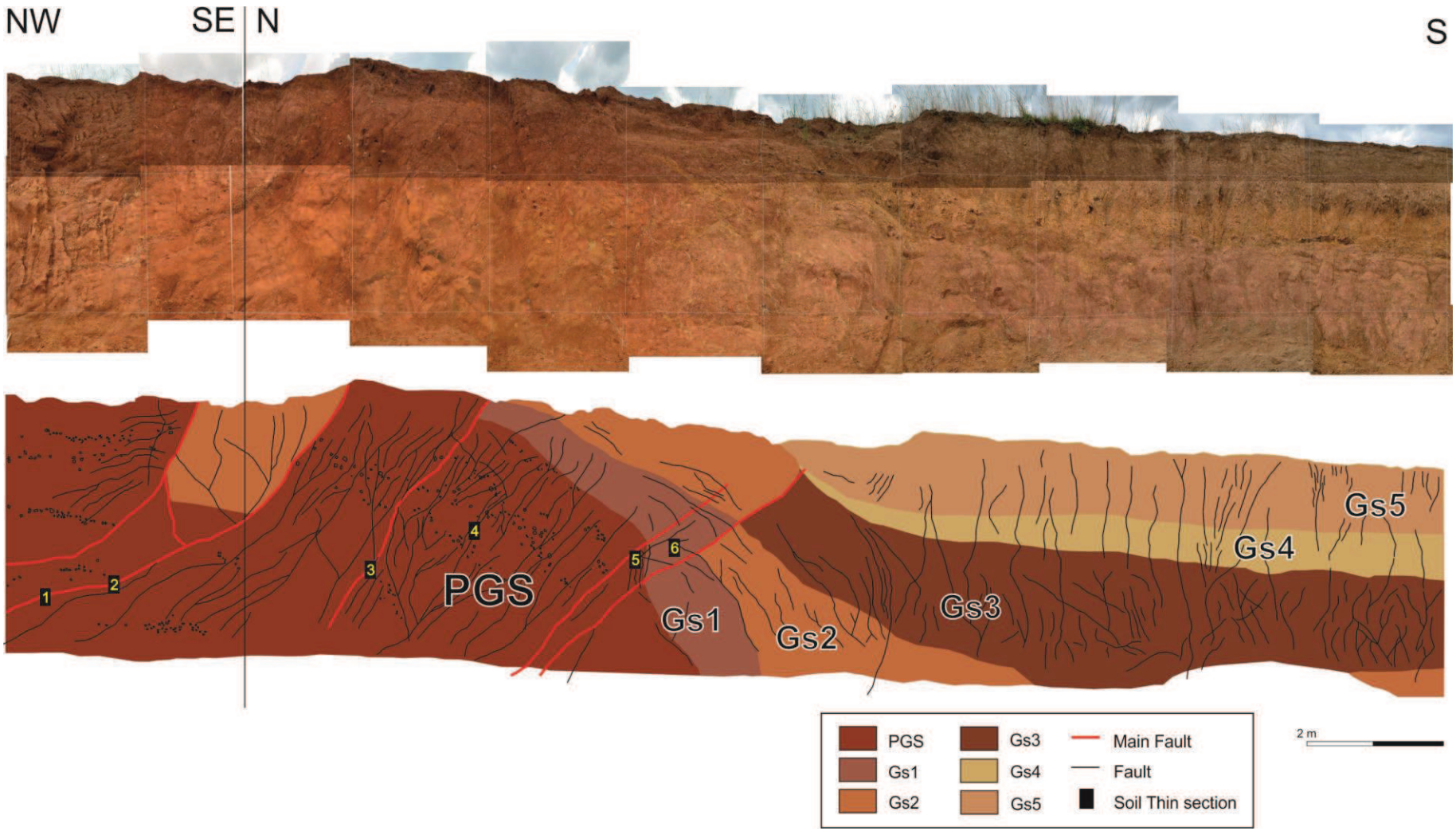

Fig. 46: LOG of the 2016 outcrop at Monte Netto. PGS, pre-growth strata; GS1 to 5, growth strata.

Livio et al., 2014		Comparison	New outcrop 2016			
Description	**Old Units**		**New Units**	**Process**	**Age**	**Description**
S2 Coarse and medium silt deposit with significant clay content (but lower than S1) and pedofeatures related to clay illuviation and weathering. PL2 Coarse and medium silt deposit (unimodal distribution) and common to frequent sandy Mn concretions (Mn pisolites).	S2+PL2 (PL2 in Zerboni et al., 2015)		Gs5	Loess	MIS 3 - MIS 2	Yellowish brown silt loam.
S3 Coarse and medium silt deposit with significant clay content and pedofeatures related to clay illuviation and weathering. PL3 Coarse and medium silt deposit (unimodal distribution) and very low sand content.	S3+PL3 (PL3 in Zerboni et al., 2015)		Gs4	Loess	MIS 4	Brown silty clay.
S4 Silty sand with a high degree of clay mobilization and accumulation of Fe-Mn. CL Fine sandy to silty deposit with common sandy Mn concretions (Mn pisolites).	S4+CL (PL4 in Zerboni et al., 2015)		Gs3	Colluvium	MIS 6	Very dark brown clay loam.
3cm of gray plastic clay overlying a grayish-yellow silty fine sand, closely alternating with gray clayey silt.	FG1		Gs2	Levee	Early-Middle Pleistocene	Reddish brown silty clay loam.
No correlation.			Gs1	Crevasse splay	Early-Middle Pleistocene	Reddish clay loam.
FG2 Fining upward coarse sand with small discontinuous lenses of microconglomerates. FG3 Matrix-supported conglomerate made of centimetric deeply weathered clasts in a reddish-brown coarse sandy matrix and with a slightly erosive basal contact.	FG2+FG3		PGS	Crevasse splay	Early-Middle Pleistocene	Reddish-brown coarse sand with small discontinuous lenses of microconglomerates.

Table 18: Comparison between the stratigraphy and age of OMNT sequence and the stratigraphy of the 2016 outcrop

In addition to the pedostratigraphic characterization, six undisturbed blocks for micromorphology of soil thin sections have been sampled. Due to the success of the micropedological approach demonstrated at Pecetto di Valenza site, deciphering two of the major stages in the sequence of tectonic events (paragraph 5.1.3; Frigerio et al., 2017), we decided to investigate the tectonic deformation at Monte Netto site also at microscale. For this reason, we extracted the six undisturbed blocks in correspondence with the main fault planes (see the location in Fig. 46). The analysis of these soil thin sections at the petrographic microscope, allowed to highlight clear crosscutting relationship recorded into microstructure, micromass and pedofeatures (e.g., clay coating, nodules and *papulae*). The interpretation and integration of these microscopic evidence into the paleoseismological reconstruction, can help deciphering a greater number of tectonic events than the ones that can be recognized at macro scale, but also can provide additional chronological constraints to the sequence of tectonic events.

In the following, the most meaningful microphotographs showing evidence of tectonic deformation are presented. The description of the deformation/crosscutting evidence and the corresponding interpretation is reported in each caption.

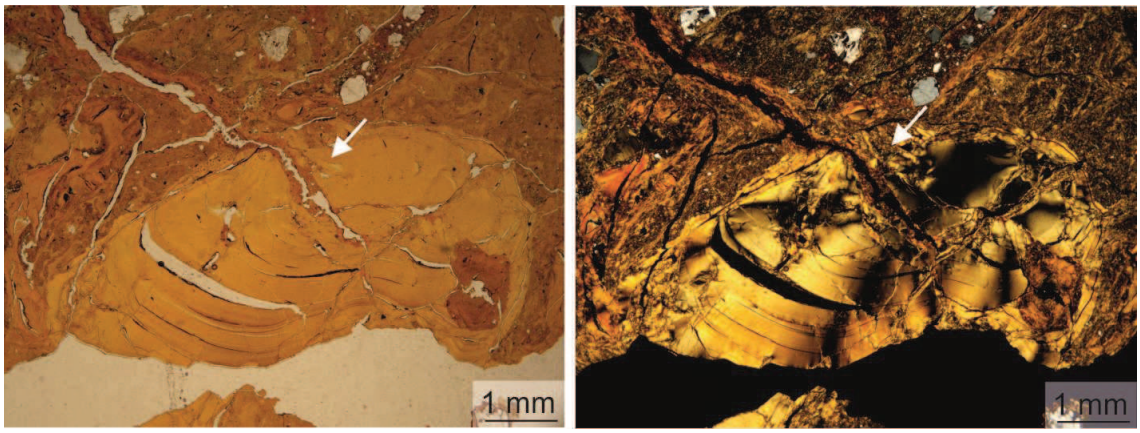

Fig. 47: Photomicrograph of thin section MNT-4 (PPL on the right; XPL on the left). The white arrow indicates a fractured clay coating filled by illuvial clay. This latter occurred after a tectonic movement, which displaced the pre-existing coating.

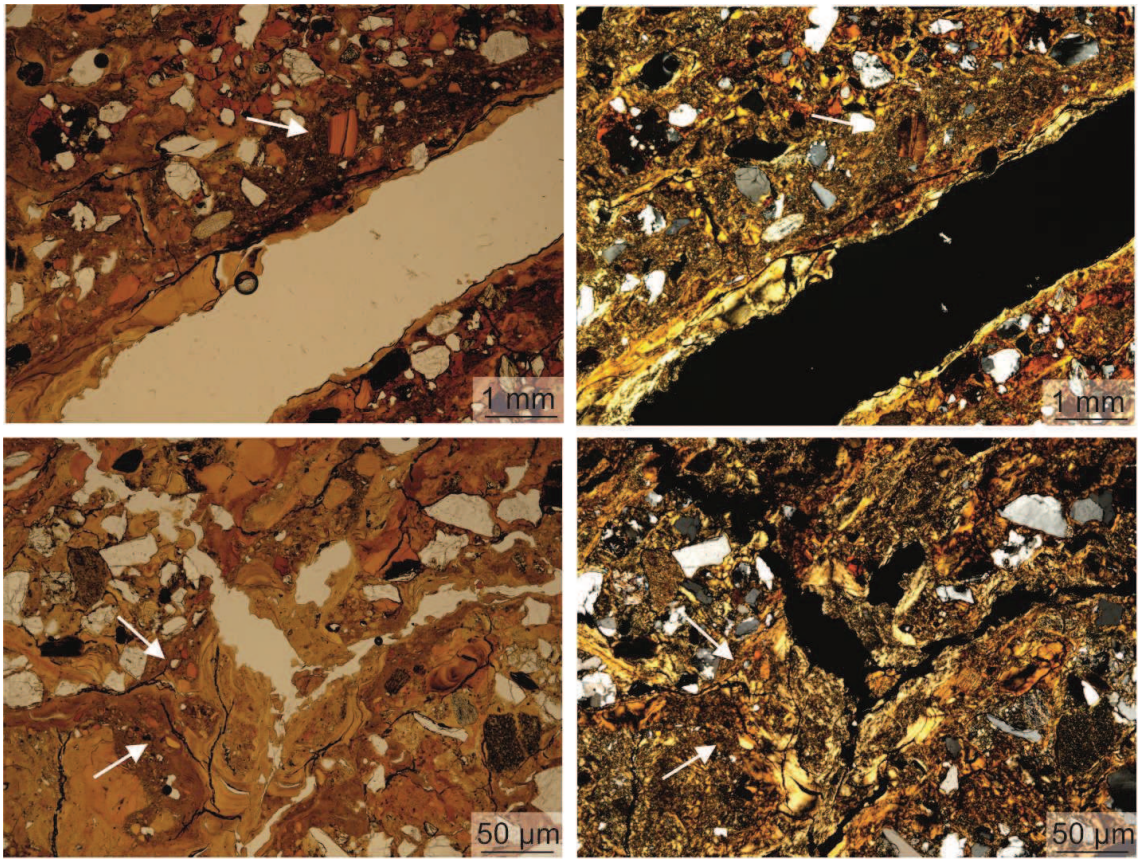

Fig. 48: of thin section MNT-2 (PPL on the right; XPL on the left). The white arrow indicates clay fragments of different colour widespread in the micromass, that can be interpreted as the reworking of pre-existing coating and infillings due to deformation events.

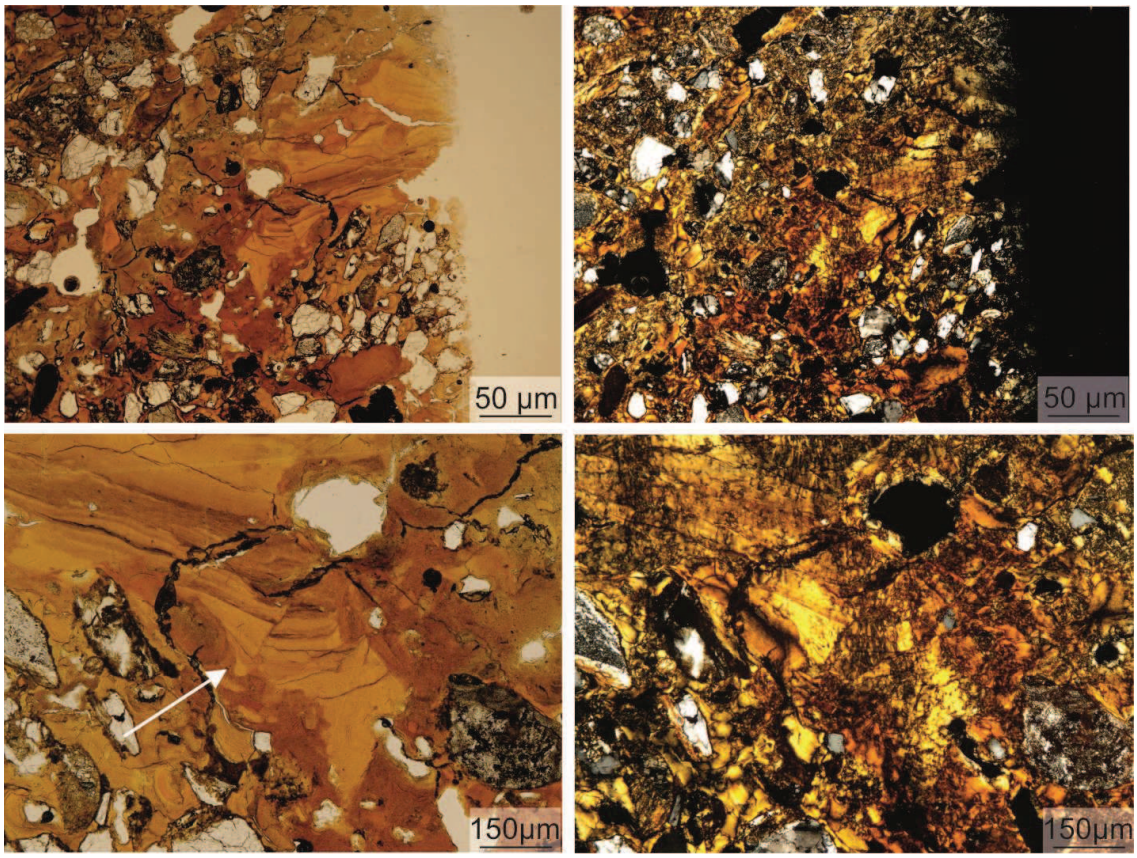

Fig. 49: Photomicrograph of thin section MNT-2 (PPL on the right; XPL on the left). The white arrow indicates a clay infilling clearly dislocated, probably due to a tectonic movement.

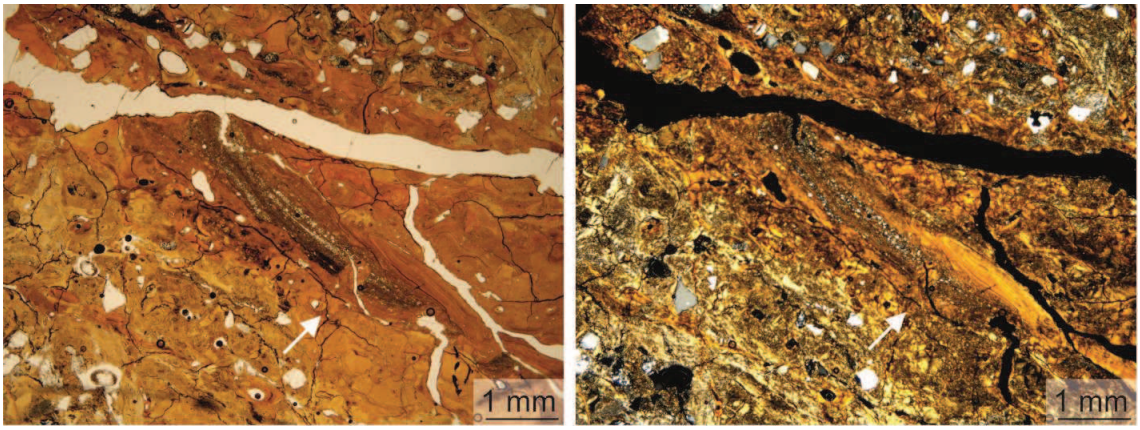

Fig. 50: Photomicrograph of thin section MNT-4 (PPL on the right; XPL on the left). The white arrow indicates a infilling of coarse material, fractured and filled by illuvial clay. The infilling of coarse material probably took place after a first deformation phase, subsequently fractured by a new tectonic movement and then filled by new illuvial clay.

5. Discussion

5.1 The Monferrato area

The field observations, the results of the pedostratigraphic analysis and the dating results obtained in the Monferrato area at Solero, Rivarone and Pecetto di Valenza sites, allow to reconstruct the recent landscape evolution of this area.

In the following, I discuss the evolution of each pedostratigraphic sequence. Then, thanks to the comparison of the studied sites, I present the reconstruction of the Alessandria and Valenza plateaux landscape evolution. Finally, the structural evidence identified and analysed at Pecetto di Valenza site, integrated with the paleopedological and geochronological data, allow to reconstruct the recent surface evolution and the paleoseismic history of this site.

5.1.1 Evolution of Solero, Rivarone and Pecetto di Valenza pedostratigraphic sequences

The field observations and the cumulative grain size distribution curves obtained for each studied site, highlight the presence of stratigraphic sequences composed by different parent material, that individuate different pedostratigraphic levels. The latter ones have been affected by different soil - forming processes, which variable intensity have been recorded into the B horizons.

All the studied pedostratigraphic sequences are composed by fluvial deposits, developed on silty to sandy silty material, covered by one or more loessic covers, which accreted during periods of rhexistasy (sensu Erhart, 1951). The identification of the parent material origin of each PL has been favoured by the comparison of the cumulative grain size distribution curves with the reference theoretical ones, (Figs.13, 23, 24, 31), which were elaborated for fresh loess and weathered loess from the PPLB (Cremaschi, 1987). The pedogenetic processes that affected each parent material during the biostasy phases (sensu Erhart, 1951) have been recorded into several pedofeatures and typical field properties. The analysis of these latter, allowed to decipher the main pedogenetic processes that took place at the studied sites, which are pedoplasmation (i.e., decrease in silt content and increase in clay content (Stoops et al., 2010)), rubification (i.e., release of iron oxides leading to a redder colour), clay translocation (sensu Cremaschi, 1987), calcite migration and recrystallization, and hydromorphy (Duchaufour, 1983; 1995).

Moreover, thanks to the available dating (AMS-^{14}C and OSL/TT-OSL dating), it is possible to give a preliminary chronological constrain to the evolution of each studied sequence.

In the following section, for each studied sites, I hypothesize the origin of the parent material of each PL and the pedogenetic processes which acted on them, as well as the timing of their deposition.

Solero

At Solero site grain size analysis confirm the existence of five pedostratigraphic levels (PL1 to PL5; Fig. 51), individuated by five different parent materials characterized by several post-depositional soil-forming process.

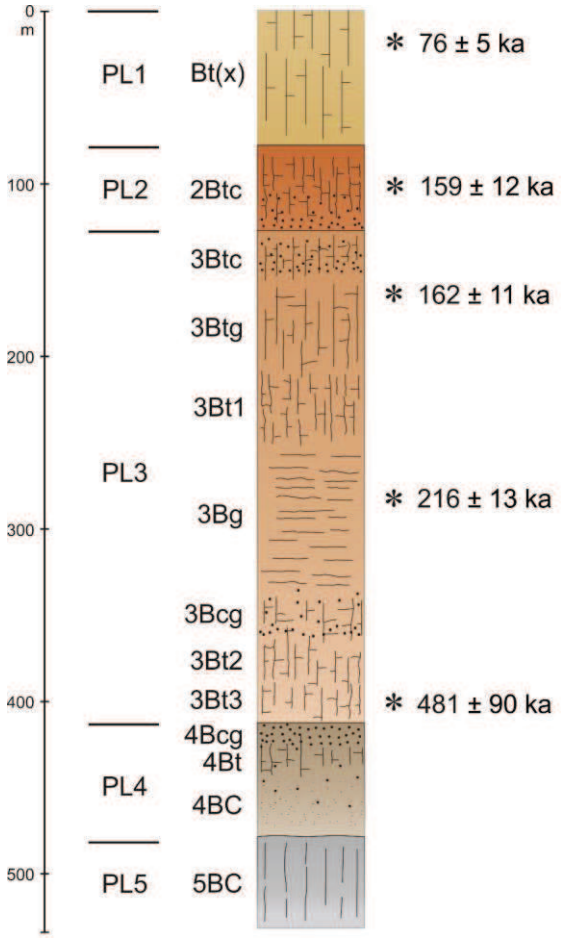

Fig. 51: Pedostratigraphic column illustrating the distribution of soil horizons and the pedostratigraphic levels at the Solero site. The results of TT-OSL dating are indicated

The oldest event recorded at Solero site led to the development of the pedostratigraphic level PL5. The cumulative grains size distribution curve obtained for this PL show a massive clay content (40%) which is consistent with a decantation environment, where the fluctuation of the water table promoted the formation of hydromorphic features (Fe-Mn nodules). The deposition of this PL, according to the TT-OSL age obtained from sample SOL-3, occurred ca. 500 ka, during the oldest fluvial aggradation phase recorded at this site.

The curves from the underlying pedostratigraphic level PL4 suggest fluvial parent material, slightly weathered at its top, highlighted by a moderate clay content and characterized by evidence of hydromorphism. This PL is only 55 cm thick, probably due to an erosional phase preceding the deposition of the overlying PL3.

The cumulative grain size distribution curves of PL3 are shifted towards the coarse fractions, suggesting a fluvial parent material. Moreover this pedostratigraphic level shows a decreasing weathering towards depth, testify by the decreasing of the clay content from 35% at the top of the PL, to less than 20% at the bottom. However, evidence of clay translocation (clay coating on voids and peds) and hydromorphism (hydomorphic mottles) are well expressed. The samples collected for the TT-OSL dating from this PL, SOL-1 from 3Btg horizon and SOL-2 from 3Bt3 horizon, date 162 ± 11 and 216 ± 13 ka respectively: these ages are consistence with the deposition of the fluvial material during two different aggradation phases, preceding the one that deposited PL2.

Indeed, also the pedostratigraphic level PL2 presents a fluvial parent material, strongly weathered. The sample from this level gave a grain size distribution curve with a high content of clay (almost 40%) and the coarse fraction rather well represented (almost 15%). The sample SOL-5, collected for the TT-OSL dating, giving an age of 159 ± 12 ka testifies that the deposition of PL2 parent material occurred during a fluvial aggradation phase, the latest recorded at Solero site. The high degree of weathering of this PL, is also testified by the reddish brown colour and by the common presence of clay coatings and Fe-Mn coatings and nodules. The formation of the latter ones has been promoted by hydromorphic processes, triggered by water-logging due to the occurrence of impervious B horizons enriched in clay at the top of the underlying pedostratigraphic level PL3.

The curve from the upper pedostratigraphic level (PL1) shows sigmoid trend and asymmetric grain size distributions with a low sand content (5%) and a clay fraction of about 25%. This curve fits well with the curves of Po Plain loess by Cremaschi (1987), falling in the range between the fresh and weathered loess. The sample SOL-4 collected from this PL for the TT-OSL dating, dates back to 76 ± 5 ka, which is consistence with a loessic depositional phase during the Upper Pleistocene.

Rivarone

The grain size analyses performed at Rivarone site show that the whole RVA sequence developed starting from the same parent material; the RVB sequence, instead, is characterized by two pedostratigraphic layers, which differ on the origin of the parent materials.

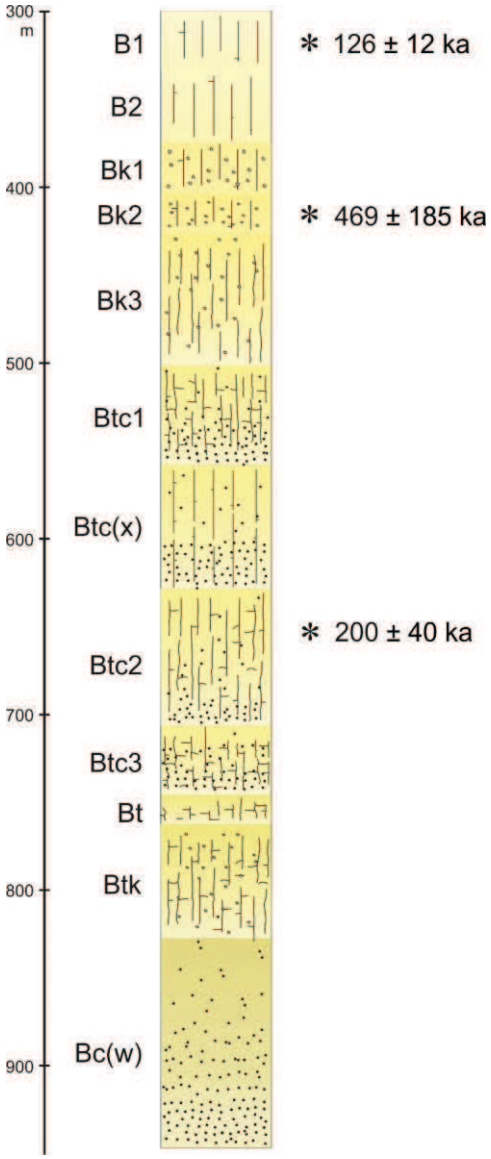

Fig. 52: Pedostratigraphic column illustrating the distribution of soil horizons of the RVA sequence, evolved starting from a parent material with the same origin. The results of TT-OSL dating are indicated.

The cumulative grain size distribution curves obtained for RVA sequence may suggest a parent material with loessic origin, on which different pedogenetic processes took place (Fig. 52). Indeed, if compared with the curves of the Po Plain loess by Cremaschi (1987), they fall into the field of existence of loess. The upper horizons, from B1 to Bk3 show curves with sigmoid trends and asymmetric grain size distributions, resulting shifted toward the curve of fresh loess. The curve from Bk1 horizon shows a high content of sand (20 %): this shifting of the curve trend toward the coarse fraction is due to the high quantities of sand-sized $CaCO_3$ nodules within this horizon. Also the Bk1 and Bk2 horizons present frequent $CaCO_3$ nodules, whose formation has been promoted by carbonate dissolution and recrystallization occurred during periods characterized by a high availability of water. The lower part of the PL, instead, from Btc1 to Bt horizons, present cumulative grain size distribution curves showing an increasing of the content of clay, which can correspond to a degree of weathering comparable to

the strongly weathered loess of the Po Plain. The abundant clay coatings identified on surface of voids and aggregates testify the high intensity of the illuviation processes, and represent the field evidence of the degree of weathering. Hydromorphic features are a further evidence of weathering (i.e., Fe-Mn nodules); their formation occurred after the illuviation of clay in the Bt horizon, due to the fluctuation of a water table.

The RVA-3 and RVA-1 samples, collected for the TT-OSL analysis and dating 126 ± 12 ka and 200 ± 40 ka respectively, gave result incompatible with the periods typical for the loess deposition, i.e., the glacial phases on the Upper Pleistocene (late MIS 4, MIS 3, possibly and MIS 2). Sample RVA-2, instead, as explained in paragraph 3.2.3 gave inconclusive results. Thinking at the depositional environment in which the RVA sequence is located, a few meters far from the Tanaro riverbank, it is reasonably possible that the fluvial dynamic have deposited a silty material, comparable with the grain size of typical loess. Therefore, I have not the certainty about the origin of the parent material composing this pedostratigraphic sequence. The micromorphology of soil thin sections could be a valuable tool to solve this issue.
Finally, looking at the cumulative grains size curves of the lowermost two soil horizons, they result shifted toward the coarse fraction, with a high content of coarse silt: in this case, I can hypothesize a fluvial origin of the parent material.

The pedostratigraphic sequence RVB appears composed by two pedostratigraphic layers (Fig. 53).

The lowermost PL2 presents poorly sorted grain size distribution curves, suggesting a fluvial parent material deposited in a decantation environment. The high content of clay ranges between 60 and 35%, corresponding with a decreasing of the degree of weathering with depth. Moreover, the presence of frequent $CaCO_3$ nodules in 2Btk and 2Bk horizons, testify that the carbonate translocation process occurred before the clay translocation one. The curve of 2Bc horizons presents a different grain size distribution, with a moderate content of coarse sand, corresponding with abundant Fe-Mn nodules, that shifted the curve trend toward the coarse fraction.

The cumulative grain size distribution curves from the uppermost PL show sigmoid trends and asymmetric distributions with a low sand content (less than 10%) and a clay content ranging between 20 and 30%. The moderate degree of weathering of this material is testified by clay pedofeatures associated with illuvial processes. The base of this level is also characterized by frequent coarse Fe-Mn nodules, whose formation have been promoted by the permanence of the water table over the underlying impervious PL2 enriched in clay. The very homogeneous grain size distribution obtained for this PL may be compared with the properties of the moderately weathered loess of the Po Plain (Cremaschi, 1987). Nevertheless, the sample RVB-1, collected for TT-OSL dating in the upper part of

this PL, dates to 87 ± 21 ka BP, which would indicate a very early onset of loess sedimentation in this area; regional data and environmental reconstructions do not completely support this possibility. The sample RVB-2, collected from the same horizon of RVB-1, and RVB-3, dating back to 135 ± 41 ka and 211 ± 46 ka respectively, result inconsistent with the Upper <Pleistocene time range of loess deposition in the Po Plain. However, as discuss for the RVA sequence, the origin of this uppermost parent material cannot be deciphered with certainty: also the fluvial dynamic may have deposited silty sediments. Moreover, it must be taken into account that the grain size analysis has been performed only for one sample from the Bt(x) horizon, which is thick more than 200 cm: probably, the analysis of all the samples collected every 20 cm, could show a highest variability of the parent material. The latter, can be deciphered through a micropedological approach.

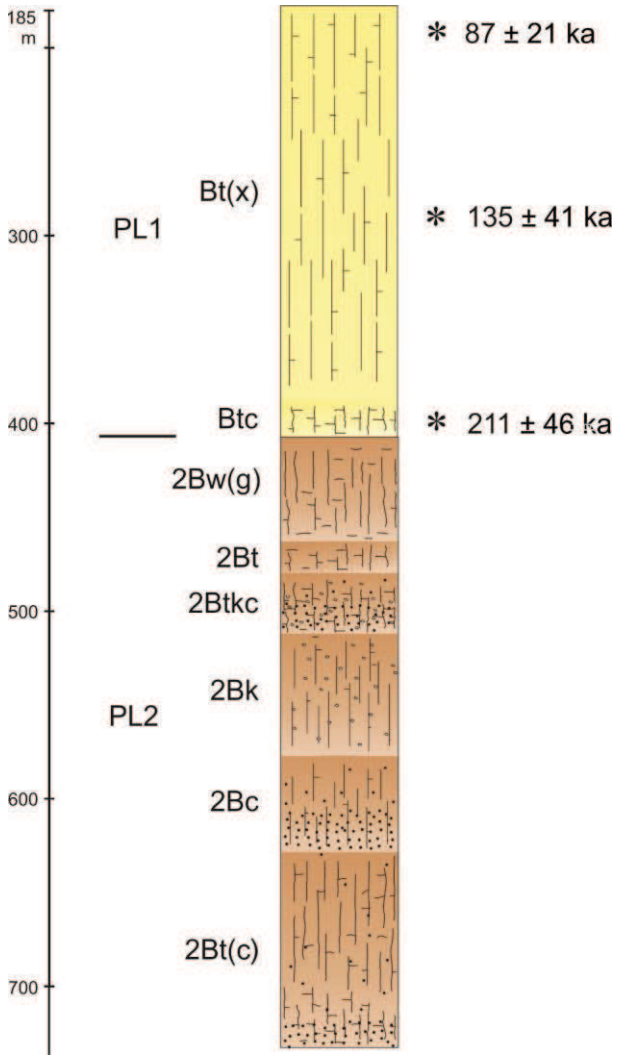

Fig. 53: Pedostratigraphic column illustrating the distribution of soil horizons and the pedostratigraphic levels at the RVB sequence, at Rivarone site. The results of TT-OSL dating are indicated

Pecetto di Valenza

At Pecetto di Valenza site, in addition to the grain size analysis, also the micromorphological analysis of soil thin sections confirm the occurrence of four pedostratigraphic levels (PL1 to PL4), which differ on the basis of the origin of parent materials and post-depositional and pedogenetic processes acting on them. According to grain size curves (Figs. 31 and 32), it is possible to make a hypothesis on the origin of the parent material of each PL, which accreted during periods of rhexistasy (sensu Erhart, 1951). The curves, in fact, shows that (i) the uppermost two PLs are formed by wind-blown sediments (loess); (ii) a clear decreasing in the intensity of weathering toward the top of the sequence, (iii) the colluvial origin of PL3, inferred from its poor sorting and (iv) curves of the weathered bedrock similar to the reference ones for shale (e.g., Krumbein and Sloss, 1963; Ricci Lucchi, 1980).

The biostasy phases (sensu Erhart, 1951) promoted, instead, a number of soil-forming processes, identified by several pedofeatures on the micromorphology of thin sections. The main pedogenetic processes that took place at the Pecetto di Valenza site are rubification (release of iron oxides leading to a redder colour), clay translocation (sensu Cremaschi, 1987), calcite migration and recrystallization, and hydromorphy (Duchaufour, 1983; 1995).

The oldest events led to the development of the pedostratigraphic level PL4, corresponding to weathered bedrock, on which different pedogenetic processes left, at the microscale, specific pedofeatures. The oldest ones are crystalline pedofeatures (calcite nodules, coatings, infillings and hypocoatings), due to carbonate translocation, which occurred during periods characterized by a high availability of water. Moreover, many calcite nodules at the top of PL4 suggest the existence of a calcrete-like horizon (4BCk), developed due to an increase of evaporation and evapotranspiration rates (Wright and Tucker, 1991). Once finished the carbonate translocation, still under a regime of greatest water availability, three distinct clay illuviation phases took place. A first illuviation is attested by pale yellow dusty clay, reworked by pedoturbation into papulae (fragmented clay coatings, sensu Brewer, 1964). A more recent illuviation phase produced brownish dusty and orange limpid clay coatings. The illuviation of dusty clay developed under degradation conditions, followed by a stable climatic period, promoting the formation of orange limpid clay coating (Kühn et al., 2010). Amorphous pedofeatures are well developed in PL4, probably due to the long standing of the water table, whose fluctuation promoted the formation of hydromorphic features. There are no chronological constraints for the pedogenetic phase acting on the parent material of PL4, and possibly it was a multi-steps process. However, micromorphological properties suggest that weathering possibly occurred under interglacial conditions, and we can tentatively suggest the MIS 7 and/or MIS 5 interglacials.

The pedostratigraphic level PL3 is composed by a highly weathered soil material that underwent erosion, colluviation, and subsequently was interested by further pedogenesis, which increased the degree of weathering of this pedological body. Under the microscope, the reddening of the micromass and the presence of textural pedofeatures belonging to three different illuvial phases suggest that the parent material of PL3 underwent strong weathering. The older illuviation is attested by brownish dusty fragments of clay coatings (papulae), which denote a reworking of the groundmass, compatible with the colluvial origin of the parent material. Also the disorthic Fe-Mn nodules, presenting sharp boundaries, are due to short-distance movements (e.g. rotations; Stoops, 2003), which is compatible with a colluvial origin. Orange dusty laminated and not laminated clay coatings and brownish dusty clay coatings suggest further illuviation phases, occurred after a secondary deposition of the layer. The orange dusty laminated and not laminated coatings indicate that the illuviation process took place in several phases. Afterwards, a more recent illuviation phase produced brownish dusty clay coatings, indicating a phase of climatic degradation characterized by soil denudation, probably due to the reduction of vegetation cover and to a significant change in the soil-water balance (Fedoroff, 1997).

The sample PEC-3, collected for the AMS-14C dating from the lower part of this level, dates back to 26300±110 years BP. This age, however, is not reliable for two reasons: i) it is younger than the age of the overlaying deposit, and ii) paleosols with similar degree of weathering were commonly observed in the Po Plain Loess Basin (PPLB; e.g., at Val Sorda (Cremaschi, 1987; Ferraro, 2009), Ghiardo (Cremaschi et al., 2015) and Monte Netto (Zerboni et al., 2015) sites, and were attributed at least to pedogenic phases occurred in the Eemian interglacial. Therefore, the sample PEC-3 was probably affected by a contamination of younger organic matter migrated from an upper level. Sample PCT-4, instead, collected at the top of the same PL and dated with the TT-OSL method, date back to 108 ± 7 ka: this age suggests the deposition by colluviation of this material during MIS 5. Moreover, it is possible to correlate the timing of the soil formation, before its colluviation on the marly bedrock, with other similar paleosols individuated in the PPLB.

The parent material of both PL1 and PL2 is loess (aeolian silt). Comparing the results of our grain size analysis with the cumulative curves elaborated for the fresh and weathered loess from the Po Plain Loess Basin (Zerboni et al., 2015), it is possible to note that both deposits fall in the field of existence of loess (Fig. 31 and 32) and show a weak-to-moderate degree of weathering (Cremaschi, 1987).

The pedostratigraphic level PL2 is a moderately weathered loess body, as attested by the reddening of the micromass detected in thin section and by the grain size distribution cumulative curve (see section 3.3.2.2). A certain degree of weathering is also confirmed by clay illuviation, which is represented by brownish dusty and layered coatings and infillings. Layered pedofeatures highlight that the illuviation

process was either active over several events and/or had variable intensity (Kühn, 2003; Kühn et al., 2010). Finally, the occurrence of amorphous pedofeatures (Fe-Mn-bearing nodules and hypocoatings) in the lower part of PL2 indicates the development of hydromorphic processes at the contact with the underlying PL3. The sample PEC-2, collected at the base of this level for AMS-14C dating, yielded and age of ca. 30000 years BP. The latter is compatible with a period marked by a lower rate of loess sedimentation and by a continuous accumulation of organic matter in the soil (a sort of cumulic soil) at the top of the pre-existing loess cover, probably deposited during MIS 3. Indeed, sample PCT-3, dated with the TT-OSL method at 75 ± 6 ka, fall in the range of time typical for the deposition of the aeolian material in the Po Plain.

The loess of pedostratigraphic level PL1 is less weathered than the one of the underlying PL2. The micromorphology of thin sections reveals the presence of dusty yellowish brown clay coatings, which testifies a phase of climatic degradation. Dusty coatings cover limpid yellowish brown clay coatings, which indicate a previous phase of illuviation under a stable vegetation cover. The amorphous pedofeatures attest the increase of hydromorphic processes with depth.

The AMS-14C age of sample PEC-1, collected at the top of PL1, dates back to 4000±30 years BP. Likely, this age did not refer to loess accretion, as it is widely accepted that loess sedimentation in northern Italy occurred up to the end of the Pleistocene (e.g. Cremaschi, 1987, 1990a, 1990b; Cremaschi et al., 2015; Amit and Zerboni, 2013). Moreover, a number of palaeohydrological records from northern Italy suggests that in Northern Italy the Early and Middle Holocene were dominated by relatively humid and warm environmental conditions (e.g., Baroni et al., 2006; Zanchetta et al., 2007; Zhornyak et al., 2011) and pollen spectra indicate for this time span a continuous vegetal cover in the Po Plain (e.g. Wick, 1996; Amorosi et al., 2004; Pini, 2004; Valsecchi et al., 2006; Kaltenrieder et al., 2010; Ravazzi et al., 2012, 2013). These conditions are incompatible with deflation and dust transportation; therefore, the radiocarbon age of sample PEC-1 refers to a pedogenetic phase occurred in the Middle Holocene under a warm climate. In the region, others loess sequences dated to the Holocene at their top, have been interpreted as the effects of a recent pedogenetic phases (Cremaschi et al., 2015; Zerboni et al., 2015). Also the OLS ages obtained from sample PCT-2 and PCT-1, 12 ± 1 ka and 3 ± 1 ka respectively, are incompatible with loess deposition: both ages date two reworking event of the loessic material, probably induced by ploughing activity.

The soil-forming processes that shaped the uppermost B horizons at Pecetto di Valenza site, can be compared with the many loess sequences found in the Po Plain (e.g. Cremaschi, 1987, 1990a, 1990b, 2004; Cremaschi et al. 2011; Giraudi, 2015). In fact, the loess deposits individuated by Giraudi (2015) on the Valenza Plateau date back to Upper Pleistocene, fitting well with our loess covers, which show

a similar degree of weathering. But the most useful comparison is with the complex pedosequence including aeolian and colluvial sediments described at Monte Netto (c. 130 km ENE form Pecetto) by Zerboni et al. (2015), which, in turn, is well related to the other loess sequence studied in the PPLB, allowing us to assume that the timing of our sedimentary events is more realistic. The Monte Netto sequence developed on a weathered fluvial/fluvioglacial deposit, on which a colluvium is deposited. Later, the colluvium was subject to an intense pedogenesis, followed by the deposition of three loess covers. This situation is similar to the one identified at Pecetto di Valenza, with the difference that our sequence developed on a marly bedrock and we have only two thin loess bodies. Moreover, the loess deposition at Monte Netto has been attributed to several cold phases during MIS 3 and MIS 2, each ones interrupted by short interstadials that allowed the weathering of every loess deposits. In particular, the rate of weathering decreases to the top of the sequence, as observed for our sequence, where PL2 is more weathered than the overlying PL1. For that reason, the correlation between the sedimentary and pedogenesis events that characterized the two different sites is more reliable.

To summarize, at Pecetto di Valenza, the pedogenesis on the bedrock started in the MIS 7 and/or 5 interglacials. The formation of the paleosol of PL3 can be attributed to an interglacial phase (possibly MIS 5e), after which, in correspondence of an areal erosion phase, it was colluviated. The loess accretion acted during MIS 3 and MIS 2, under glacial conditions, interrupted by brief interstadial phases, which allowed the weathering of loessial sediments with variable intensity.

5.1.2 The Alessandria and Valenza plateaux landscape evolution

The pedostratigraphical analysis and the dating results obtained for the sites above presented, highlight the presence of stratigraphic sequences composed by fluvial deposits, developed on silty to sandy silty material, covered by one or more loessic covers affected by different post-depositional pedogenetic processes. The comparison between the studied sequences is shown in Fig. 54. The Solero and Pecetto di Valenza sequences can be easily compared, according to the origin of the parent material and from a geochronological point of view. The Rivarone site, instead, due to its location on the actual riverbank of the Tanaro river and for the reasons discuss in the previous paragraph, needs further analysis before being compared with the other stratigraphy.

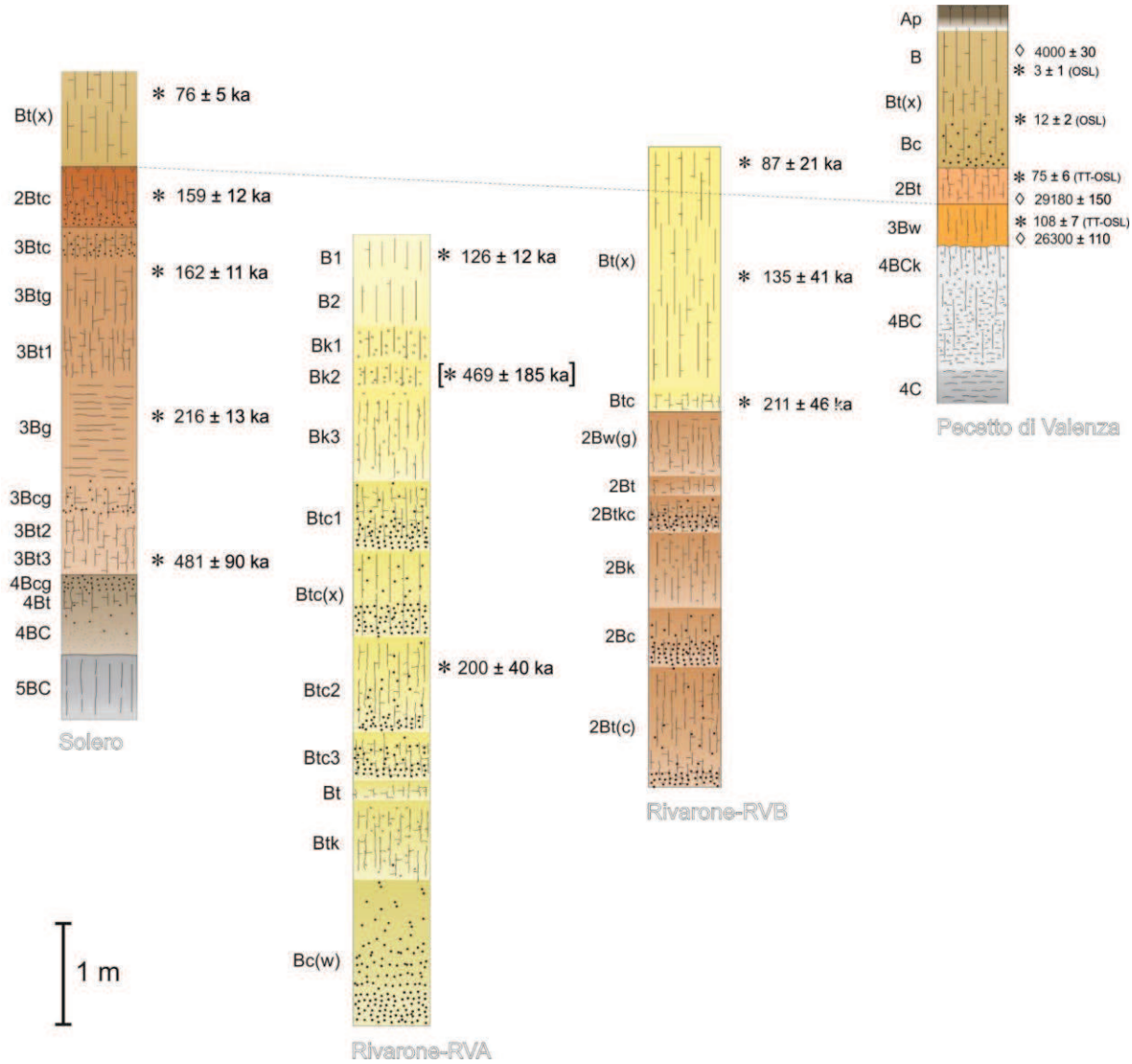

Fig. 54: Comparison between the pedostratigraphical sequences studied in the Monferrato area. At the Solero and Pecetto di Valenza site, the loess deposition took place during the same period, ca. MIS 4. For the Rivarone site (RVA and RVB sequences) instead, further analysis are required to understand the origin of the parent material, and then to make a comparison with the other sites.

The Solero site, on the Alessandria plateau, presents the pedostratigraphic sequence that can be better compared with the stratigraphy of the terraces of the Valenza plateau, described by Corsi et al., (1969) and ENEL (1984), then taken up by Giraudi (2014, 2015). These Authors identify Tertiary and Villafranchian sediments at the base of the sequence, which top present an eroded surface, shaped by the activity of paleo-streams. This surface, known in the italian literature as "platea" (ENEL, 1984b; Carraro et al., 1995; Dela Pierre et al., 2003a,b; Festa et al., 2009), is overlie by recent fluvial sediments, highly weathered, attributable to the Middle Pleistocene. These sediments are covered by two loessic covers of Upper Pleistocene age, according to indirect dating on artefacts included inside themselves.

At Solero site, the "platea" has not been directly observed. In the new geologic map of Piedmont region 1:250.000 (Piana et al., 2017), the Alessandria plateau is indicated as Middle-Upper Pleistocene alluvial deposits. Giraudi (2014, 2015) ascribes this geomorphologic unit to the Middle Pleistocene, based on indirect stratigraphic correlation with water wells (Varalda et al., 2006; ARPA Piemonte, 2014) and boreholes data (ENEL, 1984). The fluvial deposits at the Solero site, described in paragraph 3.1, present TT-OSL ages between 481 ± 90 and 159 ± 12 ka. Therefore, I can correlate these deposits with the ones dated at Middle Pleistocene on the Valenza plateau, suggesting, in this time interval, the occurrence of a fluvial aggradation phase.

The fluvial deposits at Solero are covered by a loessic cover. The deposition and preservation of loess is possible where persistent condition of stability exist, and the depositional surface is disconnected from the major fluvial drainage network. In this case, the loess deposition has been promoted by the development of a wide fluvial terrace, characterizing the Alessandria plateau. Since at Solero the loess cover dates 76 ± 5 ka, this means that the formation of the Alessandria plateau occurred at the beginning of the Upper Pleistocene. It is important to remark that alos the formation of the Valenza plateau can be attributed to the same time-window. In fact, literature data (Corsi et al., 1969; ENEL, 1984; Giraudi, 2014; 2015) indicates the presence of loess covers of late Pleistocene age preserved on the Valenza terrace surface. Therefore, it is quite clear that at the beginning of the Upper Pleistocene a major phase of fluvial incision and terrace formation occurred both in the Alessandria and Valenza areas, N and S of the Monferrato Hills.

Giraudi (2015) ascribes this phase of terrace formation to the deactivation of the Monferrato thrust front. In his model, the Monferrato thrust migrated northward until at least the late Middle Pleistocene or Upper Pleistocene, and then stopped. An alternative hypothesis is that the continuing uplift of the Monferrato region was outpaced near Alessandria and Valenza by fluvial erosion and sedimentation during the Middle Pleistocene, as observed in other areas of the W Po Plain. Therefore, this sector has been shaped by the surface processes typical of the glacial/interglacial phases, dominated by the

lateral planation of the Po River and related drainage network. This “equilibrium” has been heavily altered when the E Monferrato started to be shaped by the Tanaro River, whose recent diversion is well known in literature (Sacco, 1884; 1917; Gabert, 1962; Carraro, 1969; Carraro et al., 1995). This was a major geomorphic event, inducing regional variations in the drainage network of Piemonte and nearby areas.

The evidence of the Tanaro River diversion (Fig. 55) is recorded in the landforms and deposits at the western margin of the Poirino plateau, that can be related to a stream coming from the southern Piedmont.This stream, the Paleo-Tanaro, joined the Po River near Carmagnola. The deviation phenomena occurred in the sector near Bra, where the present river sharply changes its flow from N-S to SW-NE proceeding toward Asti. Eventually, the new trace of the Tanaro River flows again into the Po River near Bassignana. The Tanaro River diversion is supposed to be happened due to a lateral piracy, interesting a minor stream, at lower altitude, flowing toward E. The main causes of this event can be of erosive and/or tectonic origin, probably occurred in the Upper Pleistocene on the basis of the degree of weathering observed for soils covering the recent paleo Tanaro river deposits and the older ones related to the present Tanaro river. Some authors attribute the river piracy to a lateral erosion, induced by the migration of Stura stream (left tributary of the Tanaro river) toward E (Castiglioni, 1979). This event can correspond to the tectonic evolution of a buried structure that favoured the movement of the river toward E.

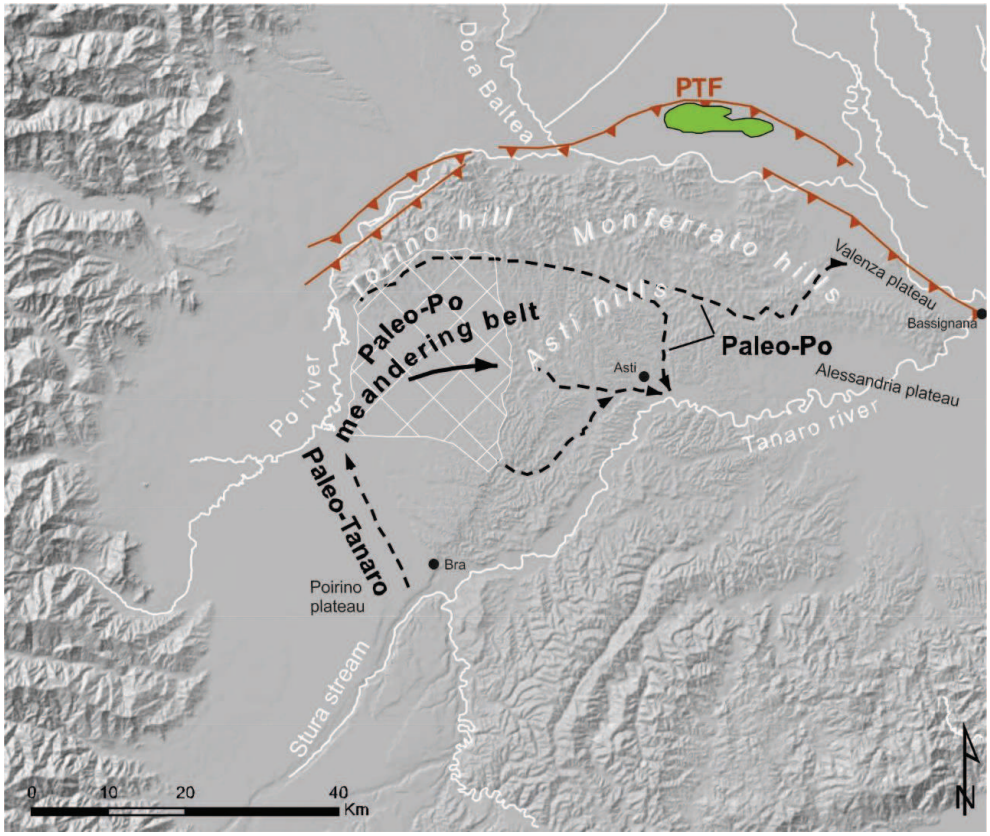

Fig. 55: Shaded relief map of the Monferrato area interested by the Tanaro diversion (modified after Michetti et al., 2012). Black dashed arrows indicate the paleo-drainage recognized in the area. The main structures of the westernomost sector of the Monferrato arc are in red (modified after Mosca et al., 2009); PTF represents the frontal north-verging thrust. The green area highlights the Trino hill.

Therefore, after the deviation, the Tanaro river started its incision activity on the Alessandria plateau, forming the terraces. On these elevated surfaces, free from the erosive processes typical of the fluvial environments, the condition suitable for the deposition of aeolian material have been created. This material has been subject to pedogenetic processes and preserved until today.

Therefore, the late Pleistocene loess cover identified at Solero, indicates that the terrace formation corresponds with the rearrangement of the drainage network, rather than a variation of the tectonic activity.

In addition, making a preliminary interpretation, it is possible to observe that the difference in elevation between the Po riverbed and the Valenza plateau is about 30 m, while for the difference in elevation between the Tanaro riverbed and the Alessandria plateau is about 15 m. Interpreting this difference in elevation as due to a tectonic uplift and extending the age of the loess identified at Solero to the loess deposits present on the Valenza terraces, it is possible to calculate the uplift rates for each plateau. For the Alessandria plateau the uplift rate is 0.2 mm/a, while for the Valenza plateau is 0.4 mm/a. Therefore, a smaller late Pleistocene uplift rate can be hypothesized for the southern sector of the Monferrato area, compared to the northern one, resulting in the overall southward tilting of the

eastern Moneferrato. This is in agreement with observations on the Valenza – Trino area, where evidence of continuing Plesitocene uplift and southward tilting has been described (e.g., ENEL, 1984; Carraro et al., 1995). For instance, the Early Quaternary paleosurface of the Pomaro Hill (Fig. 55) is clearly tilted to the south (see Bonadeo, 2014, and reference therein).

The continuing late Pleistocene to Holocene tectonic activity in the area is also confirmed by the surface faulting evidence observed at Pecetto di Valenza site (paragraphs 5.1.1 and 5.1.3). At this site, the recent deformation is recorded into a pedostratigraphic sequence developed in a secondary valley free from the drainage network due to a phenomenon of river piracy. This valley acted as sedimentary trap for the deposition of two loess covers, characterized by different degree of weathering. The age of these deposits, 108 ± 7 and 75 ± 6, are consistent with the one obtained at Solero and deduced for the Valenza plateau, thus confirming their suitability as stratigraphic markers for paleoseismological analysis in this area.

Moreover, the upper unit of the downstream Rivarone site (paragraph 5.1.1) dates 87 ± 21 ka: if the grain size analysis will confirm the loessic origin of its parent material, it will be possible to have a further confirmation of the disconnection of the Valenza plateau surface from the drainage network during the Upper Pleistocene, therefore within the same time-window observed for the Valenza and Alessandria plateau.

5.1.3 The tectono-stratigraphic and the landscape evolution of the Pecetto di Valenza site

Thanks to the innovative paleoseismological approach integrating the structural analysis with the paleoseismological and geochronological one, I was able to reconstruct the tectono-stratigraphic evolution of the Pecetto site, and, therefore, a preliminary sequence of earthquake surface faulting events which affected the study area. Figure 56 represents this evolutionary sequence, taking into account a 2D balanced retrodeformation of the section. We defined three main fault strands (namely F1, F2 and F3; Fig. 29) in order to simplify the complex fault pattern at the site. Retrodeformation was performed according to apparent offset exposed by the section wall. We divided the tectonostratigraphic history of the site into ten deformation steps, numbered from the oldest to the youngest, whose chronological constraints will be discussed in the following paragraphs. It should be taken into account that the exposed section shows only part of the paleovalley which hosted the colluvial and loess deposition. Likewise, we cannot rule out that the fault zone is wider than the Log in Figure 29. Therefore, details of the landscape evolution model as interpreted below might be modified by future geophysical prospecting and exploratory trenching. However, the collected data are certainly enough to conclude that the present-day landforms and stratigraphic record are the result of several earthquake reverse surface faulting events (i.e., linear morphogenic earthquakes, sensu Caputo, 2005) interacting with weathering, erosion, valley aggradation and loess sedimentation. It is possible to definitely rule out continuous, slow slip at the ground surface, as in the case of tectonic fault creep (e.g., Ferreli et al., 2002; McCalpin, 2009), since surface faulting reconstructed below represents instantaneous scarp-forming events during a continuous history of slope dynamics and soil development.

The different depositional features recorded in the Pecetto di Valenza sequence also allowed deducing the general evolution of the entire slope and nearby area. Figure 57 shows the main phases that modified the landscape from the geomorphological and tectonic point of view, each one represented by a morphotectonic map and by a conceptual block diagram model of the Pecetto di Valenza landscape.

- STEP 0 (Figure 56m): a small valley is subject to erosion by a secondary stream, draining from south to north. Bedding, of the Marne di S. Agata Fossili (Tortonian-Messinian), is slightly tilted probably due to surface folding induced by deeper buried structures. Repeated cycles of rock weathering and erosion are responsible for the lowering of the local relief and valley excavation.

- STEP 1 (Figure 56l): a first tectonic deformation phase (D1) is recorded by systematic conjugate jointing, pointing to a local extensional tectonic regime, probably induced by the surface

accommodation of deeper blind structures. Weathering is progressively lowering down into the bedrock, as erosion removes regolith from the surface.

- STEP 2 (Figure 56i): so far, we can infer a cyclical formation/colluviation and erosion of soil (Fig. 57a), due to a repeated downcutting and infilling of the valley. When erosion processes begin to weaken, the bedrock is finally subject to intense weathering (4BCk/4BC of PL4) by several pedogenetic processes. The oldest is the carbonate translocation process testified by the presence of crystalline pedofeatures, followed by three distinct illuviation phases, marked by three different types of textural pedofeatures. All these multi-steps weathering occurred under interglacial conditions, probably during MIS 7–MIS 5 interstadials. Weathering partially bleaches the D1 joints and a very gentle slope is now characterizing the valley-side.

- STEP 3 (Figure 56h): a major phase of colluviation, reworking older soils, occurred, according to the TT-OSL age, 108 ± 7 ka years ago, causes a partial infill of the valley (PL3). The high degree of weathering shown by this deposit, allowed attributing the soil formation, before its colluviation, to the Eemian interglacial (MIS5e). Valley floor leveling by colluvium is induced by a contemporary piracy of the stream that, at this time, definitively cut off this system tract from the local drainage system (Fig. 57b).

- STEP 4 (Figure 56g): occurrence of a subsequent phase of incision into the PL3 infilling and a slightly shifting of the thalweg to the west, probably triggered by tectonic uplift and tilting of the eastern valley side, not directly recorded at the site; at this STEP 4, we still have no evidence of scarp-forming surface rupture, and we interpreted the deformation as due to blind faulting.

- STEP 5 (Figure 56f): the main tectonic deformations of D2, including coseismic surface rupture, faults, joints and fault gouge development, can be ascribed at this time interval. The development of these features was accompanied by some weathering phases, linked to interglacial/interstadial periods, testified by two generations of textural pedofeatures. Three main fault strands cut through the sequence, crosscutting D1 structures and dying out upwards into PL3 (Fig. 57c). Part of PL3 has been partially pinched in the underlying weathered marl during the deformation movements, resulting in the formation of pocket of colluvium along the main fault strands. A minimum amount of fault throw can be inferred, assuming that PL3 thickness was almost uniform across each fault zone and thus restoring the original post-faulting geometry of the unit, prior any subsequent erosional or reworking phase. A total net slip of ca. 400 cm can be calculated during this step. This relatively large surface slip implies the reactivations of all the three fault strands during this phase, but stratigraphic constraints are lacking for distinguishing between single paleoearthquakes. We thus consider all these ruptures as a cumulative evidence of repeated linear morphogenic events. Since the fault tips for F2 and F3 are

presently located inside PL3 we can infer that the high clay content of this unit likewise resulted in a plastic response to stress, inhibiting upward fault propagation. The shallow accommodation of reverse displacement on fault was therefore distributed over relatively wide deformation zones (i.e., trishear triangular zones; e.g., Erslev, 1991).

- STEP 6 (Figure 56e): after some reworking and erosion of PL3 unit (truncated at the top), we have the sedimentation of the first aeolian deposit (PL2), leveling local relief. The deposition of this unit probably took place during the late MIS 4 (according to the TT-OSL age of 75 ± 6 ka years ago), while its alteration started from ca. 30000 years BP, testified in thin section by one generation of clay coatings. We can infer a possible reactivation of on F3 fault (Event A), following PL2 deposition, which caused a slight folding of the originally horizontal layer. Estimated slip on fault is less than 10 cm. This is the first oldest paleoearthquake slip that we are able to identify.

- STEP 7 (Figure 56d): at this time some slip on F2 and F3 faults occurred (Event B – total net slip is 44 cm), causing an upward drag-folding of PL2 bed and followed by the deposition of a new loess cover (PL1). The latter occurred during MIS 2 and subsequently underwent pedogenesis in the Middle Holocene (ca. 4000 years BP), when two illuviation phases took place. A minor erosive phase is marked by an unconformity at the top of the folded sequence, sealing all the previous deformations.

- STEP 8 (Figure 56c): during this interval we record a movement on F1 fault (Event C – slip: 20 cm) whose tip is now located close to the top of the bedrock. Slip is accommodated, above fault tip, by a gentle folding. Sub-vertical extension joints develop in the folded sector, cutting through PL2 and PL1 units.

- STEP 9 (Figure 56b): a second movement of F1 (Event D), which cuts PL2 and PL1 (Fig. 57d), is testified by a small offset at the base of PL1 (ca. 5 cm) and by crosscut relationship between F1 fault strand and sub-vertical joints. Calculated slip for this step, measured at the base of PL3 is 14 cm. F1 systematically cuts through the joint system in its uppermost sector. Offset of each joint pinpoints systematically decreases upward, thus indicating that the propagation of this sector of the fault strand is contemporary with slip accumulation. Fault ramp changes into a flat approaching the surface due to the lack of overburden load and according to typical geometries of surface thrust faults.

- STEP 10 (Figure 56a): Finally, many phases of ploughing (Ap of PL1) and reworking of the surface lead to the development of a ca. 30 – 40 cm thick level, whose base is a sharp unconformity surface.

Most of the total displacement is recorded in STEP 5, probably representing the cumulative effect of many earthquakes and coseismic ruptures. Since PL3 is cut at the top by erosion and a presumably

long time interval is not recorded, for the oldest part of the sequence we cannot distinguish each single coseismic surface rupture event. Conversely, events B to D are well preserved in the stratigraphic units and unequivocal relative chronology can be inferred by crosscut relationships. We then adopted these last events in order to calculate, through a direct method (sensu McCalpin, 2009), slip rates and recurrence intervals. Errors were calculated following the error propagation rule for values with unequal standard deviations (Geyh and Schleicher, 1990).

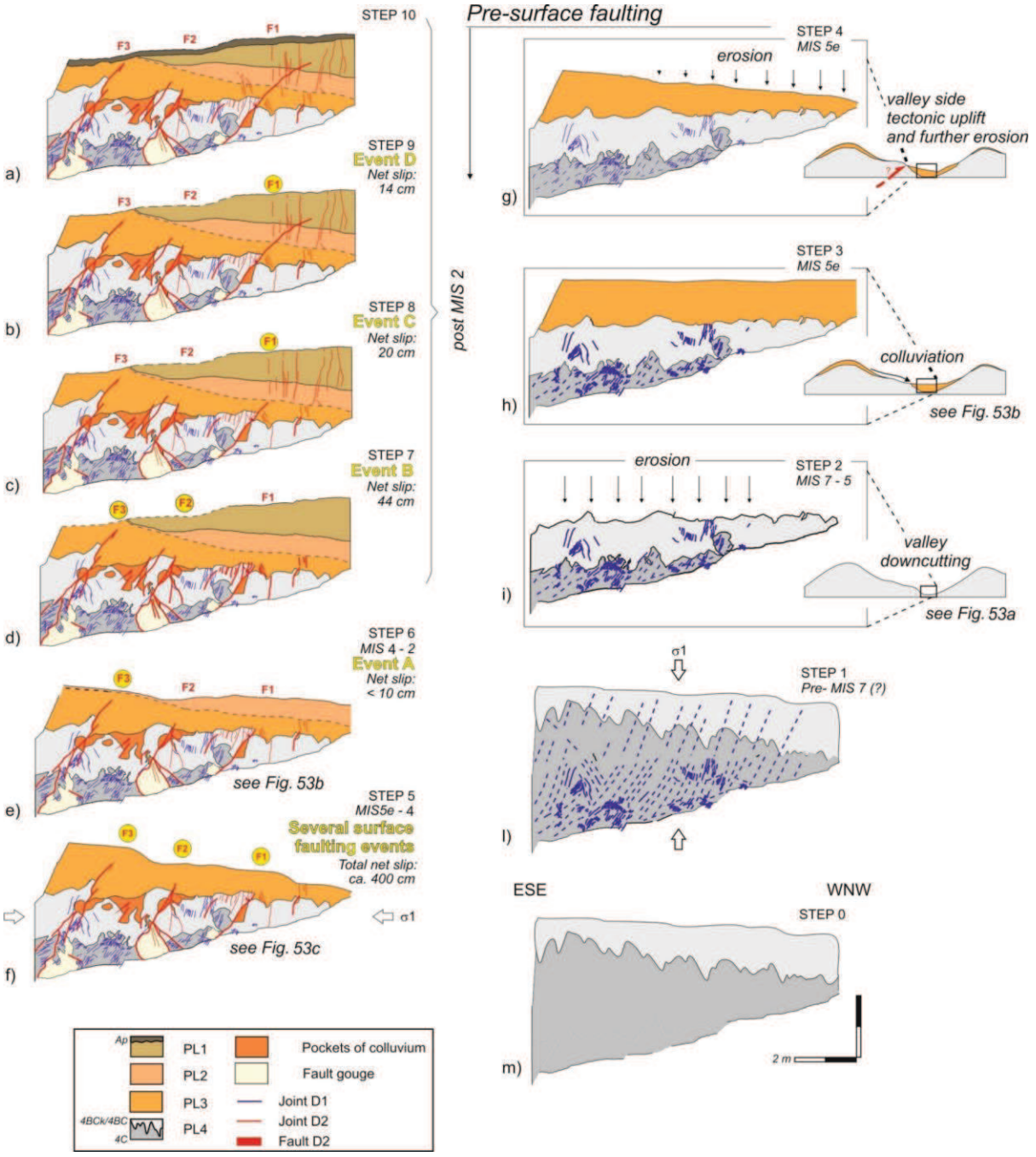

Fig. 56: a 10-step progressive retrodeformation of the logged section highlighting the progressive step-by-step coseismic deformation and paleoseismological reconstruction. Slip on each fault strand (i.e., F1, F2 and F3; Fig. 5) is here restored according to apparent displacements on the logged wall; timing is given by AMS-14C dating, pedostratigraphy and crosscut relationship between different sets of structures. Fault labels are circled while the structure is moving. White arrows on STEP 1 and 5 indicate the orientation of the principal stress (σ1) during D1 and D2 respectively, according to the observed structures. For a full description see the text; here only a brief summary is given: m) to i), hypothetical reconstruction of the evolution of the valley floor during a long-term time window previous to MIS5e, including repeated cycles of rock weathering pedogenesis and erosion; h), following a river piracy event, the valley floor is progressively infilled by colluvium and g) a supposed tectonic uplift and tilting of the valley side, not directly recorded at the site, triggered a subsequent phase of incision, slightly shifting the thalweg to the W; f) to a) is a reconstruction of the complex history of surface faulting, loess deposition and soil development. At least 4 surface faulting events (Fig. 56e to 56b) can be identified and three of them occurred in the last ca. 25 ka. For each event the relative net slip is indicated; in f) (STEP 5), the total net slip of ca. 400 cm is the result of several surface faulting events, thus representing a first cumulative evidence of repeated coseismic surface faulting.

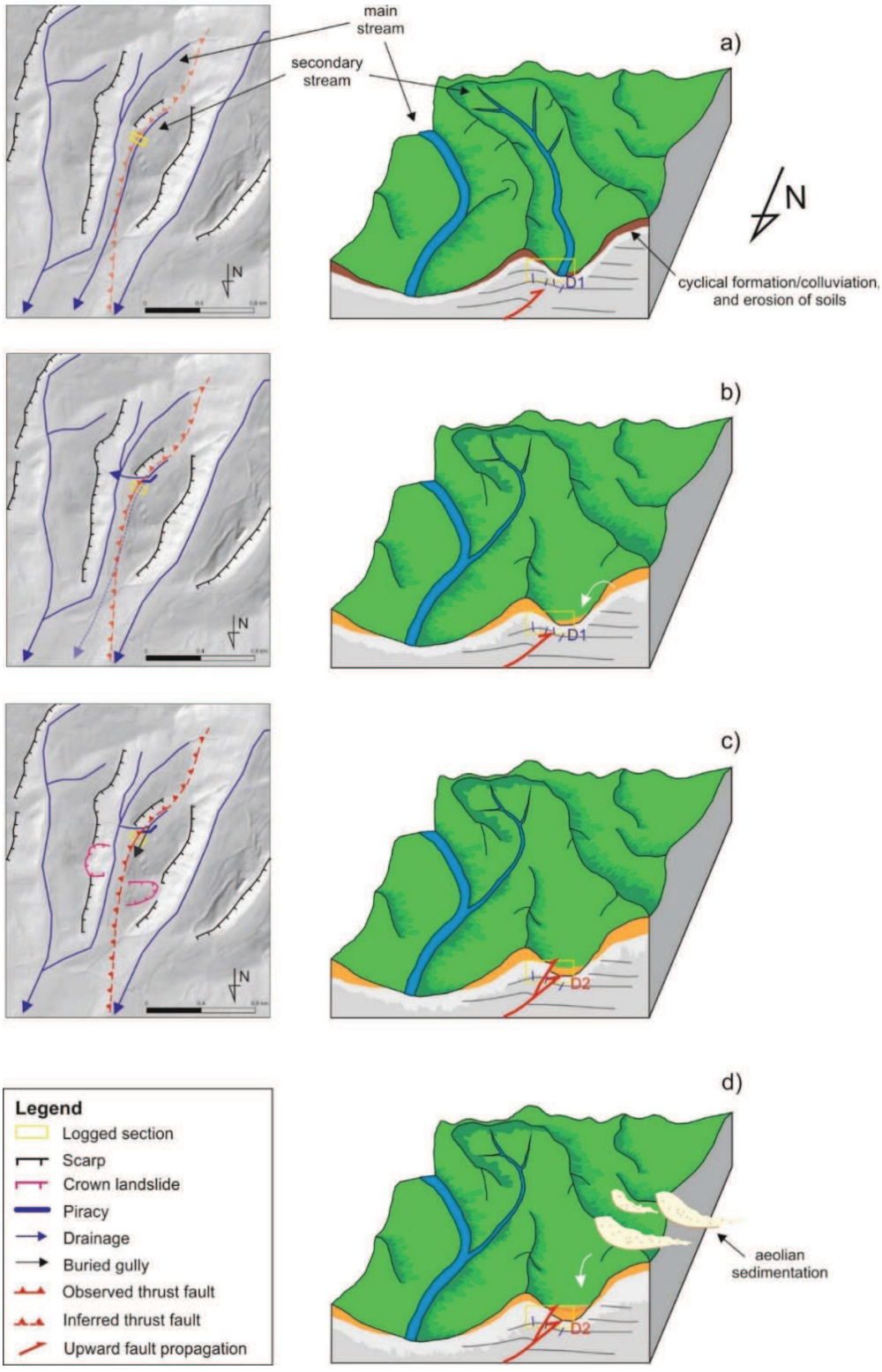

Fig. 57: Landscape evolution of the Pecetto di Valenza site: morphotectonic map, based on a hillshade model derived from a 5 m resolution DEM, on the left; conceptual 3D block diagram model of the different evolutionary phases. a) active secondary valley with deep buried tectonic structures. b) partial infilling of the secondary valley by a colluvium (PL3) after a phenomenon of stream piracy, demonstrated by an elbow of capture upstream, and upward propagation of the tectonic structures. c) upward propagation of the main tectonic structures, crosscutting PL3 to the surface. d) new upward propagation of one of the main tectonic structures, crosscutting the two loess covers (PL2 and PL1) deposited earlier.

If we consider the time interval covered by events B to D (post MIS-2 – 4 a BP) and the total net slip expressed by all the fault strands during each event, we obtain an average value of slip-per-event at surface of 26 ± 16 cm. Calculated slip rate is ± 0.08 mm/a and average return period can be estimated in 3333 ± 2055 years. If we consider these values as reliable and we extrapolate fault behavior back in time since MIS 5e, we need an average of 19 events (exactly 19 ± 11, considering uncertainty in slip per event) in order to cumulate the total slip recorded at this site and a corresponding recurrence interval of ca. 3967 – 9916 years. As discussed above, age constraints are based on limited AMS-^{14}C dating, therefore this should be regarded as a preliminary assessment.

5.2 The Monte Netto site

5.2.1 The chronological constraints from the loess/paleosols sequence investigated in 2013

Comparing the field properties and the new OSL/TT-OSL ages of the NMNT sequence presented in paragraph 5.2.1, with the characteristics of the sequence OMNT published in Livio et al. (2014) and Zerboni et al., (2015) it has been possible to correlate the pedostratigraphic levels and to obtain better chronological constraints to the paleoenvironmental evolution of this site (Fig. 58).

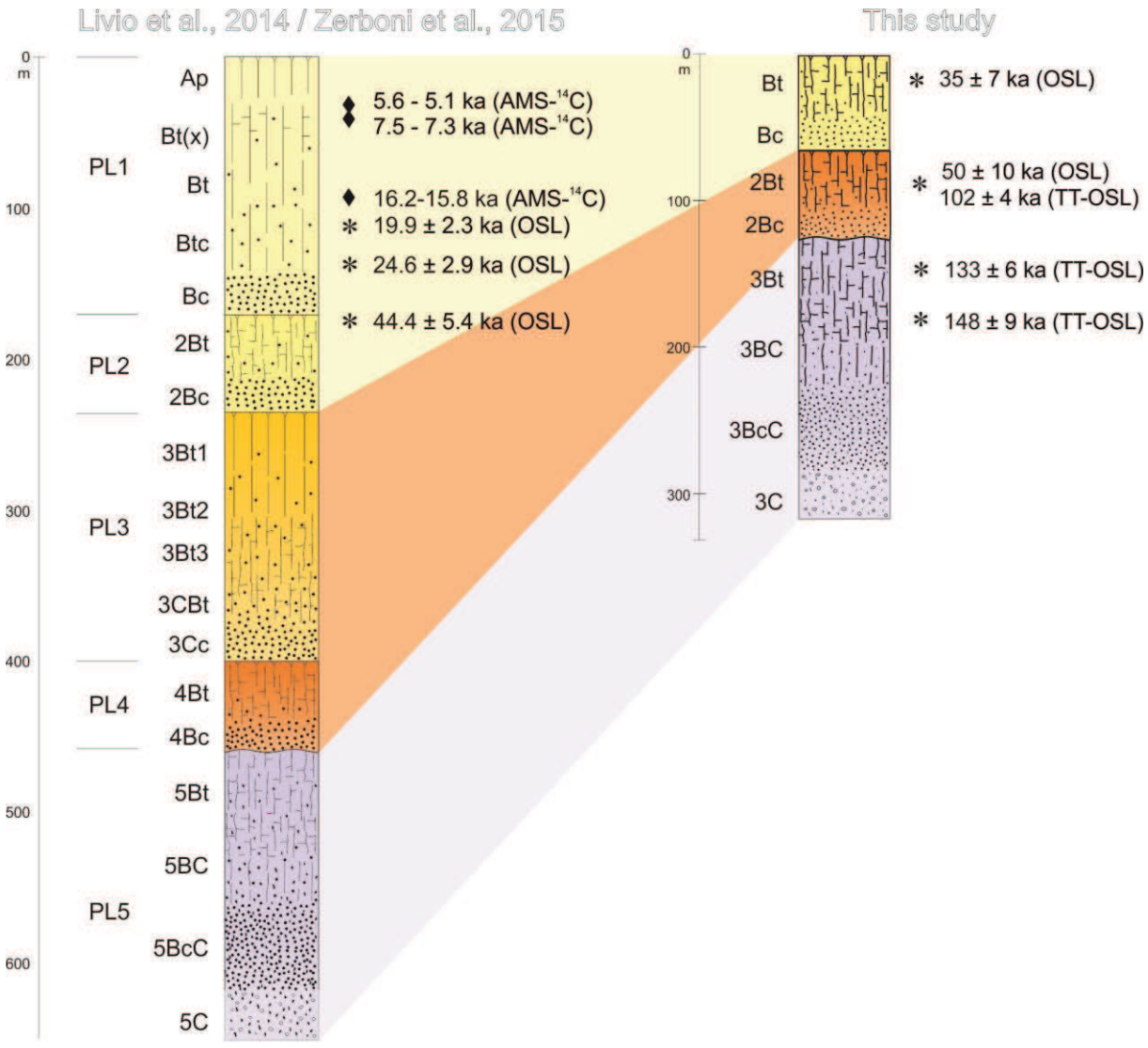

Fig. 58: Comparison between the pedostratigraphy of OMNT sequence (on the left; Livio et al., 2014; Zerboni et al., 2015) and the NMNT sequence (on the right). The OSL/TT-OSL ages are also indicated.

The pedostratigraphic level at the bottom of the sequence results composed by fluvial material, dating 148 ± 9 and 133 ± 6 ka: these ages can correspond to two phases of aggradation, on the base of a

correlation with the fluvial sequence described in Livio et al. (2014), below the loess/paleosols sequence described in Zerboni et al., (2015). The Authors, from the bottom of the sequence, identify a clast-supported fluvial conglomerate passing to a fining upward layer of interbedded silt and medium sand. Over this layer a fining upward coarse sands and conglomerates unit is described, probably representing a crevasse channel, followed by a thick overbank upward coarsening sequence. The uppermost sediments represent three or more crevasse splay episodes. Therefore, it is reasonable that the fluvial material identified at the base of OMNT sequence correspond to several phases of aggradation.

The intermediate PL represents a polycyclic paleosol, resulting from the weathering of fluvial materials (corresponding with the Eemian soil of PL4 in OMNT) and the subsequent inclusion and digestion of aeolian sediments during MIS 4, which match with the loess deposit of PL3 in OLMN. The thickness of this PL, compared with the PL3 and PL4 one of OMNT, appears condensed. As stated above, NMNT is located at the top of the anticline, whose growing played a crucial role in the formation of this PL and whose evolution can be chronologically constrained, using both the obtained OSL and TT-OSL ages. The TT-OSL age 103 $\pm$ 10 ka probably dates the last phases of fluvial aggradation, after that, the surface stabilises. This stabilization is connected to the growing of the anticline, which reaches a topographic height enough not to be covered by overbank deposits from the plain. Therefore, the pedogenetic processes started to take place on stabilized fluvial deposits. When climate turned into glacial conditions in MIS 4, the sedimentation of windblown materials started (Cremaschi, 1987; 1990a; 1990b; 2004; Cremaschi et al., 2011).

At the top of the anticline, the thickness of the loessic material is lower than in the syncline, where the growth of the fold causes a relief that acted as a topographic obstacle/sedimentary trap for the accumulation and preservation of thickest deposits. Therefore, at the top of the anticline, the reduced thickness of aeolian materials has been continuously weathered by pedogenesis and combined with the previous soil developed on the fluvial parent material. The aeolian sedimentation continued throughout the Upper Pleistocene and wind-blown sediments has been weathered until 50 ± 10 ka: this OSL age likely dates the last loessic contribution before the burial of the polycyclic paleosols. Indeed, after this phase, more intense glacial conditions in MIS 3 took place, and the strengthening of winds favoured the deposition of a thicker loess cover (Ferraro, 2009). This event is testified by the OSL age of 35 ± 7 ka obtained for the uppermost PL, developed on aeolian material and corresponding with PL2 and PL1 of OMNT. It is possible to suppose that the deposition of a thicker loess deposits has been favoured also by the interruption of the anticline uplift, or by the deceleration of the uplift rate, which allowed the deposition of a more continuous cover of loess, levelling the topographic surface between the anticline and the syncline portion of the fold.

In this framework, the combination of OSL with TT-OSL dating allowed to add more constraints to the paleoenvironmental evolutions of the Monte Netto site. In particular, also in this case, the aeolian deposition demonstrated a positive feedback with the tectonically induced surface deformation. The topographic reliefs, resulting from the progressive growth of the anticline, acted as a barrier and allowed the deposition of the loess cover, preserving the tectonic structures.

5.2.2 The 2016 outcrop as a new paleoseismological laboratory

The correlation between the pedostratigraphic levels described in Livio et al., (2014) and Zerboni et al., (2015) and the ones identified at 2016 outcrop, besides to offering the opportunity to better constrain the age of the deformed sequence as demonstrated in paragraph 4.2, also allows to investigate the fault geometry and its characteristics. This latter aspect, is beyond the aim of this project. Nevertheless, these correlation between the different stratigraphic sequences, represented the base for a paper (in preparation), in which we demonstrate that shallow stratigraphy can significantly change the potential of surface faulting from an upward propagation fault. A preliminary trishear kinematic restoration of the main fault plane and associated fold, allows to perform a grid search over the parameters regulating fault growth and propagation, i.e., fault slip, trishear angle, ramp angle, tip line position and the propagation/slip ratio (P/S). We chose the most appropriate combination of parameters to restore the top of PGS to a horizontal geometry (Fig. 59). However, a precise unfolding of the anticline resulted in a poor restoration of the fault cutoff (Fig. 59b). Conversely, a precise retrodeformation of the fault cutoff obtained by lowering the P/S value, produced a bad fold restoration (Fig. 59c). Thus, we must suppose that the fault and fold growth evolution occurred in two stages: the fault propagated faster (P/S = 7) through deeper stratigraphic units and slower through shallower stratigraphic units (P/S ca. 3). During these latest phases of deformation, several stacked bodies of aeolian sands and silts deposited, levelling the progressive structural relief cumulated by the thrust movements, and were cyclically weathered and pedogenized into a sequence of stacked paleosols.

These results are consistent with the stratigraphy described above , and with data collected from a set of deep and shallow boreholes (Livio et al., 2009). Here, from the top, the loess paleosols sequence unconformably lies over ca. 5-10 meters of overbank and colluvial deposits followed, downward, by a ca. 50 m – thick sequence of channel-facies clast-supported gravels in a sandy matrix. The latter unit, characterized by a negligible cohesion and axial strain failure, can be considered as responsible for a fast propagation of the cutting-through fault tip. Therefore, vertical and lateral changes of lithological

units would result in derived changes in the potential for surface faulting across the same fault, providing new insights into fault displacement hazard assessment.

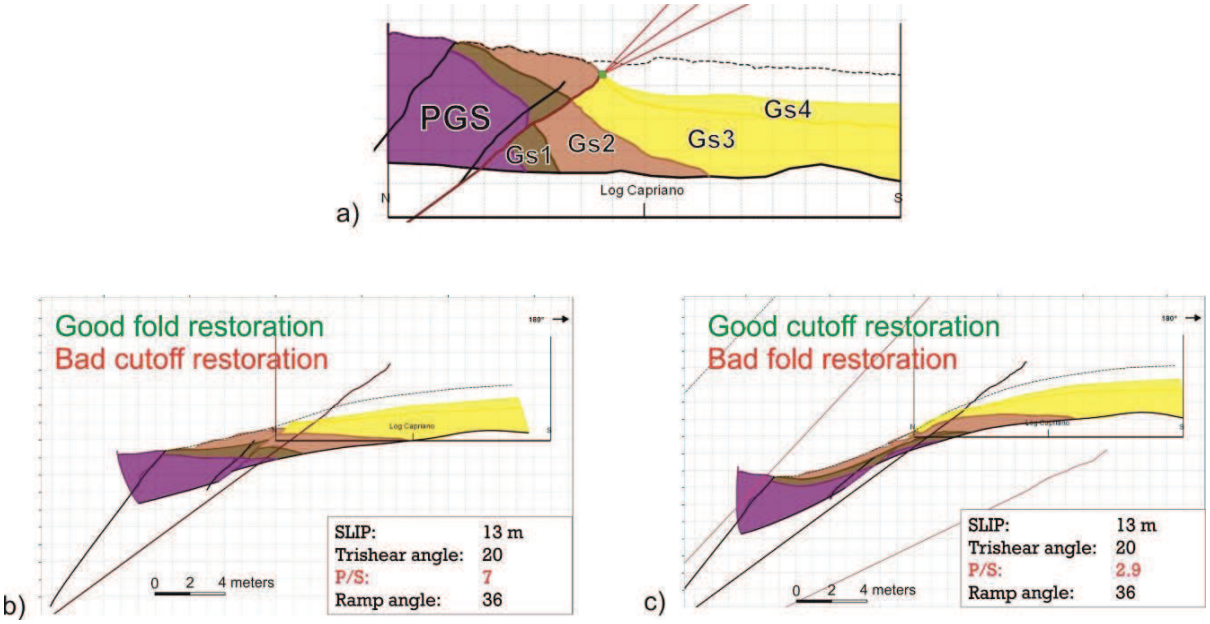

Fig. 59: Monte Netto new outcrop; a) schematic restoration through trishear kinematic modeling: note the fault strand, in red and the associated trishear triangle at the fault tip; b) retrodeformation using the parameters obtained through the inverse grid search approach: fault cutoff has not been appropriately restored; c) retrodeformation obtained using the P/S value measured at autocrop (i.e., ca. 3); fold is not appropriately restored.

In this framework, the role of the pedostratigraphic analysis into the paleoseismological one is clear. In addition, the micropedology of soil thin section, as demonstrated at Pecetto di Valenza site (paragraph 5.1.3) could help identifying at microscopic scale, tectonic evidence not visible at macroscopic scale. The identification of crosscutting relationship recorded into the natural organization of a soil, could allow to decipher a greater number of event that characterized a site. The potentiality of this approach will be extensively discussed in the next paragraph.

5.3 Comparison between the Monferrato and Monte Netto area

5.3.1 The Upper Pleistocene evolution of the Po Plain area

The paleoseismological approach applied at the Pecetto di Valenza and Monte Netto site, highlights the importance of loess/paleosols sequences as a reference stratigraphic unit. Between the aeolian sedimentation and the tectonically induced surface deformation a positive interaction exists. The terraces of the Alessandria and Valenza plateaux (Solero and Rivarone sites), the small valley at Pecetto di Valenza site and the isolated hill of Monte Netto, are landforms of tectonic origin that acted as barrier and/or sedimentary traps for the deposition and preservation of aeolian material. In particular, the interaction between pedostratigraphy and earthquake surface faulting has been identified at Pecetto di Valenza and Monte Netto site. These sites can be closely correlate, due to the loess deposition that occurred, for both sites during MIS 3 and MIS 2. This timing is consistent with other sequences identified in the Po Plain Loess Basin (PPLB), where the pedostratigraphic evolution is linked to the glacial and interglacial phases: the Bagaggera (Cremaschi et al., 1990), Val Sorda (Cremaschi et al., 1987) and Ghiardo sequences (Cremaschi and Christopher, 1984; Cremaschi, 1987; Cremaschi et al., 2011), the Fumane and Tagliente caves (Cremaschi, 1990b; Cremaschi, 2000; Peresani et al., 2008). The Ghiardo sequence, in particular, helped to understand the meaning of those samples taken from the loess unit, both at Monte Netto and Pecetto di Valenza site, which have been radiocarbon dated to the Early - Mid-Holocene, a period that cannot correspond with the loess formation. At Ghiardo, in the Holocene, due to the occurrence of local colluvial events and/or reworking due to anthropic activity (deforestation and agriculture), the upper layers of the Upper Pleistocene loess underwent a rejuvenation of the OSL signal and to the accumulation of organics in the topsoil (Cremaschi, 1987; Cremaschi et al., 2014). Probably, a rejuvenation of the uppermost loess occurred also at Monte Netto and Pecetto di Valenza site, due to a contamination of younger organic matter migrated from the active topsoil, confirming that Holocene radiocarbon ages should be attributed to a recent pedogenesis under warm climatic conditions.

In general, the OSL/TT-OSL results obtained for the loess deposits analysed in this project, are consistent with other radiometric datings available for the loess of the PPLB (e.g., Cremaschi, 1987; 1990a; 1990bM 2004; Cremaschi et al., 2011; Giraudi, 2014; 2015) and is possible to state that the loess sedimentation presumably started at the onset of glacial conditions, soon after the beginning of MIS 4. It is possible that the rate of dust accumulation increased during MIS 4 and MIS 3. As observed at Monte Netto, in the Monferrato area and elsewhere (Cremaschi et al., 2011), the persistence of glacial conditions permitted i) the increase of aridity in the area (and consequently the decrease of vegetal cover) and the strengthening of the wind responsible for deflation and dust transportation; ii)

the deposition of thick loess body on stabilized surface, that prevent them from intense erosion in subsequent interglacials/interstadials, in particular during Holocene, allowing their preservation until today.

5.3.2 Micropedology as a valuable tool in paleoseismology deciphering pedogenetic processes interacting with tectonics

The integrated paleoseismological approach applied at the Pecetto di Valenza and Monte Netto site, highlights also the key role played by the micropedological analysis of each loess/paleosols sequence.

The role of soils and paleosols is already known in paleoseismology (e.g., Nelson, 1992; Previtali, 1992; Amit et al., 1996; McCalpin and Berry, 1996; Birkeland, 1999; Rockwell, 2000; McCalpin, 2009; Livio et al., 2014): in the analysis of trench wall stratigraphy, they are typically considered as marker for event horizons (*sensu* Pantosti et al., 1993; McCalpin, 2009). Nevertheless, the potentiality of soils/paleosols to record past events also into their internal natural organization, as highlighted at Pecetto di Valenza (paragraph 5.1.3) and Monte Netto (paragraph 4.2) sites, has been largely overlooked until now.

Indeed, the review of the available literature on this topic, presented in detail in paragraph 1.2, highlights that micropedology is barely integrated to the paleoseismological research.

Previtali (1992) is one of the first authors who tried to use soils in these terms, stating that “the seismic waves also disturbed the internal arrangements of many soils, leaving behind macroturbations”. These observations, even highlighting the importance of the information included into the soil microstructure, have been too little explored through a micropedological approach and seldom integrated into a paleoseismic investigation. Indeed, in literature exist some studies that simply observe the faulting effect on soil microstructure, comparing the micromorphology of soil breccia zones with the micromorphology of unfaulted soils (Douglas, 1981; Douglas et al, 1983). Other Authors (Jim, 1990; Cetin, 1995; 1998; 2000) state that the elements of fabric (i.e., elements constituting the spatial arrangements of a soil; Stoops, 2003) of soil that underwent tectonic stress, show a preferred orientation which corresponds with the maximum principal stress direction. Nevertheless, they have not identified clear crosscutting relation that can be useful to decipher the sequence of tectonic events and, therefore, the paleoseismological evolution of the analysed site.

Only few and recent studies (Jeong & Cheong, 2005; Vanneste et al, 2008; Livio et al, 2014, Verbeeck et al, 2017; Frigerio et al, 2017), discussed the observations performed in thin section on the interaction between tectonic deformation and elements of fabric in a paleoseismic setting: the identification at microscopic scale of tectonic evidence, not visible at macroscopic scale, allowed to

establish important constraints to the paleoseismological reconstructions. These works, however, do not consider the possibility to decipher the numbers of events that characterized a site, thanks to the observation of the crosscutting relationship recorded into microstructure, micromass and pedofeatures (e.g., clay coatings, nodules, papulae). The latter, (defined by Stoops, 2003, as "discrete fabric units present in soil materials that are recognizable from an adjacent material by difference in concentration in one or more components or by a difference in internal fabric") result from the interaction of soil forming factors, including climate. Therefore, the identification of pedofeatures formed during specific climatic phases and subsequently disturbed by surface deformation, can provide relative chronological constraints useful to detail paleoseismological reconstructions.

In this light, micropedology can be useful to fill, or at least reduce, the paleoseismic record that is often incomplete, because: i) earthquakes can be too small (i.e., < 5.5) to produce detectable surface evidence, ii) the sedimentation rate must guarantee that each surface faulting event can be recorded by a sedimentary event (i.e., event horizon), iii) the evidence can be modified, obscured or removed by common surface processes. The record and preservation of the features left by paleoearthquakes can be compromised by too long earthquake recurrence intervals (e.g., in intraplate areas) or by too low accumulation rates or discontinuous sedimentation processes over time. In this framework, particularly conservative conditions are needed. The revision of the literature presented in paragraph 1.2, highlighted that all the studies have been performed in sites characterized by low sedimentation rates, low slip-rates, and the presence of loess deposits. The concomitant occurrence of these three conditions define the ideal conservative setting that can allow the preservation of primary and secondary evidence of seismic deformation in soils and sediments. Nevertheless, all the Scholars underlined that the geologic record of paleoearthquakes, especially in warm-humid climates, are rapidly degraded by chemical weathering and post-faulting pedogenesis. In such cases, macroscopic paleoseismic evidence may appear vague, but can be well preserved at the microscopic scale, and well interpreted if samples are collected where recent moisture content changes and pedological processes (such as biological activity and secondary calcite formation) are less expressed. Therefore, the micromorphological analysis becomes the only way to decipher the past processes interacting with tectonics, providing important clues in defining recurrence intervals of earthquakes and relevant implications for seismic hazard assessment.

As stated above, the potentiality of the micropedological approach integrated into the paleoseismological practice has been highlighted for the first time during the study of the Pecetto di Valenza site. The thin section coming from a pocket of colluvium located along the main fault strand (PCT-8; Fig. 29) shows a parallel sub-vertical orientation of the coarser elements of the micromass aligned along tectonic strain axis. These stress features helped constraining one of the main tectonic

deformation phases after the deposition of the colluvium, which has been involved in the displacement. Another soil thin section sampled in correspondence of the fault gouge (PCT-10; Fig. 29) presents Fe-Mn oxides-hydroxides along planar voids, corresponding, at macroscopic scale, to systematic joints. The latter are crosscut by a fault gouge, interested by illuvial clay, and locally deformed in a small-scale kink band anticline, due to a rotational component along the fault gouge. The joints filled by Fe-Mn oxides-hydroxides and illuvial clay helped marking the first stage of the deformation history of this site. Instead, the fault gouge including some fragments of illuvial pedofeatures from the base of the colluvial deposits, implies that during a further step of the tectonic history of the site, the topographic surface was coseismically offset after the deposition of the colluvium.

The importance of the information obtained from the application of this approach, prompted me to sample for soil thin section also the 2016 outcrop at Monte Netto site. The microphotographs shown in paragraph 4.2 illustrate the possibility to identify clear crosscutting relationship that can be useful to detail the sequence of events that characterized the site.

6. Conclusions

The innovative paleoseismological approach applied to this research project, integrating pedosedimentary and micropedological data, structural analyses, radiocarbon and luminescence dating with structural data, highlighted the role of loess deposits as valuable marker able to record and preserve evidence of tectonically induced deformation and earthquake surface faulting.

- In the Monferrato area, the luminescence dating of loess deposits at Solero, Rivarone, and Pecetto di Valenza sites, allowed to constrain to the Upper Pleistocene the formation and evolution of the Alessandria and Valenza plateaux, which in the existing literature have never been dated through direct radiometric methods. Moreover, thanks to the pedostratigraphic analyses, the formation of the Alessandria plateau terrace has been ascribed to the rearrangement of the drainage network following the Late Pleistocene diversion of the Tanaro River, rather than to the variation of the tectonic activity and deactivation of the Monferrato Frontal thrust (Giraudi, 2015).

- At Pecetto di Valenza site, for the first time in the Monferrato area, evidence of earthquake surface displacement has been recorded in a late Quaternary pedosedimentary sequence, formed by weathered marly bedrock, subsequently interested by slope processes (colluvium), and two events of loess deposition controlled by the fault growth at surface.
  The integrated paleoseismological approach proved to be successful in discriminating at 4 paleoearthquakes recorded at this site, with average slip-per-event of ca. 26 cm (Figs. 56 and 57). Several earlier surface faulting events are recorded in the colluvial basal unit of the section (PL3 in Fig. 29 and Fig. 56f), with an overall net slip at surface of ca. 400 cm, but the stratigraphic resolution is too limited here to discriminate among single paleoearthquake displacement. The occurrence of these scarp-forming events is the last stage in the growth of the causative reverse fault. In fact, systematic jointing observed in the damage zone allows recognizing the evolution from a blind fault to a fault, which breaks up to the topographic surface. These recent structural features are preserved thanks to the local geomorphic and geological setting, where the sedimentation/erosion rates are typically low. These conditions, occurred during the progressive growth of the fault zone that acted as a sedimentary trap, allowed the deposition of the two loess covers, becoming a marker of the tectonically induced surface deformation.
  Approximations of Late Pleistocene to Holocene slip rate along the Pecetto di Valenza reverse fault is 0.08 mm/a, and average return period can be estimated in 3333 ± 2055 years. These

estimations are consistent with typical Quaternary capable faults in the region, and fit the seismic landscape of the Po Plain (sensu Michetti et al., 2012). Observed slip-per-event of few decimetres is in line with causative earthquakes of ca. Mw 6.5 as observed from empirical relations for earthquake reverse surface faulting worldwide (Wells and Coppersmith, 1994; Lettis et al., 1997; Stirling et al., 2002). A preliminary assessment of a maximum magnitude in the order of Mw 6.5 is therefore completely reasonable also for the Monferrato Arc.
Obviously, further investigation is needed to confirm these initial estimates. Further research is also needed for the reconstruction of an accurate tectono-stratigraphic model of the Eastern Monferrato area, and for a detailed definition of the time/space relationships between the studied fault system and the Padane Thrust Front.

- A positive feedback between the aeolian deposition and the tectonically induced surface deformation has been recorded also at Monte Netto site. The geochronological characterization obtained through the OSL and TT-OSL dating methods is more detailed than the one presented in previous works (Livio et al., 2014; and Zerboni et al., 2015). These new chronological constraints, can be used to make correlations with the 2016 sequence and subsequently considered into the step-by-step restoration of the deformed sequence preliminary presented in paragraph 5.2.2. Additional constraints can be obtained from the cross/cutting relationship recorded at microscale, investigated through the micropedology of soil thin sections. As in the case of the Pecetto di Valenza site, the application of the integrated paleoseismological approach to the study of the interaction between aeolian sedimentation and active tectonics allows to define the uplift/deformation rates, the number, the magnitude, and the recurrence interval of paleoearthquakes occurred in this area.

- The potentiality of the micropedological approach into the paleoseismological practice has been highlighted in the Pecetto di Valenza study. The thin section coming from a pocket of colluvium located along one of the main fault strand, showing clear stress features, helped constraining one of the main tectonic deformation phases after the deposition of the colluvium, which has been involved in the displacement. Another soil thin section sampled in correspondence of the fault gouge, showing a set of joints systematically cut by the fault gouge, interested by illuvial clay locally deformed. The joints mark the first stage of the deformation history of this site; the fault gouge including some fragments of illuvial pedofeatures from the base of the colluvial deposits, imply that during a further step of the tectonic history of the site, the topographic surface was coseismically offset after the deposition of the colluvium.

Due to the important constraints obtained from these observation, we decided to sample for soil thin section also at Monte Netto site, along the main fault strands exposed in the 2016 outcrop. The intention is to obtain further data to constraint the kinematic restoration model above mentioned, and therefore to correctly assess the seismic hazard for this area. Indeed, the microphotographs presented in paragraph 4.2, clearly illustrates the potentiality of micropedology to decipher past pedogenetic processes interacting with tectonics. Such potentiality of the micropedological approach integrated into the paleoseismological practice, will be object of a paper focusing on the usefulness of this approach.

The paper, under preparation, aims to define an ideal workflow to follow during studies performed at site scale. The workflow starts from the definition of the ideal conditions, at regional scale, in which is possible to apply the suggested approach, arriving to the definition of diagnostic criteria useful to identify crosscutting relationship recorded into pedofeatures, microstructure and micromass, in order to help recognizing the number of events and their chronology. Particular attention will be taken defining the diagnostic criteria that allow distinguishing between elements that can be associated or not to a tectonic disturbance. In fact, pedofeatures linked to frost activity or vertic processes can be confused with those resulting from tectonic stress (Van Vliet-Lanoë, 2010; Kovda and Mermut, 2010). In the latter case, the determining factor will be the environmental setting. Also the differentiation between features displaced by coseismic rupturing instead of fault creep is a delicate issue: for this reason, is planned the image acquisition, through digital camera, of the soil thin sections from the Pecetto di Valenza and Monte Netto site, in order to construct multispectral images at plane and cross-polarized light that will be quantitatively analyses through an image analysis software (e.g., the freeware Image-J; https://imagej.nih.gov/ij/). The latter will allow ranking images and defining morphometric parameters, such as the shape of the grains, average size, roughness and smoothness, etc., to fill a numeric database subsequently subject to a multivariate statistics analysis (i.e., PCA, cluster analysis). In this way, we hypothesize to become able to decipher between features occurred during coseismic or creep movements.

It is also planned to present a collection of microphotographs from Pecetto di Valenza (paragraph 3.3.2.3) and Monte Netto (paragraph 4.2) site, as clear examples of the interplay between soil forming processes and tectonic activity. This collection is intended as a first step toward the creation of an atlas of seismopedoturbation in thin section, which can be used as a comparison tool in future paleoseismological analysis.

In conclusion, the results obtained investigating the sites discussed in this research project, clearly show that the joint research in Quaternary Geology, paleoseismology, structural analysis,

pedostratigraphy and micropedology applied to loess/paleosols sequences, might greatly improve our understanding of seismic hazard and recent landscape evolution for the Po Plain area and may offer, in the future, a methodological approach useful in other environmental contexts.

References

Aitken, M.J., 1990. Science-based Dating in Archaeology. London: Longman

Albini, P., & Rovida, A., 2010. The 12 May 1802 earthquake (N Italy) in its historical and seismological context. Journal of seismology, 14(3), 629-651.

Allmendinger, R.W., Marrett, R.A., Cladouhos, T.T., 2001. FaultKinWin: a Program for Analyzing Fault Slip Data for Windows TM Computers. Version 1.1.

Allmendinger, R.W., Marrett, R.A., Cladouhos, T.T., 2001. FaultKinWin: a program for analyzing fault slip data for Windows™ computers.

Amit, R., & Zerboni, A. 2013. Report on the INQUA-AEOMED field-trip workshop 'Reconsidering Loess in Northern Italy'(Po Plain, 1-3 July 2013). ALPINE AND MEDITERRANEAN QUATERNARY, 26(2), XI-XV.

Amit, R., Harrison, J.B.J., Enzel, Y., Porat, N., 1996. Soils as a tool for estimating ages of Quaternary fault scarps in a hyperarid environment - the southern Arava valley, the Dead Sea Rift, Israel. Catena, 28(1), 21-45 pp.

Amit, R., Zerboni, A., 2013. Report on the INQUA-AEOMED field-trip workshop 'Reconsidering Loess in Northern Italy' (Po Plain, 1-3 July 2013). AMQ - Alpine and Mediterranean Quaternary 26(2): xi-xv.

Amorosi, A., Colalongo, M., L., Fiorini, F., Fusco, F., Pasini, G., Vaiani, S., C., Sarti, G., 2004. Palaeogeographic and palaeoclimatic evolution of the Po Plain from 150-ky core records. Global Planet Chang 40: 55 –78.

Arduino E., Barberis E., Carraro F., & Forno M. G., 1984. Estimating relative ages from ironoxide/total-iron ratios of soils in the western Po Valley, Italy. Geoderma, 33(1), 39-52

Arnold, L.J., Roberts, R.G., 2009. Stochastic modeling of multi-grain equivalent dose (De) distributions: implications for OSL dating of sediment mixtures. Quat. Geochronol. 4, 204–230.

Avouac, J.P., Meyer, B., Tapponnier, P., 1992. On the growth of normal faults and the existence of flats and ramps along the El Asnam active fold and thrust system. Tectonics 11, 1–11. doi:10.1029/91TC01449

Azzaro, R., Ferreli, L., Michetti, A.M., Serva, L. & Vittori, E., 1998. Environmental hazard of capable faults: the case of Pernicana Fault (Mt. Etna - Sicily). Natural Hazards. - Vol. 17. - p. 147-162.

Balestro G., Cadoppi P., Piccardo G.B., Polino R., Spagnolo G., Tallone S., Fioraso G., Lucchesi S., Forno M.G., Perrone G., Ossella L., Campus S., Tamberlani F., Nocolò G., 2009 - Note illustrative della Carta Geologica d'Italia alla scala 1:50.000, foglio 155 Torino Ovest. Servizio Geologico d'Italia, 150 pp.

Barbero, D., Boano, P., Colla, M.T., M.G., Forno, 2007. Pleistocene terraced succession, northern slope of Torino hill. Quaternary International, 171-172, 64-71.

Baroni, C., Zanchetta, G., Fallick, A. E., Longinelli, A., 2006. Mollusca stable isotope record of a core from Lake Frassino, northern Italy: hydrological and climatic changes during the last 14 ka. The Holocene 16: 827 –837

Bartolini, C., Caputo, R., & Pieri, M., 1996. Pliocene-Quaternary sedimentation in the Northern Apennine Foredeep and related denudation. Geological Magazine, 133(03), 255-273.

Benedetti, L. C., Tapponnier, P., Gaudemer, Y., Manighetti, I., Van der Woerd, J., 2003. Geomorphic evidence for an emergent active thrust along the edge of the Po Plain: The Broni-Stradella fault. Journal of Geophysical Research: Solid Earth (1978–2012), 108(B5).

Benedetti, L., Tapponnier, P., King, G. C., Meyer, B., Manighetti, I., 2000. Growth folding and active thrusting in the Montello region, Veneto, northern Italy. Journal of Geophysical Research: Solid Earth (1978–2012), 105(B1), 739-766.

Biancotti A., Cortemiglia G.C. (1981) - Ritrovamento di loess sul "Fluviale Medio" della Scrivia presso Novi Ligure (Piemonte, Italia). Quaderni Istituto di Geologica dell'Università di Genova, 2(5), 107 -125.

Bigi, G., Cosentino, D., Parotto, M., Sartori, R., Scandone, P., 1990. Structural Model of Italy, Consiglio Nazionale delle Ricerche (CNR), Progetto Finalizzato Ge- odinamica, Quaderni de "La Ricerca scientifica", 114 (3), 1:500.000 scale, Firenze, SELCA

Birkeland, P.W., 1999. Soils and Geomorphology, 448 p. Oxford University Press, Oxford, UK.

Boccaletti, M., Bonini, M., Corti, G., Gasperini, P., Martelli, L., Piccardi, L., Tanini, C., Vannucci, G., 2004. Seismotectonic Map of the Emilia-Romagna Region, 1:250000. Re- gione Emilia-Romagna – CNR

Boccaletti, M., Bonini, M., Corti, G., Gasperini, P., Martelli, L., Piccardi, L., ... & Vannucci, G., 2004. Seismotectonic Map of the Emilia-Romagna Region, 1: 250000. Regione Emilia-Romagna–CNR.

Boccaletti, M., Corti, G., & Martelli, L., 2011. Recent and active tectonics of the external zone of the Northern Apennines (Italy). International Journal of Earth Sciences, 100(6), 1331-1348.

Boccaletti, M., Corti, G., Martelli, L., 2011. Recent and active tectonics of the external zone of the Northern Apennines (Italy), International Journal of Earth Sciences, 100 (6), 1331-1348; doi:10.1007/s00531-010-0545-y.

Bonadeo, L., 2014. Studio sismotettonico del settore della Pianura Padana occidentale compreso tra il Tortonese ed il fronte della Collina di Torino. Università dell'Insubria. Ph.D. thesis, Como, Italy, pp. 178.

Boni, A. & Casnedi, R., 1970. Note illustrative della Carta Geologica d'Italia alla scala 1:100.000, Fogli 69 e 70 Asti e Alessandria. Poligrafica & Cartevalori, Ercolano, 64 pp.
Bøtter-Jensen, L., Murray, A.S., 1999. Developments in optically stimulated luminescence techniques for dating and retrospective dosimetry. Radiat. Prot. Dosim. 84, 307–315.

Bresciani, I., & Perotti, C.R., 2014. An active deformation structure in the Po Plain (N Italy): The Romanengo anticline. Tectonics, 33(10), 2059-2076.
Brewer, R., 1964. Fabric and Mineral Analysis of Soils. John Wiley and Sons, New York, p. 470.

Bullock P., Thompson M.L., 1985. Micromorphology of Alfisols. In: Douglas L.A., Thompson M.L., (eds), Soil Micromorphology and Soil Classification. SSSA Special Publication Number 15, Madison, WI.

Bullock, P., Fedoroff, N., Jongerius, A., Stoops, G., Tursina, T., Babel, U., 1985. Handbook for Soil Thin Section Description. Waine Research Publication, Albrighton, USA.

Burrato, P., Ciucci, F., and Valensise, G., 2003. An inventory of river anomalies in the Po Plain, Northern Italy: evidence for active blind thrust faulting. Annals of Geophysics, 46(5), 865-882.

Burrato, P., Poli, M.E., Vannoli, P., Zanferrari, A., Basili, R., Galadini, F., 2008. Sources of Mw 5+ earthquakes in northeastern Italy and western Slovenia: an updated view based on geological and seismological evidence, Tectono- physics, 453 (1-4), 157-176.

Caputo, R., Pellegrinelli, A., Bignami, C., Bondesan, A., Mantovani, A., Stramondo, S., Russo, P., 2015: High-precision levelling, DInSAR and geomorphological effects in the Emilia 2012 epicentral area. Geomorphology, 235, 106-117, doi: 10.1016/j.geomorph.2015.02.002

Carminati, E., Doglioni, C., Scrocca, D., 2004. Alps Vs Apennines. In: Geology of Italy, Special Volume of the Italian Geological Society for the IGC 32 Florence-2004, Edited by U. Crescenti, S. D'Offizi, S. Merlini e L. Sacchi, 141-151.

Carminati, E., Lustrino, M., & Doglioni, C., 2012. Geodynamic evolution of the central and western Mediterranean: Tectonics vs. igneous petrology constraints. Tectonophysics, 579, 173-192.

Carminati, E., Scrocca, D., Doglioni, C., 2010. Compaction-induced stress variations with depth in an active anticline: Northern Apennines, Italy. Journal of Geophysical Research: Solid Earth (1978–2012), 115(B2).

Carnelli, F., & Frigerio, I., 2016. A socio-spatial vulnerability assessment for disaster management: insights from the 2012 Emilia earthquake (Italy). Sociologia urbana e rurale.

Carraro F., 1969. La cattura del Tanaro, in CarraroF, Petrucci F. & Tavaglini S., Note illustrative della Carta Geologica d'Italia alla scala 1:100.000: Foglio 68, Carmagnola, II ed., Servizio Geologico d'Italia, Roma 1969

Carraro, F., Collo, G., Forno, M.G., Giardino, M., Maraga, F., Perotto, A. & Tropeano, D., 1995. L'evoluzione del reticolato idrografico del Piemonte centrale in relazione alla mobilità quaternaria. In Polino R. & Sacchi R. (ed s.) Atti del Convegno "Rapporti Alpi Appennino" e giude alle escursioni (Peveragno - CN), 31 maggio-1 giugno 1994) Acc. Naz. Sc., 14, 445-461.

Carta Geo Piemonte 250K https://www.arpa.piemonte.gov.it/approfondimenti/temi-ambientali/geologia-e-dissesto/bancadatiged/immagini_2014/cartageo250k_piem_r_a.jpg

Castellarin, A., and L. Cantelli, 2000. Neo-Alpine evolution of the Southern Eastern Alps, Journal of Geodynamics, 30 (1-2), 251-274.

Castellarin, A., C. Eva, G. Giglia, G.B. Vai, E. Rabbi, G.A. Pini and G. Crestana, 1985. Analisi strutturale del Fronte Appennico Padano, Giornale di Geologia, 47 (1-2), 47-75.

Castellarin, A., L. Cantelli, A.M. Fesce, J.L. Mercier, V. Ricotti, G.A. Pini, G. Prosser and L. Selli, 1992. Alpine compressional tectonics in the Southern Alps; relationships with the N-Apennines, Annales Tectonicae, 6 (1), 62-94.

Castellarin, A., Vai, G. and Cantelli, L., 2006. The Alpine evolution of the Southern Alps around the Giudicarie faults: A Late Cretaceous to early Eocene transfer zone, Tectonophysics, 414, 203–223.

Castellarin, A., Vai, G.B., 1986. Southalpine versus Po Plain Apeninic Arcs. In: Weizel, C. Ed.), The origin of Arcs. Elsevier Science Publisher B.V., Amsterdam, pp. 253–280.

Castello B., Selvaggi G., Chiarabba C. & Amato A., 2006. CSI Catalogo della sismicità italiana 1981- 2002, versione 1.1. INGV-CNT, Roma. http://csi.rm.ingv.it/.

Castiglioni G. B (1979). Geomorfologia, UTET, Torino 1979, pp 436.

Cetin, H., 1995. Multidisciplinary technique to differentiate paleoseismic from creep displacement of faults: tested at the Meers fault, Oklahoma. Ph.D. Dissertation, Texas A&M Univ., College Station, TX.

Cetin, H., 1998. Soil–pore and particle orientations caused by active faulting: a micromorphological perspective. Soil Sci. 163 (5), 374–381.

Cetin, H., 2000. An experimental study of soil memory and preconsolidation adjacent to an active tectonic structure: the Meers fault, Oklahoma, USA. Engineering Geology, 57(3), 169-178.

Cinti, F.R., Cucci, L., Pantosti, D., D'Addezio, G., and Meghraoui, M., 1997. A Major Seismogenetic Fault in a ''Silent Area'': The Castrovillari Fault (Southern Apennines, Italy). Geophys. J. Int. 130, 322–332.

CNR, 1980. Progetto Finalizzato Geodinamica. Sottoprogetto Neotettonica. Nuovi conrtibuti alla realizzazione della Carta Neotettonica d'Italia. Parte I. Pubblicazione n. 356. Officine grafiche napoletane Francesco Giannini & Figli (1981).

CNR, 1980. Progetto Finalizzato Geodinamica. Sottoprogetto Neotettonica. Nuovi conrtibuti alla realizzazione della Carta Neotettonica d'Italia. Parte III. Pubblicazione n. 356. Officine grafiche napoletane Francesco Giannini & Figli (1981).

CNR, 1982. Contributi conclusivi per la realizzazione della Carta Neotettonica d'Italia. Progetto Finalizzato Geodinamica. Vol. 506;513 : 2 : p. 433.

CNR, 1982. Progetto Finalizzato Geodinamica. Sottoprogetto Neotettonica. Nuovi conrtibuti alla realizzazione della Carta Neotettonica d'Italia. Parte II. Pubblicazione n. 513. Officine grafiche napoletane Francesco Giannini & Figli (1981).

CNR, 1983. Structural Model of Italy, scale 1:500.000. S.E.L.C.A. Firenze (Italia).Ambrosetti P., Bosi C., Carraro F., Ciaranfi N., Panizza M., Papani G., Vezzani L. & Zanferrari A.. Neotectonic map of Italy, scale 1: 500,000. Consiglio Nazionale delle Ricerche, 1983.

CNR, 1987. Progetto Finalizzato Geodinamica. Sottoprogetto Neotettonica. Neotectonic Map of Italy at scale 1:500.000 - Sheet 1. Ambrosetti P., Bosi C., Carraro F., Panizza M., Papani G., Vezzani L. And Zanferrari A. Litografia Artistica Cartografica, Florence (Italy).

CNR, 1990. Structural model of Italy. Scale 1: 500.000. Bigi G., Cosentino D., Parotto M., Sartori R., P. Scandone. Progetto Finalizzato Geodinamica.

Corsi M., Gatto G.O., Gatto P., 1969 - Foglio 58 "Mortara" della Carta Geologica d'Italia alla scala 1:100,000. II Ed., Servizio Geologico d'Italia, Roma.

Costantini, E.A.C., Priori, S., 2007. Pedogenesis of plinthite during early Pliocene in the Mediterranean environment. Case study of a buried paleosol at Podere Renieri, central Italy. Catena 71, 425–443.

Cremaschi M, Christopher C., 1984. Palaeolithic settlement and environment in the Middle Pleistocene of Northern Italy: the Ghiardo site. The Third Conference of Italian Archaeology, vol I, The Environment. B.A.R., London, pp 87-104

Cremaschi M., 2000. Manuale di Geoarcheologia. Laterza Editore, Bari, Italy

Cremaschi M., Zerboni A., Nicosia C., Negrino F., Rodnight H., Spötl C., 2015. Age, soil-forming processes, and archaeology of the loess deposits at the Apennine margin of the Po Plain (northern Italy). New insights from the Ghiardo area. Quaternary International, 376, 173–188. DOI: 10.1016/j.quaint.2014.07.044.

Cremaschi, M. & Rodolfi, G., 1991. Il suolo - Pedologia nelle scienze della Terra e nella valutazione del territorio. La Nuova Italia Scientifica, Roma.

Cremaschi, M., & Papani, G., 1975. Contributo preliminare alla neotettonica del margine padano dell'Appennino: le forme terrazzate comprese tra Cavriago e Quattro Castella (RE). ATENEO PARMENSE. ACTA NATURALIA, 11(2), 335-371.

Cremaschi, M., 1987. Paleosols and vetusols in the Central Po Plain Northern Italy: a study in Quaternary geology and soil development. Unicopoli, Milano, Italy.

Cremaschi, M., 1990a. The loess in Northern and Central Italy: a loess basin between the Alps and the Mediterranean Sea. C.N.R., Centro di Studio per la Stratigrafia e Petrografia delle Alpi Centrale, Milano, Italy

Cremaschi, M., 1990b. Depositional and post-depositional processes in rock shelters of northern Italy during the late Pleistocene: their paleoclimatic and paleoenvironmental significance. Quaternaire 1: 51 –64.

Cremaschi, M., 2004. Late Pleistocene loess. In: Antonioli F, Vai GB (eds) Litho-palaeoenvironmental maps of Italy during the last two climatic extremes. Climex Maps Italy - Explanatory notes, Bologna, pp 34 –37

Cremaschi, M., Rodnight, H., Zerboni, A., Spötl, C., 2011. Loess in Northern Italy. New insights on dating, environment and archaeology. Il Quaternario 24: 95 –97

Crescimbene, M., La Longa, F., Camassi, R., Pino, N. A., & Peruzza, L.,2014. What's the seismic risk perception in Italy?. In Engineering Geology for Society and Territory-Volume 7 (pp. 69-75). Springer, Cham.

Davidovich, U., Porat, N., Gadot, Y., Avni, Y., Lipschits, O., 2012. Archaeological investigations and OSL dating of terraces at Ramat Rahel, Israel. Journal of Field Archaeology 37, 192–208.

Dela Pierre, F., Piana, F., Boano, P., Fioraso, G., Forno, M.G., Polino, R., Clari, P., 2003a. Carta Geologica d'Italia alla scala 1:50.000, Foglio 157 "Trino", APAT, Agenzia per la Protezione dell'Ambiente e per i Servizi Tecnici - Dipartimento Difesa del Suolo, Roma.

Dela Pierre, F., Piana, F., Fioraso, G., Boano, P., Bicchi, E., Forno, M.G., Violanti, D., Clari, P., Polino, R., 2003b. Note il- lustrative della Carta Geologica d'Italia alla scala 1:50.000, Foglio 157 "Trino", APAT, Agenzia per la Protezione del- l'Ambiente e per i Servizi Tecnici - Dipartimento Difesa del Suolo, Roma, 147 pp.

Desio, A., 1965. I rilievi isolati della Pianura Lombarda ed i movimenti tettonici del Quaternario. Rend Ist Lom Acc Sc Lett, Sez A, 99, 881-894.

Di Manna, P., Guerrieri, L., Piccardi, L., Vittori, E., Castaldini, D., Berlusconi, A., Bonadeo, L., Comerci, V., Ferrario, F., Gambillara, R., Livio, F., Lucarini, M., Michetti, A.M., 2012. Ground effects induced by the 2012 seismic sequence in Emilia: implications for seismic hazard assessment in the Po Plain. Annals of Geophysics, 55 (4), 697-703, doi: 10.4401/ag-6143

Doglioni, C., 1993. Some remarks on the origin of foredeeps, Tectonophysics, 228 (1-2), 1-20.

Douglas, L.A., 1981. Soil micromorphology and faulting. U.S. Geological Survey, Open File Report No. 81-279, 7 pp.

Douglas, L.A., Sole-Benet, A., Low, A.J., Platt, D.W. (1983). The micromorphology of two soil fault-breccias. In Soil micromorphology. P. Bullock, and C. Murphy (eds.). AB Academic Publishers, Berkhamsted, Herts, UK, pp. 347-353

Duchaufour, P., 1983. Pédologie 1: Pédogenèse et Classification. Masson, Paris

Duchaufour, P., 1995. Pédologie. Sol, Vègètation, Environnment, Masson, Paris.

Duller, G.A., & Wintle, A.G., 2012. A review of the thermally transferred optically stimulated luminescence signal from quartz for dating sediments. Quaternary Geochronology, 7, 6-20.

Duller, G.A., 2008. Luminescence Dating: guidelines on using luminescence dating in archaeology. English Heritage.

Duller, G.A.T., 2004. Luminescence dating of Quaternary sediments: recent advances. Journal of Quaternary Science 19, 183e192.

Duller, G.A.T., 2008. Single grain optical dating of Quaternary sediments: why aliquot size matters in luminescence dating. Boreas 37, 589e612.

ENEL – DCO, 1984a. Progetto per la realizzazione di una centrale elettronucleare - Area Po1.

ENEL – DCO, 1984b. Progetto per la realizzazione di una centrale elettronucleare - Area Po2.

ENEL, 1985. Interpretazione sismica a riflessione e rifrazione high-resolution , e ricostruzione strutturale, stratigrafica, tettonica e neotettonica. Rapporto finale, Gexon srl.

Erhart, H., 1951. La genèse des sols en tant que phénomène géologique. Esquisse d' une théorie géologique et géochimique. Biostasie et rhéxistasie, Masson, Paris

Erslev, E., 1991. Trishear fault-propagation folding, Geology, 19, 617–620.

Eshel, G., Levy, G.J., Mingrlgrin, U., Singer, M.J., 2004. Critical evaluation of the use of laser diffraction for particle-size distribution analysis. Soil Sci. Soc. Am. J. 68, 736–743.

Falletti, P., Gelati, R., Rogledi, S., 1995. Oligo-Miocene evolution of Monferrato and Langhe, related to deep structures. In: R., Polino, & Sacchi, R. (Eds.), Atti del convegno "Rapporti Alpi-Appennino e guide alle escursioni": Peveragno (CN) 31 Maggio - 1 Giugno 1994. Accademia Nazionale delle Scienze, 14, 1-19.

Fantoni, R., R. Bersezio and F. Forcella, 2004. Alpine structure and deformation chronology at the Southern Alps Po Plain border in Lombardy, Bollettino della Società Geologica Italiana, 123, 463-476.

FAO, 2006. Guidelines for Soil Description, fourth ed. Food and Agriculture Organization of the United Nations, Rome, Italy.

Fedoroff, N., Courty, M.A., 1987. Morphology and distribution of textural features in arid and semi-arid regions. In: N. Fedoroff, L.M., Bresson et M.A. Courty (Editeurs), Micromorphologie des Sols/Soil Micromorphology, AFES, Plasir, France, pp. 213-219.

Ferraro, F., 2009. Age, sedimentation, and soil formation in the Val Sorda loess sequence, Northern Italy. Quatern Int 204: 54 –64.

Festa, A., Boano, P., Irace, A., Lucchesi, S., Forno, M.G., Dela Pierre, F., Fioraso, G., Piana, F., 2009a. Carta Geologica d'Italia alla scala 1:50.000, Foglio 156 "Torino Est", ISPRA - Istituto Superiore per la Protezione e la Ricerca Ambi- entale, Roma.

Festa, A., Codegone, G., 2013. Geologic map of the External Ligurian Units in western Monferrato (Tertiary Piedmont Basin, NW Italy). Journal of Maps 9.1: 84-97.

Festa, A., Dela Pierre, F., Irace, A., Piana, F., Fioraso, G., Lucchesi, S., Boano, P. & Forno, M.G., 2009b. Note Illustrative della Carta Geologica d'Italia alla scala 1:50.000 Foglio 156 "Torino Est". ISPRA, Servizio Geologico d'Italia: 143 pp.

Festa, A., Ogata, K., Pini, G.A., Dilek, Y., Codegone, G., 2015. Late Oligocene-early Miocene olistostromes (sedimentary mélanges) as tectono-stratigraphic constraints to the feodynamic evolution of the exhumed Ligurian accretionary complex (Northern Apennines, NW Italy). International Geology Review, 57, 540-562.

Forno M.G., 1979 - Il “loess” della Collina di Torino. Geografia Fisica e Dinamica Quaternaria, 2, 105 -124.

Forno, M.G & Lucchesi, S., 2016. Relicts of the Pleistocene Po Plain on the Western and Southern slopes of Turin Hill (NW Italy). Journal of Maps, 12.2: 394-406.

Forno, M.G., 1982. Studio geologico dell’Altopiano di Poirino (Torino). Geogr. Fis. Dinam. Quat, 5, 129-162.

Frigerio C., Bonadeo L., Zerboni A., Livio F., Ferrario M.F., Fioraso G., Irace A., Brunamonte F., Michetti A.M. , 2017. First Evidence for Late Pleistocene to Holocene earthquake surface faulting in the Eastern Monferrato Arc (Northern Italy): geology, pedostratigraphy and structural study of the Pecetto di Valenza site. Quaternary International, 451, 143-164.

Gabert P., 1962. Le platine occidentales du Po et leurs piedmont (Piemont, Lombardie occidentale et centrale). Etude morphologique. 531 pp., 208+15 ff., 5 carte, Louis Jean,Gap.

Galadini, F., Falcucci, E., Galli, P., Giaccio, B., Gori, S., Messina, P., Moro, M., Saroli , M., Scardia, G. & Sposato, A., 2012. Time intervals to assess active and capable faults for engineering practices in Italy. Engineering geology, 139, 50-65.

Galadini, F., Galli, P., Molin, D., Ciurletti, G., 2001. Searching for the source of the 1117 earthquake in northern Italy: a multidisciplinary approach. In The Use of Historical Data in Natural Hazard Assessments (pp. 3-27). Springer Netherlands.

Galadini, F., Poli, M. E., Zanferrari, A., 2005. Seismogenic sources potentially responsible for earthquakes with M≥ 6 in the eastern Southern Alps (Thiene-Udine sector, NE Italy). Geophysical Journal International, 161(3), 739-762.

Galbraith, R.F., Roberts, R.G., 2012. Statistical aspects of equivalent dose and error calcula- tion and display in OSL dating: an overview and some recommendations. Quat. Geochronol. 11, 1–27.

Gale, S.J., Hoare, P.G., 1991. Quaternary Sediments. Belhaven Press, New York.

Galli, P., 2005. I terremoti del gennaio 1117. Ipotesi di un epicentro nel Cremonese. Il Quaternario, 18, 87-100.

Gaudant, J., Courme-Rault, M.D., Fornaciari, E., Fourtanier, E., 2010. The Upper Miocene fossil fish locality of Pecetto di Valenza (Piedmont, Italy): a multidisciplinary approach. Boll. Soc. Paleont. Ital., 49 (3), 201.

Ge, J., & Guo, Z., 2010. Neogene eolian deposits within the West Qinling Mountains: Climatic and tectonic implications. Chinese Science Bulletin, 55(15), 1483-1487.

Giglia, G., G. Capponi, L. Crispini and M. Piazza (1996). Dynamics and seismotectonics of the West-Alpine arc, Tectonophysics, 267, 143-175.

Giordano, A., 1999. Pedologia. Edizioni UTET, Torino.

Giraudi C., 2014. Quaternary studies as a tool to validate seismic hazard potential of tectonic structures: the case of the Monferrato thrust front (Vercelli Plain, NW Italy). Alpine and Mediterranean Quaternary, 27(1), 5-28.

Giraudi C., 2015. Quaternary evolution of the plain between Casale Monferrato and Valenza: Implications for the tectonics of the Monferrato thrust front. Alpine and Mediterranean Quaternary, 28(1), 71 – 92.

Giraudi C., Mottura A., Sala B., Siori M.S., Bormioli D. (2003) - The Castagnone Site (Cerrina Valley, Monferrato Hills, NW Italy): Early Pleistocene sedimentary record and biochronology. Rivista Italiana di Paleontologia e Stratigrafia,109 (3), 517-526.

Giraudi, C., 2016. The evolution of the northernmost Apennine front (Piedmont, Italy): Plio-Pleistocene sedimentation and deformation in the Po basin and Monferrato hills. Alpine and Mediterranean Quaternary, 29 (1), 2016, 45-65

Godfrey-Smith, D.I., Huntley, D.J., Chen, W.H., 1988. 'Optical dating studies of quartz and feldspar sediment extracts'. Quaternary Sci Rev 7, 373–80.

Guidoboni, E., 1986. The earthquake of December 25, 1222: analysis of a myth. Geologia Applicata e Idrogeologia, 21, 413-424.

Guidoboni, E., Comastri, A., Boschi, E., 2005. The "exceptional" earthquake of 3 January 1117 in the Verona area (northern Italy): A critical time review and detection of two lost earthquakes (lower Germany and Tuscany). Journal of Geophysical Research: Solid Earth, 110(B12).

Huntley, D.J., Godfrey-Smith, D.I., Thewalt, M.L.W., 1985. Optical dating of sedi- ments. Nature 313, 105e107.

IAEA, 2010. Seismic Hazards in Site Evaluation for Nuclear Installations. Specific Safety Guide. Series No. SSG-9.

Irace, A., Clemente, P., Natalicchio, M., Ossella, L., Trenkwalder, S., De Luca, D.A., Mosca, P., Piana, F., Polino, R., Violanti, D., 2009. Geologia e Idrostratigrafia Profonda della Pianura Padana Occidentale. Regione Piemonte, 111 p., 61 tables; La Nuova Lito Firenze 2009, ISBN 978-88- 904554-0-7, available online at http://www.regione.piemonte.it/ acqua/idrostrat.htm.

Irace, A., Monegato, G., Tema, E., Martinetto, E., Gianolla, D., Vassio, E., Bellino, L., Violanti, D., 2015. Unconformity-bounded stratigraphy in the Plio-Pleistocene continental record: new insights from the Alessandria Basin (NW Italy). Geol. J. http://dx.doi.org/10.1002/gj.2744.

Jain, M., Murray, A.S., Bøtter-Jensen, L., Wintle, A.G., 2005. A single-aliquot regenerative-dose method based on IR (1.49 eV) bleaching of the fast OSL component in quartz. Radiation Measurements 39, 309e318.

James, W.C., Mack, G.H., Monger, H.C., 1998. Paleosol classification. Quaternary International 51-52, 8–9.

Jenny, H., 1941. Factors of soil formation: A system of quantitative pedology, 281 pp.

Jeong, G.Y., Cheong, C.S., 2005. Recurrent events on a Quaternary fault recorded in the mineralogy and micromorphology of a weathering profile, Yangsan Fault System, Korea. Quaternary Research, 64(2), 221-233.

Jim, C.Y., 1990. Stress, shear deformation and micromorphological clay orientation: a synthesis of various concepts. Catena, 17(4-5), 431-447.

Kaltenrieder, P., Procacci, G., Vannière, B., Tinner, W., 2010. Vegetation and fire history of the Euganean Hills (Colli Euganei) as recorded by Lateglacial and Holocene sedimentary series from Lago della Costa (northeastern Italy). The Holocene 20:679 –695

Khatwa, A., & Tulaczyk, S., 2001. Microstructural interpretations of modern and Pleistocene subglacially deformed sediments: the relative role of parent material and subglacial processes. Journal of Quaternary Science, 16(6), 507-517.

Kim, J.C., Duller, G.A.T., Roberts, H.M., Wintle, A.G., Lee, Y.I., Yi, S.B., 2009. Dose dependence of thermally transferred optically stimulated luminescence signals in quartz. Radiation Measurements 44, 132e143.

Krumbein, W.C., Sloss, L.L., 1963. Stratigraphy and sedimentation. Freeman & Co., San Francisco, USA.

Kubiëna, W.L., 1953. Bestimmungsbuch und Systematik der Böden Europas. F. Enke Verlag, Stuttgart.

Kühn, P., 2003. Spätglaziale und holozäne Lessivégenese auf jungweichselzeitlichen Sedimenten Deutschlands. Greifswalder Geographische Arbeiten 28, Greifswald, pp 167.

Kühn, P., Aguilar, J., Miedema, R., 2010. Textural pedofeatures and related horizons. In: Stoops G, Marcelino V, Mees F (eds) Interpretation of micromorphological features of soils and regoliths. Elsevier, Oxford, pp 217-250.

Kumar, S., Parkash, B., Manchanda, M. L., & Singhvi, A. K., 1996. Holocene landform and soil evolution of the western Gangetic Plains: implications of neotectonics and climate. J. Geol, 88, 100-108.

Larson, G.J., Menzies, J., Lawson, D.E., Evenson, E.B., Hopkins, N.R., 2016: Macro- and micro-sedimentology of a modern melt-out till – Matanuska Glacier, Alaska, USA. Boreas, Vol. 45, pp. 235-251. 10.1111/bor.12149. ISSN 0300-9483.

Livio, F., Berlusconi, A., Michetti, A.M., Sileo, G., Zerboni, A., Trombino, L., Cremaschi, M., Mueller, K., Vittori, E., Carcano, C., Rogledi, S., 2009. Active fault-related folding in the epicentral area of the December 25, 1222 (Io = IX MCS) Brescia earthquake (Northern Italy): Seismotectonic implications. Tectonophysics 476, 320–335. DOI: 10.1016/j.tecto.2009.03.019.

Livio, F., Berlusconi, A., Zerboni, A., Trombino, L., Sileo, G., Michetti, A.M., Rodnight, H., Spötl, C., 2014: Progressive offset and surface deformation along a seismogenic blind thrust in the Po Plain foredeep (Southern Alps, Northern Italy). Journal of Geophysical Research: Solid Earth 119, pp. 7701–7721. DOI: 10.1002/2014JB011112.

Livio, F., Michetti, A. M., Sileo, G., Carcano, C., Mueller, K., Rogledi, S., Serva, L., Vittori, E., Berlusconi, A., 2009. Quaternary capable folds and seismic hazard in Lombardia (Northern Italy): the Castenedolo structure near Brescia, Boll. Soc. Geol. It., 128, 320-335

Madsen, A.T., Murray, A.S., 2009. Optically stimulated luminescence dating of young sediments: a review. Geomorphology 109, 3e16.

Maesano, F.E., D'Ambrogi, C., Burrato, P., Toscani, G., 2001. Long-term geological slip rates of the Emilia thrust front (Northern Apennines) from 3D modelling of key buried horizons. Geophysical Journal International, 154, 72-88.

Maesano, F.E., D'Ambrogi, C., Burrato, P., Toscani, G., 2015. Slip-rates of blind thrusts in slow deforming areas: Examples from the Po Plain (Italy). Tectonophysics, 643, 8-25.

Magri, G., Molin, D., 1986. I terremoti del 3 Gennaio 1117 e del 25 Dicembre 1222. ENEA-RTI PAS-ISPGEOL-LO,(86), 2.

Malagnini, L., Herrmann, R. B., Munafò, I., Buttinelli, M., Anselmi, M., Akinci, A., & Boschi, E., 2012. The 2012 Ferrara seismic sequence: Regional crustal structure, earthquake sources, and seismic hazard. Geophysical Research Letters, 39(19).

Mariotti, G., Doglioni, C., 2000. The dip of the foreland monocline in the Alps and Apennines. Earth Planet. Sci. Lett. 181, 191-202.

Marrett, R., Allmendinger, R.W., 1990. Kinematic analysis of fault-slip data. Journal of Structural Geology 12(8), 973–986.

McCalpin, J. P., & Berry, M. E., 1996. Soil catenas to estimate ages of movements on normal fault scarps, with an example from the Wasatch fault zone, Utah, USA. Catena, 27(3), 265-286.

McCalpin, J.P., 2009. Paleoseismology (Vol. 95). Academic Press, p. 613.

McRae, S.G., 1991. Pedologia pratica - Come studiare i suoli sul campo, Zanichelli, Bologna.

Meletti, C., D'Amico, V., Ameri, G., Rovida, A., & Stucchi, M., 2012. Seismic hazard in the Po Plain and the 2012 Emilia earthquakes. Annals of Geophysics, 55(4).

Menzies, J., Reitner, J.M., 2016: Microsedimentology ice stream tills from the Eastern Alps, Austria – a new perspective on till microstructures. Boreas, Vol. 45, pp. 804–827. 10.1111/bor.12189. ISSN 0300-9483.

Michetti, A.M. & Marco, S., 2005. Future trends in paleoseismology: Integrated study of the seismic landscape as a vital tool in seismic hazard analyses. Tectonophysics, 408(1), 3-21.

Michetti, A.M., Ferreli, L., Esposito, E., Porfido, S., Blumetti, A.M., Vittori, E., ... & Roberts, G.P., 2000. Ground effects during the 9 September 1998, Mw= 5.6 Lauria earthquake and the seismic potential of the “aseismic” Pollino region in southern Italy. Seismological Research Letters, 71(1), 31-46.

Michetti, A.M., Giardina, F., Livio, F., Mueller, K., Serva, L., Sileo, G., Fioraso, G., 2012. Active compressional tectonics, Quaternary capable faults, and the seismic landscape of the Po Plain (N Italy). Ann. Geophys. 55 (5), 969e1001. http://dx.doi.org/10.4401/ag-5462.

Michetti, A.M., Hancock, P.L., 1997. Paleoseismology: understanding past earthquakes using quaternary geology. Journal of Geodynamics, 24 (1–4), pp. 3–10

Ministero per le Politiche Agricole, 1999. Approvazione dei "Metodi ufficiali di analisi chimica del suolo", Decreto Ministeriale del 13/09/1999, Gazz. Uff. Suppl. Ordin. n° 248 del 21/10/1999.

Montone, P., Mariucci, M.T., Pondrelli S., Amato, A., 2004. An improved stress map for Italy and surrounding regions (central Mediterranean), J. Geophys. Res. 109, B10410, 10.1029/2003JB002703

Mosca P., 2006. Neogene basin evolution in the Northern Po Plain (NW Italy). Insights from seismic interpretation, subsidence analysis and low temperature (U-Th)/He thermocronology. PhD Thesis VU University Amsterdam, 190 pp.

Mosca P., Polino R., Rogledi S., Rossi M., 2009. New data for the kinematic interpretation of the Alps-Apennines junction (Northwestern Italy). Int. J. Earth. Sci., doi: 10.1007/s00531-009-0428-2

Munsell, 1994. In: Color, Munsell® (Ed.), Soil Color Charts, 1994 Rev (New Windsor).

Murphy, C.P., 1986. Thin Section Preparation of Soils and Sediments. AB Academic Publishers, Berkhamsted.

Murray, A. S., Wintle. A.G., 2000. ‘‘Luminescence Dating of Quartz Using an Improved Single-Aliquot Regenerative-Dose Protocol,’’ Radiation Measurements 32: 57–73.

Murray, A.S., Olley, J.M., 2002. Precision and accuracy in the optically stimulated luminescence dating of sedimentary quartz: a status review. Geochronometria 21, 1e16.

Muttoni G, Carcano C, Garzanti E, Ghielmi M, Piccin A, Pini R, Rogledi S, Sciunnach D (2003) Onset of major Pleistocene glaciations in the Alps. Geology 31:989 –992

Nelson, A.R., 1992. Lithofacies analysis of colluvial sediments--an aid in interpreting the recent history of Quaternary normal faults in the Basin and Range Province, western United States. Journal of sedimentary research, 62(4), pp. 607-621.

Nieto-Fuentes, R., Nieto-Samaniego, A .F., Xu, S.S., Alaniz-A lvarez, S.A., 2014. Software for determining the true displacement of faults. Comput. Geosciences 64, 35e40.

Nieto-Fuentes, R., Nieto-Samaniego, Á.F., Xu, S.S., Alaniz-Álvarez, S.A., 2014. Software for determining the true displacement of faults. Computers & Geosciences 64, 35–40.

Omori, F., 1909. Preliminary report on the Messina–Reggio Earthquake of Dec. 28, 1908, Bull. Imp. Earth. Invest. Comm., 3(2), 37–46.

Orombelli, G., 1990. Loess in Italy: an introduction. In: Cremaschi M (Ed) The loess in Northern and Central Italy: a loess basin between the Alps and the Mediterranean Sea. C.N.R., Centro di Studio per la Stratigrafia e Petrografia delle Alpi Centrale, Milano, Italy, pp 11-12

Pantosti, D., Schwartz, D., Valensise, G., 1993. Paleoseismology along the 1980 surface rupture of the Irpinia fault: implications for earthquake recurrence in the southern Apennines, Italy. Journal of Geophysical Research 98, 6561– 6577.

Pavia, G., 1989. Il giacimento a pesci messiniani di Pecetto di Valenza (Alessandria). Boll. Soc. Piem. Arch. e Belle Arti, 43, 15-21.

Peresani M, Cremaschi M, Ferraro F, Falgueres C, Bahain J-J, Gruppioni G, Sibilia E, Quarta G, Calcagnile L, Dolo J-M, 2008. Age of the final Middle Palaeolithic and Uluzzian levels at Fumane Cave, Northern Italy, using 14C, ESR, 234U/230Th and thermoluminescence methods. J Archaeol Sci 35:2986 –2996

Pieri, M., Groppi, G., 1981. Subsurface geological structure of the Po plain, progetto finalizzato geodinamica/sottoprogetto “modello strutturale. Publ. Ital. CNR 414, 1e13.

Pini, R., 2004. Late Neolithic vegetation history at the pile-dwelling site of Palù di Livenza (northeastern Italy). J Quat Sci 19: 769 –781

Poli, M.E., Burrato, P., Galadini, F., Zanferrari, A., 2008. Seismogenic sources responsible for destructive earth- quakes in NE Italy, Bollettino di Geofisica Teorica e Ap- plicata, 49 (3-4), 1-13.

Ponza, A., Pazzaglia, F.J., and Picotti, V,. 2010. Thrust-fold activity at the mountain front of the northern Apennines (Italy) from quantitative landscape analysis, Geomorphology, 123(3), 211 –231.

Porat, N., 2006. ‘‘Use of Magnetic Separation for Purifying Quartz for Luminescence Dating,’’ Ancient TL 24: 33–36.

Porat, N., 2007. ‘‘Analytical Procedures in the Luminescence Dating Laboratory,’’ Geological Survey of Israel Technical Report TR- GSI/2/2002. Jerusalem: Geological Survey of Israel (in Hebrew).

Porat, N., Duller, G.A.T., Roberts, H.M., Wintle, A.G., 2009. A simplified SAR protocol for TT-OSL. Radiation Measurements 44, 538e542.

Preusser, F., Chithambo, M.L., Götte, T., Martini, M., Ramseyer, K., Sendezera, E.J., Susino, G.J., Wintle, A.G., 2009. Quartz as a natural luminescence dosimeter. Earth-Science Reviews 97, 184e214.

Previtali, E., 1992. Seismipedoturbations in volcanic soils in North-Eastern Ecuador. Catena, 19, pp. 441–450.

Ravazzi, C., Deaddis, M., De Amicis, M., Marchetti, M., Vezzoli, G., Zanchi, A., 2012. The last 40 ka evolution of the Central Po Plain between the Adda and Serio rivers. Géomorphologie : relief, processus, environnement, 2/2012:131-154

Ravazzi, C., Marchetti, M., Zanon, M., Perego, R., Quirino, T., Deaddis, M., De Amicis, M., Margaritora, D., 2013. Lake evolution and landscape history in the lower Mincio Valley, unravelling drainage changes in the central Po Plain (N-Italy) since the Bronze Age. Quatern Int 288:195 –205

Reimer, P.J., Bard, E., Bayliss, A., Beck, J.W., Blackwell, P.G., Bronk Ramsey, C., Buck, C.E., Cheng, H., Edwards, R.L., Friedrich, M., Grootes, P.M., Guilderson, T.P., Haflidason, H., Hajdas, I., Hatte, C., Heaton, T.J., Hogg, A.G., Hughen, K.A., Kaiser, K.F., Kromer, B., Manning, S.W., Niu, M., Reimer, R.W., Richards, D.A., Scott, E.M., Southon, J.R., Turney, C.S.M., van der Plicht, J., 2013. IntCal13 and MARINE13 radiocarbon age calibration curves 0-50000 years calBP. Radio- carbon 55, 1869-1887.

Rhodes, E.J., 1988. Methodological considerations in the optical dating of quartz. Quaternary Science Reviews 7, 395–400.

Rhodes, E.J., 2011. Optically stimulated luminescence dating of sediments over the past 200,000 years. Annual Review of Earth and Planetary Sciences, 39, 461-488.

Ricci Lucchi, F., 1980. Sedimentologia I. Materiali e tessitura dei sediment. CLUEB, Bologna, Italy.

Rittenour, T.M., 2008. Luminescence dating of fluvial deposits: applications to geomorphic, palaeoseismic and archaeologic work. Boreas 37, 613e635.

Roberts, H.M., Duller, G.A.T., 2004. Standardised growth curves for optical dating of sedi- ment using multiple-grain aliquots. Radiat. Meas. 38, 241–252.

Rockwell, T. K., 2000. Use of soil geomorphology in fault studies. Quaternary Geochronology: Methods and Applications, 273-292.

Rossi, M., Mosca, P., Polino, R., Rogledi, S., Biffi, U., 2009. New outcrop and subsurface data in the Tertiary Piedmont Basin (NW-Italy): unconformity-bounded stratigraphic units and their relationships with basin-modification phases. Rivista Italiana di Paleontologia e Stratigrafia, 115(3), 305-335.

Rovida, A., Locati, M., Camassi, R., Lolli, B., Gasperini, P. (Eds.), 2016. CPTI15, the 2015 version of the Parametric Catalogue of Italian Earthquakes. Istituto Nazionale di Geofisica e Vulcanologia. http://dx.doi.org/10.6092/INGV.IT-CPTI15.

Sacco F., 1889 - Il bacino Terziario e Quaternario del Piemonte. Atti Società Italiana di Scienze Naturali, 31-32, 135-281, 289-398, 331-390.

Sacco F., 1917. L'evoluzione del Fiume Tanaro durante l'Era Quaternaria. Atti della Soc. Italiana di Sc. Naturali, Vol. LVI.

Sacco, F., 1884. L'alta valle padana durante l'epoca delle terrazze in relazione con il contemporaneo sollevamento della circostante catena alpina-appenninica. Atti della Regia Accademia delle Scienze di Torino, 19, 3-24

Scardia G, Muttoni G, Sciunnach D, 2006. Subsurface magnetostratigraphy of Pleistocene sediments from the Po Plain (Italy): constraints on rates of sedimentation and rock uplift. Geol Soc Am Bull 118(11/12):1299 –1312.

Scardia, G., De Franco, R., Muttoni, G., Rogledi, S., Caielli, G., Carcano, C., Sciunnach, D., Piccin A., 2012. Stratigraphic evidence of a Middle Pleistocene climate-driven flexural uplift in the Alps. Tectonics, vol. 31, p. TC6004

Scrocca, D., Carminati, E., Doglioni, C. and Marcantoni, D., 2007. Slab retreat and active shortening along the central-Northern Apennines, In: O. Lacombe, J. Lavè, F. Roure and L. Verges (eds.), "Thrust belts and foreland basins: From fold kinematics to hydrocarbon systems", Frontiers in Earth Sciences, 471-487.

Serva L., 1990. Il ruolo delle scienze della terra nelle analisi di sicurezza di un sito per alcune tipologie di impianti industriali; il terremoto di riferimento per il sito di Viadana (MN). Role of Earth sciences in the safety analysis of the site of a particular typology of an industrial plant; the reference earthquake at Viadana - Boll. Soc. Geol. It., 109, 2, 375-411.

Singh, S., Parkash, B., Rao, M. S., Arora, M., & Bhosle, B., 2006. Geomorphology, pedology and sedimentology of the Deoha/Ganga–Ghaghara Interfluve, Upper Gangetic Plains (Himalayan foreland basin)—extensional tectonic implications. Catena, 67(3), 183-203.

Soil Survey Staff, 2010. Keys to Soil Taxonomy, eleventh ed. Natural Resources Conservation Service, US Department of Agriculture, Washington, DC, USA, p. 342.

Srivastava, P., Rajak, M. K., & Singh, L. P., 2009. Late Quaternary alluvial fans and paleosols of the Kangra basin, NW Himalaya: Tectonic and paleoclimatic implications. Catena, 76(2), 135-154.

Stoops, G., 2003. Guidelines for analysis and description of soil and regolith thin sections. Soil Science Society of America, Inc., Madison, Wisconsin, USA.

Stoops, G., Marcelino, V. and Mees, F., Eds., 2010. Interpretation of Micromorphological Features of Soils and Regoliths. Elsevier, Oxford.

Stoops, G., Marcelino, V., Mees, F., 2010. Interpretation of Micromorphological Features in Soil and Regoliths. Elsevier Science Ltd, Amsterdam.

Stoops, G., Schaefer, C.E.G.R., 2010. Pedoplasmation: Formation of Soil Material. In: Stoops, G., Marcelino, V. and Mees, F. (eds), Interpretation of Micromorphological Features of Soils and Regoliths. Elsevier, Oxford.

Stuiver, M., Reimer, P.J., Reimer, R., 2013. Calib Radiocarbon Calibration Version 7.0. http://calib.qub.ac.uk/calib/.

Sturani, C., Sampò, M., 1973. Il Messiniano inferiore in facies diatomitica nel Bacino terziario Piemontese. Mem. Soc. Geol. It., 12, 335-358.

Terhorst, B., Ottner, F., 2003. Polycyclic luvisols in Northern Italy: paleopedological and clay mineralogical characteristics. Quatern Int 106 –107: 215 –231

Thomsen, K.J., Bøtter-Jensen, L., Denby, P.M., Moska, P., Murray, A.S., 2006. Devel- opments in luminescence measurement techniques. Radiation Measurements 41, 768-773.

Toscani, G., Burrato, P., Di Bucci, D., Seno, S., Valensise, G., 2009. Plio-Quaternary tectonic evolution of the northern Apennines thrust fronts (Bologna-Ferrara section, Italy): seismotectonic implications, Italian Journal of Geosciences (Bollettino della Società Geologica Italiana), 128, 650-613.

Tsukamoto, S., Duller, G.A.T., Wintle, A.G., 2008. Characteristics of thermally transferred optically stimulated luminescence (TT-OSL) in quartz and its potential for dating sediments. Radiation Measurements 43, 1204e1218.

Turrini, C., Angeloni, P., Lacombe, O., Ponton, M., Roure, F., 2015. Three-dimensional seismo-tectonics in the Po Valley basin, Northern Italy. Tectonophysics, doi: 10.1016/j.tecto.2015.08.033

Valsecchi, V., Tinner, W., Finsinger, W., Ammann, B., 2006. Human impact during the Bronze Age on the vegetation at Lago Lucone (northern Italy). Veg Hist Archaeobot 15: 99 –113

Vanneste, K., Mees, F., Verbeeck, K., 2008. Thin-section analysis as a tool to aid identification of palaeoearthquakes on the “slow”, active Geleen Fault, Roer Valley Graben. Tectonophysics, 453(1), 94-109.

Verbeeck, K., Wouters, L., Vanneste, K., Camelbeeck, T., Vandenberghe, D., Beerten, K., ... De Grave, J. (2017). Episodic activity of a dormant fault in tectonically stable Europe: The Rauw fault (NE Belgium). Tectonophysics, 699, 146-163.

Wang, X.L., Lu, Y.C., Wintle, A.G., 2006a. Recuperated OSL dating of fine-grained quartz in Chinese loess. Quaternary Geochronology 1, 89e100.

Wang, X.L., Wintle, A.G., Lu, Y.C., 2006b. Thermally transferred luminescence in fine-grained quartz from Chinese loess: basic observations. Radiation Measurements 41, 649e658.

Wick, L., 1996. Late-glacial and early-Holocene palaeoenvironments in Brianza, N Italy. Il Quaternario 9: 653–660.

Wintle, A.G., Murray, A.S., 2006. A review of quartz optically stimulated lumines- cence characteristics and their relevance in single-aliquot regeneration dating protocols. Radiation Measurements 41, 369–391.

WRB, 2006. World Reference Base for Soil Resources 2006. World Soil Resources Reports 103. FAO, Rome.

Wright, V., P., Tucker, M., E., 1991. Calcretes: an introduction. In Wright, V.P. & Tucker, M.E. (eds.), Calcretes. IAS Reprint Series, Volume 2. Blackwell, Oxford, pp. 1–22.

Xu, S., Nieto-Samaniego, A.F., Alaniz-Álvarez, S.A., 2009. Quantification of true displacement using apparent displacement along an arbitrary line on a fault plane. Tectonophysics 467(1), 107–118.

Zaidner, Y., Frumkin, A., Friesem, D., Tsatskin, A., Shahack-Gross, R., 2016. Land- scapes, depositional environments and human occupation at Middle Paleolithic open-air sites in the southern Levant, with new insights from Nesher Ramla, Israel. Quat. Sci. Rev. 138, 76e86.

Zanchetta, G., Drysdale, R., N., Hellstrom, J.,C., Fallick, A., E., Isola, I., Gagan, M., K., Pareschi, M., T., 2007. Enhanced rainfall in the Western Mediterranean during deposition of sapropel S1: stalagmite evidence from Corchia cave (Central Italy). Quat Sci Rev 26: 279–286.

Zerboni, A., Trombino, L., Cremaschi, M., 2011. Micromorphological approach to polycyclic pedogenesis on the Messak Settafet plateau (central Sahara): formative processes and palaeoenvironmental significance. Geomorphology 125, 319–335.

Zerboni, A., Trombino, L., Frigerio, C., Livio, F., Berlusconi, A., Michetti, A.M., Rodnight, H., Spottl, C., 2015. The loess-paleosol sequence at Monte Netto: a record of climate change in the Upper Pleistocene of the central Po Plain, northern Italy. J. Soils Sediments 15, 1329e1350. http://dx.doi.org/10.1007/ s11368-014-0932-2.

Zhornyak, L., V., Zanchetta, G., Drysdale, R., N., Hellstrom, J., C., Isola, I., Regattieri, E., Piccini, L., Baneschi, I., Couchoud, I., 2011. Stratigraphic evidence for a “pluvial phase ” between ca 8200e7100 ka from Renella cave (Central Italy). Quat Sci Rev 30:409 –417.